Longitudinal studies and the development of gene therapy for ovine neuronal ceroid lipofuscinoses

---

A thesis

submitted in partial fulfilment

of the requirements for the Degree of

Doctor of Philosophy

at

Lincoln University

by

Nadia Lesley Mitchell

Lincoln University

2016

Declaration

Parts of this thesis have been submitted and accepted for publication and/or presented in advance of submission of the thesis.

Publications

- Amorim I.S., Mitchell N.L., Palmer D.N., Sawiak S.J., Mason R., Wishart T.M., Gillingwater T.H. (2015). Molecular neuropathology of the synapse in sheep with CLN5 Batten disease. Brain and Behaviour 5: e00401.

- Sawiak S.J., Perumal S.R., Rudiger S.R., Matthews L., Mitchell N.L., McLaughlan C.J., Bawden C.S., Palmer D.N., Kuchel T and A.J. Morton (2015). Rapid and progressive regional brain atrophy in CLN6 Batten disease affected sheep measured with longitudinal magnetic resonance imaging. PLoS ONE 10: e0132331.

- Palmer D.N., Neverman N.J., Chen J.Z., Chang C-T., Houweling P.J., Barry L.A., Tammen I., Hughes S.M. and N.L. Mitchell (2015). Recent studies of ovine neuronal ceroid lipofuscinoses from BARN, the Batten Animal Research Network. Biochimica et Biophysica Acta 1852:2279-2286.

- Perentos N., Martins A.Q., Watson T.C., Bartsch U., Mitchell N.L., Palmer D.N., Jones M.W. and A.J. Morton (2015). Translational neurophysiology in sheep: Measuring sleep and neurological dysfunction in CLN5 Batten disease affected sheep. Brain 138, 862-874.

- Hughes S.M., Hope K.M., Xu J.B., Mitchell N.L. and D.N. Palmer (2014a). Inhibition of storage pathology in prenatal CLN5-deficient sheep neural cultures by lentiviral gene therapy. Neurobiology of Disease 62, 543-550.

Official Documentation

- Environmental Protection Agency: Section 26 Determination (2015). Application (APP202443) sought to determine whether *Ovis aries* (sheep) injected with recombinant Adeno-Associated Viral (AAV)-derived non-replicating vectors and constructs were new organisms for the purpose of the Hazardous Substances and New Organisms (HSNO) Act (1996). Decision on 28 October 2015 in Lincoln University's favour, actioned 11 November 2015.

Presentations

- Mitchell N.L., Wicky H.E., Schoderböck L., Barrell G.K., Wellby M.P., Russell, K.N., Bland, R., Hughes, S.M and D.N. Palmer (2015) Viral-mediated gene therapy prevents disease development in ovine models of neuronal ceroid lipofuscinosis. 20th European Study Group on Lysosomal Diseases (ESGLD) Workshop and Graduate course, 30 September – 4 October 2015, Pozzuoli (Naples), Italy (Invited oral presentation).

- Mitchell N.L., Barrell G.K., Wellby M.P., Wicky H.E., Palmer D.N. and S.M. Hughes (2014) Gene therapy using adeno-associated virus serotype 9 in the sheep brain. 14th Congreso Internacional de Lipofuscinosis Ceroideas Neuronales (Enfermedad de Batten), 22-26 October 2014, Cordoba, Argentina (Invited oral presentation).

Statement of candidate contribution

The data presented in this thesis are the original work of the author and do not incorporate material that has been previously submitted for another degree at any University, except where specifically indicated in the text. However, as the studies described in this thesis were integrated within the Lincoln University Batten disease research programme and/or BARN (Batten Animal Research Network) initiatives, there are strong collaborative components. In particular, viral vectors were prepared in the laboratory of Dr. Stephanie Hughes, Otago Viral Vector Facility, University of Otago, as part of a large-scale project jointly funded by CureKids NZ and the Australian and American chapters of the Batten Disease Support and Research Association (BDSRA) to assess viral vector-mediated gene therapy in ovine models of NCL. Further longitudinal *in vivo* biomarkers of disease progression, including electroretinography and three-dimensional intracranial and ventricular modelling, were developed by Katharina Russell as part of her PhD studies at Lincoln University and utilised in the latter part of this study. MRI analyses were performed in collaboration with Dr. Tracey Melzer at the New Zealand Brain Research Institute.

Twenty years from now you will be more disappointed
by the things that you didn't do than by the ones you did do.
So throw off the bowlines.
Sail away from the safe harbor.
Catch the trade winds in your sails.
Explore. Dream. Discover.

Mark Twain

Dedicated to my family
Including the woolly ones

Abstract of a thesis submitted in partial fulfilment of the
requirements for the Degree of Doctor of Philosophy.

Longitudinal studies and the development of gene therapy for ovine neuronal ceroid lipofuscinoses

by

Nadia Lesley Mitchell

The neuronal ceroid lipofuscinoses (NCLs, Batten disease) are a group of fatal inherited lysosomal storage diseases characterised by progressive neurodegeneration, cortical atrophy, and blindness. Currently there are no effective treatments. Naturally occurring animal models exist, including two forms in sheep which are representative of the different NCL protein defects. A lesion in a soluble lysosomal protein (CLN5) causes NCL in Borderdale sheep, whilst South Hampshire sheep have a defective intracellular endoplasmic reticulum membrane-bound protein (CLN6). This subdivision has consequences for the planning of therapies. This thesis compares the progressive neuropathological changes, and examines the efficacy of viral-mediated *in vivo* gene therapy, in these two NCL sheep models.

An immunohistochemical study revealed that, despite very different gene products and subcellular localisations, the pathogenic cascade was remarkably similar for CLN5 and CLN6 affected sheep. Dysregulated glial activation preceded regionally specific neurodegeneration in both disease models and both occurred well before clinical onset. Neuropathological changes were more advanced in the CLN5 model, which correlated with the earlier onset of clinical symptoms in these sheep, but by end-stage disease CLN5 and CLN6 brains were similarly affected. Windows for best therapeutic efficacy were established and these data highlight the translational utility of the sheep brain for testing human gene therapies.

Lentiviral vectors have been shown to mediate successful gene delivery to the ovine brain yet the efficacy of adeno-associated viral (AAV) vectors has not been tested in sheep. Stable, predominantly neurotropic, transgene expression was evident one month after intracerebroventricular (ICV) and intraparenchymal (IP) delivery of AAV9 to the normal sheep brain. However with a greater spread and no evidence of vector or procedural neuroinflammation or toxicity, the ICV approach proved most efficacious in sheep.

Deficiencies in soluble lysosomal proteins are deemed particularly amenable to *in vivo* gene therapy via the normal lysosomal enzyme trafficking system and the phenomenon of 'cross-correction'. To test this paradigm in sheep, six pre-clinical CLN5 deficient lambs were treated with combinatorial ICV and IP injections of either lentiviral or AAV9 vectors expressing ovine *CLN5*. Both vector platforms afforded sustained protection against stereotypical disease in these sheep. Cognitive and neurological function was preserved, whilst longitudinal neuroimaging revealed normalisation of intracranial volume and structural brain integrity. Quality of life was profoundly improved for the treated sheep and, apart from delayed-onset visual deficits, treated sheep well exceeded the typical lifespan of untreated animals.

Defects in membrane-bound proteins are generally considered harder therapeutic targets. However the current study indicates that gene therapy is also possible for these NCL forms. Whilst five similarly injected pre-clinical CLN6 deficient sheep developed stereotypical CLN6 disease, one AAV9-*CLN6* treated animal was clinically indistinguishable from age-matched control animals through the 24-month follow up period. *Post mortem* neuropathological studies revealed significant correction of neurodegeneration, normal cortical laminar organisation and a reversal in disease-associated glial activation.

These encouraging results of sustained therapeutic and functional efficacy in large animal models of NCL provide a strong rationale for the clinical translation of viral-mediated gene transfer to human patients with CLN5 and CLN6 disease. In fact, the findings of this thesis have encouraged a Phase I/II CLN6 clinical trial which has just begun.

Keywords: Batten disease, neuronal ceroid lipofuscinosis, lysosomal storage disorder, animal models, sheep, brain, neurodegeneration, neuroinflammation, neurogenesis, gene therapy, vector, adeno-associated virus, lentivirus, transduction.

Acknowledgements

I have found to complete a PhD you need to surround yourself with many different people; firstly those who know more than you do! Add to the mix those who encourage you, those who make you want to explore and keep learning. For me, this thesis would not have been possible without the following such people.

Foremost I am indebted to my supervisor, Prof. David Palmer, who over the past 15 years has opened up a world of opportunities for me. Thank you for introducing me to the Battens community, for your constant belief in me and for providing a 'blend' of motivation, support, responsibility and freedom during this time. We've shared (and survived!) some ups and downs through this process but I'm thrilled to play a part in fulfilling one of your life-long goals – seeing a therapy come to fruition in NCL. How exciting was it to see those treated sheep run free in the paddock at 26 months of age?! Your knowledge of NCL is boundless and if I could one day know even half as much as you do, then I would be happy. Much love to you and Jeanette always. Oh, and guess what? I *finally* finished 'Lucky Jim'!

I whole-heartedly thank my co-supervisor, Assoc. Prof. Graham Barrell, for his enthusiasm, surgical expertise and incredible way with words. My writing benefits tremendously from your keen and able eye. I am so fortunate to work with some other amazing colleagues at Lincoln University, whom I cannot thank enough: Martin Wellby for your boundless knowledge and skills, initiative and willingness to be involved in anything and everything; Katharina Russell (DVM, Copenhagen, Denmark) for your invaluable veterinary and imaging skills, positive energy and for *months* of helping me shovel sheep poo! To my office-mate Dr. Hannah Lee, thank you for your friendship, open advice, many de-stressing swims and runs and for generally keeping me (semi-)sane! I thank Drs Graham Kay and Robin MacFarlane for sharing your skills with me over the years, and Jarol Chen for paving the PhD pathway, your passion and constant smile are invigorating. In your own way, you have all inspired me to want to keep learning and I am *so* appreciative of your help. The cake is on me!

I warmly thank our BARN colleagues, particularly Drs. Stephanie Hughes (University of Otago) and Imke Tammen (University of Sydney), and Hollie Wicky (University of Otago). These long-standing collaborations have been rewarding, your expertise and support have been instrumental in this project and I value your friendship. Locally, I acknowledge more recent collaborators at the New Zealand Brain Research Institute (Dr. Tracy Melzer) and the Department of Radiology, University of Otago, Christchurch (Assoc. Prof. Nigel Anderson) for their neuroimaging contributions and general enthusiasm about this project. I look forward to expanding these studies further when I commence post-doctoral studies with you.

I gratefully acknowledge the following funding groups: the John W and Carrie McLean Trust for my PhD scholarship; CureKids NZ, the Batten Disease Support and Research Association (BDSRA), Lysosomal Diseases New Zealand (LDNZ), Batten Disease NZ, and the Faculty of Agriculture and Life Sciences, Lincoln University for the financial support for this study and my conference travel grants.

My deepest gratitude goes to animal technicians and research farm staff, particularly Amy Smaill, Robin McAnulty, Chris Logan, James Meyer, Colin Pettigrew and Hélène de Batz. Without their dedication, care and *hours* of weekend work this project simply would not have been possible. To my woolly friends, what a sacrifice you have made in the name of research. I have loved the many hours spent in the field observing, monitoring and just 'playing' sheep. What a totally under-rated species you are! Sheep are curious, intelligent, gregarious animals and we could all learn from their fellowship.

To put a human face to NCL, we are incredibly fortunate as research scientists in this field to interact with patients, parents, family advocacy groups and clinicians. The NCL families I have met, both in New Zealand and internationally, drive me to want to answer many of the outstanding questions we still have about this disorder. As a mother, I stand in admiration of your strength and perserverance in such adversity.

I would not be here today without all of my family and friends outside of work. I thank my parents, John and Anne, and sister Alika, for their supportive discussions through this time, child-minding and for instilling in me a strong 'work ethic' and love of education! Thank you Gately grandparents for your love and holiday support. In particular, I want to thank the 'Thursday night walkers' for your constant support and for always renewing my energy. What an inspirational group of strong and beautiful women, I value your friendship more than you know.

Finally, but by no means least, to the three amazing men in my life – you are my world and this PhD would not have been possible without your support. Karl, you are the calm to my storm. Always willing to help, be it finishing my immunostaining, chasing sheep or 'last minute' dashes to pick up the boys from school! You're my best friend, dependable beyond belief and the *greatest* dad to our wee people. Jackson and Ethan, this thesis is for you. Your smiling faces, hugs and funny stories make me *so* happy every day. I want you to know that if you work hard, good things can come your way. I've loved sharing many 'sheepy times' with you all but now it's time for that Gately-Mitchell 'holiday' that I promised you! *Love love love you*. Let's keep exploring together…

Table of Contents

List of Tables

List of Figures

List of Abbreviations

Only abbreviations that appear more than once and in more than one chapter are displayed.

AAV	adeno-associated virus
AAV9	adeno-associated virus, serotype 9
BARN	Batten Animal Research Network
BBB	blood brain barrier
bp	base pair
cDNA	complementary DNA
CDS	coding DNA sequence
CLN/CLN	NCL causing gene/protein
CNS	central nervous system
CRS	clinical rating score
CSF	cerebrospinal fluid
CT	Computed tomography
DAB	3, 3'-diaminobenzadine
DNA	deoxyribonucleic acid
DPX	p-xylene-bis(pyridinium bromide)
EPA	Environmental Protection Agency (NZ)
ER	endoplasmic reticulum
ERG	electroretinography
ERT	enzyme replacement therapy
GABA	γ-aminobutyric acid
gDNA	genomic deoxyribonucleic acid
GFAP	glial fibrillary acidic protein
GFP	green fluorescent protein
GSB4	Griffonia simplicifolia isolectin type I-B4
HIV-1	human immunodeficiency virus 1
ICV	intracerebroventricular
INCL	infantile NCL
IP	intraparenchymal
kDa	kilodalton(s)

kB	kilobase
LFB	Luxol fast blue
LINCL	late infantile NCL
LOD	logarithm of the odds
LSD(s)	lysosomal storage disease(s)
LV	lentiviral
MND(U3)	myeloid sarcoma virus (U3 element)
MPS	mucopolysaccharidosis
MRI	magnetic resonance imaging
mRNA	messenger ribonucleic acid
NCL	neuronal ceroid lipofuscinosis
NGS	normal goat serum
PBS	phosphate buffered saline, pH 7.4
PBST	phosphate buffered saline, pH 7.4, containing 0.3% Triton X-100
PCR	polymerase chain reaction
PLR	pupillary light reflex
PME	progressive myoclonic epilepsy
PPT1	palmitoyl protein thioesterase 1
PSA-NCAM	poly-sialated neural cell adhesion molecule
RNA	ribonucleic acid
SAP	sphingolipid activator proteins (saposin)
scAAV	self complementary AAV
SEM	standard error of the mean
ssAAV	single stranded AAV
sub c	subunit c of the mitochondrial ATP synthase
SVZ	subventricular zone
TPP1	tripeptidyl peptidase I
TU	transducing units
vg	viral genomes
VSV-G	vesicular stomatitis virus glycoprotein

Chapter 1

Introduction

1.1 Neuronal ceroid lipofuscinosis – an overview

The neuronal ceroid lipofuscinoses (NCLs; Batten disease) refer to a group of fatal, incurable lysosomal storage diseases that collectively constitute one of the most common types of inherited neurodegenerative diseases in childhood. Given advances in genetic diagnoses, the traditional estimate of incidence of 1:12,500 live births worldwide (Rider & Rider, 1988) now seems realistic. The disease is genetically heterogeneous with mutations in any one of thirteen genes (designated *CLN1-8, 10-14)* proposed to cause NCL, however the functions of the proteins encoded by these genes and the underlying pathological mechanisms are still largely unclear. As a group they are defined by the near-ubiquitous accumulation of protein, either subunit c of mitochondrial ATP synthase or saposins A and D, in lysosome-derived organelles (storage bodies) and regionally specific neurodegeneration with resultant severe brain atrophy (Mole *et al*., 2011). As well as the progressive and selective loss of neurons, widespread gliosis is seen through the central nervous system (CNS) supporting a causative role of disease-associated neuroinflammation in pathogenesis. Patients suffer from progressive psychomotor deterioration, retinal degeneration resulting in loss of vision, seizures, and premature death between 7 years of age and early adulthood (Mole *et al*., 2005). Despite considerable efforts, there are no effective treatments.

Various genetically engineered or naturally occuring animal models of the human NCL subtypes exist. Gene 'knock-out' or 'knock-in' NCL mutant mice, with progressive neurodegenerative phenotypes, have been used to delineate disease pathophysiology and in the development of novel therapeutics (reviewed by Shacka, 2012). Spontaneous NCL forms occur in mice (Bronson *et al.,* 1993, 1998) and also in larger animals which serve key translational therapeutic roles. These include ovine, bovine, caprine, canine, equine, feline and porcine species (reviewed by Bond *et al*., 2013; http://www.ucl.ac.uk/ncl/animal.shtml and Section 1.2). Affected sheep, in particular, recapitulate many of the clinical and neuropathological features of the human disease. Several novel aspects underlying NCL pathogenesis have been identified in the CLN6 sheep model and extended to human patients, including the nature of the stored material, the precocious activation of glial cells and the selectivity of neuronal loss. The gyrencephalic ovine brain is similar in size and physical organisation to non-human primates and is ideally suited for the validation of new therapies. These facts have led to this longitudinal investigation into the ovine disease progression, and therapeutic efficacy and translatability of viral-mediated gene transfer in established CLN5 and CLN6 NCL sheep models.

1.1.1 Genetic classification

Historically the NCLs were classified into four forms based on the age of onset of clinical symptoms, infantile, late-infantile, juvenile and adult with a plethora of eponyms coined for these (Haltia, 2003). However advances in molecular genetics and biochemical technologies, particularly whole exome sequencing, have resulted in the identification of 446 mutations in over a dozen NCL genes (http://www.ucl.ac.uk/ncl/mutation.shtml) and demonstrated much more genetic heterogeneity than was initially thought. Mutations in several NCL genes can cause a similar clinical and histopathological phenotype, for example late infantile variant NCL can be caused by mutations in *CLN5*, *CLN6*, *CLN7* or *CLN8* (Warrier *et al*., 2013). Phenotypic heterogeneity has also been reported recently, with mutations in the same gene leading to very different disease courses (Kousi *et al*., 2012; Warrier *et al*., 2013). All these considerations prompted the development of a new NCL nomenclature with classification based on the defective gene as well as the age of onset (Williams & Mole, 2012; Table 1.1). Nevertheless the more recently identified NCL subtypes (*CLN11–14*) do not meet all the classification criteria (clinical, neuropathological and ultrastructural commonality) and there is less certainty over their inclusion into the NCL family (Palmer *et al*., 2013).

Interestingly too, mutations in some of these recently described NCL genes are also linked to other more common neurodegenerative diseases (Table 1.1). A homozygous mutation in the progranulin gene, *CLN11/GRN*, was claimed to cause adult onset NCL in a single-family report (Smith *et al*., 2012). Yet heterozygous mutations in the same gene are a major cause of frontotemporal lobar degeneration (Benussi *et al*., 2008), the second most common type of early-onset dementia. Mutations in *CLN12/ATP13A2* generally cause a rare juvenile Parkinsonism disorder, Kufor-Rakeb syndrome (Ramirez *et al*., 2006) but have been implicated in a family with juvenile onset NCL with learning difficulties (Bras *et al*., 2012), as well as a causative role in a Tibetan terrier canine model of NCL (Wöhlke *et al*., 2011). Mutations in *CLN14/KCTD7* have been described in three diseases; infantile-onset NCL, infantile progressive myoclonic epilepsy (PME) and opsoclonus-myoclonus ataxia-like syndrome (Van Bogaert *et al*., 2007; Blumkin *et al*., 2012; Staropoli *et al*., 2012).

Previously defined NCL genes have also been recently shown to intersect genetically and pathophysiologically with other neurodegenerative disorders. Compound heterozygous missense and splice site variants in *TPP1*, the gene typically mutated in classic late-infantile CLN2 NCL, cause an autosomal recessive spinocerebellar ataxia 7 (SCAR7) (Sun *et al*., 2013). SCAR7 patients present with pyramidal signs and cerebellar ataxia, but none of the ophthalmologic abnormalities or epilepsy seen in the CLN2 disease. Moreover, mutations in the *CLN6* gene cause two distinct subsets of NCL: variant late infantile onset, and adult-onset NCL with PME but no visual dysfunction. Recently *CLN6* mutations have also been documented alongside *CLN14/KCTD7* in PME patients with no evidence of lysosomal storage (Andrade *et al*., 2012).

Table 1.1 Genetic classification of the NCLs (modified from http://www.ucl.ac.uk/ncl/, Cotman *et al*., 2013; Kollmann *et al*., 2013; Warrier *et al*., 2013)

NCL gene	Genotype-Phenotype correlation*	NCL gene product	Cellular localisation	Major storage component	Ultrastructural features
CLN1	**Classic infantile,** late infantile, juvenile, adult	PPT1	Lysosomal matrix	SAP A and D	GROD
CLN2	**Classic late infantile**, juvenile, protracted, *SCAR7*	TPP1	Lysosomal matrix	sub c	CL
CLN3	**Classic juvenile**	CLN3	Endo-lysosomal membrane	sub c	CL, FP
CLN4/DNAJC5	Adult autosomal dominant (Parry disease)	CSPα	Cytosolic/ vesicular membrane	SAPs A and D	CL, GROD, FP
CLN5	**Variant late infantile**, juvenile, adult, protracted	CLN5	Lysosomal matrix	sub c	CL, FP, GROD, RL
CLN6	**Variant late infantile**, protracted, adult Kufs Type A, *PME*	CLN6	ER membrane	sub c	CL, FP, GROD, RL
CLN7	**Variant late infantile**, juvenile protracted	MFSD8	Lysosomal membrane	sub c	CL, FP, GROD, RL
CLN8	**Late infantile**, protracted, *EPMR/Northern epilepsy*	CLN8	ER/ER-Golgi membrane	sub c	CL, FP
CLN10/ CTSD	**Congenital**, late infantile, juvenile, adult	Cathepsin D	Lysosomal matrix, extracellular	SAP A and D	GROD
CLN11/GRN	**Adult**, *Frontal temporal lobe dementia (when heterozygous)*	Progranulin	Extracellular	n.d.	FP
CLN12/ATP13A2	**Juvenile***, Kufor-Rakeb syndrome*	P-type ATPase	Lysosomal membrane	n.d.	FP, GROD
CLN13/CTSF	**Adult Kufs type B**	Cathepsin F	Lysosomal matrix	n.d.	FP, GROD
CLN14/KCTD7	**Infantile**, *Infantile PME, OMA*	KCTD7	Cytosolic/ membrane associated	sub c?	FP, GROD

* Typical phenotype caused by complete loss of gene function (bold) whereas "milder" mutations result in a later age of onset, a more protracted disease course or in some cases a non-NCL disease phenotype also associated with the gene (italic).

The NCL genes, encoded proteins and their cellular localisations, ultrastructural findings as well as typical clinical onsets and phenotypes are presented. The different cellular localisations are highlighted in grey shades, with light grey for soluble lysosomal enzymes/proteins and dark grey for membrane-associated proteins. Abbreviations: **CL**, curvilinear profile; ***CLN1*** etc, ceroid lipofuscinosis, neuronal 1 etc; **CSPα**, cysteine string protein; **DNAJC5**, DnaJ (Hsp40) homolog, subfamily C, member 5; **EPMR**, progressive epilepsy with mental retardation; **ER**, endoplasmic reticulum; **FP**, fingerprint profile; **GROD**, granular osmiophilic deposits; **KCTD7**, potassium channel tetramerization domain-containing protein 7; **MFSD8**, major facilitator superfamily domain containing 8; **n.d.**, not determined; **OMA**, opsoclonus-myoclonus ataxia-like syndrome; **PPT1**, palmitoyl protein thioesterase I; **PME**, progressive myoclonic epilepsy; **RL**, rectilinear profile; **SAP**, sphinglolipid activator protein; **SCAR7**, autosomal recessive spinocerebellar ataxia type 7; **sub c**, subunit c of the mitochondrial ATP synthase; **TPP1**, tripeptidyl peptidase I.

1.1.2 Gene product classification

Aside from genetic classification, the NCL gene products fall into two general subclasses – *bona fide* soluble glycosylated lysosomal enzymes (CLN1, CLN2, CLN10, CLN13) and glycoproteins (CLN5), or predicted transmembrane proteins of unknown function (see Table 1.1).

The function of most of the NCL proteins and their natural substrates are unknown, but their intracellular localisations provide some hints. The soluble subset of NCL gene products are typically known lysosomal enzymes. For example, *CLN1* and *CLN2* encode soluble lysosomal hydrolases, palmitoyl protein thioesterase (PPT1) (Vesa *et al*., 1995) and tripeptidyl peptidase 1 (TPP1) (Sleat *et al*., 1997) respectively. The lysosomal proteases cathepsin D (CTSD) and cathepsin F (CTSF) are encoded by *CLN10* (Siintola *et al*., 2006) and *CLN13* (Smith *et al*., 2013) respectively. A lack of cathepsin D activity causes a congenital NCL in children and sheep (Tyynelä *et al*., 2000; Siintola *et al*., 2006) whilst cathepsin F deficiency results in an adult onset NCL. *CLN5* encodes a soluble lysosomal glycoprotein of unknown function (Sleat *et al*., 2005, 2006, 2007) (see Section 1.4.2). The *CLN11* gene encodes progranulin, a secreted protein that is localised within the ER and endosomal-lysosomal system (Cenik *et al*., 2012). Its function is unknown, however it is highly expressed in neurons and activated immune cells, therefore has a proposed role in neuronal function and inflammation (Jian *et al*., 2013).

The second group of NCL associated proteins are putative polytopic membrane proteins, thought to functionally reside in the lysosomal membrane or in pre-lysosomal organelles. *CLN3* probably encodes a lysosomal or endosomal membrane protein (Ezaki *et al*., 2003; Fossale *et al*., 2004; Kyttälä *et al*., 2004), whilst the *CLN7/MFSD8* gene encodes a putative lysosomal transporter (Siintola *et al*., 2007). Overexpression studies suggest that the CLN12 protein, ATP13A2, is also localised to the lysosome (Ramirez *et al*., 2006) and is possibly a transmembrane P-type ATPase transporter of cations or glycolipids (Bras *et al*., 2012). NCL gene products CLN6 and CLN8 are reportedly ER-resident proteins. CLN6 has been documented to modulate the endocytosis of exogenous proteins (Heine *et al*., 2004; Mole *et al*., 2004) (see Section 1.3.2) whilst CLN8 recycles between the ER and the ER-Golgi intermediate compartments (Lonka *et al*., 2000, 2004). Two other NCL gene products, CLN4 and CLN14, are cytosolic yet appear to associate with vesicular membranes. *CLN4/DNAJC5* encodes a cysteine-string protein alpha chaperone protein with a likely role in neuronal synaptic activity (Fernández-Chacón *et al*., 2004) whilst the CLN14 protein, potassium channel tetramerization domain-containing protein 7 (KCTD7), may modulate ion channel activity (Azizieh *et al*., 2011).

1.1.2.1 Interactions between NCL gene products

Coherent ideas as to why deficiences in separate NCL gene products result in a similar clinical, pathological and biochemical phenotype remain elusive. Most characterised NCL proteins are located in the endosomal-lysosomal system, being trafficked through or resident in the ER-Golgi system, suggesting that they may participate along a single common pathway (Weimer *et al*., 2002), or in intersecting or parallel pathways that, when dysfunctional, result in the shared pathology (Cotman *et al*., 2013). Links have been described for many of the NCL proteins (reviewed by Kollmann *et al*., 2013). In particular, the CLN5 protein may have a central role, having been suggested to interact with PPT1/CLN1, TPP1/CLN2, CLN3, CLN6 and CLN8 *in vitro* (Vesa *et al*., 2002; Lyly *et al*., 2009; von Schantz *et al*., 2009). Of these, the CLN5-CLN1 interaction is of considerable interest as the co-expression of CLN1/PPT1 in cell culture can restore the lysosomal trafficking of the most common CLN5 mutant Y392X (Lyly *et al*., 2009). However given these were protein overexpression studies, conditions of which could have a detrimental effect on protein structure (*e.g.* dimerisation, incorrect glycosylation, cleavage and folding) or result in protein retention in the ER, described *in vitro* interactions need to be considered carefully for biological significance.

1.2 Animal models of NCL

Systematic studies of the pathological changes in the NCLs, both early and with disease progression, and proof of therapeutic concept have only been possible in genetically-defined animal models of the disease. For these studies, experimental mouse models have proven valuable. A panel of naturally occurring and knock-in or knock-out murine mutants for CLN1, CLN2, CLN3, CLN5, CLN6, CLN8, CLN10 and CLN13 exist (http://www.ucl.ac.uk/ncl/mouse.shtml, Cooper *et al*., 2006; Shacka, 2012). Mice have the advantage of a clearly defined and uniform background, well-known genetics and a short reproductive cycle thus providing large numbers of affected progeny. However mice are not ideal for the validation and pre-clinical translation of CNS-directed NCL therapeutics, given their brains are non-gyrencephalic and much smaller than those of humans (Figure 1.1) and the neuropathology is generally milder. Current therapeutic trials in NCL employ human patients in whom the disease is often too advanced for any reasonable assessment of efficacy (see Section 1.6.4). Large animal models of NCL bridge this gap. Naturally-occurring NCL forms that recapitulate key molecular, pathologic and/or clinical features of NCL phenotype have been reported in cats (Green & Little, 1974; Nakayama *et al*., 1993; Bildfell *et al*., 1995; Weissenböck & Rössel, 1997), cattle (Read & Bridges, 1969; Harper *et al*., 1988; Hafner *et al*., 2005), dogs (Palmer *et al*., 2011), ferrets (Nibe *et al*., 2011), goats (Fiske & Storts, 1988), horses (Url *et al*., 2001), pigs (Cesta *et al*., 2006) and sheep (Jolly & West, 1976; Jolly *et al*., 1982; Järplid & Haltia, 1993; Woods *et al*., 1994; Cook *et al*., 2002; Jolly *et al*., 2002). The majority of large animal NCL models under active study presently are domesticated production (*e.g.* sheep) or companion (*e.g.* dog) animals.

This thesis focusses on the comparative neuropathology and clinical characterisation of two ovine models of NCL, specifically CLN5 affected Borderdale (Jolly *et al*., 2002) and CLN6 affected South Hampshire sheep (Jolly & West, 1976), and the efficacy of gene therapy in these translational model systems. These forms of NCL in sheep are representative of two different protein classes; a lesion in a soluble lysosomal protein (CLN5) and a defective intracellular ER membrane-bound protein (CLN6). This subdivision of protein defects has consequences for the planning of therapies. For this reason, the next sections of this review will introduce sheep as a pre-clinical model, describing the known characteristics of the CLN5 and CLN6 variants in humans and animals and focussing on what has been discovered about disease pathogenesis from studies in NCL sheep and other animal models. The final section will review enzyme replacement and gene therapy as treatment strategies for NCL.

1.2.1 Sheep as a pre-clinical model

Of the larger species models, sheep (*Ovis aries*) are ideal pre-clinical subjects to fill the translational gap for NCL. The clinical progression and course of neuropathology in ovine NCL closely follows that in affected children (see Sections 1.3.1 and 1.4.1). In marked contrast to mice, which are ~2800 times smaller than a typical adult patient, sheep are similarly sized to humans, weighing 3.5 - 4.5 kg at birth and 80 – 110 kg as adults. This makes them much more suited for surgical manipulation and clinical evaluation, including CNS imaging. Their gyrencephalic brains are comparable in size (Figure 1.1), complexity and physical organization to those of non-human primates, neonates and small children, thus particularly relevant to paediatric neurodegenerative disorders such as NCL and obviating the need for scale-up of treatment doses for human patients. Sheep share similar spine dimensions, cerebrospinal fluid (CSF) volumes and pulmonary and cardiac parameters to humans (Scheerlinck *et al*., 2008). As domestic production animals, they have been selectively bred for ease of handling and economic management. The longevity of sheep (9 - 12 years) allows considered longitudinal assessments of therapeutic efficacy. The high level of understanding of ovine reproductive technology, anatomy, physiology and veterinary care provides benefits for their role in a translational capacity.

Sheep are also ideally suited as behavioural models. Their docile nature permits training, their aptitude for shape and colour discrimination (Morton & Avanzo, 2011) and excellent facial (Kendrick *et al*., 2001; Peirce *et al*.,2001) and olfactory recognition (Sánchez-Andrade *et al*., 2005; Nowak *et al*., 2011) suggest a good capacity for learning and memory. Moreover, they have been shown to tolerate repetitive behavioural testing without signs of stress (Morton & Avanzo, 2011; Wilkes *et al*., 2012).

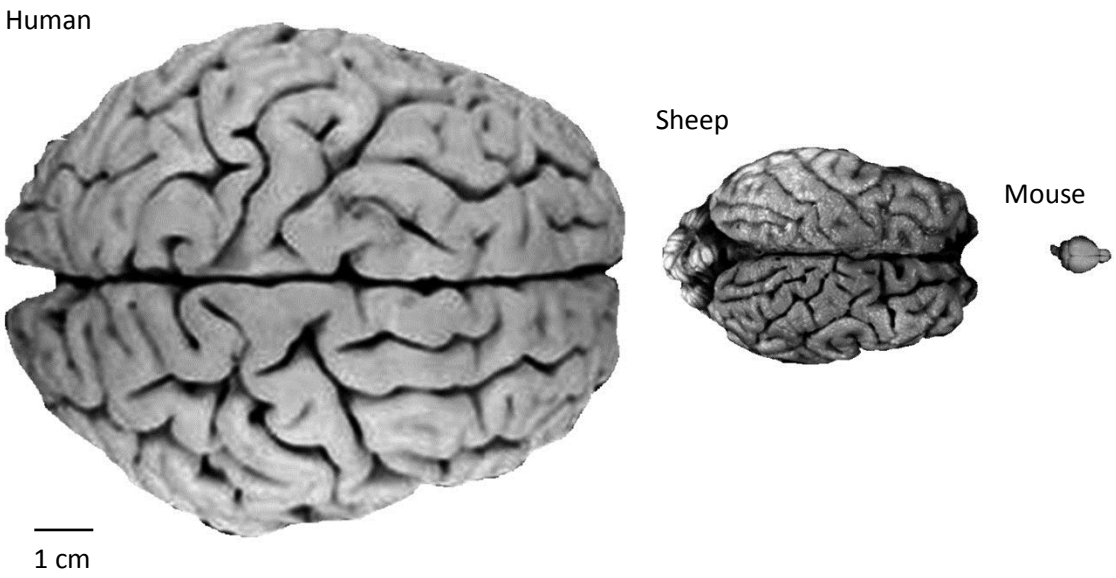

Species (adult)	Average brain weight (g)	Average body weight (kg)
Human (*Homo sapiens*)	1400	65
Sheep (*Ovis aries*)	140	55.5
Mouse (*Mus musculus*)	0.4	0.023

Figure 1.1 Comparison of average human, sheep and mouse brains and body weights
Note the human-like gyrencephalic sheep brain which, at 140 grams by maturity, is larger than that of many non-human primates, one-tenth that of a human adult and more comparable to that of a neonate or small child. In comparison, the mouse brain is lissencephalic and weighs at most 0.4g.

In addition to the different forms of ovine NCL, a number of other naturally occurring diseases of the CNS have been identified in sheep, including the monogenic neurodegenerative LSDs, GM1 and GM2 gangliosidoses, Gaucher, Pompe and Tay-Sachs diseases (Table 1.2). A transgenic ovine model of Huntington's disease has also been generated (Jacobsen *et al*., 2010). With the recent completion of a fully annotated sequence of the sheep genome (Jiang *et al*., 2014; http://genome.ucsc.edu/cgi-bin/hgGateway) and advanced technologies like next generation sequencing to screen populations of sheep for genetic variants resembling human diseases, many new ovine models of human diseases could be easily identified (PInnapureddy *et al*., 2015).

Table 1.2 Naturally occurring genetic diseases of the ovine CNS

Disease	Gene	Description	Sheep breeds affected	References
Adult-onset Alexander disease	*? GFAP*	Astrocytic disorder	Merino	Kessell *et al*., 2012
Cerebellar abiotrophy	*?*	Purkinje cell atrophy	Merino, Wiltshire	Harper *et al.,* 1986; Johnstone *et al*., 2005
Cerebellar cortical atrophy	*?*	Daft lamb disease	Blackface, Border Leicester, Charollais, Corriedale, Welsh Mountain	Innes & MacNaughton, 1950; Bradley & Terlecki, 1977; Terlecki *et al*., 1978; Milne & Schock, 1998
Degenerative thoracic myelopathy	*?*	Spinal cord degeneration	Merino	Harper *et al*., 1991
Gaucher disease type 1	*GBA*	Glucocerebrosidosis	Southdown	Karageorgos *et al*., 2011
GM1 gangliosidosis (human type 3)	*?*	GM1 gangliosidosis	Romney, Suffolk	Prieur *et al*., 1991; Ryder & Simmons, 2001
Krabbe disease	*? GALC*	Globoid cell leukodystrophy	Poll Dorset	Pritchard *et al*., 1980
Lissencephaly with cerebellar hypoplasia	*RELN*	Lissencephaly	Churra	Pérez *et al*., 2013; Suárez-Vega *et al*., 2013
Lower motor neuron disease	*AGTPBP1*	Spinal muscular atrophy	Romney	Anderson *et al*., 1999; Zhao *et al*., 2012
Morquio B disease	*?*	Mucopolysaccharidosis IVB	Suffolk	Ahern-Rindell *et al*., 1988
Murrurundi disease (segmental axonopathy)	*?*	Encephalopathy	Merino	Harper *et al*., 1986
Neuroaxonal dystrophy	*?*	Muscular dystrophy	Coopworth, Merino, Perendale, Romney	Cordy *et al*., 1967; Harper & Morton, 1991; Finnie *et al*., 2014
Neuronal ceroid lipofuscinosis	*CLN5*	Neurodegenerative disease	Borderdale	Jolly *et al*., 2002
	CLN6		Merino, South Hampshire	Jolly & West, 1976; Cook *et al*., 2002
	CTSD		Swedish Landrace	Tyynelä *et al*., 2000
	?		Rambouillet	Edwards *et al*.,1994
Pompe disease	*?*	Glycogen storage disease	Corriedale, Merino	Manktelow & Hartley, 1975
Tay-Sachs disease	*HEXA*	GM2 gangliosidosis	Jakob	Torres *et al*., 2010; Wessels *et al*., 2014
Thalamic cerebellar neuropathy	*?*	Neuropathic disorder	Merino	Bourke *et al*.,1993

Lysosomal storage diseases are boxed
? = gene not known or unconfirmed

1.3 CLN6 NCL

1.3.1 CLN6 in New Zealand South Hampshire sheep

The best characterised NCL animal model, especially at a biochemical and pathological level, is the CLN6 form identified in New Zealand South Hampshire sheep over four decades ago (Jolly & West, 1976; Jolly *et al*., 1980, 1989). The disease progression and course of neuropathology in this model is well described and closely parallels that in the human disease, particularly the severe cortical atrophy, profound neuronal loss, storage body accumulation and retinal degeneration (see Section 1.5). Affected sheep are apparently normal at birth but develop clinical symptoms between 10 and 14 months of age, notably progressive psychomotor decline and blindness as a result of atrophy of the occipital cortex and loss of retinal photoreceptors, with premature death when aged about two years (Mayhew *et al*., 1985; Jolly *et al*., 1989). The specific storage of subunit c of mitochondrial ATP synthase was first discovered in these sheep (Palmer *et al*., 1989, 1992; Fearnley *et al*., 1990; Palmer, 2015). Regionally defined and selective loss of cortical neurons in the CLN6 affected sheep brain is preceded by prenatal neuroinflammation, starting from particular cortical foci later associated with symptomology and becoming more generalised with disease progression (Oswald *et al*., 2001, 2005, 2008; Kay *et al*., 2006). These findings have subsequently been confirmed in human and other mammalian NCL models hence the CLN6 sheep are often regarded as a prototype of the NCLs.

1.3.2 The CLN6 gene and protein

The human *CLN6* gene is located on chromosome 15q21-23 (Sharp *et al*., 1999), and contains 7 exons, encoding a putative 311 amino acid protein (Gao *et al*., 2002; Wheeler *et al*., 2002) (Figure 1.2). To date, 71 mutations in the *CLN6* gene have been described in diverse geographical populations across all habitable continents (http://www.ucl.ac.uk/ncl/cln6.shtml). Seventy-three per cent of CLN6 patients are homozygous for their mutation (Kousi *et al*., 2012).

Positional cloning localised the *CLN6* gene responsible for the South Hampshire disease to a region on sheep chromosome 7 homologous with the 15q21–23 human *CLN6* region (Broom *et al*., 1998). The ovine *CLN6* ortholog has an identical gene structure of 7 exons, encoding a predicted 311 amino acid polypeptide (Figure 1.2) and 90% sequence homology to human *CLN6* (Tammen *et al*., 2006). Long-range PCR amplification of the part of the ovine genome, followed by SOLiD (sequencing by oligonucleotide ligation and detection) next-generation DNA sequencing identified the disease-causing mutation in the South Hampshire sheep as a 402 base pair (bp) deletion and 1 bp insertion in ovine *CLN6*, namely g.-251_+150del and g.+150_151insC (Mohd Ismail, 2014). The mutation is predicted to lead to the deletion of the ATG start codon, the whole of exon 1 and the flanking 5' non-coding sequence.

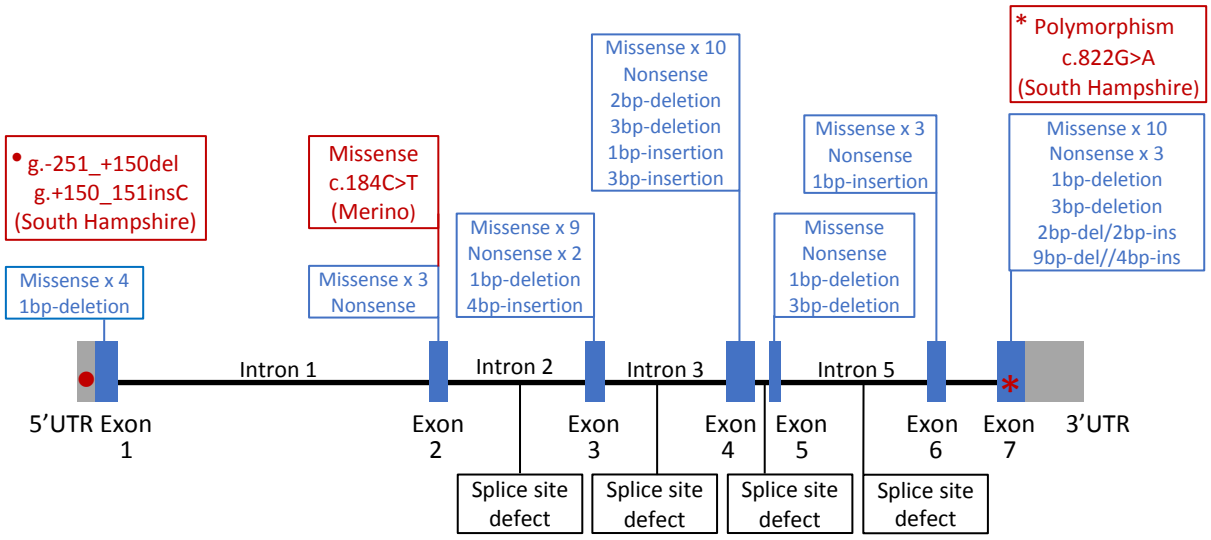

Figure 1.2 Disease-causing mutations identified within the *CLN6* gene

Schematic of the *CLN6* gene (drawn to scale) with the locations of all known human disease-causing mutations depicted in blue. Intron 4 is represented by the black line between introns 3 and 5. A naturally occurring form of CLN6 in South Hampshire sheep results from a large deletion and a single base insertion in the GC-rich 5' end of the gene (red) (Mohd Ismail, 2014). Given this region is extremely difficult to amplify, a silent allelic variant (c.822G>A) in exon 7 of ovine *CLN6* is used instead as an indirect test for preclinical diagnosis of affected South Hampshire sheep (Tammen *et al*., 2006). The South Hampshire flock is configured now such that all heterozygous sheep are GA and all affected animals AA. Additionally a single substitution in exon 2 (c.184C>T) results in ovine CLN6 in Australian Merino sheep (Tammen *et al*., 2006). The Merino mutation codes for a major amino acid exchange (p.Arg62Cys) and is very similar to a human disease-causing substitution, p.Arg62His.

The CLN6 protein is a 27 kDa integral membrane protein of unknown function. Two independent studies, using immunocytochemistry and subcellular fractionation, concluded that human and sheep CLN6 is an ER-resident protein (Heine *et al*., 2004; Mole *et al*., 2004). This ER-residency is seen in both neuronal and non-neuronal cells (Mole *et al*., 2004; Heine *et al*., 2007). The mature CLN6 protein has been modelled to contain a cytoplasmic N-terminus, seven transmembrane domains and a C-terminal directed towards the ER lumen (Heine *et al*., 2007). Expression of retention signals in the first 49 amino acids of the N-terminal and in the carboxy-proximal transmembrane domains six and seven are predicted to maintain the ER localisation of CLN6 (Heine *et al*., 2007). The protein bears no sequence homology to other known proteins but it is highly conserved across mammalian species (Heine *et al*., 2004). Human and sheep CLN6 are 92% identical, with the majority of differences in the poorly conserved N-terminus. The exact function of the CLN6 protein remains elusive, however studies indicate that CLN6 modulates the endocytosis of exogenous lysosomal proteins (Heine *et al*., 2004; Mole *et al*., 2004).

1.3.3 Human CLN6 disease

Mutations in the *CLN6* gene cause an autosomal recessive, progressive neurodegenerative disorder with bimodal presentation of both late infantile (Lake & Cavanagh, 1978) and adult-onset NCLs (Arsov *et al*., 2011). The disease is characterised by regionally specific neuronal loss, with the abnormal specific accumulation of subunit c of mitochondrial ATP synthase in lysosome derived storage bodies in CNS neurons and in somatic cells outside of the nervous system (Palmer *et al*., 1989, 1992; Goebel *et al*., 1999; Palmer, 2015). The late infantile form manifests at 3 to 5 years of age with developmental and mental retardation, followed by speech impairment, seizures, ataxia and myoclonus (Mole *et al*., 2005). Patients lose vision and motor coordination between the ages of 4 and 10 years (Teixeira *et al*., 2003b) with premature death before the third decade of life (Mole *et al*., 2005). More recently cases of teenage progressive onset myoclonus epilepsy (Andrade *et al*., 2012) and Kufs disease Type A (Arsov *et al*., 2011) have been attributed to mutations in the CLN6 gene. The latter typically presents around the age of 30 years, but onset ranges from teenage to as late as the fifth decade, with progressive myoclonus epilepsy and intellectual deterioration. Strikingly the teenage/adult onset forms of CLN6 have no retinal involvement and vision is preserved. There is no specific treatment for the CLN6 disease, except for palliative care and the management of psychiatric symptoms which is limited as seizures do not respond well to traditional anti-convulsant medications (Mole *et al*., 2011).

1.3.4 Other CLN6 animal models

Aside from the CLN6 South Hampshire sheep model used in this thesis, other naturally occurring NCLs in animals were subsequently localized to CLN6, such as the *nclf* mouse (Bronson *et al*., 1998; Gao *et al*., 2002; Wheeler *et al*., 2002) and the Australian Merino sheep (Tammen *et al*., 2001, 2006) (Figure 1.2). The *nclf* mouse model is publically available for purchase from the Jackson laboratory (Bar Harbor, Maine, USA). Homozygous *nclf* mice develop progressive retinal atrophy early in life, with ataxia, neurodegeneration and ultimately paralysis and death by 9 months of age (Bronson *et al*., 1993). A CLN6 Merino flock is maintained at the University of Sydney, Australia. The disease manifests in Merino sheep at 7 - 12 months of age, with clinical signs and disease progression remarkably similar to that seen in the South Hampshires (Tammen *et al*., 2001; Cook *et al*., 2002; Palmer *et al*., 2011). Affected sheep suffer from gross brain atrophy and usually die before 24 months. A study characterising the neuropathological changes in the affected Merino sheep brain is underway (Katharina Russell, PhD, Lincoln University). A missense mutation in the *CLN6* gene has been reported to cause NCL in Australian Shepherd dogs however a colony has not been established. Closely related dogs were not genotyped and screening failed to find any other affected individuals (O'Brien *et al*., 2008; Katz *et al*., 2011).

1.4 CLN5 NCL

1.4.1 CLN5 in New Zealand Borderdale sheep

Fifteen years ago, a second naturally occurring ovine NCL was identified in New Zealand Borderdale sheep (Jolly *et al*., 2002) and the causative mutation was found to be in *CLN5* (Frugier *et al*., 2008). Blindness is the first clinical sign in affected Borderdales, with presentation from 10 - 11 months of age. Again subunit c of mitochondrial ATP synthase was found to be the abnormally stored component of the lysosomal inclusion bodies. The course of the CLN5 form was predicted to be similar to the CLN6 form in sheep, although the brain atrophy was reported to be more severe (Jolly *et al*., 2002). One of the major objectives of this study was to characterise the Borderdale model by defining the progressive extent of neuronal loss, neuroinflammation and neurogenesis in a similar way as has been published for the South Hampshire CLN6 form. The Borderdale sheep provide an ideal resource for studying CLN5 NCL, and soluble enzyme forms of NCL in general, complementing the membrane protein mutation in the CLN6 South Hampshire model.

1.4.2 The CLN5 gene and protein

The *CLN5* gene maps to human chromosome 13q22 and 36 disease-causing mutations have so far been identified in it (http://www.ucl.ac.uk/ncl/cln5.shtml) (Figure 1.3). The majority of patients carry a 2 bp deletion in exon 4 (c.1175delAT), which results in a truncated protein (Savukoski *et al*., 1998; Holmberg *et al*., 2000). Interspecies variation is almost exclusively concentrated in the N-terminus of the polypeptide, coded for by the GC-rich exon 1, but the rest of the coding sequence is highly conserved (Frugier *et al*., 2008). For example, human and sheep CLN5 share 84% homology.

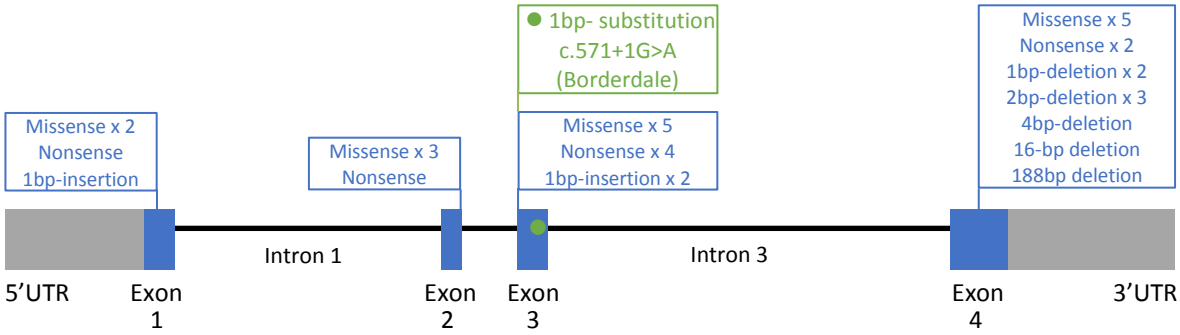

Figure 1.3 Disease-causing mutations identified within the *CLN5* gene
Schematic of the *CLN5* gene (drawn to scale) with the locations of the known human mutations depicted in blue. Intron 2 lies between exons 2 and 3. A naturally occurring form of CLN5 in Borderdale sheep results from a single substitution at a consensus splice site (green), with resultant excision of exon 3 thus a truncated putative protein (Frugier *et al*., 2008).

The ovine *CLN5* gene, located on sheep chromosome 10, also contains 4 exons and encodes a predicted 361 amino acid protein (Frugier *et al*., 2008). A substitution of the first nucleotide in intron 3 (c.571+1G>A, Figure 1.3) segregates with the disease and was identified as the disease-causing mutation (Frugier *et al*., 2008). This mutation disrupts the normal splicing consensus sequence at the 5' end of the intron 3, resulting in the excision of exon 3.

The human *CLN5* gene has four possible methionine initiation sites, translation from which would produce polypeptides with molecular masses ranging from 39 to 47 kDa (Klockars *et al*., 1999; Isosomppi *et al*., 2002; Vesa *et al*., 2002). Initially it was suggested that the most 5' upstream was the functional site in humans, providing an open reading frame of 1380 bp coding for a 407-amino acid 47 kDa polypeptide with two transmembrane domains (Savukoski *et al*., 1998). Subsequent protein expression studies and alignment with the mouse gene, which contains only one start site, led to the proposal that the most 3' AUG in humans (AUG62) was the major initiation site, resulting in a 38 kDa lysosomal-targeted protein, with an N-terminal signal sequence that is cleaved after entering the ER (Isosomppi *et al*., 2002; Holmberg *et al*., 2004; Mole *et al*., 2004). However later alignment of the human, bovine, canine, murine and ovine *CLN5* showed that the third human methionine is evolutionally conserved and thus may be the true initiator (Houweling *et al*., 2006; Frugier *et al*., 2008). Realignment would generate a CLN5 protein of 358 amino acids. All of the CLN5 isoforms lack homology to any protein of known function however there is strong evidence that CLN5 is a soluble lysosomal glycoprotein. Eight potential N-glycosylation sites have been identified and CLN5 contains a signal peptide which is cleaved in the ER and the mature polypeptide is localised to the lysosome (Isosomppi *et al*., 2002; Holmberg *et al*., 2004; Schmiedt *et al*., 2010). Three mannose-6-phosphate moieties are connected to asparagine residues 320, 330 and 401, which interact with the lysosomal targeting mannose-6-receptors, enabling CLN5 transport from the Golgi to the lysosome (Sleat *et al*., 2005, 2006, 2007) and rendering it soluble.

1.4.3 Human CLN5 disease

The late infantile variant CLN5 disease is particularly prevalent in Finland, first described there in children who share the same founder mutation (Savukoski *et al*., 1998). However the disease is not confined to the Finnish population, now being recognised worldwide in a broad ethnic diversity (Xin *et al*., 2010). CLN5 disease presents with motor difficulties and visual deficits between the ages of 4 and 7, progressing to mental and motor deterioration, ataxia, myoclonic epilepsy, and loss of vision by the age of 7 to 10 years (Santavuori *et al*., 1982, 1991; Holmberg *et al*., 2000; Xin *et al*., 2010). Age at death in CLN5 patients is highly variable, ranging from 10 to 30 years, with one patient surviving until the age of 41 (Holmberg *et al*., 2000; Moore *et al*., 2008).

Neuropathologically, human CLN5 manifests as generalised cerebral and extreme cerebellar atrophy (Autti *et al*., 1992; Tyynelä *et al*., 1997). The latter is a particularly striking abnormality in neuroimaging studies (Autti *et al*., 1992; Holmberg *et al*., 2000) and in autopsy specimens (Tynnelä *et al*., 1997). In late stage disease, an almost complete loss of thalamic neurons and Purkinje cells in the cerebellum is reported, whilst the cortical neurons in laminae III and V are most vulnerable, undergoing moderate loss with enlargement of the cell soma of those remaining (Tynnelä *et al*., 1997). Subunit c of mitochondrial ATP synthase is the main protein stored (Tynnelä *et al*., 1997). Widespread astrocytosis can be seen in the cortex and cerebellum of CLN5 patients and CLN5 knockout mice (Tyynelä *et al*., 2004; von Schantz *et al*., 2009).

1.4.4 Other CLN5 animal models

Naturally occurring CLN5 NCLs in Devon cattle (Harper *et al*., 1988; Houweling *et al*., 2006), Border Collie (Taylor & Farrow, 1988; Melville *et al*., 2005) and Golden retriever dogs (Gilliam *et al*., 2015) present with a disease course and pathogenesis matching human CLN5. A small herd of Devon cattle was maintained at the University of Sydney but as the animals developed clinical signs from 9 months of age, they became aggressive (Imke Tammen, personal communication), dying about two years later (Harper *et al*., 1988). The CLN5 Borderdale ovine model was deemed easier to maintain, because of the greater ease of handling sheep, so CLN5 Devon cattle are no longer under active study however frozen semen from affected bulls has been stored. CLN5 affected Border Collies and Golden retrievers present with a progressive neurological disease between 15 and 22 months of age, dying before the age of three years (Taylor & Farrow, 1988; Melville *et al*., 2005; Gilliam *et al*., 2015). Research colonies of these CLN5-deficient dogs do not currently exist. However a number of carrier dogs have been retained under private ownership and semen stocks are maintained. A CLN5 exon 3 knock-out mouse model has also been generated (Kopra *et al*., 2004), which has provided insights into the spatiotemporal expression of CLN5 in the CNS (Holmberg *et al*., 2004) but these mice lack the severe brain atrophy characteristic of the sheep and human diseases.

1.5 NCL pathogenesis – what has been learnt from animal models?

1.5.1 Storage body accumulation

In addition to a similar clinical phenotype, the NCLs share the common accumulation of Sudan black and Luxol fast blue positive fluorescent electron dense storage material within autophagic vacuoles (lysosomes) of most nerve cells, and many other somatic cells. These lysosomal inclusions display distinctive ultrastructural patterns, visualised by electron microscopy, described as curvilinear, fingerprint, granular osmiophilic deposit or rectilinear profiles, depending on the NCL phenotype and tissue (Table 1.1). Direct protein sequencing unequivocally established the specific storage of subunit c of mitochondrial F_1F_0 ATP synthase, first in the CLN6 South Hampshire sheep model (Palmer *et al*., 1989; Fearnley *et al*., 1990) (see Section 1.3.1), and then in the CLN2 and CLN3 human diseases and some animal models (Fearnley *et al*., 1990; Palmer *et al*., 1992; Palmer, 2015). Subsequent subunit c storage has been identified by direct sequencing and/or immunohistochemistry in CLN5, CLN6, CLN7, CLN8 and CLN14 human forms (Faust *et al*., 1994; Ezaki *et al*., 2000; Haltia, 2006; Staropoli *et al*., 2012) and other animal models (Fearnley *et al*., 1990; Martinus at al., 1991; Jolly *et al*., 1994; Palmer *et al*., 1997; Url *et al*., 2001; Cook *et al*., 2002; Katz *et al*., 2005; Melville *et al*., 2005; Frugier *et al*., 2008). Of the remaining NCL forms, the sphingolipid activator proteins (SAPs) A and D are the major proteins accumulating in CLN1 and CLN10 (Tyynelä *et al*.,1993; Siintola *et al*., 2006), some uncharacterised non-neuronal storage has been reported for the CLN12 form (Bras *et al*., 2012) whilst the molecular composition of the stored material in the more recently described adult forms (CLN4, CLN11 and CLN13) have not been determined.

Until recently the neuropathology seen in the NCLs was considered to be consequent to the storage body accumulation, but there was a growing body of evidence against this. Despite ubiquitous storage in most cells and most tissues, there is no obvious disruption to cellular function or specific tissue or organ failure (Palmer *et al*., 2013; Palmer, 2015). Even within the central nervous system (CNS), where storage accumulation is widespread and progressive, only selective neuronal populations degenerate during the disease progression (Oswald *et al*., 2005, 2008) whilst others can maintain a substantial storage burden to no obvious detriment. For instance, the accumulation of storage material in the Purkinje cerebellar cells of the ovine CLN6 model does not correlate with any disease-related changes, with no measurable atrophy and only minimal neuroinflammation in the cerebellum even at end-stage disease (Graham Kay, personal observation). Additionally the clearance of large amounts of CNS-derived storage material after viral-mediated gene therapy in CLN1 mice did not impact on neuron survival or improve the clinical outcome (Griffey *et al*., 2006). Thus, it is now thought that neurodegeneration and storage body accumulation are independent manifestations of the NCL genetic mutations (Palmer *et al*., 2013).

1.5.2 Selective neuron loss

The other unifying pathological hallmark of NCL is regionally specific neurodegeneration. The disease selectively manifests in the CNS, with progressive loss of neuronal structure and function which is linked to the profound atrophy documented in all human NCL forms (Haltia, 2003, 2006) and in the ovine NCL models used in the current study (Mayhew *et al*., 1985; Jolly *et al*., 1989, 2002; Oswald *et al*., 2001, 2005). However not all brain regions are equally affected by the neurodegeneration. The cerebral cortex is severely affected in all NCL forms, whereas the pathology in other regions of the CNS varies. Histological studies of human NCL brains are limited to autopsy tissue by which stage neuronal loss is widespread (Bennett & Rakheja, 2013) and, whilst brain imaging studies on human patients provides some insight into the sequential anatomical and functional changes (Peña *et al*., 2001; Autti *et al*., 2008; Paniagua Bravo *et al*., 2013), elucidation of the progressive and selective nature of neurodegeneration has relied on animal model studies.

Given the widespread cortical neurodegeneration at end-stage disease, it could be assumed that neuronal loss would occur to a similar extent throughout the diseased brain. Remarkably though, studies of early neurodegeneration revealed regional selectivity. Comprehensive *post mortem* studies showed that the development of CLN6 affected sheep brains proceeded normally for the first four months after birth, then progressively reversed, diverging from that of age-matched controls which continued to grow (Oswald *et al*., 2005). Gross atrophy of the cerebral cortex was apparent from six months, with a reduction in cortical thickness commencing and progressing fastest in the parieto-occipital and visual cortices, the regions first associated with clinical symptomology. By 12 months of age atrophy was apparent in all cortical regions (Figure 1.4). In contrast, the subcortical nuclei and cerebellum of CLN6 affected brains retained a normal appearance, even at an advanced disease stage.

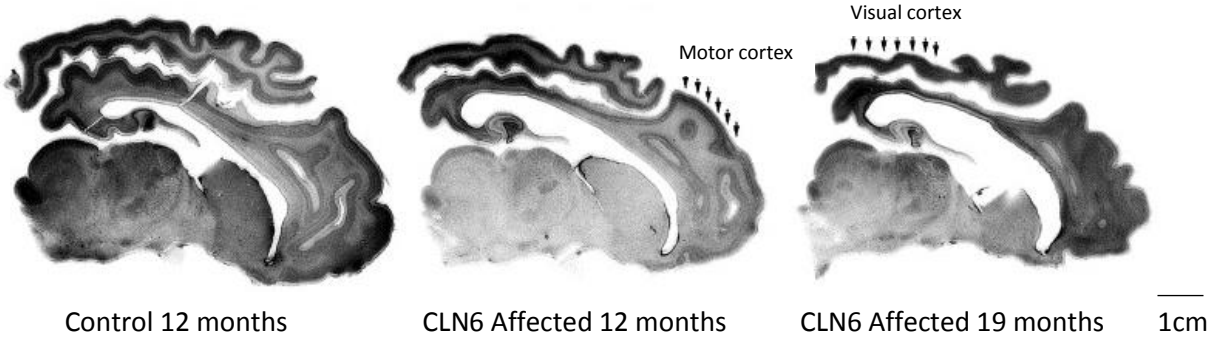

Figure 1.4 Cortical atrophy in ovine CLN6 compared to normal control animals
At 12 months there is marked atrophy of the cerebral cortex in CLN6 affected sheep compared to age-matched controls. By 19 months, this is even more pronounced, especially in the visual cortex (modified from Oswald *et al*., 2005).

A spatiotemporal survey of cortical interneuron phenotypes in CLN6 affected sheep demonstrated selective neuronal loss, with cellular location and connectivity the overriding influences rather than early preferential loss of specific cell types (Oswald *et al*., 2008). Interneurons are specialised nerve cells whose primary role is to form connections between other types of neurons, creating neural circuits. Within the CNS, interneurons are primarily inhibitory using γ-aminobutyric acid (GABA) neurotransmission and can be categorised into subtypes based on the surface markers they express. Consistently, populations of inhibitory GABAergic interneurons have been shown to be vulnerable in human, mouse and sheep NCLs (Williams *et al*., 1977; Cooper *et al*., 1999; Mitchison *et al*., 1999; Oswald *et al*., 2001; Bible *et al*., 2004; Pontikis *et al*., 2004; Tyynelä *et al*., 2004; Kielar *et al*., 2007). Study of the ovine CLN6 model revealed an early and severe loss of parvabumin-positive GABAergic interneurons, which began in the visual and parieto-occipital cortices (Oswald *et al*., 2008), paralleling the regionally specific neurodegenerative changes and cortical atrophy (Oswald *et al*., 2005). Loss of somatostatin and neuropeptide Y-positive interneurons followed the same regional trend but later in disease progression, whilst calretinin and calbindin-positive neuron populations were relatively well preserved, confirming the marked differences in the survival of different interneuron subtypes and between different brain regions during disease progression.

Studies in NCL mouse models have surprisingly shown that, despite profound cortical degeneration, the thalamus appears to be pathologically targeted early in disease progression (Pontikis *et al*., 2005; Kielar *et al*., 2007; Partanen *et al*., 2008; Kuronen *et al*., 2012; Morgan *et al*., 2013). In most NCL murine forms, loss of thalamic relay neurons preceded neurodegeneration in the corresponding cortical region to which they project. However the sequence of neuron loss is reversed for CLN5 mutant mice, with an earlier susceptibility of cortical neurons than thalamic ones (von Schantz *et al*., 2009). An explanation for this difference has not been elucidated but indicates the contrasting consequences of the different gene mutations. Morphometric analysis from a longitudinal MRI study indicated some thalamic atrophy in the CLN6 affected sheep brain at end-stage disease (Sawiak *et al*., 2015), but no early neuronal loss from the ovine thalamocortical system has been observed in histological studies in sheep (Oswald *et al*., 2005, 2008; Kay *et al*., 2011).

1.5.3 Neuroinflammation

NCL is not simply a disease of neurons. A primary role for glial activation has been implicated in NCL pathogenesis. Spatiotemporal studies in ovine NCL established that reactive astrocytosis and microglial activation begins in prenatal, pre-symptomatic CLN6 affected sheep brains, long before significant storage body accumulation or neuronal loss (Oswald *et al*., 2005; Kay *et al*., 2006). Hypertrophic and proliferating perivascular macrophages and activated astrocytes were present at 40 and 20 days before birth respectively, spreading to form reactive clusters in the cortex at birth. The glial activation proceeded in a progressive, regionally specific manner, beginning in the visual, parieto-occipital and somatosensory cortices, the regions associated with the later development of neurodegeneration, atrophy and clinical symptoms (Kay *et al*., 2006). Activation in the primary motor and entorhinal cortices followed (Oswald *et al*., 2005). Localised microglial and astrocyte activation, which precedes and accurately predicts where subsequent neuronal loss will occur, has since been substantiated in multiple mouse models of NCL (Pontikis *et al*., 2004, 2005; Kielar *et al*., 2007; Partanen *et al*., 2008; Macauley *et al*., 2009; von Schantz *et al*., 2009; Kuronen *et al*., 2012; Schmiedt *et al*., 2012; Thelen *et al*., 2012; Morgan *et al*., 2013). Neuroinflammation has also been indicated as a major contributor to disease pathogenesis in many neurodegenerative CNS disorders, including Alzheimer disease, Huntington's disease, Parkinson disease, multiple sclerosis and amyotrophic sclerosis (Block & Hong, 2005; Mrak & Griffin, 2005; McGeer & McGeer, 2007; Eikelenboom *et al*., 2006).

A CNS injury or insult can result in reactive gliosis through a transient inflammatory response, as glial cells endeavour to remove the insult whilst providing trophic support to neurons. However, chronic inflammation is thought to be detrimental to neurons, creating a neurotoxic environment due to elevated levels of inflammatory cytokines and chemokines, and pro-apoptotic molecules accelerating cell death (Stoll & Jander, 1999; Streit *et al*., 2004; Lyman *et al*., 2014; Lee & MacLean, 2015). It follows that drug inhibition or suppression of neuroinflammation in NCL may be neuroprotective and thus therapeutic. However chronic oral administration of a broad-spectrum anti-inflammatory, minocycline, to pre-symptomatic CLN6 affected lambs did not change the course of the disease (Kay & Palmer, 2013). Molecular dissection of the ovine CLN6 neuroinflammatory cascade, by quantitative PCR, Western blot and immunohistochemistry revealed a complex but uncontrolled pathway with differential regulation of a number of genes but could not identify causal initiators of neuroinflammation or potential druggable targets (Chen, 2016).

1.5.4 Extended neurogenesis

Evidence of extended neurogenesis has also been found in the CLN6 sheep model (Dihanich *et al*., 2009, 2012). Neurogenesis, the generation of new neurons from precursor neural stem (progenitor) cells, was traditionally thought to occur only during embryonic or perinatal development (Ming & Song, 2005). However, active adult neurogenesis has been found to occur in two specific neurogenic regions of the brain; the subgranular zone in the hippocampal dentate gyrus where new granule cell neurons are generated, and the subventricular zone (SVZ) of the lateral ventricles, where neuroblasts are generated and migrate through the rostral migratory stream to the olfactory bulb to differentiate into interneurons (Eriksson *et al*., 1998; Gage, 2000).

Like humans, the normal sheep SVZ is stratified and is the main site of progenitor cell proliferation and adult neurogenesis (Brus *et al*., 2010, 2013; Low *et al*., 2013). However immunohistochemical staining for newly generated and migratory neurons revealed a band of immunoreactive cells and fibres along the SVZ much more prominently in the CLN6 diseased state than in the normal sheep brain (Dihanich *et al*., 2009, 2012). Newly generated SVZ neurons migrated through the rostral migratory stream but also radially away from the SVZ, via white matter tracts, aggregating to form large clusters in the outer laminar layers of the cerebral cortex of older affected animals, particularly in the regions undergoing neurodegeneration. The clusters contained mature and immature neuronal cells, but not glial cells, and were absent in normal brains. Analysis of human CLN6 autopsy brains revealed newly generated neurons in lamina II and the deeper laminae of the cerebral cortex, supporting the idea that ongoing neurogenesis occurs even in the severely diseased brain (Dihanich *et al*., 2012). Upregulation of neurogenesis has also been reported on brain trauma or after neuronal death in a number of other neurodegenerative diseases, including Alzheimer, Huntington's and Parkinson disease (Curtis *et al*., 2003; Winner *et al*., 2011). Thus it seems plausible that this is an intrinsic attempt at "self-repair" in the diseased brain. This finding is pertinent for therapy in NCL, as it could indicate an accessible key target site for viral-mediated gene correction of neural progenitor cells, daughters of which differentiate into neuroblasts and new neurons and migrate globally through the brain, allowing cross-correction of diseased neurons (or glia).

1.5.5 Loss of vision and retinal degeneration

Visual failure also occurs in most forms of NCL. Sequential studies in the CLN6 ovine model have shown that the visual deficits have two components, primary central (cortical) blindness and a secondary peripheral (retinal) lesion (Mayhew *et al*., 1985). Early loss of vision is probably due to the atrophic changes and neuronal loss seen in the occipital (visual) cortex of the CLN6 affected sheep from 6 months, well before the onset of visual deficits at 10 - 14 months of age (Oswald *et al*., 2005). The occipital cortex is unlikely to be able to correctly process and interpret input coming from the still intact retina. An alternative primary upstream insult to the dorsal lateral geniculate nucleus (LGN), with selective loss of these neurons, has been suggested to cause cortical lesions, optic atrophy and retrograde retinal dysfunction in the CLN3 mutant mouse model (Weimer *et al*., 2006). Patients with central blindness lack a menace response (a blink elicited by a threatening, sudden movement towards the eye) (see Table 1.3). Stimulation of this reflex is used as a diagnostic procedure in human and veterinary medicine to determine whether a subject's post-retinal visual system has suffered damage. The menace response is cortically-mediated, with the afferent arm involving visual fibres through the optic nerve, optic chiasm and LGN to the occipital cortex. The information generated in the contralateral occipital cortex is projected efferently to the motor cortex and ipsilateral facial nerve to generate the blink movement. Responses to other subcortical neuro-ophthalmic tests (*e.g.* direct and consensual pupillary light response (PLR), dazzle and palpebral reflexes) (see Table 1.3 and Section 3.3.1) are intact in early-stage ovine NCL, allowing some distinction between light and dark, colour, general shape and the ability to perceive moving but not static objects. The appearance of the NCL retina is initially normal in all species under funduscopy (Katz *et al*., 2008; Hainsworth *et al*., 2009). Electroretinography (ERG), which measures the electrophysiological response of the retina to visual stimulation, is also relatively normal during the early central (post-retinal) blindness phase in the canine and ovine disease course (Graydon & Jolly, 1984; Mayhew *et al*., 1985; Weleber, 1998; Katz *et al*., 2008).

However temporal pathophysiological studies in NCL animal models, particularly dogs and sheep, have shown that with disease progression, the structural integrity of the NCL retina is also compromised through selective loss of neuroretinal cells. Retinopathy in sheep results from the degeneration of rod and cone photoreceptor cells and bipolar neurons of the outer nuclear layer (Graydon & Jolly, 1984; Mayhew *et al*., 1985; Goebel, 1992). This mirrors historic morphologic findings from autopsied human eyes at end stage disease (Goebel *et al*., 1977; Schochet *et al*, 1980; Traboulski *et al*., 1987). There is an accumulation of storage material in the photoreceptor cells and retinal ganglion cells. Despite prominent storage in the latter neurons, they show few signs of degeneration, even at advanced stages of retinal atrophy (Graydon & Jolly, 1984; Mayhew *et al*.,

1985; Goebel, 1992), reinforcing the theory that storage body accumulation *per se* does not cause the retinopathy.

As the disease progresses to involve both cortical and retinal lesions, NCL patients become functionally blind although some light-dark perception may be retained (Mink *et al*., 2013). At this stage, PLR and dazzle reflexes are depressed (Table 1.3) however, as these are sub-cortical responses and not routed through the visual cortex, they cannot be regarded as "true" indicators of central vision or retinal function. In fact, comparatively few functional photoreceptor cells are required for a positive PLR. ERG provides a better longitudinal *in vivo* measure of retinal dysfunction. ERG responses can still be elicited during the functional blindness phase but become increasingly abnormal, and by end-stage NCL disease scotopic and photopic ERG extinction has been reported for human patients and affected dogs and sheep (Graydon & Jolly, 1984; Mayhew *et al*., 1985; Weleber, 1998; Haltia, 2003; Katz *et al*., 2008; Sanders *et al*., 2011).

Table 1.3 Clinical neuro-ophthalmic tests to assess loss of vision in NCL

Lesion	Menace response*	Pupillary light response*	Dazzle reflex*	Palpebral reflex*	ERG	Fundus	Vision
Visual cortex	-	+/-	+	+	+	Normal	-
Retina	-	-	-	+	-	Normal or abnormal	-

* These tests are described in further detail in Section 3.3.1

The ovine eye closely resembles the human eye. Whilst lacking a fovea, a central depression of cones in the human retina, sheep eyes share the typical multi-layered human retinal structure. They also possess an extra layer, the tapetum lucidum, which lies directly behind the retina and reflects visible light back through the retina, increasing the light available to the photoreceptors and providing this species with superior night vision. In NCL, ideal therapeutic interventions will ameliorate degeneration in both the retina and the CNS regions associated with vision. Because of the size of the large animal eye, particularly those of sheep, they represent an ideal resource for characterising the similar pathological changes associated with loss of vision and for testing and translation of potential therapeutic strategies.

1.5.6 Therapeutics for NCL

Although much has been discovered about the genetics, cell biology and pathogenesis of NCL (described above), a key question still remains in developing therapeutics for this group of diseases: ***Are the pathological changes described in NCL haltable or reversible?***

1.6 Gene and enzyme replacement therapeutic options for NCLs

Most treatment strategies for LSDs, including the NCLs, are based on the seminal observation that small amounts of lysosomal proteins and enzymes are secreted and can be recaptured and targeted to the lysosomes of adjacent and distal enzyme-deficient cells (Fratantoni *et al*., 1968). Enzyme replacement and gene therapies take advantage of this physiologic lysosome-specific trait termed 'cross-correction', and the normal lysosomal enzyme trafficking system. Nascent lysosomal enzymes are synthesised and glycosylated in the rough endoplasmic reticulum (RER) before undergoing vesicular transport to the Golgi apparatus for post-translational modification including the addition of mannose and/or mannose-6-phosphate (M6P) moieties (Kornfeld, 1987). These modified proteins then bind integral membrane mannose-6-phosphate receptors (M6PR) in the Golgi and the majority are trafficked to the mature lysosome. However 5 - 20% of the M6P-modified enzymes are secreted extracellularly and are taken up by neighbouring cells through a M6PR-mediated endocytic clearance pathway (Kaplan *et al*., 1977). The plasma membrane receptors involved are the cation-independent M6PR (Kornfeld, 1987), which is ubiquitously expressed, or the mannose receptor, found only in cells of the reticuloendothelial system (Achord *et al*., 1978) and both mediate the endocytosis and subsequent lysosomal targeting of the secreted enzymes.

Fortunately for therapy, the amount of enzyme needed in the lysosome for phenotypic correction of an individual cell is only a small percentage of 'normal' amount. It is widely accepted that enzyme activity representing as little as 1 - 5% of normal levels in the CNS can be sufficient to rescue phenotype in experimental models of LSD (Sands & Davidson, 2006). Successful treatment will however require direct therapy to, or systemic therapy that targets, the CNS. One of the greatest challenges is bypassing the blood brain barrier to repair or prevent the neurodegeneration and restore the CNS functionality.

1.6.1 The blood brain barrier

The blood brain barrier (BBB) separates the brain, spinal cord and CSF from the blood and represents a major obstacle to the delivery of therapeutics to the CNS. It is a network of cerebral blood vessels lined by endothelial cells and supporting cells, such as astrocytes, neurons, pericytes and perivascular microglia. The blood capillaries of the BBB are rarely more than 8 to 25 μm from each neuron (Schlageter *et al*., 1999). Endothelial cells of the BBB differ from those elsewhere in the body, by forming a physical barrier through continuous intercellular tight junctions, with low endocytic activity and thus extremely low rates of vesicular transport and permeation. The BBB has been reported to deprive the brain of greater than 98% of neurotherapeutic compounds in visceral circulation (Pardridge, 2002). Excluded are large or hydrophobic molecules, such as viruses or conventional gene

vectors, large pharmaceuticals and corrective proteins or enzymes, which cannot passively cross the BBB from the blood circulation to the neural tissues (Scherrmann, 2002).

1.6.2 Enzyme replacement therapy

Enzyme replacement therapy (ERT) typically involves repeated (life-long) intravenous administration of an exogenous lysosomal enzyme into affected patients. From the bloodstream, the recombinant enzyme enters enzyme-deficient cells, through the secretory pathway described above, partially restoring deficient lysosomal enzymatic function with subsequent reversal of tissue pathology. This strategy has been successful in some non-neuropathic LSDs, and Food and Drug Administration (USA)-approved ERTs are now available for Fabry, Gaucher and Pompe diseases as well as mucopolysaccharidosis (MPS) types I, II, and VI (reviewed by Ohashi, 2012). Unfortunately, in some patients, repeated ERT administration has triggered immune responses to the infused enzyme, blocking efficacy and neutralising product activity (Wang *et al*., 2008). Moreover, although ERT strategies effectively treat the visceral manifestations of LSDs, the enzymes in systemic circulation either do not traverse the BBB or in therapeutic quantities, and hence do not resolve the neuropathic disease (Sands, 2014).

ERT strategies are being explored in the NCLs but are likely to only be effective for the subtypes involving soluble proteins (*e.g.* CLN1, 2, 5, 10 and 13). To circumvent the BBB limitations, deficient enzyme has been administered directly to the CSF through intracerebroventricular (ICV) delivery in a naturally occurring canine model of CLN2. This approach has proved successful, with widespread distribution of active enzyme through the brain and reduced neuronal storage (Vuillemenot *et al*., 2011) and attenuation of brain atrophy, neurological and cognitive decline and increased lifespan in CLN2 affected Dachshunds following biweekly recombinant human tripeptidyl peptidase-1 (rhTPP1) ERT (Katz *et al*., 2014). Subsequently, a clinical study evaluating the potential therapeutic value of rhTPP1 administration into the CSF of children with CLN2 disease was initiated (NCT01907087, http://clinicaltrials.gov). Promising interim results reported that ICV-administered rhTPP1 was well tolerated and described stabilization in disease progression for some of the treated patients (Schulz *et al*., 2016).

1.6.3 Gene therapy

Gene therapy offers an alternative or supplementary option to ERT for the NCLs which have significant CNS lesions. It can pertain to either the *ex vivo* genetic modification of donor cells or to the introduction of a correct copy of a defective gene into host cells *in vivo* for therapeutic benefit. For the NCL forms resulting from mutations in soluble lysosomal proteins (CLN1, 2, 5, 10 and 13) genetic correction of a small subset of neural cells may be sufficient to correct large regions of the

CNS via diffusion through the brain parenchyma and the phenomenon of “cross-correction”. Gene therapy is considered less likely to correct the deficit of membrane bound NCL proteins (CLN3, 6, 7, 8 and 12), unless they are involved in the processing of diffusible agents, such as neurotrophic factors, which can rescue neighbouring cells. Despite this, gene therapy using viral vectors is being investigated for membrane-bound and soluble protein forms of NCL as a potential treatment, with the hope that sufficient expression of the corrective gene product could compensate for the disease-related deficiency.

Viral-mediated gene therapy uses modified viruses to infect a small percentage of target host cells, delivering a corrective copy of a mutated gene to these cells, and hijacking the host cell machinery to make functional therapeutic protein to either stabilise or reverse a clinical disease state. The viruses used are termed vectors and have been rendered replication-deficient by the deletion of the structural and packaging (replication) elements of the viral genome. The only viral DNA sequences remaining in the viral vector are the terminal repeats into which the therapeutic constructs are packaged (described below). Such a virus can efficiently enter a cell, but can neither cause a ‘viral disease’ nor replicate. The key features of some viral vectors currently in use for gene therapy of the LSDs are described in Table 1.4. HIV-1-derived lentiviral and adeno-associated viral vectors, encoding either a reporter gene or therapeutic NCL genes were delivered to the sheep CNS *in vivo* in the current study. These vectors will be discussed in greater detail.

Table 1.4 Biological properties of gene therapy viral vectors in current use for the lysosomal storage diseases

Viral vector	Adenovirus	Adeno-associated virus (AAV)	Lentivirus (HIV)	Retrovirus
Family	*Adenoviridae*	*Parvoviridae*	*Retroviridae*	*Retroviridae*
Pathogenicity of parent virus	Yes	No	Yes	Yes
Transgene capacity	37 kB	4.7 kB ssAAV 2.2 kB scAAV	8 - 10 kB	8 kB
Genome	dsDNA	ssDNA	ssRNA	ssRNA
Chromosomal integration	No (episome)	No (circular episome)	Yes	Yes
Transduction of non-dividing cells	Yes	Yes	Yes	Yes
Immunogenicity	High	Low	Limited	Limited
Duration of expression	Transient	Stable	Stable	Stable
Use in human clinical trials *	21.7%	6.2%	5.2%	18.9%
Advantages	Large packaging capacity Transient delivery	Low host immunogenicity Persistent delivery	Low host immunogenicity Persistent delivery	Low host immunogenicity Persistent delivery
Limitations	Host immunogenicity Transient delivery	Small packaging capacity	Risk of insertional mutagenesis Immunodeficiency origin	Risk of insertional mutagenesis Relies on target cell mitosis

* The Journal of Gene Medicine Clinical Trial site, http://www.abedia.com/wiley/ (May 2016). Other platforms make up the remaining 48 % of viral vectors used in human clinical trials (*e.g.*retrovirus)

1.6.3.1 Lentiviral vectors

Lentiviruses are relatively large (100 - 120 nm), enveloped single stranded RNA retroviruses, common examples being feline and type I human immunodeficiency viruses (FIV and HIV-1). They transduce multiple cell types in the brain, including both dividing and post-mitotic cells like glia and terminally differentiated neurons, resulting in high-level and long-term transgene expression *in vivo* (*e.g.* Bosch *et al.*, 2000; Consiglio *et al.*, 2001; Jarraya *et al.*, 2009; Lattanzi *et al.*, 2010; Palfi *et al.*, 2014). The host tropism of lentiviral vectors can be expanded with different promoters and by pseudotyping with a variety of envelope glycoproteins (Wong *et al.*, 2004; Cronin *et al.*, 2005; Jakobsson & Lundberg, 2006). For example, lentiviruses pseudotyped with VSV-G (vesicular stomatitis virus) are typically neurotropic (Naldini *et al.*, 1996a, 1996b; Blömer *et al.*, 1997; Kordower *et al.*, 1999; Jakobsson *et al.*, 2003) with low activity in glial cells *in vivo* (Brooks *et al.*, 2002; Jakobsson *et al.*, 2003). Reduced storage and improved cognitive function has been reported after lentiviral-mediated CNS-directed gene transfer in murine models of the LSDs, type I Gaucher disease, mucopolysaccharidoses IIIA, VII, and IIIB and metachromatic leukodystrophy (Bosch *et al.*, 2000; Brooks *et al.*, 2002; Gieselmann, 2008; Di Domenico *et al.*, 2009; McIntyre *et al.*, 2014; Dahl *et al.*, 2015).

Replication-incompetent HIV-1 lentiviral vectors can be engineered whereby the viral genes and their promoter have been replaced by an alternative expression cassette comprised of an exogenous cellular promoter juxtaposed to a transgene encoding the desired therapeutic protein (Figure 1.5).

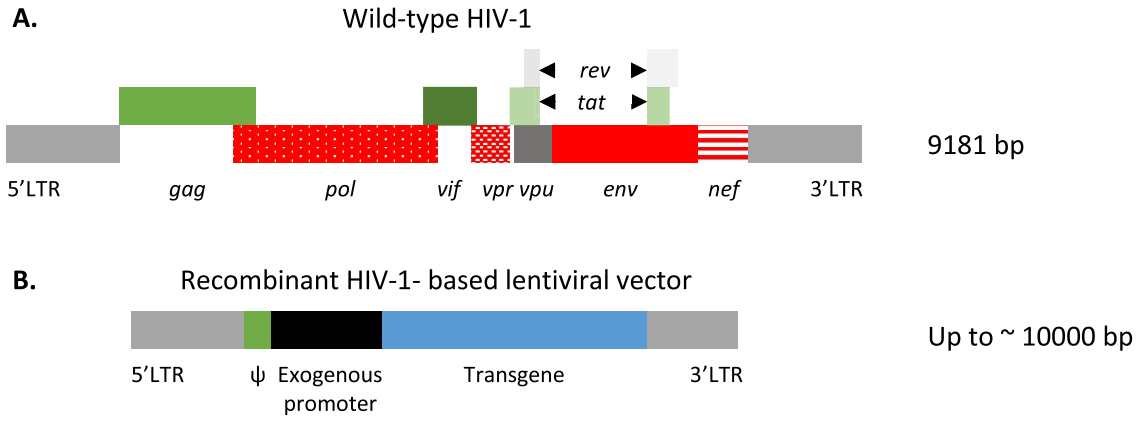

Figure 1.5 Structure of the wild-type HIV-1 and recombinant lentiviral genome

A. Wild-type HIV-1 has a linear 9.7 kb positive-sense single-stranded RNA genome, and contains nine open reading frames required for replication and virulence, between two long terminal repeats (LTRs). The nine viral genes are *env* (envelope), *gag* (capsid and matrix), *rev* and *tat* which encode viral regulatory proteins and *vif*, *vpr*, *vpu* and *nef* which encode viral accesory proteins.

B. Recombinant HIV-1-based lentiviral vectors contain the gene of interest, an exogenous promoter and a packaging signal (ψ) from the viral *gag* gene between the HIV-1 LTRs but the recombinant genome lacks any other viral genes.

A lentiviral vector uses receptor-mediated cell entry and once it is inside the host cell, the reverse transcriptase enzyme, encoded by *pol*, produces a double stranded DNA copy of the RNA viral genome (Temin & Baltimore, 1972). Lentiviral DNA enters the nucleus and is integrated directly into the host genome by the virally encoded integrase enzyme. This has both advantages and disadvantages. Integration allows persistence within the host cell for its lifetime, through repeated cell division, providing permanent expression of the gene delivered in host cells. On the other hand, the chance of insertional mutagenesis is increased with integrating vectors. This risk was highlighted following *ex vivo* gene therapy trials using a murine leukaemia retrovirus to treat X-linked severe combined immunodeficiency (SCID) (Cavazzana-Calvo *et al*., 2000; Gaspar *et al*., 2004). The clinical benefit was tempered by the development of T-cell acute lymphoblastic leukaemia in 20% of patients that was directly attributable to the vector randomly integrating next to, and activating, a specific oncogene (Hacien-Bey-Abina *et al*., 2003; McCormack & Rabbitts, 2004). Fortunately lentiviral vectors have a lower tendency to integrate into potentially carcinogenic hot-spots than other retroviruses (Cattaglio *et al*., 2007).

1.6.3.2 Adeno-associated viral vectors

Adeno-associated viruses (AAVs) are small (20 - 25 nm), non-enveloped single stranded DNA parvoviruses. Although AAVs naturally infect humans and other species, they have no known pathogenicity (Lin & Ertl, 2008). They are classified as a dependovirus, as they rely on co-infection with helper virus (*e.g.* adenovirus or herpesvirus) to complete the viral life cycle and cause a productive infection (Atchison *et al*., 1965; Buller *et al*., 1981; Bauer & Monreal, 1986; Conway *et al*., 1997).

Numerous different AAV serotypes have been identified with variable CNS tropism. After direct delivery to the murine brain parenchyma, AAV serotypes 1, 2, 7, 8, 9 and rh10 primarily result in neurotropism whilst AAV5 is more efficient in transducing neurons and glial cells to a lesser extent (Cearley & Wolfe, 2006; Gray & Samulski, 2011). Of these, AAV1, AAV9 and AAVrh10 exhibit superior spread and transduction efficiency. AAV4 preferentially targets astrocytes, even after intrastriatal injection, and including those astrocytes in the subventricular zone lining the lateral ventricles after ICV delivery (Davidson *et al*., 2000; Burger *et al*., 2004; Liu *et al*., 2005a, 2005b; Cearley & Wolfe, 2006; Markakis *et al*., 2010).

Recombinant AAV vectors have risen to prominence for the treatment of the CNS disease associated with LSDs, because of their ability to transduce non-dividing post-mitotic cells and to confer long-term stable gene expression for up to 10 years (Mingozzi & High, 2013), with minimal associated inflammation or toxicity (McCarty *et al*., 2004; Gonçalves, 2005). Therapeutic effectiveness using AAV has been shown recently in animal models of a number of LSDs, including α-mannosidosis, GM1-

gangliosidosis, GM2-gangliosidosis (Tays-Sachs and Sandhoff diseases), Krabbe disease, metachromatic leukodystrophy, MPS types I, IIIA, IIIB, and VII, and Niemann-Pick A as well as the CLN2 form of NCL (*e.g.* Liu *et al*., 2005b; Sondhi *et al*., 2005, 2012; Fu *et al*., 2011; Haurigot *et al*., 2013; McCurdy *et al*., 2015; Ribera *et al*., 2015; Rockwell *et al*., 2015).

The genes that encode packaging (replication) and structural proteins are removed from the viral genome to generate therapeutic recombinant AAV vectors and are replaced with a transgene expression cassette (Figure 1.6). Removal of the viral genes renders the vectors non-integrative, replication-deficient and minimizes potential immune response risks.

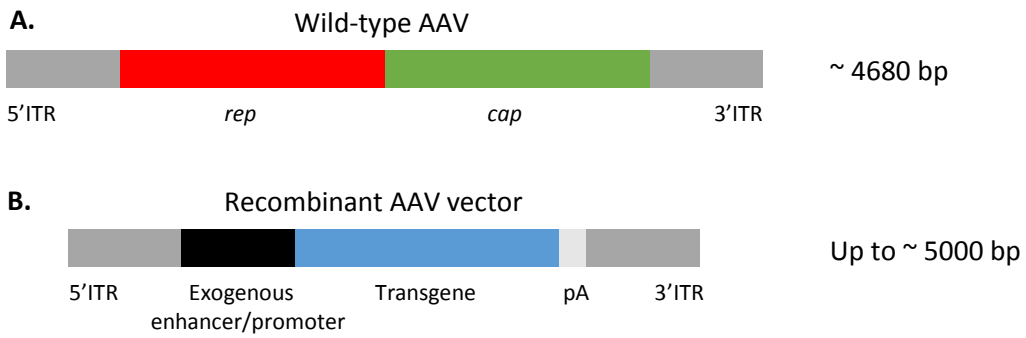

Figure 1.6 Structure of the wild-type adeno-associated virus (AAV) and recombinant AAV genome
A. Wild-type AAV has a linear single-stranded DNA genome of ~4.7 kb, containing two open reading frames, *rep* required for replication and virion assembly and *cap* that encodes the structural viral capsid proteins. The virus does not encode a polymerase and uses cellular polymerases for genome replication. The genes are flanked by two 145 bp inverted terminal repeats (ITRs) which are required as signals for packaging.
B. Recombinant AAV vectors lack the *rep* and *cap* viral genes, hence rendering them replication-deficient. Instead the gene of interest, an exogenous enhancer and/or promoter and a polyadenylation signal (pA) reside between the AAV ITRs, the only viral sequences retained from the parent virus.

AAVs enter the cell through receptor mediated endocytosis. Inside the cell, an AAV translocates its genome into the nucleus where it is made into double-stranded DNA. This DNA persists as an episome with only sporadic transgenic integration, thereby reducing the potential for insertional mutagenesis and oncogenesis. No evidence for tumorigenesis from AAV vectors was reported in a large study of over 600 mice (Bell *et al*., 2005), although an increased incidence of hepatocellular carcinoma (HCC) has been noted in several long-term mouse studies following systemic administration of AAV vectors (Bell *et al*., 2006; Donsante *et al*., 2007). AAV2-related insertional mutagenesis has also been reported in human HCC (Nault *et al*., 2015) yet this remains contentious,

being found in only 7% of HCC tumours compared with 21% of adjacent normal liver tissue samples (Berns *et al*., 2015).

1.6.4.1 Gene therapy approaches to bypass the blood brain barrier

The most direct gene therapy stratagem developed to anatomically bypass the BBB is via direct stereotaxic injection of viral vectors into the brain parenchyma. This approach has been used in a number of animal model studies (Di Domenico *et al*., 2009; Jarraya *et al*., 2009; Haurigot *et al*., 2013), including the current study, as well as in human gene therapy trials for infantile NCL (INCL) (Worgall *et al*., 2008) and MPSIIIA (Tardieu *et al*., 2014). An alternative mechanical way is to administer viral vectors into the CSF of the ventricular system, allowing distribution through the CSF flow and hence a more global delivery. This approach is tested in sheep in the current study and has been gaining in popularity as a therapeutic delivery route (Haurigot *et al*., 2013; McIntyre *et al*., 2014; Katz *et al*., 2015).

The BBB can also be breached biologically. Certain AAV serotypes can cross the intact BBB, including AAV9 into neonatal mice (Foust *et al*., 2009) and into adult non-human primates (Gray *et al*., 2011), as well as AAVrh8 and rh10 into adult mice (Yang *et al*., 2014). A number of these vectors can also undergo axonal transport, mainly in the retrograde but sometimes the anterograde direction. Vectors can enter the synaptic terminals and be transported in the retrograde direction within axons to the cell somas where transgene expression is induced. Targeted delivery to regions rich in efferent and afferent projections has the advantage of transferring genes to cells in regions distal to the vector injection site, improving efficacy. For example, AAV serotypes 1, 9 and rh10 can be disseminated along axonal projections in both directions after injection into the ventral tegmental area in mice, a region in the midbrain with known neural circuitry (Cearley & Wolfe, 2007).

1.6.4 Gene therapy in the NCLs

Most reported NCL cases are caused by mutations in the *CLN1*, *CLN2* and *CLN3* genes. The former two encode soluble lysosomal proteins of known function and as such are regarded to be the most amenable to gene or enzyme replacement therapies. The first demonstration of gene therapy in NCL was performed by Sands and colleagues, using intracranial injection of AAV2 expressing human *CLN1* cDNA into a neonatal mouse model of infantile NCL (INCL) (Griffey *et al*., 2004). Approximately 15% of normal enzyme activity was detected at the injection sites, with partial correction of phenotype. Despite functional improvements, there was no increase in longevity in AAV2-*CLN1* treated INCL mice (Griffey *et al*., 2006).

Therapeutic studies in late infantile NCL (LINCL) are well advanced. Direct central nervous system delivery of AAV2 expressing human *CLN2* cDNA into mice, rats and non-human primates mediated

long-term gene expression in the brain with partial correction of hallmark NCL cellular pathologies (Haskell *et al*., 2003; Hackett *et al*., 2005; Sondhi *et al*., 2005; Passini *et al*., 2006; Cabrera-Salazar *et al*., 2007). The *CLN2* gene encodes a lysosomal serine protease, tripeptidyl peptidase-1 (TPP-I), which is secreted from expressing cells *in vivo* and endocytosed into non-expressing cells, trafficking via the classical mannose-6-phosphate receptor mechanism (Lin & Lobel, 2001). TPP1 activity at the injection sites after intraparenchymal (IP) delivery into the various animal models ranged from 0.5- to 7-fold higher than endogenous levels (Haskell *et al*., 2003; Passini *et al*., 2006) indicating the feasibility of this approach in the clinic. The resultant Phase I clinical trial (NCT00151216; https://clinicaltrials.gov) (Crystal *et al*., 2004), administering AAV2-h*CLN2* through 12 parenchymal injections into the CNS of 10 children with moderate to severe LINCL phenotype, demonstrated a reduction in the rate of neurological decline, but not a complete halt in pathology (Worgall *et al*., 2008). Minor, ephemeral humoral responses to the vector were reported in 40% of subjects. This study highlighted that the clinical course was not the ideal estimate of therapeutic efficacy, given the different mutations and considerable variation seen between individual humans suffering from the same NCL variant.

The safety and efficacy of a second-generation AAVrh.10, a serotype derived from the rhesus monkey, to mediate *CLN2* delivery was studied in a number of animal models (Sondhi *et al*., 2007, 2012). Recent initiation of parallel Phase I and Phase I/II clinical trials for children with mild to moderate and moderate to severe cases and to uncommon genotypes of LINCL respectively followed (NCT01161576, NCT01414985). Children received delivery of one of two viral vector doses (2.85 x 10^{11} or 9 x 10^{11} viral genomes (vg) total) into 12 parenchymal locations through six entry sites. No adverse safety events were noted but reports on efficacy will not be made until the completion of the trial in 2016 (Crystal, 2014).

Development of gene therapies for the lesser common NCLs has long been a major initiative within the BARN research programme (Palmer *et al*., 2015). Neural cell cultures, isolated from foetal sheep (Kay *et al*., 1999), have proven beneficial in testing the efficacy of gene therapy prior to whole animal studies (Linterman *et al*., 2011; Hughes *et al*., 2014a). The transgenic expression, transduction efficiency and cell tropism of lentiviral vectors have been tested in mixed cultures of neural precursors (neuroblasts), mature neurons, astrocytes and microglia generated from both South Hampshire CLN6 and Borderdale CLN5 affected sheep. Lentiviral vectors, pseudotyped with VSV-g and under the control of a constitutive myeloproliferative sarcoma virus promotor (MND) were used to deliver a green fluorescent protein (*GFP*) reporter gene to control and CLN6 affected neural cultures (Linterman *et al*., 2011). A greater tropism for neuronal and neuroblast cells was seen over glia. More recently, a significant diminution of storage body accumulation was observed in CLN5-deficient neural cells after transduction with a *CLN5* expressing lentiviral vector (Hughes *et al*., 2014a). Both findings supported the use of lentiviral mediated gene transfer *in vivo.*

A program of direct lentiviral injections into sheep brains *in vivo* was initiated. Despite positive indications from murine studies (Fu *et al*., 2003), no transduction of cells followed intracisternal injections of lentiviral *GFP* constructs in sheep, however columnar infusion into the cortical parenchyma resulted in stable yet localised GFP transduction evident up to 80 day post-injection (Linterman *et al.,* 2011). Of importance was the targeted transduction of ependymal and subependymal cells along the extent of the ventricular surface, including type B astrocytic cells, thought to be equivalent to the *bona fide* human adult neural stem cells (Doetsch *et al*., 1999). These findings were encouraging for human translation. Given the restricted parenchymal spread of lentiviruses (Cetin *et al*., 2006; Lerchner *et al*., 2014), an alternative ICV injection strategy was attempted in the current study. Targeted correction of the ependyma lining the ventricles could result in protein secretion into the cerebral spinal fluid (CSF) for circulation to the entire CNS, whilst transduced neuroblasts could provide an alternative route for the spread of the gene product to the degenerating cortex in NCL patients via the chain migration of neuroblastic granule cells (see Section 1.5.4). The reported long-term transduction efficiency and spread of AAV vectors in the CNS, described above, also supported their inclusion in the therapeutic trials in ovine NCL detailed in this thesis.

Chapter 2

Experimental rationale

2.1 Research objectives

Spontaneous and genetically engineered large animal models are being used increasingly for translational studies of human neurological disorders to supplement the current reliance on small animal models, such as rodents, that do not fully replicate the many size- and age-related aspects of the human nervous system (Aigner *et al*., 2010; Dolezalova *et al*., 2014; Chang *et al*., 2015; Pinnapureddy *et al*., 2015). Sheep constitute a powerful species for such studies. With their comparable size, human-like gyrencephalic brain and relative longevity, sheep are ideal translational candidates for paediatric neurodegenerative disorders, including neuronal ceroid lipofuscinosis (NCL).

The naturally occurring ovine models of CLN5 and CLN6 NCL exhibit close mimicry to the relevant human NCL pathology. The prolonged disease course of ovine NCL (up to 24 months) permits development and analysis of the clinical effectiveness and longer term consequences of potential gene and pharmacological therapies. To do so, it is important that rigorously defined quantitative *in vivo* signatures (biomarkers) are identified for following disease progression and then evaluating therapeutic efficacy. As the causative mutations of ovine CLN5 and CLN6 have been identified and preclinical molecular genetic diagnoses have been developed (Tammen *et al*., 2006; Frugier *et al*., 2008), affected sheep can be genotyped at birth and detailed analysis of the clinical course and the progression of pathological changes in the ovine disease can be carried out from a perinatal stage, with observable pathology but no overt symptoms, through to advanced disease at 18 - 24 months of age. Longitudinal biomarkers of disease progression in sheep, including non-invasive *ante mortem* behavioural, neurological and cognitive parameters and neuroimaging, can be correlated with *post mortem* neuropathological findings and then used to evaluate therapeutic approaches. Studies such as these are rarely possible using human material or patients.

One therapeutic approach trialled in sheep has been gene therapy. Although genetically distinct, NCLs can be broadly divided into two categories: one in which the mutation results in a defective transmembrane protein (*e.g.* CLN6), and the other in a deficient soluble lysosomal enzyme (*e.g.* CLN5). Among the NCLs, those caused by soluble enzyme deficiencies are considered good candidates for gene therapy through the normal lysosomal enzyme trafficking system and the phenomenon of cross-correction, whereby affected cells take up soluble enzyme from the surrounding environment (reviewed by Sands & Davidson, 2006). Viral-mediated gene therapy could

transduce target cells, causing them to express the corrective gene, and provide the surrounding cells and tissue with a continuous supply of soluble functional enzyme. Once secreted, the corrective enzyme can be endocytosed by neighbouring enzyme-deficient cells via the return plasma membrane mannose-6-phosphate receptor pathway, potentially correcting their deficiency (see Section 1.6). *In vitro* cross-correction studies and *in vivo* preclinical studies in animal models support the hypothesis that restoration of 5 – 10% of normal enzyme activity would be sufficient to facilitate normal cellular function (Sands & Davidson, 2006), indicating that only a subset of cells may need to be genetically modified to secrete the deficient enzyme to cross-correct other cells at a distance.

In contrast, defects in membrane-bound proteins are predicted to be harder to correct, unless the transmembrane protein is involved in the processing of secreted proteins. Chimeric studies in sheep have shown this may be the case in ovine CLN6 (Barry, 2011). Chimeras, generated from normal and CLN6 affected sheep embryos, showed no evidence of neurodegeneration or disease-associated glial activation, despite having varied ratios of normal to affected tissue composition and the sheep retained their vision, long after natural disease progression in affected animals. This intimates a neuroprotective role of normal cells over diseased cells and suggested that attempts at gene therapy may be warranted even in the case of membrane-bound defects.

2.2 Research aims and hypotheses

The first aim of this study was to elucidate the pathological changes within the diseased brain and to define windows for possible therapeutic intervention. The preclinical and progressive changes in the CNS of the ovine CLN6 model have already been described (Oswald *et al*., 2005, 2008; Kay *et al*., 2006) however data from the Borderdale CLN5 model are presently limited, and a proper definitive time course neuropathological study was required. The current study sought to provide comparative and quantitative histological and immunohistochemical measures of the sequential changes in both disease models relative to the normal brain. The variables analysed were cortical thickness, astrocytosis, microglial activation, storage body accumulation and neurogenesis. Expression of the endogenous CLN5 and CLN6 proteins in the normal sheep brain was also examined for the first time. Results are described in Chapter 4.

The second aim was to test the efficacy and tropism of adeno-associated virus serotype 9 (AAV9) as a gene transfer vector in the normal sheep brain. Naïve, juvenile sheep received injections of AAV9 expressing a marker gene (green fluorescent protein; GFP) into the brain parenchyma or cerebral lateral ventricles and GFP expression through the CNS was analysed one month later (Chapter 5).

Lastly, Chapters 6 and 7 describe longitudinal *in vivo* monitoring of the efficacy of lentiviral- and AAV9-mediated delivery of the therapeutic NCL genes to pre-clinical CLN5 and CLN6 affected sheep.

Chapter 3

General Materials and Methods

3.1 Animals

Experimental flocks of sheep (*Ovis aries*) with CLN5 and CLN6 neuronal ceroid lipofuscinoses have been developed and were maintained by mating 7 - 8 month old homozygous affected ram lambs with heterozygous adult ewes, to give a 1:1 ratio of affected and heterozygous offspring each year. A separate flock of unaffected Coopworth sheep served as controls for some of these studies. In 2013, to sustain genetic variation, improve reproductive performance and increase flock numbers, homozygous ram lambs of both genotypes were outbred to normal Coopworth ewes. Resultant obligate heterozygous ewe lambs were retained within the respective CLN5 and CLN6 breeding flocks.

Animals were maintained under standard New Zealand pastural and husbandry conditions on University farms. Animal procedures were carried out in compliance with the New Zealand Animal Welfare Act (1999), approved by the Lincoln University Animal Ethics Committee, and conducted in accordance with US National Institutes of Health guidelines.

3.1.1 Gene injected (treated) animals

Approval for the use of recombinant lentiviral and AAV vectors was obtained from the NZ Environmental Protection Authority (EPA) (GMD004899) and all experimental gene therapy procedures were approved by the Lincoln University Animal Ethics and Institutional Biosafety Committees.

CLN5 and CLN6 affected sheep, assigned for gene therapy, were weaned early (sections 6.2.2 and 7.2.2), housed indoors and fed initally on calf start-mix (Reliance Feeds, Rolleston, New Zealand) and chaffed lucerne. They were transferred to an indoor Physical Containment 2 sheep facility, in compliance with EPA requirements, from one week prior to surgery until trial completion. All animals used were healthy and clinically normal at the commencement of the study. Once in the containment facilty, sheep were housed in individual pens and fed a mixed daily ration of chaffed hay and lucerne (up to 400 g/day), and a pelletised lucerne feed concentrate (Seales Winslow, Ashburton, New Zealand and Dunstan Nutrition Ltd, Hamilton, New Zealand; up to 800 g/day). Feed was top-dressed for 3-month restricted periods of time with 3% common salt (sodium chloride) and 0.5% ammonium chloride to stimulate water consumption and acidify urine respectively, as preventative measures against urinary calculi. During the study, sheep received daily oral

administration of 50 mg ammonium molybdate and 500 mg soldium sulphate for 3 week periods to abrogate concentrate-feed induced copper toxicosis. Sheep were housed under a natural daylight regimen, monitored daily with any abnormal behaviours recorded, and weighed monthly. Every 6 months, jugular blood samples were sent to Gribbles Veterinary Pathology, Christchurch, NZ for plasma copper testing, and haematological and biochemical analysis for signs of liver or other organ damage.

3.1.2 Genotyping

The causative mutations of ovine CLN6 and CLN5 have been identified (see Sections 1.3.2 and 1.4.2) and preclinical molecular genetic diagnoses developed (Tammen *et al*., 2006; Frugier *et al*., 2008).

3.1.2.1 Ovine CLN6 genotyping

The large disease-causing mutation in the South Hampshire sheep falls in the 5' region of the gene, a very difficult region to amplify by PCR (Mohd Ismail, 2014). Instead an indirect DNA test was used to genotype lambs born into the CLN6 flock. This test exploits a silent single nucleotide polymorphism marker (c.822G>A) in the coding region of *CLN6*, 111 bp downstream of the 5′ end of exon 7, which introduces a differential cut site for the restriction enzyme *Hae* II (Tammen *et al*., 2006). This silent substitution shows tight linkage with the disease (LOD score of 13.3, $\theta = 0.01$). In brief, amplification from genomic DNA (as above), enzymatic cleavage and agarose gel separation of the products allowed allelic discrimination (Figure 3.1). The CLN6 South Hampshire flock has been configured so that all normal sheep used carry only the G allele, affected sheep carry only the A allele and South Hampshire heterozygotes carry both. This test has proven to be entirely reliable over 15 years and 800 sheep, as judged by subsequent clinical and pathological diagnosis.

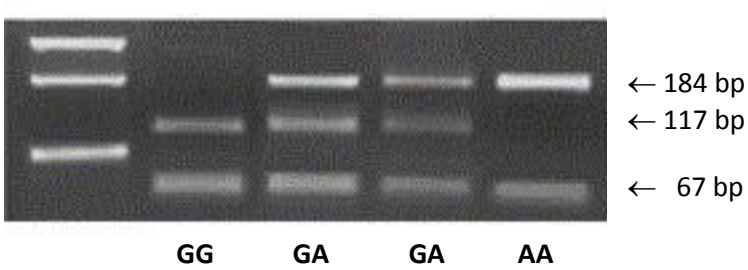

Figure 3.1 An indirect test for the preclinical diagnosis of ovine CLN6
Restriction enzyme detection of the discriminatory c.822G>A polymorphism in ovine CLN6 in South Hampshire sheep (Tammen *et al*., 2006). A 251bp PCR product cleaved with *Hae* II results in a differential banding pattern for unaffected (GG), heterozygous (GA) and CLN6 affected (AA) sheep Lane 1 contains a size standard with 300, 200 and 100 bp bands visible.

3.1.2.2 Ovine CLN5 genotyping

The ovine CLN5 disease is caused by a nucleotide substitution at a consensus splice site in the *CLN5* gene (c.571+1G>A) with subsequent excision of exon 3. This mutation was detected by either reverse-transcription PCR amplification of mRNA over the exon 3/ intron 3 splice site or by sequencing a PCR product amplified from genomic DNA which spans this region (Frugier *et al*., 2008) (Figure 3.2). In brief, RNA isolated from whole blood using PureLink Total RNA blood kits (Invitrogen, Carlsbad, CA, USA) was converted to cDNA using SuperScript III RNase H reverse transcriptase (Invitrogen) and oligo $d(T)_{15}$ primers. *CLN5* cDNA was amplified with primers in exons 2 and 4 to give a differential banding pattern on agarose gel electrophoresis (Figure 3.2A).

Alternatively, sheep genomic DNA was extracted from heparinized venous blood by NaCl fractionation (Montgomery & Sise, 1990), from Whatman FTA cards (Whatman, Brentford, Middlesex, UK) or from EDTA blood samples using QIAamp DNA mini extraction kits (Qiagen, Hilden, Germany). *CLN5* gDNA was amplified with primers in exon 3 and intron 3 and the 538 bp PCR product sequenced at the Lincoln University Sequencing Facility, using Big Dye terminator v3.1 Cycle sequencing (Applied Biosystems, Foster City, CA, USA). Pre-sequencing clean-up was performed with CleanSEQ Dye-Terminator removal kits (Agencout Bioscience Corporation, Beverly, MA, USA) and samples were sequenced on an Applied Biosystems 3130xl Genetic Analyzer (Figure 3.2B).

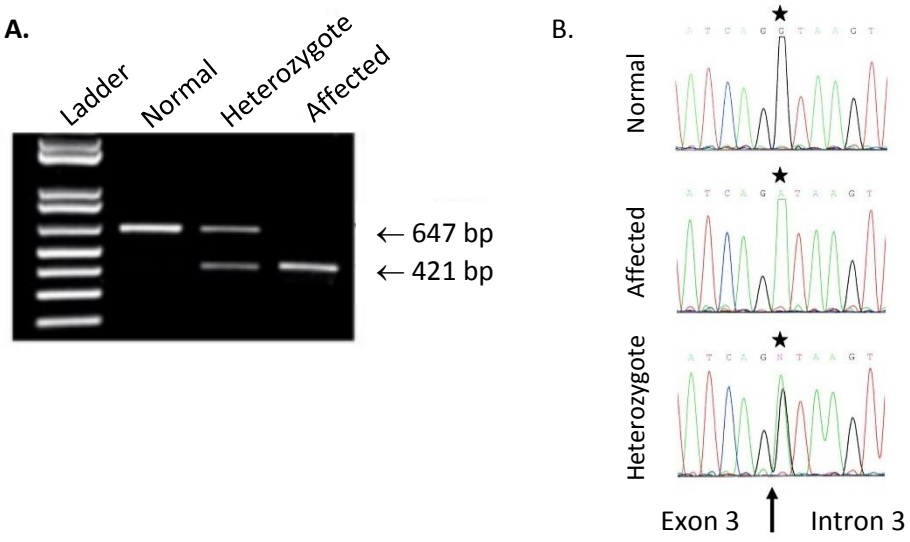

Figure 3.2 Alternative methods for the genetic diagnosis of ovine CLN5

A. Reverse-transcriptase PCR of *CLN5* between exons 2 and 4 shows retention of exon 3 in normal transcripts (647 bp) whilst exon 3 is lacking in affected transcripts (421 bp). Both bands are seen in the heterozygote. Sequencing the two bands confirmed this observation (Frugier *et al*., 2008).

B. Comparative sequence analysis of normal, affected and heterozygous *CLN5* PCR products from genomic DNA. The affected sheep electropherogram shows the substitution c.571+1G>A (*). Note the presence of both alleles (G/A) in the heterozygote Borderdale animal. The arrow indicates the exon 3/intron 3 boundary (Frugier *et al*., 2008).

3.2 Gene therapy protocols

Whilst this section describes the general gene injection strategy, specific protocols, including cloning of the NCL transgenes, delivery doses and target sites are included in the appropriate chapters.

3.2.1 Viral constructs and *in vitro* analysis

Full-length ovine *CLN5* (GenBank accession number NM_001082595; Frugier et al., 2008) and *CLN6* (GenBank accession number NM_001040289; Tammen et al., 2006) cDNA was cloned at Lincoln University (see Sections 6.2.3 and 7.2.3). Both lentiviral and AAV9 constructs expressing these cDNAs were produced, titred and *in vitro* analyses performed by Batten Animal Research Network (BARN) collaborators, led by Dr. Stephanie Hughes based at the Otago Viral Vector Facility, University of Otago (Dunedin, New Zealand). The viral constructs were then transported to Lincoln University for *in vivo* administration to the sheep brain.

3.2.1.1 Lentiviral constructs

HIV-1 derived lentiviral plasmids (Meyerrose *et al*., 2008) expressing ovine *CLN5* or *CLN6*, under the control of the myeloid proliferative U3 enhancer element (MNDU3) and pseudotyped with the vesicular stomatitis virus glyocprotein (VSV-G), were packaged using a third generation packaging system (Zufferey *et al*., 1998). Briefly, 293FT cells (Life Technologies, Carlsbad, CA, USA) were transfected with plasmids containing the NCL transgene, packaging and VSV-G envelope genes in OptiMEM containing Lipofectamine-2000 (Life Technologies) (Linterman *et al*., 2011). Media was recovered 48 hours post-transfection, concentrated by ultracentrifugation at 25,000 rpm for 90 min, resuspended in PBS containing 40 mg/mL lactose, and stored at -80°C until required. Functional viral titres were determined by serial dilutions on HT1080 cells (ATCC, Manassas, VA, USA)

3.2.1.2 Recombinant adeno-associated virus serotype 9 (AAV9) constructs

Recombinant AAV (serotype 9; AAV9) constructs of ovine *CLN5* or *CLN6* were produced, under the control of the MNDU3 promoter. In brief, 293FT cells (Life Technologies) were triple transfected with plasmids encoding the *CLN5* or *CLN6* transgene; the pAAV2/9 packaging plasmid (containing AAV2 *rep* and AAV9 *cap* viral genes); and the pAd delta F6 Helper plasmid containing the adenoviral genes required to drive AAV replication (University of Pennsylvania, Philadelphia, PA, USA). Cells were harvested 48 hours post-transfection, and cell pellets frozen at -80 °C before sodium deoxycholate and benzonase-driven cell lysis and iodixanol gradient purification. Purified virus was concentrated in a centrifugal concentrator and stored at -80 °C. Genomic titres were determined by quantitative real-time PCR analysis of woodchuck hepatitis virus post-transcriptional regulatory element (WPRE) expression (Clark *et al*., 1999). Functional titres were were determined by serial dilutions on 293FT cells, with confirmation by *in vitro* immunofluorescence 72 h post-infection (McClure *et al*., 2011).

3.2.2 *In vivo* viral injections

The design, planning and stereotactic gene injections were carried out by a team consisting of Nadia Mitchell, Martin Wellby and Dr. Graham Barrell at Lincoln University, based on stereotactic surgical procedures described previously (Linterman *et al*., 2011).

Sheep were fasted overnight. Intravenous anaesthesia was induced with a mixture of ketamine hydrochloride (7.5 mg/kg live weight (LW); PhoenixPharm Distributors Ltd, Auckland, NZ) and diazepam (0.3 mg/kg LW; Ilium, Troy Laboratories NZ Pty Ltd, Auckland, NZ). Sheep were then intubated (8 – 9.5 mm cuffed endotracheal tube) and maintained on isoflurane inhalation (2 – 4% in oxygen), within a closed circuit system. A dose of buprenorphine hydrochloride (Temgesic, 324 µg/ animal; Reckitt Benckiser (NZ) Ltd, Auckland, NZ) was given intramuscularly for analgesia.

With the sheep in the sternal recumbency position, the head was secured for injection in a stereotactic frame (Kopf, model 1630; David Kopf Instruments, Tujunga, CA, USA) and the surgical site clipped and prepared for surgery by repeated scrubs with povidone-iodine solution (Biodine, VetPharm NZ Ltd, Auckland, NZ), an alcohol spray and subsequent draping. Following a medial skin incision and retraction of the underlying musculature and fascia, bregma (the junction of the sagittal and coronal sutures on the top of the skull) was identified. Three mm holes were drilled through the frontal and/or parietal bones at co-ordinates relative to bregma (Figure 3.3, I1 and I2). These co-ordinates and the needle depths differed slightly for each study, depending on the age of the animals and the underlying parenchymal or ventricular target, and are described in the appropriate chapters.

For the parenchymal injections, two 25 µl Hamilton syringes (Harvard Apparatus, Holliston, MA, USA) with 26 gauge needles were lowered into each hemisphere of the brain using a stereotaxic manipulator. Two µl of viral vector solution was infused at the greatest depth over 30 secs, then the complete needle unit was withdrawn 0.5 mm and the process repeated until the full volume was discharged. The syringe was left in place for 5 min after the specified dose was administered to ensure tissue penetration, before slow retraction.

The intracerebroventricular injections used the same drill holes as the parietal injections but the needle was directed 10° rostral for the latter to avoid following the same needle tracks. To establish the depth of the tissue-ventricle interface, a 500 µl Hamilton syringe with a 26 gauge needle filled with sterile saline was lowered into the brain. The ventricular interface was indicated by the positive flow of CSF once the ventricle was reached. Viral vector solution was infused at a rate of 0.1 mL/ min. After the full volume had been dispensed, the syringe was left in place for a further min before removal.

The wound was closed with a continuous subcuticular suture, followed by interrupted skin sutures that were removed 10 days post-surgery. An intramuscular non-steroidal anti-inflammatory (meloxicam, Metacam 20, 0.5 mg/kg LW; Boehringer Ingelheim (NZ) Ltd, Auckland, NZ) and subcutaneous antibiotic (procaine and benzathine penicillin, Duplocillin LA, 12,000 IU/kg LW, Intervet Schering Plough Animal Health Ltd, Upper Hutt, NZ) was administered, and the animals were observed until full recovery. Intramuscular buprenorphine (Temgesic, 324 µg/ animal) was given every 8 h for 2 days for analgesia. Sheep were monitored and rectal temperatures recorded daily for 3 weeks post-surgery. Non-absorbable sutures were removed one week after surgery.

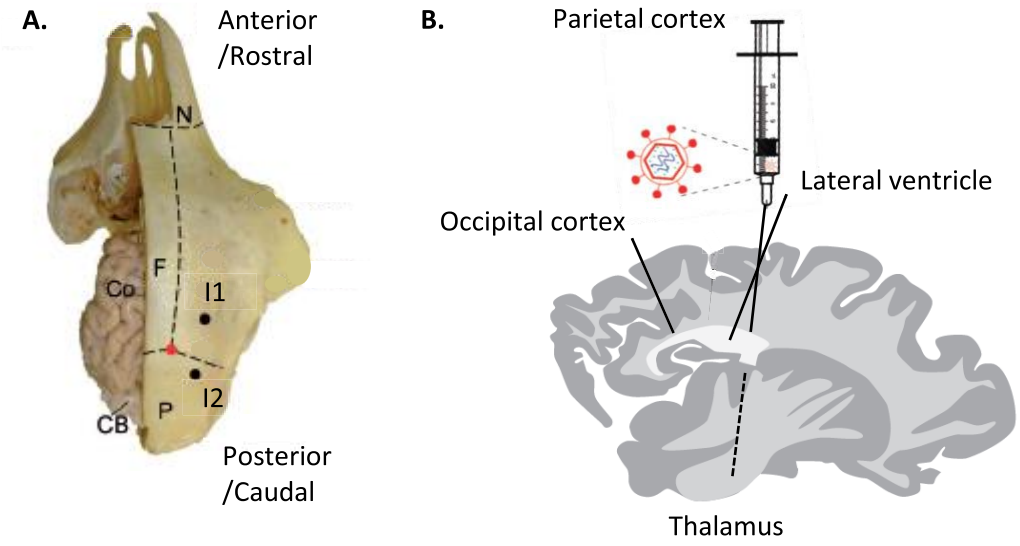

Figure 3.3 Viral vector injection sites in the ovine brain

A. Burr holes are shown by the black dots on the right side of the skull, with equivalent positions on the left hand side. The injection site 1 (I1) targeted the parietal cortex, thalamus and lateral ventricle whilst the occipital cortex was injected through I2. Coordinates were determined with reference to the intersection (bregma) of the transverse suture that separates the frontal (F) and parietal (P) bones. Suture positions are indicated by dotted lines. Part of the skull has been removed to show the brain *in situ*: the dorsal surface of the cortex (Co) and the cerebellum (CB) are partially visible.

B. Location of the bilateral injections in a representative sagittal sheep brain section and the underlying target sites. The two cortical injections per hemisphere were delivered as a columnar infusion, from the subventricular zone at the deepest point to near the pial surface at the shallowest. Targeted thalamic injections were performed in the proof-of-concept AAV9-*GFP* study through the same needle track as the parietal cortex (Chapter 5). Multiple bolus injections were administered to the lateral ventricles.

3.3 Clinical progression and staging of ovine NCL

The methodology for clinically staging neuronal ceroid lipofuscinosis was based on previous clinical descriptions of the ovine form of the disease (Mayhew *et al*., 1985; Westlake *et al*., 1995; Cook *et al*., 2002) and neurological prototypes in goat (Konold *et al*., 2010) and sheep (Passler *et al*., 2012). The general health and neurological status of normal (heterozygous) and affected lambs of both genotypes were assessed monthly in conjunction with the affected lambs which had undergone CLN5 or CLN6 gene therapy. Live weight and body condition score data were also collected.

Initially a full neurological examination following the method of Konold (2010) was carried out on each sheep. Many of the parameters examined, such as the five spinal reflexes and some of the cranial nerve reflex tests, were not found to be helpful in the diagnosis of NCL hence these components were abandoned and a modified procedure was adopted (Appendix A).

3.3.1 Neuro-opthalmic and auditory testing

In the adapted testing paradigm, sheep were handled individually for basic neuro-opthalmic examination including assessment of the cranial nerves (CN) involved in ocular function (Optic II, Oculomotor III, Trigeminal V and Facial VII), the central visual pathways and the visual cortex. The tests (and their possible points of lesion) included:

1. Menace response (CN II and VII, visual cortex and cerebellum), characterised by an eyelid blink, ocular retraction and head aversion as the examiner rapidly moved a finger toward the eye from a medial and rostral direction.
2. Palpebral and corneal reflexes (CN V and VII), which elicited involuntary blinking of the eyelids by touch stimulation of the lateral or medial canthi and the cornea respectively.
3. Direct and consensual pupillary light responses (CN II and III, and central visual pathways excluding the visual cortex), indicated by the constriction of both pupils upon shining a light beam in a nasotemporal direction toward the temporal region of the retina.
4. Dazzle reflex (CN II and VII, retina, and subcortical visual pathways), characterised by an involuntary aversion response (blinking, globe retraction, third eyelid protrusion and/or head movement) to intense illumination of the eye.
5. Visual tracking (CN II, visual cortex and all areas involved in motor function), evidenced by following a visual stimulus without auditory or olfactory clues.

Auricular (acoustic startle) reflexes (CN VII) - the movement of the pinna in response to a loud noise (handclap) - were also tested. Visual and auditory reflexes were assessed as normal, decreased or absent. Mentation, gait, head carriage and postural traits, as well as manifest tremor or seizure

onset, were assessed while sheep were herded up a set of stairs and a graded slope to the testing facility. The functionality of the optic cranial nerve II, visual cortex and all cerebral areas associated with motor function were subsequently assessed by behavioural vision testing through negotiation of a maze (see Section 3.4).

Finally the sheep were assigned a clinical rating score from the scale in Table 3.1 by two independent evaluators (including the author). Where there was a discrepancy in scores between assessors, the scores were averaged.

Table 3.1 Clinical rating criteria for assessing neurological dysfunction in sheep

Clinical score	Clinical phenotype	Clinical status
5	Normal	Normal
4	Pre-clinical	Low head carriage
		Propensity to crouch, baulk and stumble
		Normal visual and acoustic reflexes
3	Blind	Head tilt/stargazing
		Visual deficits
		Decreased or lost menace (blink) response
		Loss of visual tracking
		Reduced herding
2	Overt/neurological	Onset of motor, cognitive and proprioceptive deficits*
		Decreased startle to auditory stimuli
		Decreased pupillary light reflex
		Wide stance
1	Advanced	Progressive disease
		+/- induced tetanic seizures
		Localised tremors
		Minimal pupillary light and absent dazzle reflexes
		Repetition in activities (compulsive circling)
		Low mentation
		Somnolence
		Non-responsiveness to external stimuli
		Loss of body condition
		Hindlimb paresis
0	Terminal	Spontaneous tetanic seizures

* Motor and proprioceptive dysfunction was evidenced by ataxia, stumbling, dragging of the feet, and intermittent episodes of localised muscle tremors (particularly of the ears, eyelids, lips, and hind limbs). Behavioural changes from this age included a reduced awareness of surroundings, repetitive actions (aimless circling, teeth grinding) and feeding abnormalities (dribbling and inefficient or sham eating)

3.4 *In vivo* cognitive maze testing

A simple closed-field maze behavioural task was utilised to assess the visual and cognitive faculties of normal (heterozygous), NCL deficient sheep, and affected sheep of both genotypes who had received gene therapies. A 15.5 m x 3.5 m outdoor maze was constructed beside wooden yards between two existing buildings (Figure 3.4), with a start box and goal pen positioned at opposite corners of the maze. The wooden yards were 1.2m high and covered in opaque shade cloth. Internal barriers were positioned as visual obstacles around which the sheep manoeuvred to reach the goal area. These moveable fence panels were open-barred to enable animals to view conspecifics at the opposite end of the maze, providing motivation for sheep to traverse the maze and join their flockmates.

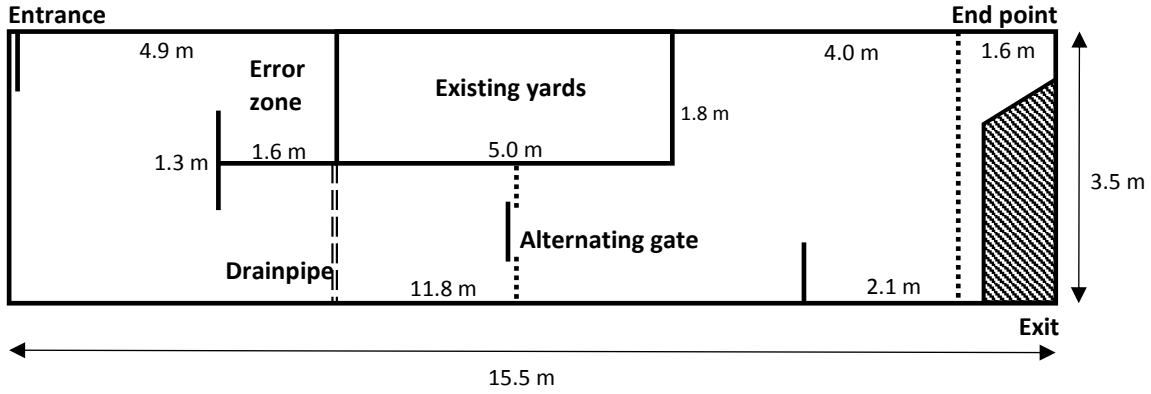

Figure 3.4 Configuration of the maze

Sheep for testing were housed in a group pen, before being released individually into a race by a handler for entry into the testing arena and maze negotiation. Conspecifics were penned in the shaded goal area near the exit. Food, in the form of lucerne pellets, was also available there. A drainpipe (5 cm diameter; dashed line) was included as an extra hindrance. The middle gate (dotted) alternated from left to right between runs. The handler remained at the entrance during each maze run, out of sight of the traversing sheep.

Maze testing was conducted under daytime photopic light between the hours of 9:00 am and 1:00 pm. Prior to each test, sheep were given a 15 min habituation period as a group, to allow them to explore the testing area. Animals were then randomly allocated, with half used as conspecifics and penned in the goal pen at the opposite end of the maze whilst the remainder were housed in the group pen near the maze entry. Individual sheep were released from the group pen by a handler, entering a race which led onto the maze entry. Timing commenced on entry and the criterion for successful completion was exit from the maze in 2 min or less. Reward for completion consisted of entry into the goal area with conspecifics and food (lucerne pellets). If an animal failed to traverse the maze in less than 2 min, they were steered to the exit by a handler. Sheep negotiated the maze twice on each testing day and the configuration of the maze remained unchanged between runs, except for the position of the gap at the middle gate, which alternated between left and right to reduce a learning effect.

Total times required to successfully traverse the maze and any errors committed (failure to enter the maze arena unassisted and the sum of time spent in the error zone) were recorded by the handler at the time and verified from video footage. The handler was not blinded to the disease status of the sheep but retrospective video analysis and maze grading (Table 3.2) was performed by a second, independent investigator in a blinded fashion, to eliminate observer bias.

Table 3.2 Criteria for assessing cognition and behaviour during maze negotiation

Maze score	Descriptor
5	Traverse the maze with no pauses or difficulty
4	Traverse the maze but with small pauses
3	Traverse the maze with no major difficulty but overt behavioural phenotype*
2	Traverse the maze with or without pauses, but missed entry
1	Traverse with errors
0	Failure to traverse (needs assistance)

*Behavioural phenotypes included low head carriage, crouching when walking through gateways, self-spooking, stumbling, circling or a reluctance to walk in and around shadows or across the drainpipe, contact with or failure to avoid obstacles

3.5 *In vivo* quantitative neuroimaging

Computed tomography (CT) scans were performed every 2 months on animals who received intracranial gene therapy. Sheep were fasted overnight. Anaesthesia was induced with a single intravenous injection of a mixture of diazepam (0.5 mg/kg LW) and ketamine (10 mg/kg LW). The anaesthetised sheep was then loaded into the CT scanning stretcher in the sternal recumbency position, with the feet tucked under the body. Coronal slices 1 mm thick were scanned at 5-mm intervals, 120 kV, 160 mA, 2 s on a GE ProSpeed CT Scanner (GE Healthcare, Hyogo, Japan) and intracranial volumes were determined by the Cavalieri method from the areas of each slice using STAR (Sheep Tomogram Analysis Routines) software (version 3.9; Biomathematics and Statistics Scotland (BioSS), Dundee Scotland, and Scottish Agricultural College (SAC), Perth, UK). Intracranial volumes from the experimental animals were then compared with historical cohorts of untreated affected and heterozygous control sheep of both genotypes.

Magnetic resonance imaging (MRI) was performed in collaboration with Dr. Tracy Melzer, at the NZ Brain Research Institute. Sheep were anaesthetised with higher doses of diazepam (1 mg/kg LW) and ketamine (15 mg/kg LW) delivered intravenously, loaded in the supine position into the 3 Tesla HDx MRI scanner (General Electric, Fairfield, Connecticut, USA) and scanned.

3.6 Ophthalmology and electroretinography

Ophthalmic examinations were performed on the treated sheep by an independent veterinary ophthalmologist (Dr. Steve Heap, McMaster and Heap Veterinary Practice, Christchurch, NZ) who was blinded to treatment. Pupils were dilated with a short acting mydriatic agent (Mydriacyl, tropicamide 1%; Alcon NZ Ltd) 30 min prior to indirect ophthalmoscopy with a wireless indirect headset and a hand held lens.

Electroretingraphic (ERG) and funduscopic techniques to monitor disease-associated loss of vision longitudinally were developed by Katharina Russell (Lincoln University) as part of her PhD studies. Both techniques were performed on treated sheep at 27 months of age. Pupils were dilated 30 min prior to ERG with Mydriacyl and 15 min later, sheep were sedated with an intravenous injection of diazepam (0.1 mg/kg) and ketamine (10 mg/kg). The trachea was intubated and oxygen was delivered through a closed circuit anaesthetic machine. Anaesthesia was maintained using 1-4% isoflurane. Each animal was laid in lateral recumbency and its eyelids retracted with a lid speculum. Two subdermal electrodes (Eickemeyer Veterinary Equipment Inc, Tuttlingen, Germany) were placed on the sheep's head; the first (ground) overlying the occipital tuberosity and the second reference electrode 1 cm caudal to the lateral canthus of the eye. A gold-plated corneal contact lens was placed on the cornea with sterile saline solution. All preparations were conducted in ambient lighting.

Photopic (cone) responses were examined first. A light stimulator (Eickemeyer) was held 2 cm from the eye and flashed 4 times at 0.8-sec intervals. The light-adapted ERG waveform, an average of 4 responses, was recorded on the provided software (Eickemeyer). The sheep was then dark-adapted for 5 min, with scotopic (rod) recordings taken at the start and completion of this adaptation. The ERG was then repeated on the opposite eye. ERG waveforms in all recordings were evaluated, and the amplitudes and latencies of the a- and b-waves measured as part of Katharina Russell's doctorate studies.

Fundus appearance was documented using a ClearView digital fundus camera (Eickemeyer) with images archived on the Optibrand ClearView Optical Imaging System (Eickemeyer).

3.7 Euthanasia and tissue collection

Sheep for neuropathological analyses were euthanized by penetrating captive bolt stunning between cervical vertebrae C1 and C2 followed by immediate exsanguination, and brain perfusion fixation performed as before via one of the carotid arteries with 10% formalin in 0.9% NaCl, pH 7.4, after the blood was first cleared with 0.9% NaCl at 37 ^{o}C (Oswald *et al*., 2005). The brains were removed intact, bisected at the sagittal midline and left in fixative (10% formalin) for a further 7 days. Fixed brains

were then equilibrated in cryoprotective solution (10% ethylene glycol, 20% sucrose in 0.9% NaCl) at 4°C for 5 days and stored frozen at -80 °C until they were sectioned. Sequential 50 µm sagittal brain sections were cut through the medio-lateral extent of one hemisphere using a freezing sliding microtome (MICROM International, Walldorf, Germany). Sections were collected, one per well, into 96-well plates containing cryopreservative (30% ethylene glycol, 15% sucrose and 0.05% sodium azide in phosphate buffered saline, pH 7.4) and stored at -20 °C until required.

3.8 Histology and immunohistochemical methods

For Nissl and Luxol fast blue (LFB) histological staining, formalin fixed sagittal brain sections (from mediolateral levels 2 – 5, see Figure 4.1) were mounted in a solution of 0.5% gelatine and 0.05% chromium potassium sulphate on glass slides and air-dried overnight. Mounted slides were then dehydrated through a series of ethanol dilutions and cleared in xylene. One set of sections was rehydrated through the ethanol gradient, equilibrated in water and then incubated for 10 min in a pre-warmed Nissl staining solution (0.05% cresyl violet acetate C5042; Sigma-Aldrich, St. Louis, MO, USA, 0.05% acetic acid in water) at 37 °C and rinsed in water. They were then dehydrated through the ethanol gradient, and cleared in xylene prior to coverslipping with DPX (BDH, Poole, England). Another set of sections was equilibrated in ethanol, incubated for 24 h at 40 °C in an air-tight container in LFB staining solution (0.1% Solvent Blue 38, S3382; Sigma-Aldrich, 95% ethanol), rinsed in 70% ethanol for 3 min, incubated in 0.05% lithium carbonate, 10 min, taken through the alcohol gradient back to xylene, then mounted in DPX.

For immunohistochemistry, the primary antibodies used were rabbit anti-sheep CLN5 and CLN6 (both 1:500, polyclonal; Dr. Stephanie Hughes, University of Otago, Dunedin, NZ) to detect endogenous and exogenous protein; rabbit anti-cow glial fibrillary acidic protein (GFAP, 1:5000; Z0334, polyclonal; Dako, Ely, England) to detect astrocytes; a biotinylated form of the α-D-galactose specific isolectin I-B4 from *Griffonia simplicifolia* (GSB4, 1:500; B-1205; Vector Laboratories, Burlingame, CA, USA) for microglia and mouse anti- PSA-NCAM (1:1000; MAB5324, monoclonal; Chemicon, Temecula, CA, USA) for newly generated and migrating cells. All antibodies were diluted in 10% Gibco normal goat serum (NGS) (Life Technologies NZ Ltd, Auckland, NZ) in phosphate buffered saline (PBS), pH 7.4, containing 0.3% Triton X-100 (PBST).

Routine immunohistochemical detection was carried out using an avidin-biotin amplification system. For each antigen, sections from all ages and levels were processed simultaneously as a batch. All steps were performed on a rocking platform, and were followed by three 10 min washes with PBS. Test cryosections were thawed and blocked for 30 min with either 1% H_2O_2 in PBS (anti-CLN5, CLN6 and GFAP) or 1% H_2O_2 in 50% methanol in PBS (anti-PSA-NCAM and GSB4), 30 min, at room temperature. Sections were then pre-incubated in 15% NGS in PBST prior to overnight incubation at

4 °C in primary antibody. Immunoreactivity was detected using the appropriate secondary antibodies; biotin-conjugated affinity purified IgM (1:500; AP500B; Chemicon) for PSA-NCAM and biotinylated goat anti-rabbit IgG (1:1000; B7389; Sigma-Aldrich) for all other antigens for 2 h at room temperature, followed by ExtrAvidin peroxidase (1:1000; E2886; Sigma-Aldrich) for 2 h at room temperature. Staining was visualized by incubation in 0.05% (0.5 mg/ml) 3, 3'-diaminobenzadine (DAB; D5637; Sigma-Aldrich) and 0.01% H_2O_2 in PBS. The optimal incubation period with DAB substrate solution was tested for each antigen (Table 3.3) and negative control sections, in which either the primary or secondary antibody was omitted, were included in all staining runs. No immunostaining was observed in any of the negative control sections. Sections were mounted in a solution of 0.5% gelatine and 0.05% chromium potassium sulphate on glass slides, air dried, dehydrated in 100% ethanol, cleared in xylene and coverslips mounted with DPX. Further unstained sections were mounted as above, air dried and coverslipped with glycerol for observation of fluorescent storage body accumulation.

Table 3.3 Primary antibodies, with associated DAB incubation times

Primary antibody	Concentration	Host	Supplier	DAB incubation time (min)
CLN5	1:500	Rabbit	In-house	7
CLN6	1:250 - 1:500	Rabbit	In-house	7
GFAP	1:5000	Rabbit	Dako	7
GSB4	1:500		Vector	5
PSA-NCAM	1:1000	Mouse	Chemicon	3

3.9 Microscopy

Digital images of CLN5, CLN6, GFAP, GSB4, Nissl and PSA-NCAM stained sections were obtained with a Nikon Digital Sight DSFi1 camera attached to a Nikon Eclipse 50i model microscope (Nikon Instruments Inc., Tokyo, Japan) utilising NIS-Elements Software (Nikon Instruments). A second set of images, representative of the upper and lower layers of selected cortical regions, were acquired with the x20 objective for GSB4 stained sections and for sections immunostained for GFAP. The microscope lamp intensities, exposure times, condenser aperture settings, video camera set-up and calibration, and use of neutral density filters were kept constant for capturing all images of a particular immunostain. Digital images were saved as .tif and .jpg files and figures and photomontages prepared in Corel Photopaint 12 (Corel Co., Ontario, Canada). For GSB4 and GFAP threshold analysis, digital images (RGB, .jpg, three different fields per section per animal) were analysed with the public domain Image J programme (version 1.28u; National Institutes of Health (NIH), Bethesda, MD, USA). Red bandwidth filters were applied for the DAB images, and the number

of pixels with brightness levels above a set threshold was expressed as a percentage of the total pixel area. Threshold values for images of a particular immunostain at the same magnification were set so that positively stained structures at low reactivity were still selected, but not background staining in regions of high reactivity. Data were transferred to Microsoft Excel 2013 (Microsoft Corp., Seattle, WA, USA) for analyses.

Cortical and commissural thickness in Nissl and LFB stained sections, respectively, were measured with the x4 objective on a Nikon Eclipse 50i microscope using NIS-Elements Software (Nikon). Perpendicular distances were measured from the surface of the pia mater to the boundary between the grey and white matter in the cerebral cortex. In the cerebellum, the cortical thickness of the anterior lobe at sagittal level 4 was measured from the pial surface to the granular boundary with the white matter. The thickness of the corpus callosum at sagittal level 5 was measured. At least 25 measurements were taken at regular intervals for each region.

Unstained sections were examined using a Nikon Eclipse 50i microscope, fitted with a 450-490 excitation/510 emission filter set for observation of fluorescent storage body accumulation.

3.10 Statistics

All statistical analysis was performed in Microsoft Excel 2000. For the neuropathological studies, means (% area stained, cortical/commissural thickness) and the corresponding standard errors of the mean (SEM) were computed for each brain region for each animal. These means were used in a one way analysis of variance (ANOVA) to test each region separately for differences between normal and affected sheep, and between upper and lower cortical layers within affected sheep. A *P*-value less than 0.05 was considered statistically significant.

For the gene therapy efficacy and behavioural studies, quantitative data are presented as means $\pm$ SEM. ANOVA was performed for each time interval separately for the maze data to determine whether transit times varied between the cohorts. Mean transit times were then compared between cohorts using the Student's *t*-test. Differences were considered significant if $P \leq 0.05$.

3.11 Special methods

Special methods relating to particular experiments are included in the appropriate chapters.

Chapter 4

Comparative Neuropathology

4.1 Introduction

Detailed quantitative information about the neuropathological changes in human NCL is limited. Typically qualitative histological studies have been restricted to end-stage *post mortem* material, and are often based on small samples from non-specific regions of the brain. These describe the severe gross atrophy of the brain, widespread neuroinflammation and characteristic storage body accumulation within remaining neurons and neuroglial cells (Haltia, 2003; Tyynelä *et al*., 2004; Bennett & Rakheja, 2013). Very few life-threatening pathological changes are reported outside of the brain. However these studies provide little analysis on the morphological evolution of the condition, namely any causal relationships between these end-stage phenomena and pathogenic changes occurring during disease progression. If therapies are to be delivered when and to where they can be most effective, there is a need to study the progressive pathological changes that lead up to the end stages of the disease.

Animal models provide an invaluable resource for characterising the temporal and spatial neuropathological cascades in NCL. Naturally occurring forms of NCL in sheep are particularly useful, because their large complex brain closely resembles that of humans and the prolonged disease progression faithfully reflects the human pathology. Systematic studies of ovine CLN6 in New Zealand South Hampshire sheep have provided a detailed quantitative and qualitative assessment of storage body accumulation, glial activation and cortical atrophy in affected sheep brains from pre-natal to advanced disease stages (Oswald *et al*., 2005, 2008; Kay *et al*., 2006). Affected newborns are clinically normal but develop obvious clinical symptoms resembling human NCL from 10 – 14 months of age. Sheep with CLN6 disease rarely survive past 24 months. Although prenatal lysosomal storage has been reported in affected sheep (Jolly *et al*., 1989), this is sparse but evenly distributed throughout the brain at birth (Oswald *et al*., 2005; Kay *et al*., 2006). In contrast, early reactive and neurodegenerative changes are regionally selective. Prenatal astrocytic activation and progressive perinatal transformation of microglia to brain macrophages precedes neurodegeneration in the ovine CLN6 sheep model (Oswald *et al*., 2005; Kay *et al*., 2006). Localised reactive changes commence from specific foci in certain superficial laminae of the neocortex, which are predictive of those regions that subsequently degenerate. Importantly for therapeutic consideration, these pathological changes are occurring well before a clinical phenotype is observed in affected animals.

Subsequent studies describing pathogenesis in several murine NCL disease models (Pontikis *et al*., 2005; Weimer *et al*., 2006; Kielar *et al*., 2007; Partanen *et al*., 2008; Macauley *et al*., 2009; von Schantz *et al*., 2009; Kuronen *et al*., 2012; Schmiedt *et al*., 2012) revealed a similar pathological phenotype with generalised thinning of the cortex and widespread regional atrophy, pronounced astrocytosis and microglial activation. However a consistent finding from the murine studies was the early vulnerability of the thalamocortical system, neuronal loss commencing in thalamic relay nuclei and subsequently within the corresponding cortical regions. The reason why the thalamus is pathologically targeted early in murine NCLs is not clear (Cooper 2006). However, in marked contrast to the other murine forms, cortical neuron loss preceded that in the thalamus in CLN5 mutant mice (von Schantz *et al*., 2009), which correlates with the large animal and human NCLs in which cortical lesions are foremost (Mayhew *et al*., 1985; Jolly *et al*., 1989; Palmer *et al*., 2011). Also, the overt atrophy seen in ovine and human NCLs (Jolly *et al*., 1989; Oswald *et al*., 2001; Haltia, 2003; Palmer *et al*., 2011) is not nearly so apparent in most NCL murine models (Cooper *et al*., 2006; Cooper, 2010), with the exception of the CLN2 knockout mice (Sleat *et al*., 2004). These findings highlight the discrepancies between the mouse and human NCLs and emphasise the translational usefulness of larger animal NCL models with their more complex human-like CNS.

A large animal model of *CLN5* deficiency has been described in New Zealand Borderdale sheep (Jolly *et al*., 2002; Frugier *et al*., 2008). Specific lysosomal storage of subunit c of mitochondrial ATP synthase has been shown in these sheep and preliminary studies indicate the clinical disease and neuropathological progression closely follows that seen in CLN6 South Hampshire sheep (Jolly *et al*., 2002; Frugier *et al*., 2008). Clinical onset is slightly earlier in the ovine CLN5 model, being apparent from 10 -11 months of age, and affected sheep reach a humane endpoint between 22 - 24 months of age. Whilst the CLN6 disease results from a defective endoplasmic reticulum-resident transmembrane protein (Mole *et al*., 2004; Heine *et al*., 2004), the *CLN5* gene product is a soluble lysosomal glycoprotein which traffics via the mannose-6-phosphate pathway (Holmberg *et al*., 2004; Sleat *et al*., 2005, 2007) and this form of NCL is deemed to be a strong candidate for gene therapy. *In vitro* studies showed that lentiviral-mediated cross-correction of *CLN5* deficient neurons is possible (Hughes *et al*., 2014a) and gene therapy approaches are more likely to succeed if targeted to where the pathology is first apparent. This chapter provides a comparative description and quantitative assessment of the neuropathological cascade in ovine CLN5 and CLN6 brains during disease progression, whilst determining temporal windows in which to administer therapeutic intervention before the cascade becomes fatally damaging.

4.2 Materials and Methods

4.2.1 Animals

The breeding, maintenance and diagnosis of the CLN5 and CLN6 sheep flocks are described in Chapter 3. A series of brains from CLN5 affected sheep aged 1 day (newborn), and 4, 6, 9, 12, 15, 18 and 24 months, were used together with age-matched control sheep brains. In parallel, brains from CLN6 affected sheep aged 2, 6, 9, 12, 18 and 24 were processed for comparative analysis and to replicate the findings of Oswald *et al.* (2005). At each age, one control and one to four affected sheep brains of each genotype were selected for analysis.

4.2.2 Tissue preparation and sectioning

Sheep were killed by exsanguination, the brains perfusion fixed *in situ* and processed as described in Section 3.7. Each brain was weighed, post-fixed, bisected down the sagittal midline, equilibrated in cryoprotectant and stored at -80 °C until sectioning.

Subsequently, 50 µm serial sagittal sections were cut through the medio-lateral extent of the left hemisphere (Section 3.7) and cryopreserved in 96-well plates at -20 °C. For all subsequent analyses, matched series of sections from each animal were selected at five medio-lateral levels (Figure 4.1), as previously described (Oswald *et al.*, 2005). Digital images of the tissue blocks, taken during sectioning, aided in the matching of sections to the five sagittal levels. The CNS regions, with corresponding sagittal levels that were used in the quantitative image analyses, are summarised in Table 4.1.

4.2.3 Histological analysis, quantification and statistics

Histological and immunohistological staining was carried out as described in Section 3.8. For Nissl staining, sections from two to four individual CLN5 affected sheep brains were processed at each timepoint to test for inter-animal variation. Sequential sections from one brain of each genotype at each age were then used for all subsequent immunohistochemical and lectin histochemical studies. Cortical thickness measurements, thresholding image analysis methods and statistical analysis are described in Sections 3.9– 3.10. All histological processing and subsequent analyses were performed with no prior knowledge of genotype.

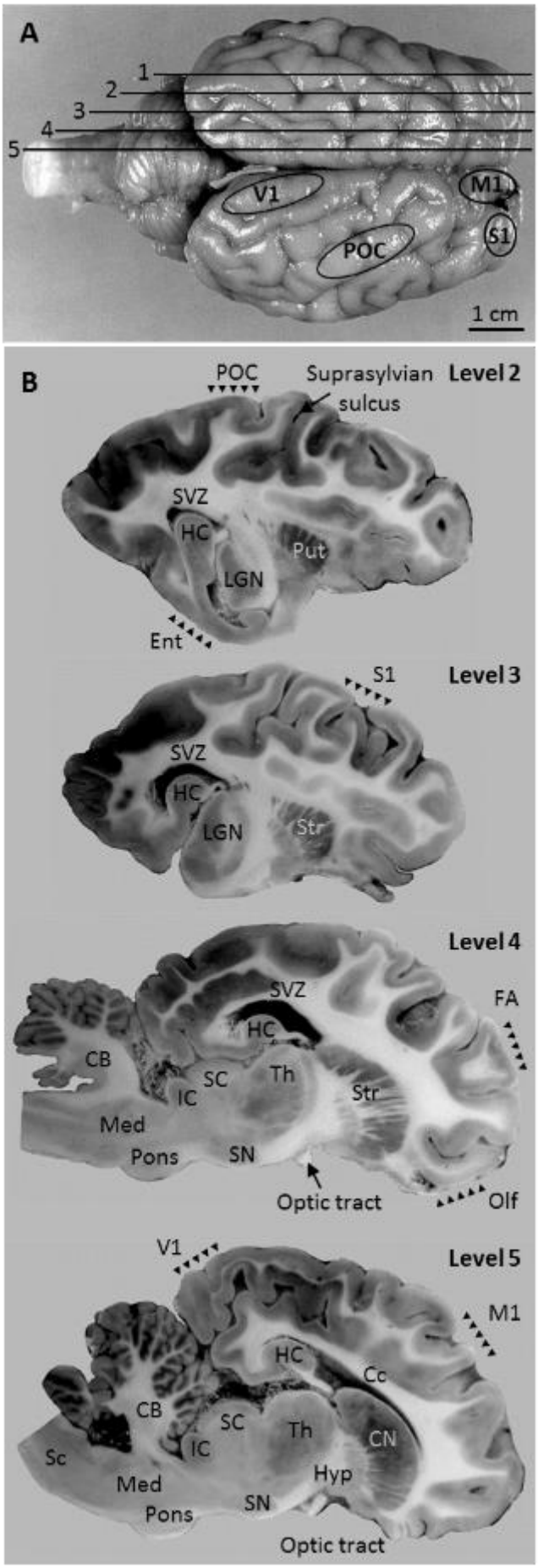

Figure 4.1 Anatomical structure of the normal sheep brain (adapted from Oswald *et al*., 2005)

A. Dorsal view of a brain from a one year old control sheep. Sagittal levels (1-5) from which serial sections were taken for analysis are shown.

B. Representative sagittal levels 2, 3, 4 and 5 are depicted, with the key brain regions under study indicated.

Abbreviations: **CB** cerebellum; **Cc** corpus callosum; **CN** caudate nucleus; **Ent** entorhinal cortex; **FA** frontal association cortex; **HC** hippocampal formation; **Hyp** hypothalamus; **IC,** inferior colliculus; **LGN** lateral geniculate nucleus; **M1** primary motor cortex; **Med** medulla; **Olf** olfactory cortex; **opt** optic tract; **POC** parieto-occipital cortex; **Put** putamen; **S1** somatosensory cortex; **Sc** spinal cord; **SC** superior colliculus; **SN** substantia nigra; **Str** striatum; **SVZ** subventricular zone; **Th** thalamus; **V1** primary visual cortex.

Table 4.1 CNS regions and sagittal section levels in which they were investigated (adapted from Oswald, 2004)

Level		1	2	3	4	5
	Symbol	Lateral				Medial
Hippocampus	HC	**	***	**	**	*
Entorhinal cortex	Ent	**	***	*		
Parieto-occipital cortex	POC	**	***	*		
Primary somatosensory cortex	S1		**	***		
Lateral geniculate nucleus	LGN		**	***		
Striatum	Str			***		
Cerebellar cortex	CB		*	**	***	**
Frontal association cortex	FA			*	***	*
Optic tract	Opt			*	***	*
Olfactory cortex	Olf			*	***	
Superior colliculus	SC				***	**
Corpus callosum	Cc				**	***
Thalamus	Th				**	***
Caudate nucleus	CN				**	***
Primary visual cortex	V1					***
Primary motor cortex	M1					***

4.3 Results

4.3.1 General organisation and development of the ovine NCL brain

Normal sheep brains grew rapidly from birth to reach an early peak at 4 months. After a 3% decline in mean normal brain mass at 6 months, brain growth recommenced, approaching a plateau at 12 months and mature weight by 24 months (Table 4.2). At birth, affected sheep brains of both genotypes appeared to be normally developed and although divergent in weight from the normal newborn brain, this difference was not significant. The brain masses of CLN5 and CLN6 affected sheep also peaked at 4 months of age, falling behind normal controls at this stage by 11% and 19% respectively, marking the start of progressive brain atrophy. This decline was more obvious in the CLN6 affected brain which was reduced to 69% and 54% of the normal brain weight by 12 and 24 months of age, respectively (Table 4.2). In contrast, the CLN5 affected brain mass changes were less overt, plateauing on average at 79.3 $\pm$ 0.8 g from 6 to 12 months, however this converged to 58% of normal brain weight by 24 months of age (Table 4.2).

Table 4.2 Mean brain weight of normal and affected sheep from birth to 24 months of age

Age (m)	Normal (g)	CLN5-/- (g)	CLN6-/- (g)	CLN5 / Normal	CLN6 / Normal
0 – 1	58.0 $\pm$ 1.7* (*n*† = 11)	55.5 $\pm$ 1.4 (*n* = 2)	52.4 $\pm$ 3.2 (*n* = 9)	96%	90%
2	74.1 $\pm$ 2.5 (*n* = 5)		70.4 $\pm$ 2.3 (*n* = 7)		95%
4	92.1 $\pm$ 3.7 (*n* = 13)	81.8 $\pm$ 0.7 (*n* = 2)	74.7 $\pm$ 3.3 (*n* = 7)	89%	81%
6	89.2 $\pm$ 1.7 (*n* = 17)	79.5 $\pm$ 2.2 (*n* = 5)	70.4 $\pm$ 3.6 (*n* = 6)	89%	79%
9	92.2 $\pm$ 2.2 (*n* = 9)	78.4 $\pm$ 1.6 (*n* = 4)	68.2 $\pm$ 2.1 (*n* = 5)	85%	74%
12	98.2 $\pm$ 1.6 (*n* = 16)	79.5 $\pm$ 1.1 (*n* = 16)	67.7 $\pm$ 5.6 (*n* = 5)	81%	69%
15		76.1 $\pm$ 1.8 (*n* = 7)	66.2 $\pm$ 1.9 (*n* = 8)		
18	98.1 $\pm$ 1.1 (*n* = 16)	71.2 $\pm$ 1.5 (*n* = 13)	66.0 $\pm$ 2.4 (*n* = 18)	73%	67%
24	106.1 $\pm$ 1.5 (*n* = 17)	62.0 $\pm$ 1.0 (*n* = 5)	57.5 $\pm$ 2.5 (*n* = 8)	58%	54%

* Standard error of the mean (SEM)
† Number of brains collected. One to four brains of each category was used for subsequent analysis
No brains were available to be analysed at those ages where values are missing

By 6 months, the disparate effect of the diseases on the cerebral hemispheres was macroscopically apparent, with obvious volume loss in the parietal and occipital lobes, medial and caudal to the suprasylvian sulcus, of both CLN5 and CLN6 affected brains. By 18 months, gross atrophy of the cerebral hemispheres, with concomitant dorsoventrally flattened, narrowed gyri and widened sulci, was evident (Figure 4.2). Whilst the CLN6 affected cerebral cortex was more severely shrunken overall, the CLN5 affected frontal lobe, medial and rostral to the pseudosylvian sulcus, was discernibly more atrophied than that in the CLN6 affected brain. In contrast to the marked cerebral

atrophy, the cerebellum and subcortical structures of both genotypes retained normal appearance, even at 24 months.

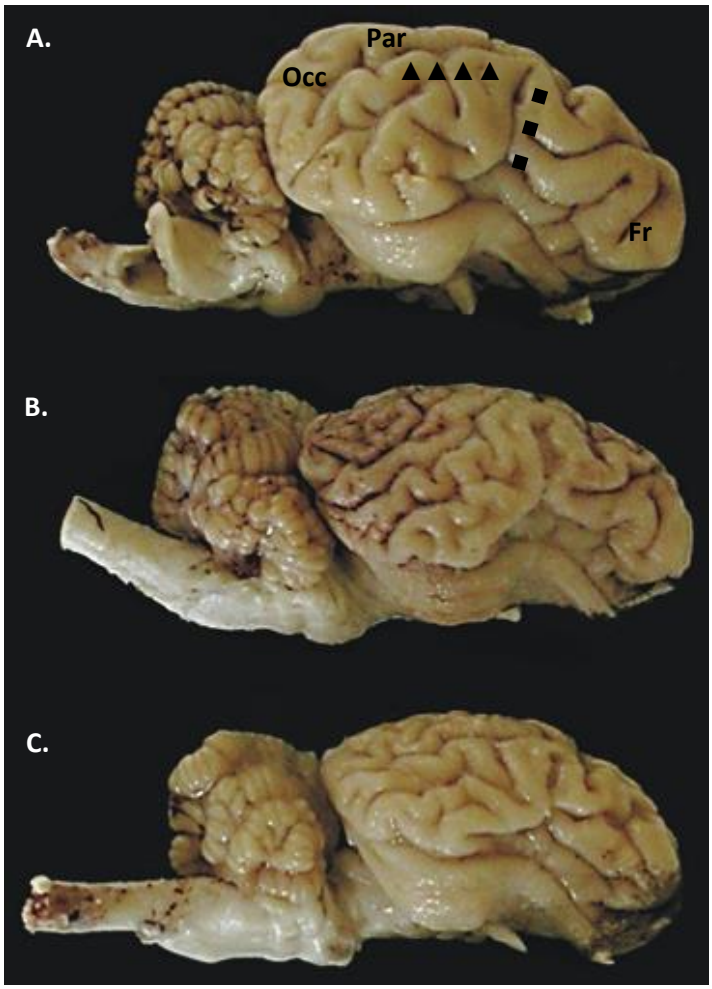

Figure 4.2 Lateral view of the normal and affected sheep brain
Perfused brains from **A.** a 19.4 month old normal Coopworth sheep, **B.** a 19.2 month old CLN5 affected Borderdale and **C.** a 19.3 month old CLN6 affected South Hampshire. Note the marked atrophy of the diseased cerebral hemispheres and the relative sparing of the cerebella. Brain weights were 99, 74.86 and 60.75 g respectively. The suprasylvian sulcus (▲), pseudosylvian sulcus (■), parietal (Par), occipital (Occ) and frontal (Fr) lobes are indicated.

4.3.2 Regional atrophy and cortical thinning

The unifying pathological hallmark of NCL is severe neurodegeneration. In order to quantify this, Nissl stained sections from CLN5 and CLN6 diseased sheep brains were analysed for neuronal cytoarchitecture and by measurement of cortical thickness, to compare spatiotemporal changes with disease progression (Figure 4.3). Distinct neuronal laminae were evident across the normal cortical mantle (Figure 4.4), with pronounced thickening of the normal cortical layers over time to reach maturity by 12 months (Figure 4.5). In contrast, the NCL affected ovine cerebral cortices never attained full maturity; instead regionally specific cortical thinning and neurodegeneration commenced. Preceding or coinciding with the neuronal loss was perturbation of the cytoarchitectonic layers and the progressive appearance of clusters of densely packed cellular aggregates at the layer I/II boundary throughout the affected cerebral cortex of both genotypes. Control sheep brains did not contain these cellular aggregates, except in the entorhinal cortex. In all

affected cortical regions, the neuronal atrophy was more pronounced in the upper layers (II-III) with the lower cortical layers (V-VI) better preserved, especially the lamina V pyramidal cells.

It was previously reported that the cytoarchitecture of the cerebellum, hippocampus and all cortical regions of the CLN6 affected brains appear normal at birth (Oswald *et al*., 2005; Kay *et al*., 2006). However, even by the earliest age in the current study (2 months), loss of layer definition was observed in the CLN6 affected primary visual and parieto-occipital regions with aggregation of cells at the I/II laminar boundary (Figure 4.4). These degenerative changes spread from the visual and parieto-occipital cortices to the somatosensory cortex at 6 months, reaching the motor cortex by 12 months, and the entire cortical mantle by 18 months, corroborating the findings of Oswald *et al* (2005). Cortical thickness measurements demonstrated that the rate of active thinning differed between the regions but followed a similar pattern (Figure 4.5), to the cytoarchitectural changes albeit delayed. The visual and parieto-occipital regions were affected most and earliest (from 2 months). The thickness of the CLN6 affected somatosensory cortex increased comparatively normally up to 9 months, delayed atrophy commenced in the entorhinal and frontal cortices from 12 months, and the motor cortex was relatively spared until 18 months of age. By 24 months, significant atrophy was seen across the CLN6 affected cerebral cortex with the primary visual, entorhinal, and primary motor areas reduced to 37%, 56%, and 61% of the respective normal thicknesses.

The CLN5 affected brain was also normal in appearance at birth, except for a mild disturbance in the laminar architecture and small cellular clusters at the layer I/II interface of the primary visual cortex. The same clusters and loss of layer definition reached the parieto-occipital and somatosensory CLN5 cortices by 4 months of age. Degenerative changes in the CLN5 entorhinal, frontal association and motor cortices were detected from 6 - 9 months, some 3 - 6 months earlier than in the CLN6 affected brain. However, despite the earlier cortical laminar reorganisation in the CLN5 brain, the affected brains of both genotypes reached the same pathological endpoint at 24 months of age with obvious layer I/II cellular aggregates and few cortical neurons remaining (Figure 4.4).

As in the CLN6 model, active thinning in the CLN5 affected brain became apparent at different ages in different cortical regions. There was a near linear decline in the visual, parieto-occipital and somatosensory cortices from birth. Atrophy became apparent in the frontal cortex from 9 months and was not apparent in the entorhinal and motor cortex until 15 months (Figure 4.5). The neurodegenerative cascade began earlier in most regions of the CLN5 affected brain than in the CLN6 affected brain, however, despite this earlier onset of atrophy, cortical thickness measurements from CLN5 and CLN6 affected sheep brains converged, and were very similar by 24 months (Figure 4.5).

The major point of difference was seen in the cortices of the frontal lobe. At 24 months there was an 11% greater reduction in the thickness of the CLN5 frontal association cortex compared to that of the

CLN6 brain ($P \leq 0.0001$). Additionally the motor cortex of the CLN5 affected sheep brain shrank dramatically from 15 months of age to be 59% that of normal thickness by 18 months, a 20% greater reduction than in the same region in an age-matched CLN6 affected animals. This discrepancy was still statistically significant (P = 0.0006) at 24 months when the CLN5 and CLN6 motor cortex thicknesses were reduced to 54% and 61% of normal respectively (Figure 4.4).

Progressive atrophic changes in the cortical grey matter were accompanied by white matter tract changes. Occipital white matter loss with disease progression was macroscopically overt (Figure 4.3). The thickness of the corpus callosum in normal brains increased to plateau at 1323 $\pm$ 30 µm (n = 7) by 18 - 24 months, whereas it remained relatively unchanged in NCL affected sheep throughout postnatal development (CLN6 affected 724 $\pm$ 30 µm (n = 5); CLN5 affected 756 $\pm$ 18 µm (n = 8)).

The subcortical structures were remarkably preserved in sharp contrast to the gross atrophy of the cortex in both ovine disease models. Nissl staining revealed no overt depletion of cells in the affected thalamic nuclei, colliculi or striatum and neuronal populations in these resembled those seen in control sections. Cerebellar cortical thickness was also relatively constant from birth to 24 months in normal (513 $\pm$ 5 µm; n = 10), CLN5 affected (511 $\pm$ 5 µm; n = 18) and CLN6 affected (495 $\pm$ 7 µm; n = 5) sheep brains, demonstrating the relative sparing of the cerebellum in ovine CLN5 and CLN6 NCLs (Figure 4.5).

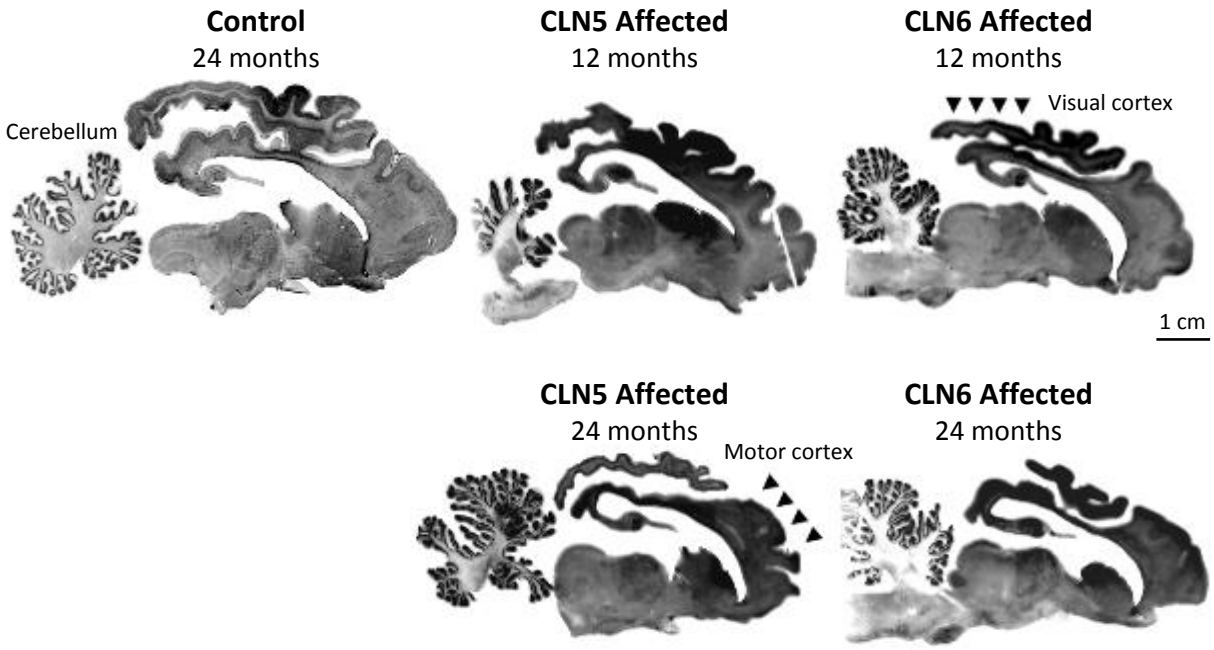

Figure 4.3 Progressive cortical atrophy in CLN5 and CLN6 affected sheep
Nissl stained sagittal sections (Level 5) show gross atrophy of the cerebral cortex in CLN5 and CLN6 affected sheep at 12 months, which is more pronounced at 24 months, especially in the visual cortex. The vulnerability of the motor cortex is also highlighted in CLN5 affected sheep. In contrast, the cerebellum is relatively spared in both disease models.

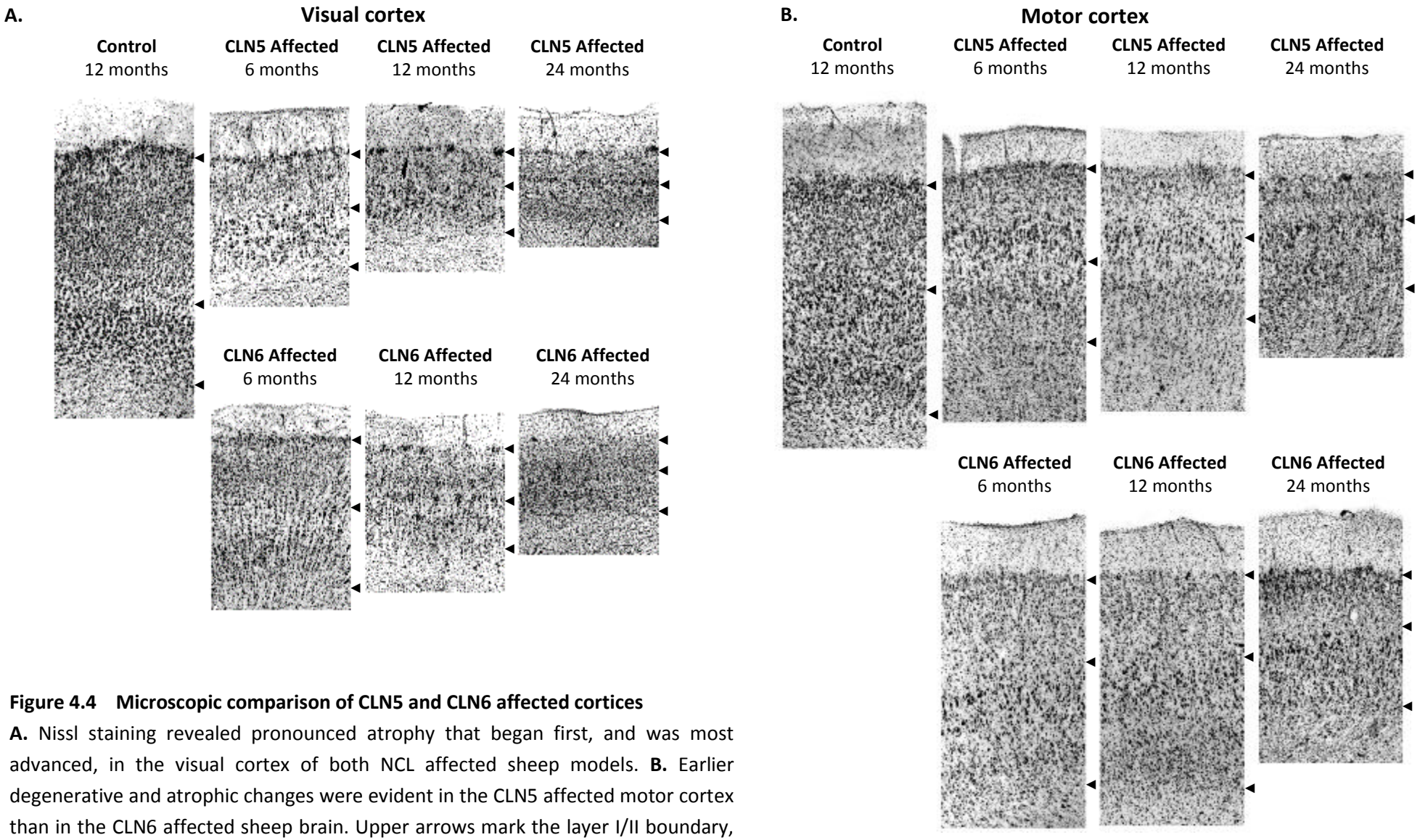

Figure 4.4 Microscopic comparison of CLN5 and CLN6 affected cortices

A. Nissl staining revealed pronounced atrophy that began first, and was most advanced, in the visual cortex of both NCL affected sheep models. **B.** Earlier degenerative and atrophic changes were evident in the CLN5 affected motor cortex than in the CLN6 affected sheep brain. Upper arrows mark the layer I/II boundary, the middle arrows indicate layer IV, and the lower arrows mark the layer VI/WM boundary. Scale bar represents 500 μm.

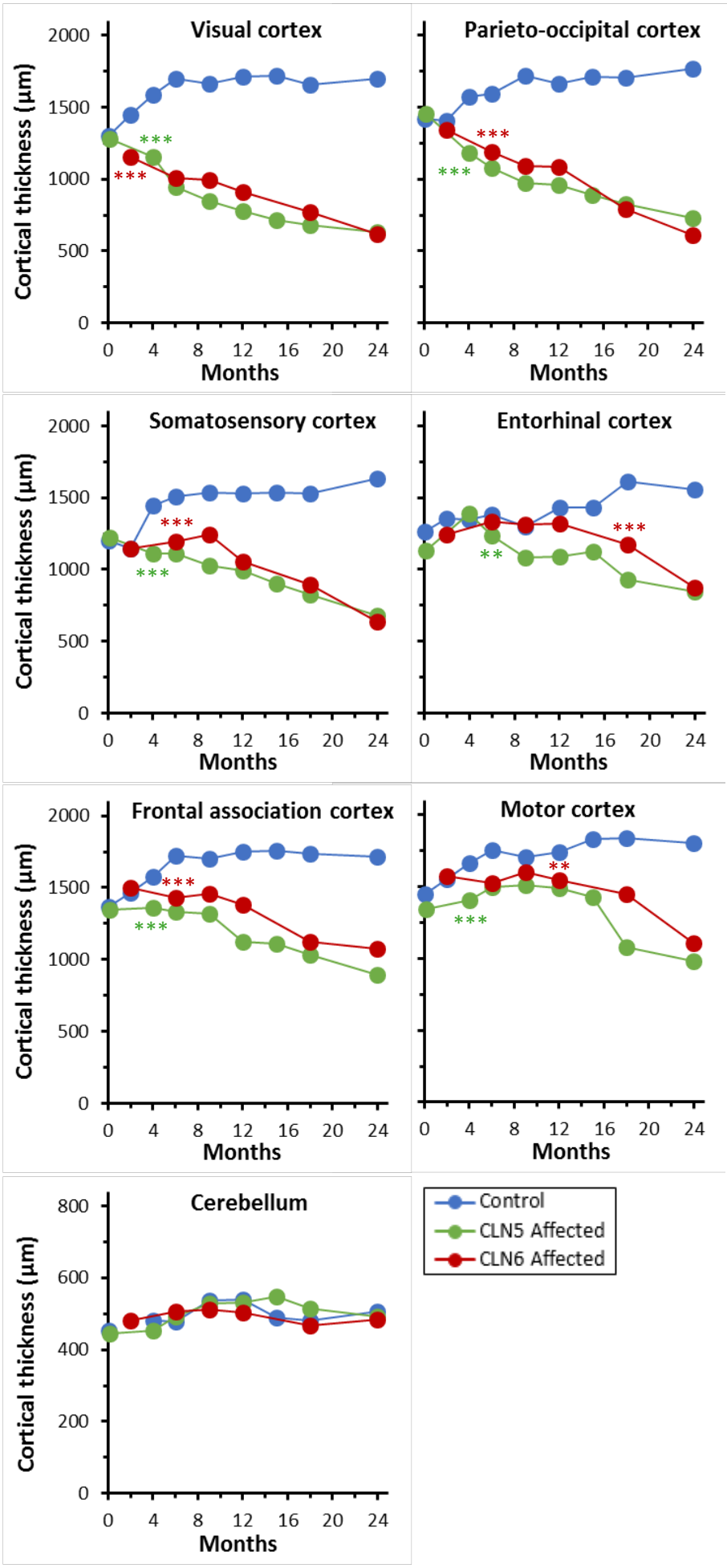

Figure 4.5 Quantitative assessment of the cortical thinning in CLN5 and CLN6 affected sheep brains

Cortical thickness measurements from Nissl stained brain sections revealed progressive thinning of the affected cortical mantle, but at various rates in different cortical regions. Compared with age-matched controls (blue), significant atrophy was first evident in the primary visual cortex in both disease models from 2 to 4 months of age and subsequently observed in the parieto-occipital and somatosensory cortices at 4 to 6 months. Earlier declines in the cortical thicknesses of most regions were evident in CLN5 affected brains (green) compared with the CLN6 affected brains (red). However in most regions, measurements converged for both genotypes by 24 months of age. At this age, only the CLN5 affected frontal association and motor cortices were statistically thinner than the same CLN6 affected regions ($P \leq 0.001$). Results are means of at least 25 measurements. Standard errors for each point are not displayed but were within 0.5 – 5.2% of the means. Due to the progressive nature of the disease, only the first ages from which difference between control and affected thicknesses become significant are indicated (** $P \leq 0.05$, *** $P \leq 0.001$).

4.3.3 Progressive glial activation

Because glial activation is proposed to play a central role in the pathogenesis of NCL, the glial cell response was assessed over disease progression by immunohistochemistry, using glial fibrillary acidic protein (GFAP) as an astrocytic marker and by GSB4 lectin histochemistry to detect microglia. Similarly to findings in CLN6 affected sheep, a prominent early response was detected with each of these markers in the CLN5 ovine model, which was at first restricted to individual laminae in the same cortical regions initially undergoing neurodegeneration, but which subsequently spread to involve all cortical laminae and subcortical regions (Figure 4.6 - Figure 4.11). Neither activated astrocytes nor microglia were detected in the cerebellum of either ovine NCL model, even at advanced disease.

4.3.3.1 Regional astrocytosis

Low-level GFAP reactivity was limited to protoplasmic astrocytes in lamina I adjacent to the pial surface or distributed evenly within the grey matter laminae)in the control brains at all ages (Figure 4.7). These had short, highly branched processes. More intense GFAP immunopositivity was seen in the white matter of control sheep, due to the presence of quiescent astrocytes along the white matter tracts. These either exhibited the typical stellate morphology or were associated with the capillary vasculature. In marked contrast, discrete foci of reactive hypertrophic astrocytes were present as early as birth in the pre-symptomatic CLN5 affected brains. Similarly to observations in perinatal CLN6 affected sheep (Oswald *et al*., 2005; Kay *et al*., 2006), this upregulation of GFAP immunoreactivity in the CLN5 affected brains was initially regionalised to the first areas to undergo neurodegeneration (the visual and parieto-occipital cortices), with significantly more activation in the superficial laminae (II and III) than the lower cortical layers ($P \leq 0.005$). A distinct band of hypertrophied activated astrocytes formed initially in these laminae. With age, reactive glia spread to form a dense network in affected brains of both genotypes throughout laminae II - VI as more cortical and subcortical regions became involved.

Quantitative thresholding image analysis demonstrated progressive astrocytosis occurring within the cortex of affected sheep of both genotypes (Figure 4.8). Whilst significant increases in GFAP immunoreactivity were most pronounced in the primary visual cortex of both disease models, there were some regional differences between them. Temporal plots of the percentage of GFAP immunopositivity showed subcortical regions and the visual and parieto-occipital cortices were largely uniformly affected between the two disease models. However staining intensity in the CLN5 affected motor cortex increased earlier than in the same region in the CLN6 affected brains (Figure 4.7). A band of hypertrophied astrocytes in laminae II-III of the CLN5 affected motor cortex was revealed at 6 months, whilst sparse activated cells were present only in the molecular layer I of the

age-matched CLN6 brain. Even at end-stage disease (24 months) GFAP immunoreactivity was considerably greater in the CLN5 than in the CLN6 affected motor cortex.

Figure 4.8 reveals an increase in GFAP immunoreactivity in the caudate nucleus and the lateral geniculate nucleus with age, which was representative of other subcortical structures. In particular, hypertrophic astrocytes were seen both macroscopically and microscopically in the CLN5 and CLN6 affected thalamus from 12 months of age (Figure 4.6). However this progressive activation of subcortical astrocytes was considerably more delayed than in the cortex with far fewer cells involved. Of interest too, the affected white matter was intensely stained at birth, but this dramatically declined with disease progression before increasing again at end-stage disease (Figure 4.8).

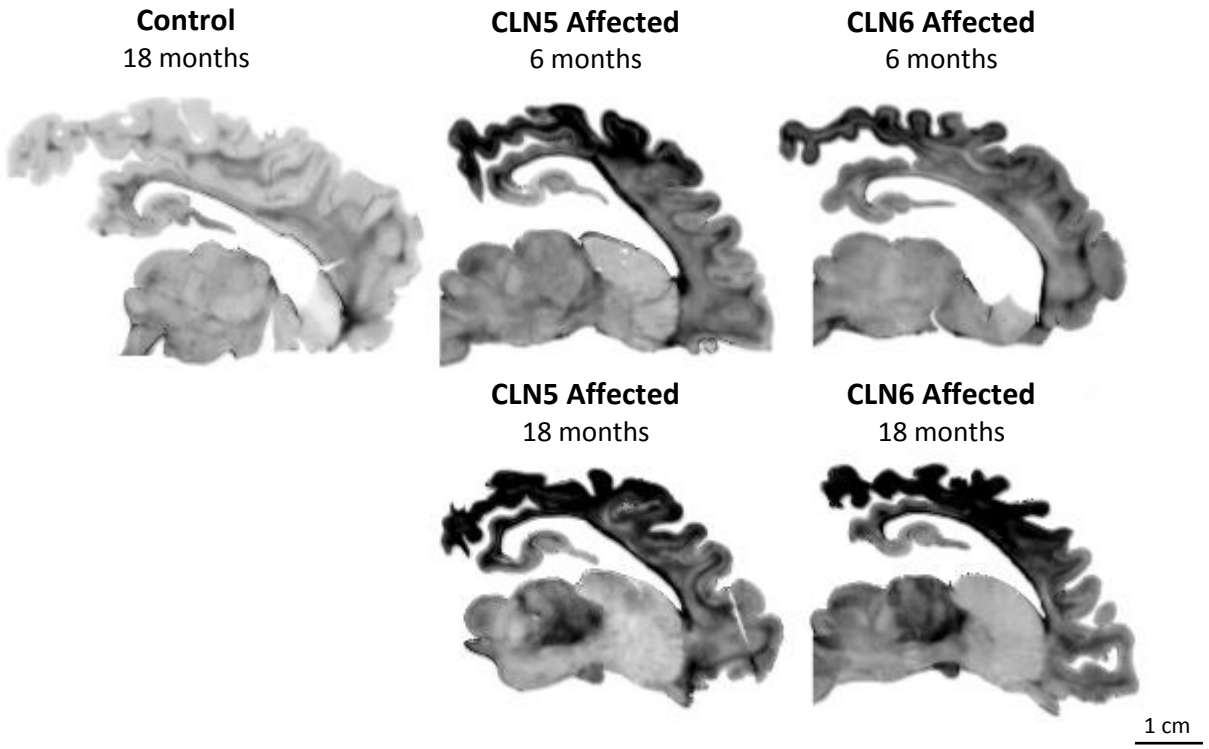

Figure 4.6 Comparative astrocytosis during ovine NCL disease progression
GFAP stained sagittal sections (Level 4/5) showing widespread and progressive activation of astrocytes in the NCL affected sheep brains with age. Note the increased activation in the CLN5 affected brain at 6 months and the delayed subcortical involvement in both ovine disease models.

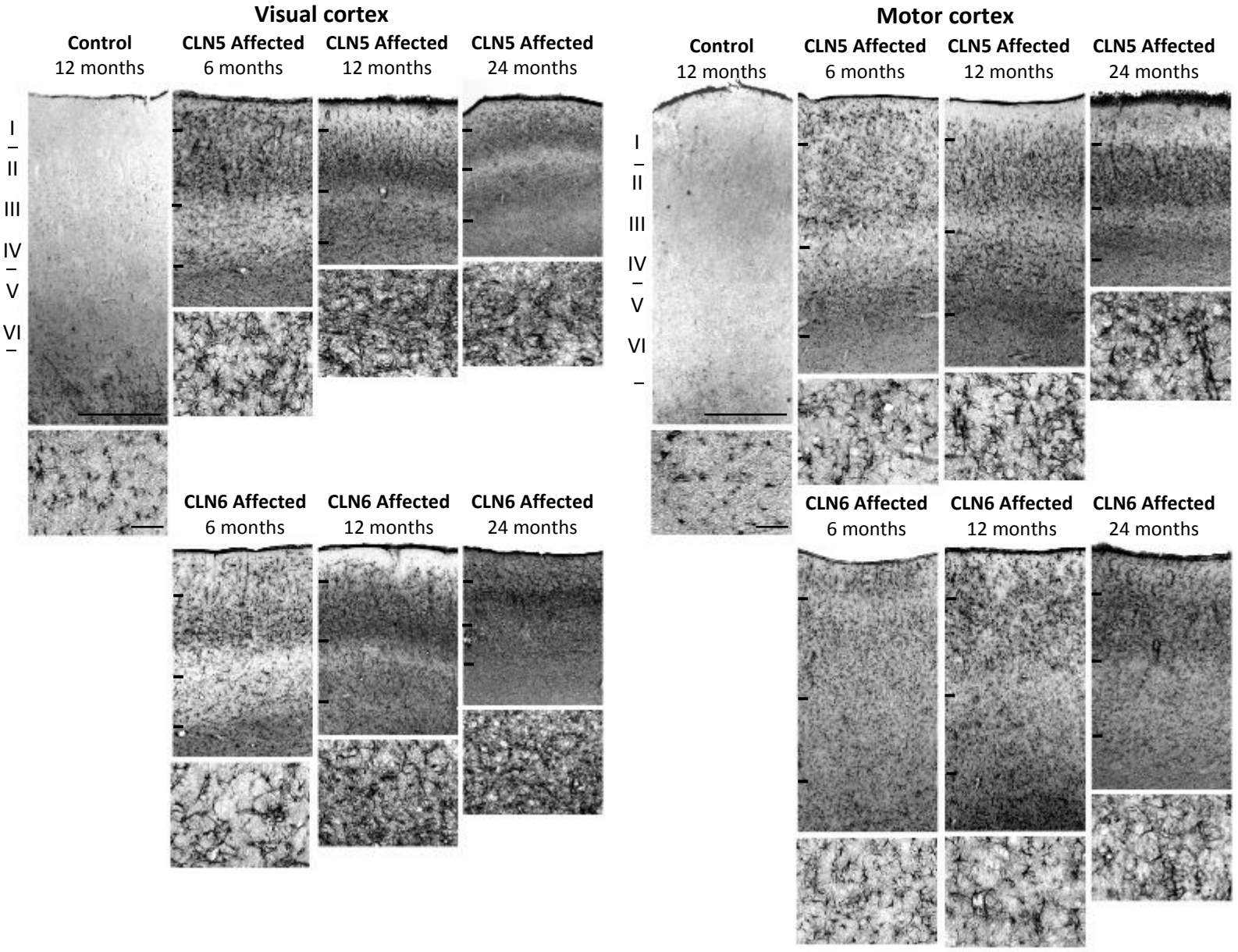

Figure 4.7 GFAP expression in the CLN5 and CLN6 affected visual and motor cortices

Increasing astrocytosis (upper image) was revealed in the affected brains of both genotypes, spreading from initial specific foci in the upper cortical layers (lower image) to form a dense glial network across all cortical layers with disease progression. Note the earlier astroglial involvement (dark staining) in the CLN5 affected cortex, especially seen at higher magnification (lower boxes). Scale bars represent 500 μm (upper) and 50 μm (lower).

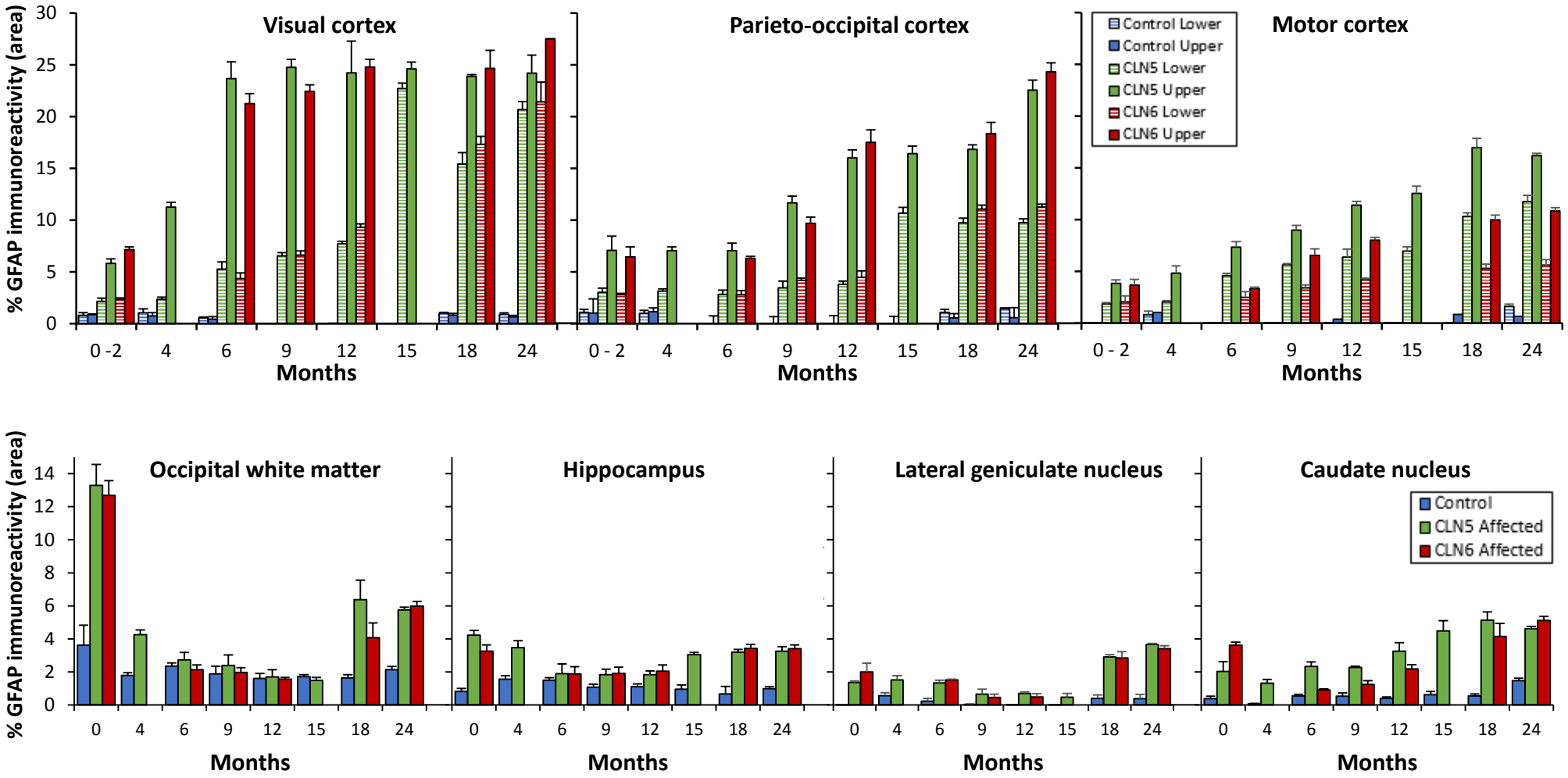

Figure 4.8 Astrocytic activation in the CLN5 and CLN6 affected sheep brain

Quantitative thresholding image analysis of GFAP immunostaining in upper (I-III) and lower (IV-VI) laminae of different brain cortices and subcortical brain regions of control and CLN5 and CLN6 affected sheep of different ages. Results are expressed as the mean percentage areas that stained above a threshold value for at least 10 fields, showing the standard error of the mean (vertical bars). No astrocytic activation was found in the cerebellum of either ovine disease model.

4.3.3.2 Microglial activation

The GSB4 lectin, also referred to as I-B4, acts as a common neuroinflammatory marker in the brain, labelling vascular endothelia, as well as perivascular macrophages and activated (amoeboid) microglial cell populations (Streit, 1990). GSB4 staining followed a similar pattern to GFAP immunostaining, being markedly increased in the cortical grey matter of both CLN5 and CLN6 affected brains compared with controls (Figure 4.9), with initial foci of activated microglia in the upper laminae (II-III) of the parieto-occipital and visual cortices. These foci were detected in the CLN5 neocortex as early as birth and in the CLN6 affected brain by 2 months. As the disease progressed, the numbers of activated cells and clusters increased to form a conspicuous band in these cortical regions of the CLN5 affected brain by 6 months and in the CLN6 affected brain by 9 months, with subsequent activation in the somatosensory, entorhinal and motor cortices in both disease models. This microglial activation spread to the deeper laminae with time, particularly to VI and the white matter/grey matter boundary of both disease models. From 12 months of age all CLN5 affected cortical layers contained intensely stained cells, whilst these were not evident in the CLN6 affected brain until 18 months. Compared with the weakly stained and highly ramified microglia in the cortex of control sheep, many of the microglia in the CLN5 and CLN6 deficient sheep displayed enlarged soma with short thickened processes, typical of an amoeboid or brain macrophage-like morphology (Figure 4.10).

These trends were consolidated by quantification of GSB4 staining. Thresholding image analysis of GSB4 staining revealed activated microglia first in the visual and parieto-occipital cortices, and later in the motor cortex in both disease models (Figure 4.11). However activation in all cortical regions of CLN5 affected brains began before that in CLN6 affected brains, and was considerably greater. Strong GSB4 reactivity in controls was evident only in the neonatal white matter.

Progressive activation of subcortical nuclei was delayed compared with the cortical activation. On a gross level, there was some staining of GSB4-positive staining in subcortical regions of both the CLN5 and CLN6 affected brain at 6 months (Figure 4.9) but this was not associated with cell bodies and was interpreted as neuropil staining of unattributed biological significance. By 12 months, activated microglia were present in the lateral geniculate nucleus and in other thalamic nuclei in both disease models. Initially activated cells in these regions were small but rounded with only weakly stained processes. By late to end-stage disease at 18 – 24 months they had morphed into activated brain macrophages, yet overall subcortical activation was minor compared with that in the affected cortices.

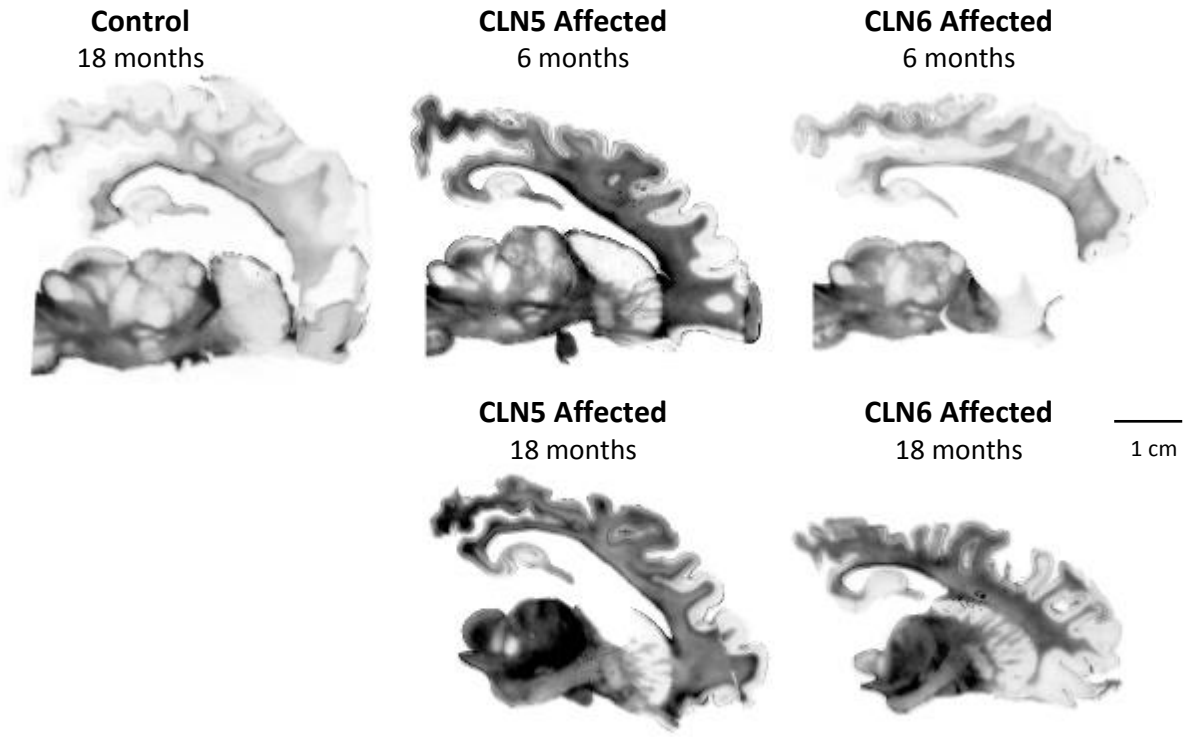

Figure 4.9 Comparative microgliosis during ovine NCL disease progression

GSB4 stained sagittal sections (Level 4/5) showing widespread and progressive microglial activation in the NCL affected sheep brains with age. Note the greater activation in the CLN5 affected brain at 6 months compared with that in the age-matched CLN6 affected brain.

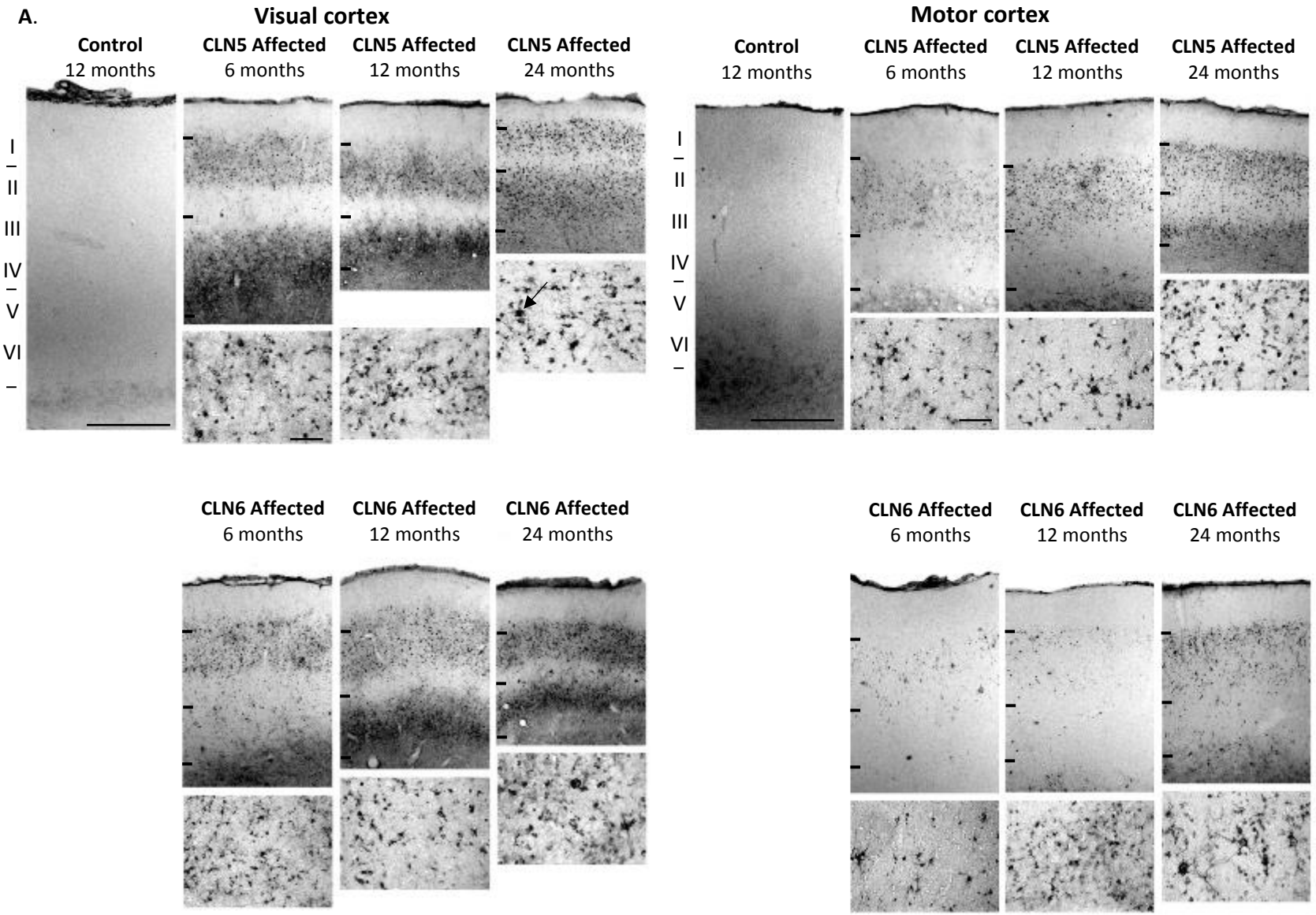

Figure 4.10 Microgliosis in the CLN5 and CLN6 affected visual and motor cortices

GSB4 expression in the CLN5 and CLN6 affected visual and motor cortices (upper image) showing the increase in microglial activation with age, from initial hyper-trophic foci in the upper laminae II and III (lower image) which spread to encompass all cortical laminae. Brain macrophages were progressively noted in the affected brains of both genotypes at higher magnification (arrows, lower boxes). Note the earlier microgliosis (dark staining) in the CLN5 affected cortex. Scale bars represent 500 μm (upper) and 50 μm (lower).

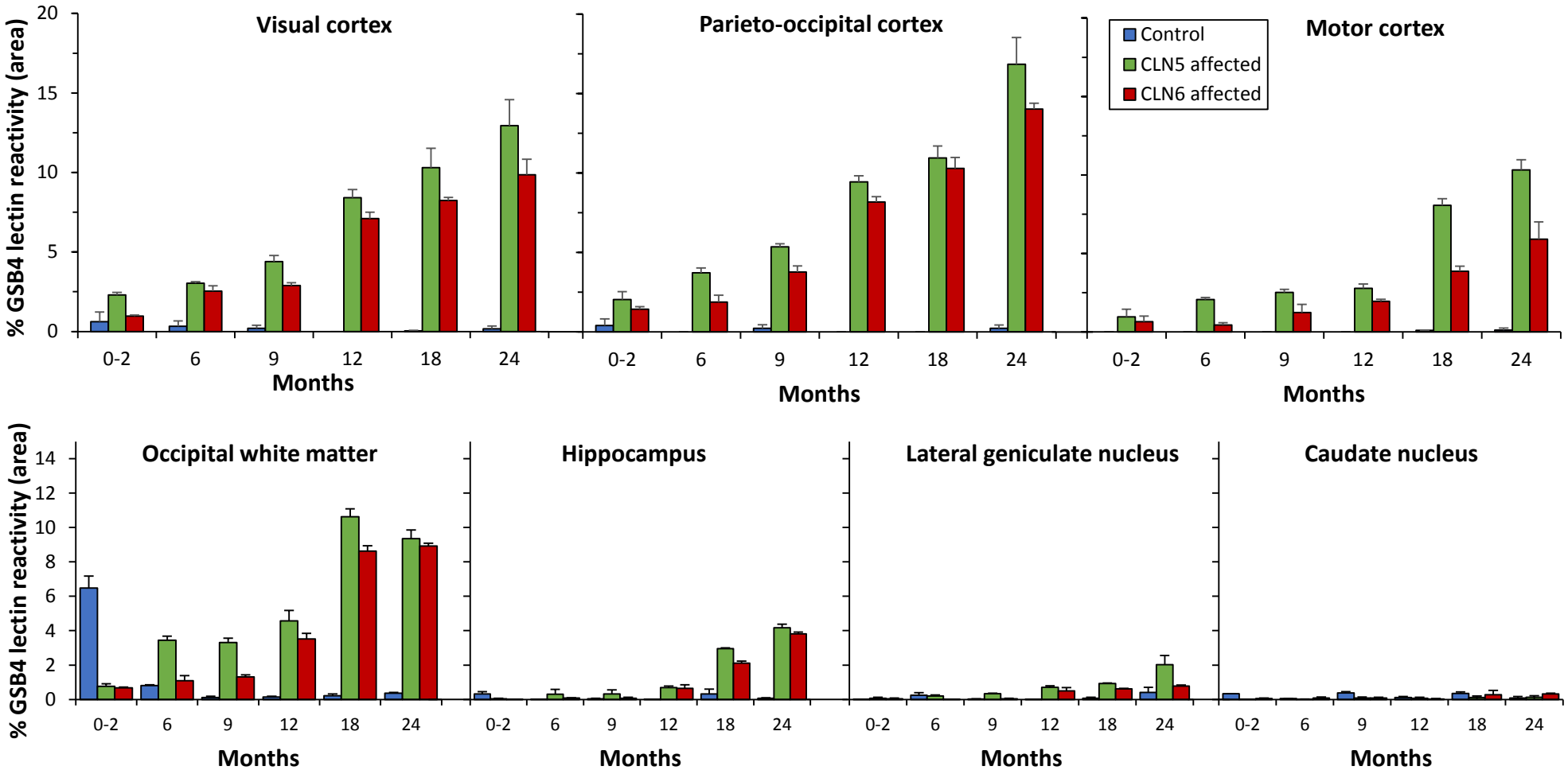

Figure 4.11 Microglial activation in the CLN5 and CLN6 affected sheep brains

Quantitative thresholding image analysis of GSB4 staining across different cortices (laminae II-VI) of control and CLN5 and CLN6 affected sheep brains of different ages. Results are expressed as the mean percentage area that stained above a threshold value in at least 10 fields, showing the standard error of the mean (vertical bars). No microglial activation was found in the cerebellum of either ovine disease model.

4.3.4 Storage body accumulation

Fluorescent lysosomal storage body accumulation is another hallmark of the NCLs. Punctate accumulation in different regions of affected brains was quantified by fluorescent microscopy and image analysis. In the initial disease stages, aggregates of fluorescent material were confined to cells with characteristic neuronal morphology in both disease models. These included neurons in the subcortical nuclei and across all laminae of the cerebral cortex, pyramidal cells of the hippocampus, and all Purkinje cells of the cerebellum. As the disease progressed, lysosomal storage appeared also in non-neuronal cells of both disease forms.

Accumulation was revealed as early as birth in all regions analysed in the CLN5 affected sheep brain and became more pronounced with age (Figure 4.12). Age-matched newborn CLN6 brain sections were not available but prenatal accumulation has been reported for this form (Jolly *et al*., 1989), and at 12 days after birth (Oswald *et al*., 2005). Accumulation was evident at the earliest time-point of 2 months in the current study. The earlier onset seen with the other neuropathological markers for the CLN5 sheep model did not reflect in the comparative storage body analyses. There was no significant difference between the two ovine disease models with respect to storage body onset and accumulation, which followed a near linear pattern in the neocortex from birth to end-stage disease (Figure 4.13).

All subcortical regions analysed showed slower percentage increases in storage body accumulation than was observed in the cortex, apart from comparable, albeit delayed, cumulative responses detected in the cerebellum, hippocampus and the lateral geniculate nucleus of the thalamus (Figure 4.13). By end-stage disease, storage material was universal throughout all grey and white matter regions.

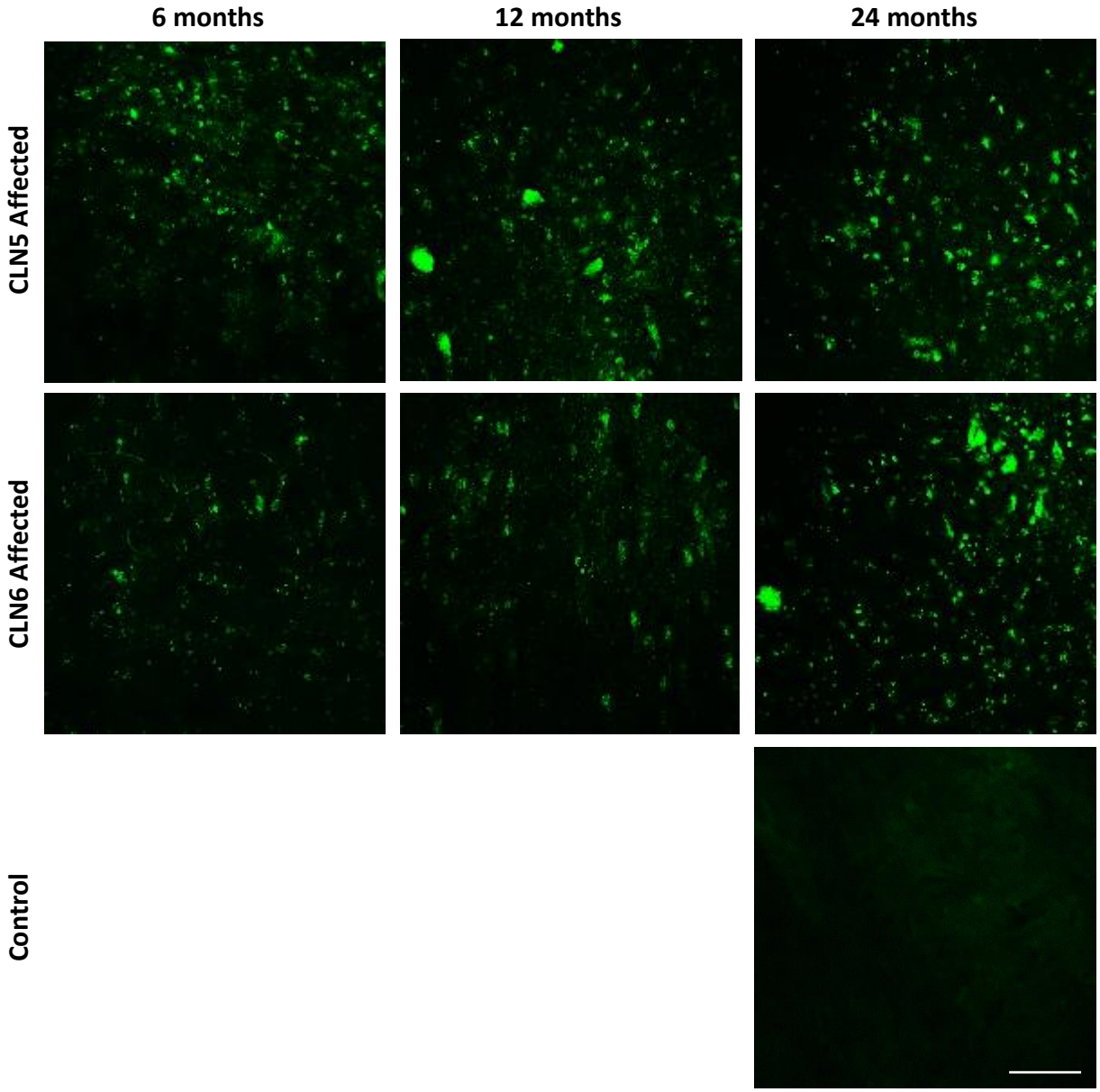

Figure 4.12 Comparative storage body accumulation during ovine NCL disease progression
Fluorescent (450-480 nm excitation, 490-530 nm emission) imaging of storage body accumulation in the parieto-occipital cortex of the CLN5 and CLN6 affected sheep brains compared with an unaffected control brain. Images are from 50 μm cortical sections, hence the thickness of the section makes the punctate nature of the storage harder to see. Scale bar represents 50 μm.

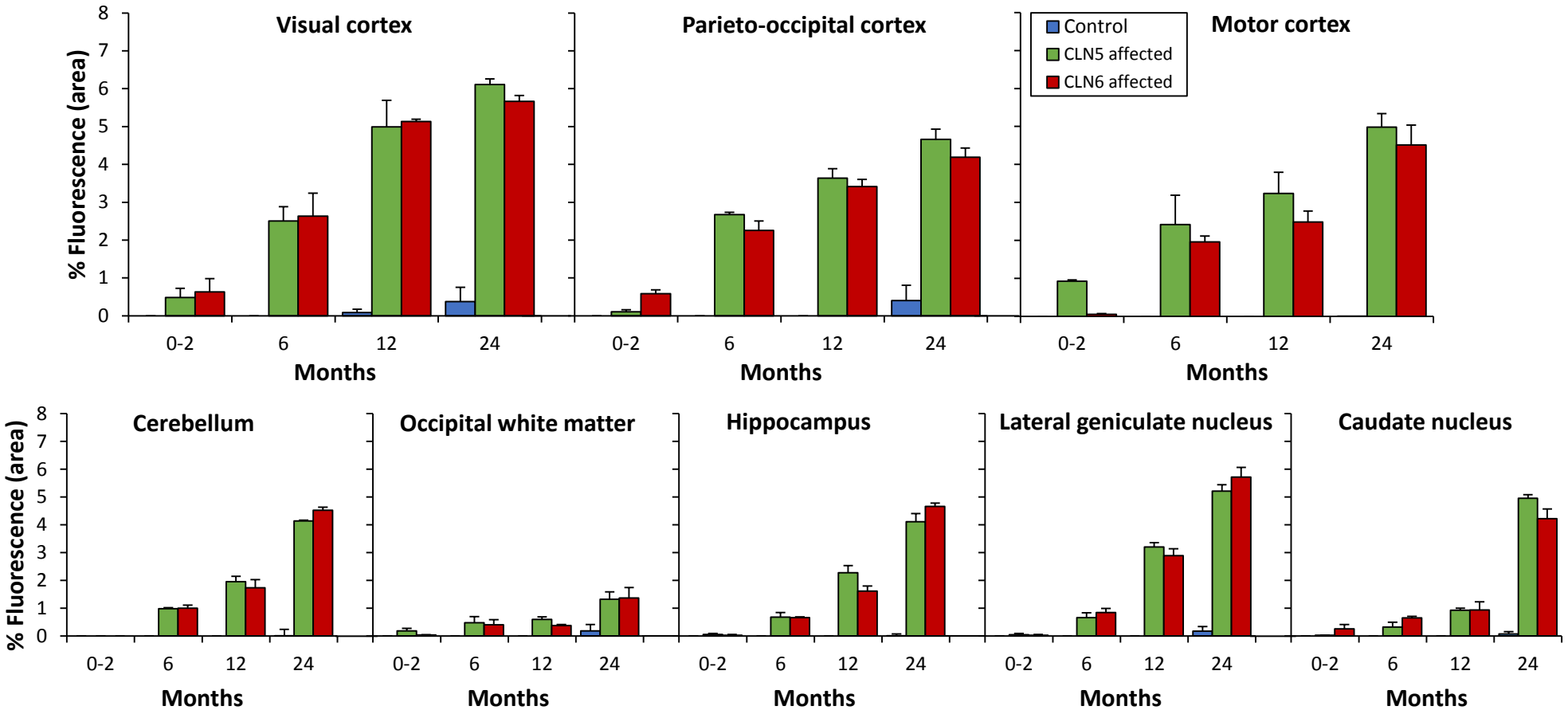

Figure 4.13 Accumulation of fluorescent storage bodies in CLN5 and CLN6 affected sheep

B. Quantitative thresholding image analysis of storage body accumulation in different brain regions of CLN5 and CLN6 affected sheep compared with controls. Results are expressed as the average percentage area containing fluorescence above a threshold value in at least 10 fields, showing the standard error of the mean (vertical bars). Cortical values are means for all layers.

4.3.5 Neurogenesis

The discovery of extended neurogenesis in the subventricular zone (SVZ) of CLN6 affected sheep suggested an intrinsic attempt at cell replacement within the diseased brain (Dihanich *et al*., 2009, 2012). Consequently the extent of neurogenesis was explored in the CLN5 affected brains to verify if this was a disease-specific phenomenon, using an immunohistochemical marker for developing and migrating neurons, poly-sialated neural cell adhesion molecule (PSA-NCAM),.

Markedly increased PSA-NCAM immunoreactivity was observed in both the CLN5 and CLN6 affected sheep brains along the entire rostro-caudal extent of the SVZ lining the lateral ventricle. Whilst SVZ neurogenesis was evident in the normal sheep brain, particularly in the early neonatal period, this was greatly enhanced in the CLN5 and CLN6 diseased brains. Intensely stained cells and fibres oriented tangentially to the ventricle, particularly at the rostral regions of the SVZ, formed a conspicuous band of endogenous neurogenesis in the affected sheep (Figure 4.14). As well as the normal migration of newly-generated neurons through the rostral migratory stream to the olfactory bulb, there was evidence of radial migration of these cells in the diseased brains, extending away from the SVZ along white matter tracts towards the deep laminar layers of the degenerating cortex (Figure 4.11A). Migratory PSA-NCAM positive cells, with intensely stained perikaryon and multiple dendritic processes, were detected through all cortical regions, particularly the upper laminae, in both the CLN5 and CLN6 affected brains. Here they formed densely packed clusters (or spheres) at the layer I/II boundary with fibrous dendritic processes. These were congruous with the developing cellular aggregates revealed in the diseased sheep cortex by Nissl staining (see Section 4.3.2). By comparison, in the adult normal brain, punctate staining was observed in sparse individual cells and along neuritic processes in the cortex but there were no clusters.

Neurogenesis was particularly pronounced in the CLN5 affected brain at 6 months of age, much more so than in the CLN6 ovine model. There was considerable evidence of neurogenic activity in the SVZ and layer I/II PSA-NCAM-positive cellular aggregates were present across the entire CLN5 cortical mantle. In the CLN6 affected brain at the same age, these aggregates were mainly restricted to the occipital cortex, whilst elsewhere in the cortex they were similar in morphology to the control. From 12 to 18 months, both disease models were identical in their presentation, resembling the 6 month CLN5 profile described above. Interestingly, at end-stage disease (24 months) very few cortical immunoreactive clusters were seen in the CLN5 affected brain, whilst dense spheres still existed in the CLN6 model.

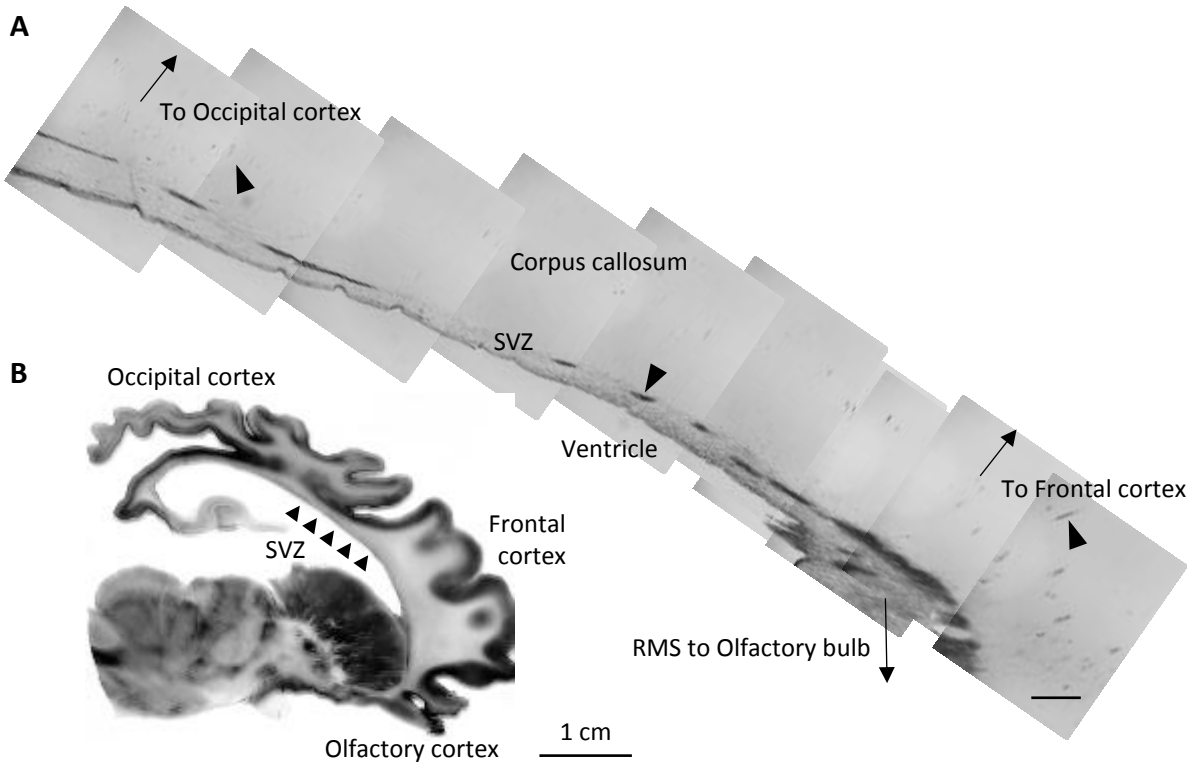
A
To Occipital cortex
Corpus callosum
SVZ
B
Occipital cortex
Ventricle
To Frontal cortex
SVZ
Frontal cortex
RMS to Olfactory bulb
Olfactory cortex
1 cm

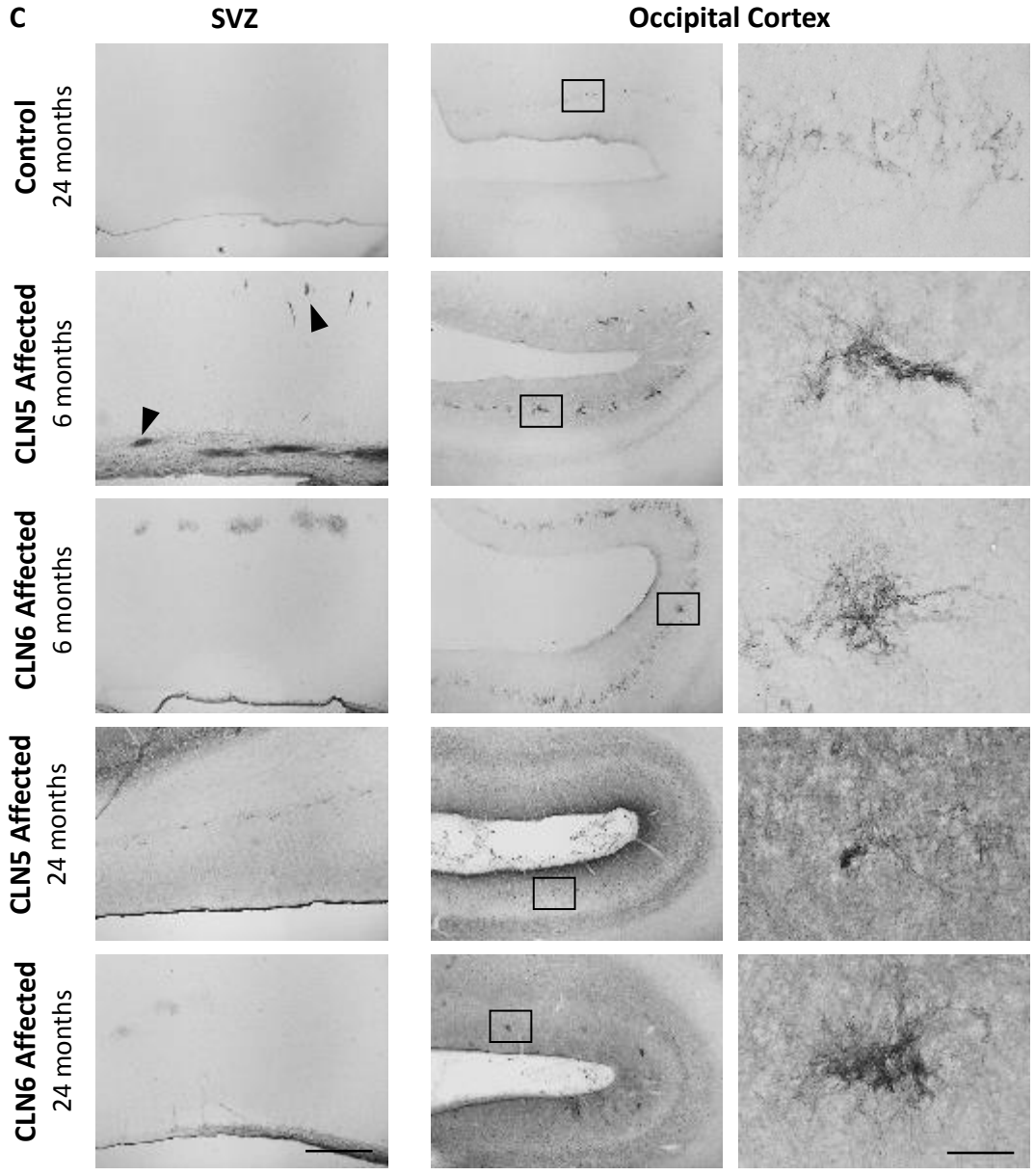
C
SVZ
Occipital Cortex
Control
24 months
CLN5 Affected
6 months
CLN6 Affected
6 months
CLN5 Affected
24 months
CLN6 Affected
24 months

Figure 4.14 Extended neurogenesis in the CLN5 and CLN6 affected sheep brain
PSA-NCAM immunohistochemistry revealed a band of extended adult neurogenesis along the subventricular zone (SVZ) in affected sheep. **A.** As well as migrating through the usual rostral migratory stream (RMS) to the olfactory bulb, newly generated PSA-NCAM-positive cells and fibres could be seen radiating perpendicularly and tangentially from the 6 month CLN5 affected SVZ (arrowheads) along white matter tracts to the degenerating cortex. **B**. The neurogenic band and degenerating cortical regions are shown in an 18 month old CLN5 affected PSA-NCAM stained sheep brain section. **C.** Newly generated cells travelled along the SVZ and, once in the cortex, clustered at the layer I/II boundary. Scale bars represent 500 μm in **A,C** (left and middle) and 50 μm in **C** (right).

4.3.6 Spatial expression of CLN5 and CLN6 in the sheep brain

When developing therapies for genetic disorders, it is useful to know where the endogenous proteins are expressed. With this in mind, the expression patterns of these endogenous NCL proteins were explored using the recently developed novel sheep-specific polyclonal CLN5 and CLN6 antibodies (Hughes *et al*., 2014b). CLN6 reactivity was intrinsically weaker than that for CLN5. Nevertheless, CLN5 and CLN6 immunohistochemistry in the developing normal sheep brain resulted in a very similar, mainly neuronal, pattern of expression. Both endogenous CLN5 and CLN6 proteins were widely expressed throughout the brain during postnatal development, but were particularly evident in the cortical neurons, pyramidal cells of the hippocampus, periventricular epithelia and paraventricular thalamic cells, subcortical striatal and hypothalamic neurons as well as the cerebellar Purkinje cells (Figure 4.15). At a subcellular level, granular CLN5 and CLN6 immunostaining was predominantly localized to the neuronal cell soma, and along neurites of larger immunopositive cells. No expression was seen in the CLN5 affected sheep tissues with the CLN5 antibody nor in the CLN6 affected tissues with the CLN6 antibody (Figure 4.15A, E insets).

The strongest CLN5 and CLN6 immunoreactivities were detected in the hippocampus from birth to adulthood (Figure 4.15A,E-G). The most prominent expression was seen in the pyramidal cells in both CA3 and CA2 regions, the hilus and the granule cells of the dentate gyrus. In the sheep cerebral cortex, CLN5- and CLN6-positive cells were found across the cortical laminae II-VI, but were prominent in layers II-II and at the white matter/ gray matter boundary (Figure 4.15B). Both proteins were expressed in the Purkinje (PCL) and granular (GCL) cell layers of the cerebellum (Figure 4.15D). In the neonatal cerebellar cortex, weak endogenous CLN5 and CLN6 expression was observed in mitotically active cells of the external granular cell layer (EGL) but as the brain developed these cells migrated to populate the internal granular cell layer with subsequent loss of the EGL in the mature cerebellum. Additionally, an increase in immunoreactivity with both antibodies was detected in the molecular layer of the cerebellum, first seen at six months of age.

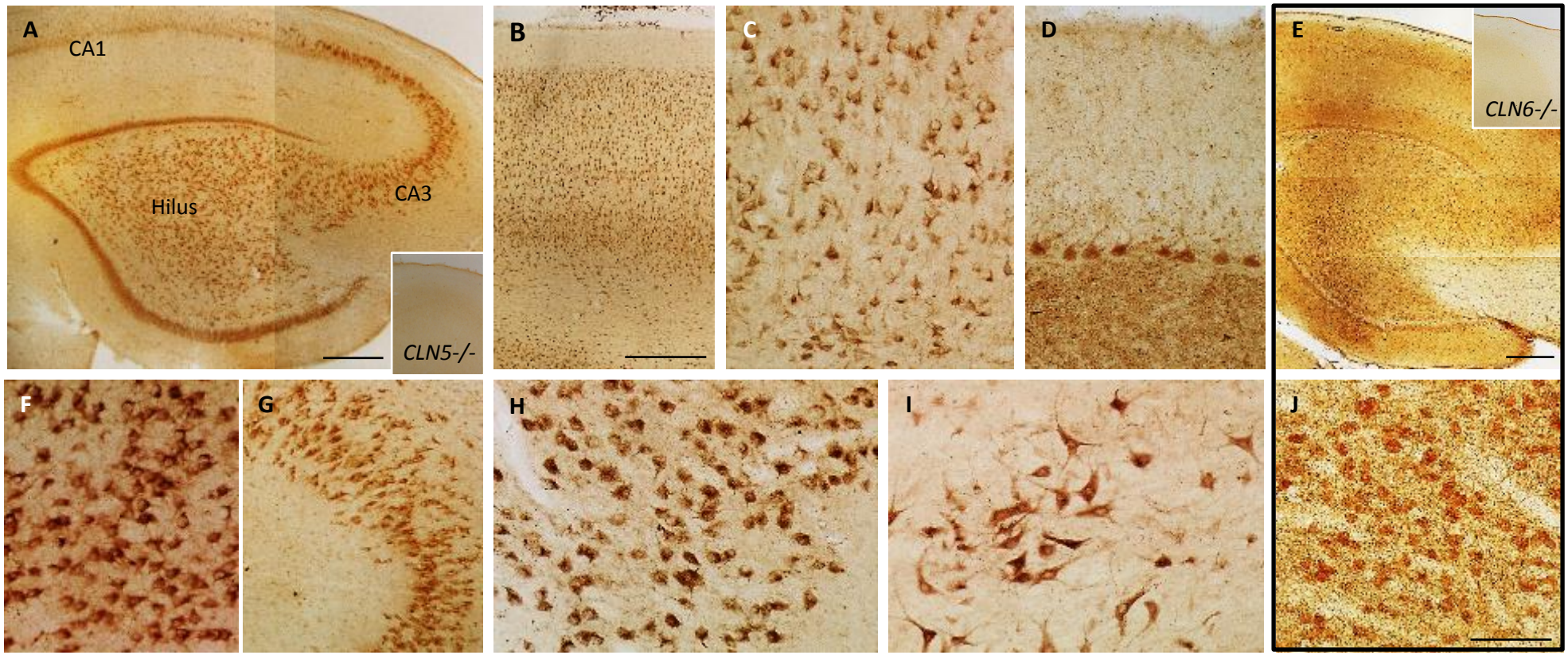

Figure 4.15 Expression of endogenous CLN5 and CLN6 proteins in the normal adult sheep brain

Strong CLN5 immunostaining in hippocampal pyramidal cells (**A**), cortical neurons of laminae II-VI in the frontal lobe (**B**, inset **C**), cerebellar Purkinje cells (**D**), hilar (**F**) and CA3 cells (**G**) of the hippocampus, hypothalamic neurons (**H**) and the paraventricular cells of the thalamus (**I**). CLN6 expression (boxed) was considerably weaker but was co-localised to the same cell populations, as seen in the hippocampus (**E**) and paraventricular thalamic cells (**J**). Insets on **A** and **E** demonstrate the lack of CLN5 and CLN6 expression in the hippocampus of CLN5 and CLN6 affected brains respectively. Scale bars represent 500 μm in **A,B,E** and 100 μm in **C,D,F-J.**

73

4.4 Discussion

This work provides the first detailed description of progressive pathological changes in the CNS of Borderdale CLN5 affected sheep. Despite the very different genotypes and subcellular localisation of the defective proteins, it was surprising that similar neuropathological themes emerged for both CLN5 and CLN6 affected sheep, including the cortical regionality of neurodegeneration and atrophy, together with early and localised microglial activation, pronounced hypertrophy of astrocytes, brain-wide storage body accumulation and enhanced neurogenesis. The data serve to highlight the similarities of these two ovine models, whilst also showing that despite having pathological endpoints that resemble one another, these are reached by pathogenic cascades that differ between NCL subtypes.

4.4.1 Common themes in ovine NCL pathogenesis

4.4.1.1 Progressive neuropathological phenotype in the cortex

The NCLs are traditionally characterised by the near-ubiquitous accumulation of protein in lysosome-derived storage bodies and profound neurodegeneration, with severe resultant brain atrophy (Mole *et al*., 2011). The common assumption was that the storage body accumulation caused the characteristic neuropathology, but this idea no longer seems plausible (Palmer *et al*., 2013; Palmer 2015). Instead a central role for disease associated neuroinflammation has been proposed. That neuroinflammation actually precedes neurodegeneration was first established in the CLN6 ovine model (Oswald *et al*., 2005; Kay *et al*., 2006) and has subsequently been reported in murine NCLs (Pontikis *et al*., 2005; Kielar *et al*., 2007; Partanen *et al*., 2008; Macauley *et al*., 2009; von Schantz *et al*., 2009; Kuronen *et al*., 2012; Schmiedt *et al*., 2012; Morgan *et al*., 2013). The current study extends these observations to include the CLN5 ovine model.

Proliferating perivascular macrophages and activated astrocytes were detected in the CLN6 affected sheep brain as early as 20 and 40 days before birth (Kay *et al*., 2006). These progress to discrete foci of reactive hypertrophic astrocytes and activated microglia in CLN6 affected cortical regions at birth, and were also seen in the pre-symptomatic CLN5 affected neonatal cortex in the current study. They were initially localised to the superficial laminae (II and III) of the affected visual and parieto-occipital sheep cortices. However, their presence did not appear to disturb neuronal development overtly, with cerebellar and cortical laminae in both ovine models well-defined at birth (this study; Kay *et al*., 2006). The gross anatomy and brain weight increases in the perinatal ovine NCL brain also suggest that the affected brain of both genotypes follows a relatively normal developmental path until 4 months of age (Table 4.2).

With time, a progressive process of dysregulated glial activation becomes established. Consistently in both ovine disease models, reactive changes spread in a regionally specific manner from the visual, parieto-occipital and somatosensory cortices to the frontal association cortex, before spreading progressively across the cortical mantle and then into subcortical regions with maturation (Figure 4.8). Later neurodegeneration followed gliosis in the same regional and temporal order in both the CLN5 and CLN6 affected sheep brains and, as in human NCLs (Cooper *et al*., 2006; Cooper, 2010), cortical regions were foremost (Figure 4.3). This ordered primacy of neuroinflammation over neurodegeneration in NCL supports the theory that activated glia serve as sensitive predictors of subsequent neuronal dysfunction or loss (Raivich *et al*., 1999; Streit, 2000, 2002). Each cortical region in affected sheep demonstrated a similar sequence of glial activation, from initial superficial foci to later involvement of successively deeper cortical laminae. The cortical regions first targeted and most affected by the glial activation, namely the parieto-occipital and visual cortices, were also those later associated with the onset of phenotypic symptomology.

The early activation of glia in ovine NCL pathogenesis would suggest it is not solely a response to neuronal insult (this study; Oswald *et al*., 2005; Kay *et al*., 2006). Prominent glial activation has been reported as a common sequelae in many neuropathic LSDs, including Gaucher disease, GM1 and GM2 gangliosidosis, Niemann-Pick type C, Sandhoff disease and mucopolysaccharidoses I , IIIA and IIIB (Wada *et al*., 2000; Baudry *et al*., 2003; Jeyakumar *et al*., 2003; Ohmi *et al*., 2003; Farfel-Becker *et al*., 2011; Wilkinson *et al*., 2012). It is usually interpreted as a protective response to neurodegeneration. Healthy glia are in a quiescent resting state. On CNS insult, by an event such as neurodegeneration, damaged/dying neurons release molecular cues which trigger astrocytic hypertrophy and activation (Rama Rao & Kielian, 2015; Thundyil & Lim, 2015). Astroglial dysfunction can affect neuronal survival through the loss of neurotrophic support and critical homeostatic function, as well contributing to neuroinflammatory processes through robust chemokine secretion (Bosch & Kielian, 2015; Rama Rao & Kielian, 2015). Similarly on CNS disruption, microglia, the principal neuroinflammatory cells in the CNS parenchyma, undergo morphological transformation to amoeboid brain macrophages. These recognise and remove damaged neurons by phagocytosis whilst concurrently secreting pro-inflammatory cytokines and activating an innate immune response (Ransohoff & Perry, 2009; Schwartz & Shecter, 2010). Whilst acute neuroinflammation is typically self-limiting, collective evidence indicates persistent inflammation can itself elicit neuronal damage (Raivich *et al*., 1999; Streit *et al*., 2004; Lyman *et al*., 2014; Lee & MacLean, 2015), likely to further perpetuate the inflammatory cycle and progressive CNS pathology seen in NCL.

It is still unclear what causes the initial activation in the NCLs. A molecular dissection of the neuroinflammatory cascade in ovine CLN6 revealed that the process was complex, and despite differential regulation of a number of genes, no causal initiators of neuroinflammation were

recognised (Chen, 2016). In collaboration with colleagues at the University of Sydney, a transcriptomic approach is planned on ovine CLN5 and CLN6 CNS tissues to compare gene expression in pre-clinical disease stages with the aim of identifying early targets for effective therapeutic drug interventions.

The NCLs are also pathologically typified by the intracellular accumulation of punctate fluorescent storage bodies (Mole *et al*., 2005). Sparse storage material was apparent at birth in both affected sheep models (this study; Oswald *et al*., 2005; Kay *et al*., 2006), accumulating through the brain with disease progression but the distribution was neither focal nor did it correlate temporally or spatially with glial activation or neurodegeneration. Whilst cortical accumulation of storage material was near-linear (Figure 4.13), storage burden was spread across all laminae of the affected cortex. Despite large amounts of lysosomal storage in the soma of the Purkinje cells at end-stage ovine CLN5 and CLN6 disease, there was no indication of atrophy or neuroinflammation in the cerebellum in the current study. This observation is not novel, but is consistent with previous findings in the CLN6 sheep model that neurodegeneration and storage body accumulation are independent manifestations of the genetic lesion (Mayhew *et al*., 1989; Jolly *et al*., 1989; Palmer *et al*., 2002; Oswald *et al*., 2005, 2008; Kay *et al*., 2011).

An important question for therapy is when does the pathogenic cascade become fatally damaging to neurons? Atrophy of the cerebral cortex in ovine NCL is not uniform but instead follows the same delayed pattern as glial activation, and both of these pathological events occur well before the animals become symptomatic. Consistent with the advanced symptomology and more rapid course of ovine CLN5 (Chapter 6), the onset of neuropathology was earlier in all analysed regions of the CLN5 affected brain than in ovine CLN6 brain regions. Measurable increases in glial markers and declines in cortical thickness could be seen from early perinatal stages in the CLN5 parietal and occipital lobes, with the frontal association cortex affected from 9 months of age (during early- to mid-stage disease) and generalised neuronal loss and atrophy across the cortical mantle observed by 15 months of age. The early targeting of the visual and parieto-occipital cortices was also seen in the CLN6 ovine model, however atrophy was delayed until 9 months of age in the somatosensory cortex, the frontal association and entorhinal cortices until mid-stage disease at 12 months and the motor cortex was not affected until late in disease progression at 18 months of age. The CLN6 measurements corroborated well with those of Oswald *et al.* (2005), and extended those findings to show very delayed, albeit significant, atrophy in the CLN6 motor cortex at terminal disease.

Quantitative measures of atrophy and glial activation demonstrated the greater involvement of the frontal lobe in the ovine CLN5 disease. At end-stage disease, cortical thickness measurements for both genotypes converged for all regions, except the primary motor and frontal association cortices

(Figure 4.5). These two regions were macroscopically more atrophied in the CLN5 affected brains than in the CLN6 affected brains (Figure 4.4). In mammalian anatomy, the frontal association cortex is located in the prefrontal cortex, which has been implicated in executive function and complex cognitive behaviour (Yang & Raine, 2009). Although sheep have not been shown to have the equivalent of a human prefrontal cortex, rodents do (Dalley *et al*., 2004), hence it seems logical that sheep would too as they are capable of performing tasks that require this brain region (Morton & Avanzo, 2011). The frontal lobe also contains the primary motor cortex, which generates neural impulses that control the execution of movement. Atrophy in these regions correlates with the declining motor, proprioceptive and cognitive function seen with disease progression in the CLN5 Borderdale sheep (Chapter 6). Motor deficits particularly manifest with stiffness in the legs and hind-limb paralysis much earlier and more abundantly in the CLN5 affected sheep than in CLN6 affected sheep (Chapter 6).

Given the earlier atrophic changes in the CLN5 affected sheep brain, one would expect this to manifest in the brain mass data as well. This was not the case. The CLN5 affected brain mass was greater at all time points, only converging with the CLN6 affected brain mass at terminal disease. This may be rationalised by the smaller size of the of the CLN6 South Hampshire sheep, which are smaller in stature, and of the fact that the CLN6 flock is longer established, and despite some out-breeding, have been maintained by heterozygous ewe/ homozygous affected ram crosses for over forty years. Collated results from this model include historical and newly collected data points. The CLN5 Borderdale flock was established more recently, through homozygous out-breeding with another large sheep breed (Coopworth), which likely influences the overall mature size of the sheep and their brains.

By end-stage ovine NCL disease at 22- 24 months of age, relatively few cortical neurons were left and overall atrophy was similar in both models. Consistent with findings in human NCL autopsy tissue and other model species, selective neuronal populations were lost. Neurons within laminae II and III were preferentially lost from both the CLN5 and CLN6 affected neocortices (Figure 4.4). Previous reports have described the loss of specific gamma amino-butyric acid (GABA)-ergic interneurons in human and murine NCLs, as well as in the CLN6 sheep model (Williams *et al*., 1977; Braak & Goebel, 1979; Cooper *et al*., 1999; Mitchison *et al*., 1999; Oswald *et al*., 2001, 2008; Bible *et al*., 2004; Pontikis *et al*., 2004; Tyynelä *et al*., 2004; Kielar *et al*., 2007). The interneuron loss seen in the CLN6 affected sheep brain follows the pattern of glial activation (Oswald *et al*., 2008), whereas Kay *et al* (2011) showed that the specific loss of gonadotrophin-releasing hormone (GnRH) secreting neurons of the hypothalamus was not associated with glial activation or storage body accumulation. This suggests cellular location and connectivity, rather than phenotype, are important determinants of neuronal

survival in ovine CLN6. A future examination of interneuron survival in the CLN5 model would confirm if this was general to ovine NCL.

Neuroinflammation is also purported to both enhance and suppress neurogenesis. Inflammatory factors released during acute inflammation are postulated to stimulate neurogenesis, whereas those released by extended, chronic uncontrolled inflammation reportedly create an environment which is more detrimental to neurogenesis (Whitney *et al*., 2009). This correlates well with the marked increase in adult neurogenesis evident in the CLN6 sheep model (Dihanich *et al*., 2009, 2012) and demonstrated in the current study in CLN5 affected sheep brains (Figure 4.14). An equivalent neurogenic capacity was detected in the hippocampus, cerebellum and subventricular zone (SVZ) of control and CLN5 affected neonatal brains. This showed an age-related decline in the control brains. However neurogenesis continued in the affected brains and did not appear to be 'turned off'. As early as 6 months of age, newly-generated neural progenitor cells could be seen migrating on the usual rostral migratory stream destined for the olfactory bulb, but also radially along white matter tracts towards the affected cortical regions undergoing neurodegeneration (Figure 4.14A). Large spherical aggregates were observed at the lamina I/II interphase in the degenerating cortex. These have been shown to contain both immature and mature neuronal cells but not glial cells in CLN6 affected sheep tissue (Dihanich *et al*., 2009). Their progressive appearance also became apparent after Nissl staining of the affected ovine cortical tissue (Figure 4.4). Equivalent aggregates have been reported in human CLN6 autopsied cortical tissue but not in any cortical regions of the CLN6 mouse model, even at advanced disease stages (Dihanich *et al*., 2012). There have been no previous reports of this phenomenon in human or murine CLN5 tissue.

Neuroinflammation and neuronal death have been reported to trigger upregulated neurogenesis in other models of brain injury and neurodegenerative disease (Magavi *et al*., 2000; Arvidsson *et al*., 2002; Curtis *et al*., 2003, 2005; Winner *et al*., 2011). Multiple steps are involved, including proliferation, migration, differentiation, survival and integration of the newly formed neurons into the CNS circuitry (Ming & Song, 2005). It is not clear what factors signal the observed cellular proliferation and migration in the ovine NCL brain, but it may be that the local micro-environment in the diseased brain resembles conditions seen during development and this is sufficient to maintain ongoing neurogenesis. Regardless, the increase evidenced in the current study was insufficient to compensate for the progressive cell loss observed in NCL. Moreover, neurogenesis in the CLN5 affected sheep was significantly reduced at advanced disease, which may be because of the chronic detrimental effects induced by the chronic duration of the neuroinflammation.

4.3.1.5 Interconnectivity and delayed subcortical neuropathology

No overt neuropathology was detected in the ovine NCL cerebellum during the study. The gross morphology of the cerebella in both ovine disease models remained unaltered during the disease and the size of the affected cerebella approximated normal (Figure 4.3). End-stage MRI studies on the affected sheep corroborated this structural finding (Amorim *et al*., 2015; Sawiak *et al*., 2015). This contrasts with the characteristic cerebellar pathology reported in human CLN5 and CLN6. Cerebella from human CLN6 patients may be normal or show some atrophy (Peña *et al*., 2001; Cannelli *et al*., 2009), but it has been reported that the cerebellum in human CLN5 cases is severely atrophied, with an almost complete depletion of cerebellar granule and Purkinje cells observed *post mortem* (Tyynelä *et al*., 1997; Goebel *et al*., 1999; Haltia, 2003). Brain imaging of human CLN5 patients reveals atrophy of the cerebellum to be the most striking abnormality (Autti *et al*., 1992), yet only dilated cerebellar sulci without gross degeneration is seen in MRI or CT studies of a canine Border collie CLN5 model (Koie *et al*., 2004; Mizukami *et al*., 2012). Only mild cerebellar atrophy has been reported for Devon cattle with a naturally occurring CLN5 NCL (Jolly *et al*., 1992). The reason why cerebellar pathology does not manifest in ovine NCL, particularly CLN5, is unclear. The sheep in the current study did not die from the disease, being euthanised for humane reasons. It may be that the degenerative effects of the disease that manifest initially in the cerebral cortex of the ovine NCLs were simply delayed in the cerebellum and sheep did not live long enough to exhibit cerebellar pathology.

The effect of the disease on the thalamus is more contentious. Whilst the main pathological target in multiple forms of NCL is the cortex (Haltia, 2003; Palmer *et al*., 2013), there is evidence that the thalamus is affected earlier in the disease progression than the cortex in murine models of CLN1, 2, 3, 6, 8 and 10 (Pontikis *et al*., 2004, 2005; Weimer *et al*., 2006; Kielar *et al*., 2007; Partanen *et al*., 2008; Kuronen *et al*., 2012). In contrast though, neuronal loss in the cortex preceded that in the thalamus in the CLN5 knock-out mouse (von Schantz *et al*., 2009). MRI studies on humans show decreased T2 intensity in the thalamus at the time of diagnosis in a Costa Rican CLN6 patient (Peña *et al*., 2001) and in some CLN5 cases (Holmberg *et al*., 2000) whilst an almost complete loss of thalamic neurons has been reported in *post mortem* human CLN5 brain tissue at end-stage disease (Tynnelä *et al*., 1997).

The thalamus represents a structure that harbours high levels of neural interconnectivity. Every sensory CNS system (with the exception of olfactory) includes a thalamic nucleus that receives sensory signals and relays them through thalamocortical projections to the associated primary cortical region. Reciprocal corticothalamic fibres then relay the processed feedback information to the respective thalamic nuclei, in a process termed ‘top-down’ processing (Rauschecker, 1998; Granger & Hearn, 2007). For instance, in the visual system, sensory input from the retina is sent to

the lateral geniculate nucleus (LGN) of the thalamus, which in turn projects to the visual cortex of the occipital lobe. In turn, the LGN receives strong feedback connections from the primary visual cortex (Cudeiro & Sillito, 2006; Sillito *et al*., 2006).

The current study is consistent with others of ovine NCL that showed that subcortical (including thalamic) degeneration was limited to very late in the disease progression at most (Mayhew *et al*., 1985; Oswald *et al*., 2005, 2008; Kay *et al*., 2011). Whilst sparse activated microglia and astrocytes were first evident from 12 months of age in the affected sheep thalami, this was significantly delayed compared with the cortical reactive changes which originated in the visual and parieto-occipital cortex. Only at late stage disease were GFAP and GSB4 expression levels upregulated in the reciprocal LGN (Figure 4.8 and Figure 4.11). Nissl staining in the current study revealed no obvious qualitative changes in the subcortical or thalamic architecture and although MRI scans of CLN5 and CLN6 sheep reported some subcortical atrophy (Amorim *et al*., 2015; Sawiak *et al*., 2015), these imaging studies were performed at end-stage disease, when the entire brain was atrophied. Kay *et al*. (2011) found the cross-sectional area of the CLN6 affected thalamus was reduced by only about 5%. The gross normality of the thalamus in the ovine NCLs compared with that in murine models would suggest that the pathogenic pathways may be species-specific (Kay *et al*., 2011) and any disruption in the thalamocortical network in affected sheep would result from the cortical degeneration rather than vice versa.

Interestingly, the cortical laminae targeted in CLN5 and CLN6 NCL seem to differ between species. Layer V neuron vulnerability has been reported for human and murine CLN6 (Elleder *et al*., 1997) whilst the laminar loss of neurons in human CLN5 is targeted to laminae III and V (Tyynelä *et al*., 1997) and to laminae IV-VI in CLN5 knock-out mice (von Schantz *et al*., 2009). As neurons within the individual cortical laminae are morphologically unique, with specific axonal projections to different CNS regions, one might expect neuronal cell loss within each lamina to produce distinct phenotypes. For instance, commissural and associative neurons reside within the laminae II and III which are most affected in the ovine NCLs. These neurons have projections across the midline to the contralateral hemisphere or to other ipsilateral cortical locations respectively (Greig *et al*., 2013). Potentially their loss could have significant consequences on inter-hemispheric and intracortical co-ordination of neuronal activity. The deeper neuronal laminae V and VI contain pyramidal and multiform neurons which mainly send efferent projections to subcortical structures, such as the basal ganglia and thalamus. Loss of these neurons would likely disrupt the reciprocal interconnections between the cortex and subcortex.

4.4.2 Spatial expression of endogenous CLN5 and CLN6 in the sheep brain

Detection of sites of endogenous protein expression are important when designing therapies for genetic disorders, however the availability and/or generation of high quality antibodies to the NCL proteins has always been problematic. Neither the ovine CLN5 nor CLN6 proteins were amenable to production in bacteria, *Escerichia coli*, whilst recombinant protein expression in mammalian cells lines yielded only small quantities of purified protein (unpublished PhD observations, Janet Xu, Lincoln University). Sheep-specific CLN5 and CLN6 antibodies were recently developed with collaborators at the University of Otago and the current study set out to characterise endogenous protein expression in the normal sheep brain using them. Immunohistochemical staining with the CLN5 antibody was particularly successful, whilst the CLN6 antibody had weaker immunopositivity and had to be used at a much higher concentration.

Spatial co-expression of both proteins was detected throughout the brain but the most prominent expression was seen in the hippocampal formation, hypothalamus, cerebral cortex and the developing cerebellum. This recapitulates the gene and/or protein expression patterns previously shown for CLN2 (Fabritius *et al*., 2014), CLN3 (Luiro *et al*., 2001; Fabritius *et al*., 2014), CLN5 (Holmberg *et al*., 2004; Fabritius *et al*., 2014), CLN6 (Thelen *et al*., 2012) and CLN8 (Passantino *et al*., 2013) in the murine brain. Expression of the CLN5 and CLN6 proteins appears to be developmentally regulated. Although this was not quantified, they did correlate with regions of active neurogenesis in the sheep brain, supporting a hypothesized role in embryonic neurogenesis and the development of neural networks (Fabritius *et al*., 2014). These neurogenic sites include the SVZ, hippocampus and cerebellum. In the normal sheep hippocampus, the pyramidal cells in both CA3 and CA2 subfields of Ammon's horn, the hilus and the granule cells of the dentate gyrus were strongly immunoreactive with both antibodies. Stronger expression was seen in the ovine CA3 subfield than in CA1 (Figure 4.15A). This correlated with CLN5 immunohistochemical findings in the mouse brain (Holmberg *et al*., 2004; Fabritius *et al*., 2014) but contrasted with those detected in CLN6 mice by *in situ* hybridization (Thelen *et al*., 2012), where higher *CLN6* expression was observed in the CA1 region.

CLN5- and CLN6-positive cells in the normal sheep brain were typically neuronal in morphology. Collaborative studies at the University of Otago showed that CLN5 immunoreactivity in normal sheep brain sections co-localised with a neuronal marker (NeuN) and GABAergic interneuron markers, calretinin and parvalbumin (unpublished Summer Studentship observations, Kristina McIntyre, 2014). Whilst a quantitative PCR study by Holmberg *et al.* (2004) demonstrated murine *CLN5* mRNA expression in glial cell cultures, the ovine CLN5 protein was not detected in astrocytes by co-localisation in sheep brain tissue (Kristina McIntyre, 2014).

A correlation between NCL protein expression and the distinct laminar neurodegeneration and astrocytic activation seen in ovine NCL does not seem likely. Both proteins are expressed across cortical laminae II-VI, particularly in II-III. These are the same laminae that show early upregulation of astrocytosis and microgliosis but then are progressively lost in the affected sheep brain. However, although strong CLN5 and CLN6 expression is observed in the hippocampus and cerebellum, neither of these structures exhibit significant atrophy or neuroinflammation in ovine NCL.

Taken together, the CLN5 and CLN6 co-expression findings from the current study suggest that expression of the NCL genes is cross-regulated and that the gene products operate together in a common pathway to cause a similar clinical phenotype.

4.4.3 Implications for clinical therapy

Whilst the mechanisms that underlie selective neuronal vulnerability in NCL have not yet been fully elucidated, targeted therapies may be beneficial for this disorder. As NCLs are primarily neurodegenerative diseases and endogenous CLN5 and CLN6 expression is predominantly in neurons and interneurons (Figure 4.15), neurotrophic gene therapies which replace the mutated gene product with a functional protein are likely to be most effective. Therapy can be directed to the regions most affected by the disease, namely the cortex, or more widespread to allow global correction. Such treatments will be explored in greater detail in the following chapters of this thesis but the general thought is that greater therapeutic efficacy will be achieved if delivered early in the disease process (Cabrera-Salazar *et al*., 2007). As evident above, there is an ideal pre-clinical therapeutic window during which an ordered neuroinflammatory cascade and a neurogenic 'self-repair' response are underway but neurodegeneration and brain atrophy is negligible. For these ovine NCLs, this would be in the first four months of life. Realistically though, as definitive diagnosis of NCL can take from months to several years (Batten Disease Family Association UK), most human patients will have developed symptoms before any treatment is initiated. Affected sheep at 6 – 14 months of age thus represent ideal early- to mid-stage disease models. Although neuropathology and clinical symptoms are established, gene therapies at this stage may be able to halt further disease progression.

A further therapeutically relevant approach is targeted towards the extended yet spatially limited endogenous neurogenesis along the SVZ and within the cerebral cortex of CLN5 and CLN6 affected sheep. Although cell proliferation is upregulated in the diseased brain, the newly generated cells will carry the same genetic defect and hence any attempt at self-repair will inevitably fail. Yet if some of these neurogenic cells could be corrected early in the disease by gene therapy, it may be sufficient to halt disease pathology before it becomes irreversible. Intracerebroventricular administration during early stages of disease, of viral vectors expressing the corrective NCL gene, may be able to cross the

ependymal cell barrier resulting in transduction of cells in the SVZ, from which neurons are generated before migrating to their final destination in the brain parenchyma. This could facilitate widespread dissemination of transduced neurons throughout the CNS, allowing treatment of the global brain defects of NCL. Equally for NCL subtypes with soluble protein deficits (*e.g.* CLN1, 2, 5 and 10), corrected ependymal cells could secrete the missing protein into the CSF circulation for uptake by other protein-deficient cells.

Evidence presented in this study and by others (Oswald *et al*., 2005; Kay *et al*., 2006) of early activation of glial cells highlights their central role in NCL pathogenesis. As a chronic inflammatory response can be detrimental to both neuronal survival and neurogenesis (Raivich *et al*., 1999; Stoll & Jander, 1999; Streit *et al*., 2004; Whitney *et al*., 2009; Lyman *et al*., 2014; Lee & MacLean, 2015), early suppression of inflammation may be an important treatment strategy. The chronic oral administration of an anti-inflammatory drug, minocycline, alone to pre-clinical CLN6 affected sheep did not have any neuropathological benefits or prevent the clinical course of the disease (Kay and Palmer 2013). Anti-inflammatory neuroprotection may have a better effect in the treatment of the NCLs when given in combination with other therapies which correct the genetic defect (see Section 8.3.4).

4.5 Conclusion

Given the different class and subcellular location of the defective proteins in the ovine CLN5 and CLN6 models, the phenotypic similarities between the two forms were remarkable. In both, cortical neurodegeneration is presaged by dense glial activation and these neuropathological events display regional selectivity. The parieto-occipital and visual cortices were first affected pre-clinically in both CLN5 and CLN6 disease models, with subsequent reactive and atrophic changes spreading to the somatosensory and entorhinal cortices during early- to mid-stage disease, and reaching the frontal association and motor cortices later in the disease process. Consistent with the advanced onset of clinical disease, the reactive and neurodegenerative changes were more pronounced earlier in the CLN5 Borderdale sheep brain. However sub-cortical involvement only occurs very late in the disease progression in both sheep models. By end-stage disease, NCL affected sheep brains weigh only 54% to 58% of a normal brain, with most of the atrophy involving the cerebral cortex in which few neurons remain. Concurrent with the progressive neuroinflammation and neurodegeneration in ovine NCL, extended yet spatially limited endogenous neurogenesis occurs along the SVZ and within the cerebral cortex of affected CLN5 and CLN6 sheep. While this self-repairing mechanism may be effective in maintaining neuronal functionality at early and mid-stages of the disease, it fails at more advanced phases.

The current assumption for NCL therapies, particularly gene therapy, is a need for global repair of neurons. However the regionality and selectivity of neuron loss suggest that targeted therapeutics might prove most effective. If delivered early in the disease process, therapies could either be directed to at-risk cells or to the neural progenitor cell in the SVZ, aiming to preserve the beneficial effects of enhanced neurogenesis and taking advantage of the latent potential of the diseased brain to orchestrate a self-repair response.

Chapter 5

AAV9 mediated gene transfer in the normal sheep brain

5.1 Introduction

Lysosomal storage diseases (LSDs) are a heterogeneous group of inherited disorders resulting from the deficiency of one or more enzymes, transporter or other proteins that normally reside within the lysosomal compartment (Neufeld, 1991; Platt *et al*., 2012). More than 50 different forms of LSDs are known to occur in humans, with an aggregate incidence estimated at 1 in 5000 live births (Fuller *et al*., 2006). At least 75% of LSDs have a significant central nervous system (CNS) component (Sands & Haskins, 2008). Animal homologs of the neuropathic LSDs exist. Genetically engineered murine models recapitulate aspects of the corresponding human diseases but the mouse physiology, anatomy and lifespan differs significantly from that of humans. In contrast, naturally occurring diseases in larger animals, such as sheep, more faithfully reflect the human neuropathological, biochemical and phenotypic manifestations, making them a better replica for the development and testing of new therapies. Following the dogma that restoration of 5% of normal enzyme activity via genetically corrected cells should restore normal cellular function in LSDs (Sands & Davidson, 2006), gene therapy becomes an attractive treatment option for these diseases.

Lentiviruses have been widely used as gene delivery vectors to the CNS (*e.g.* Naldini *et al*., 1996b; Bosch *et al*., 2000; Consiglio *et al*., 2001; Lattanzi *et al*., 2010) due to their ability to stably integrate the gene cargo into the genome of both mitotic and post-mitotic host cells, persisting through cell division and thus conferring long-term gene delivery to stem cells and neurons. Previous experiments have shown efficient lentiviral mediated gene transfer to the sheep brain, transducing neurons, neuroblasts and astrocytes *in vivo* (Linterman *et al*., 2011). Spread beyond the intracerebral sites of injection was limited, or the vector was retained within ependymal layers when injected directly into the lateral cerebral ventricles. Recently, recombinant adeno-associated viruses (AAVs) have emerged as the preferred gene delivery vector for the treatment of neurological disorders, including the neuropathic LSDs. Advantages include their broad cellular and tissue tropism, safety, reportedly mild immune response *in vivo*, and their capability to support long-term transgene expression (Worgall *et al*., 2008; Zhang *et al*., 2011; Leone *et al*., 2012; Tardieu *et al*., 2014; Yang *et al*., 2014). Unlike lentiviruses, AAVs do not integrate into the host genome, instead persisting in an extrachromosomal state as episomal concatemers in the host cell nucleus. In dividing cells the episomal DNA is not replicated with the host cell DNA and the AAV genome is lost at mitosis. However in post-mitotic cells, such as differentiated neurons, AAV episomes remain intact for the life of the host cell, providing sustained transgene expression and therapeutic protein production. Tissue specificity is

determined by the capsid serotype (Zincarelli *et al*., 2008). Several AAV serotypes (*e.g.* AAV1, 5, 9, rh10) mediate widespread transduction of the CNS in animal model systems (Burger *et al*., 2004; Cearley & Wolfe, 2006; Markakis *et al*., 2010; Swain *et al*., 2014) yet only AAV1 has been tested in the sheep brain, targeting short interfering RNA to the hypothalamus in a gene knockdown approach (Dufourny *et al*., 2008).

Much interest has centered on AAV serotype 9 for CNS-directed gene transfer, due to its proven spread and efficiency of transduction, and predominant neuronal tropism (Foust *et al*., 2009; Gray *et al*., 2013; Samaranch *et al*., 2013; Swain *et al*., 2014). It has been shown to undergo efficient axonal transport within the brain (Cearley & Wolfe, 2006) and crosses the blood-brain barrier (BBB) to transduce neurons and glia within the brain and spinal cord (Foust *et al*., 2009; Gray *et al*., 2011). With clinical translation in mind, determining the optimal route of administration and the scalability from rodent models to larger animal species is essential. This proof-of-concept study set out to determine the effectiveness of AAV9 as a gene transfer vector in the normal sheep brain and how two distinct delivery routes affected transduction patterns of this vector. More specifically, it was questioned whether transduction of the brain and spinal cord parenchyma would be better achieved via direct parenchymal injections or by intracerebroventricular (ICV) infusion of sheep. Based on previous studies it was hypothesized that intraparenchymal (IP) administration of AAV9 expressing an enhanced green fluorescent marker protein (*eGFP,* hereafter termed GFP) gene driven by a ubiquitous promoter would result in a more focal distribution of the vector in the ovine brain, whereas a more global transduction may be achieved by direct ICV delivery. If so, widespread improvement in neuropathology may be achieved by AAV9-mediated ICV delivery of disease-modifying transgenes into large mammalian brains, suggesting an effective treatment route for the neurodegenerative pathology seen in some human lysosomal storage diseases.

5.2 Materials and methods

5.2.1 Viral vector

Recombinant adeno-associated viral vector, serotype 9, expressing enhanced green fluorescent protein, (AAV9.CB7.Cl.eGFP.WPRE.rBG), was purchased from the vector core at the University of Pennsylvania (cat # AV-9-PV1963; viral titre 3.6 x 10^{13} viral genomes (vg)/ mL, Philadelphia, PA, USA). The vector genome encoded AAV2 inverted terminal repeats (ITRs) flanking a transcription unit containing GFP under the control of the CAGS promoter (CB7 promoter with chicken beta-actin intron (CI)) and pseudotyped with AAV9 capsid proteins. The importation and use of the recombinant AAV9 vector was approved by the New Zealand Environmental Protection Authority (Permits GMC100166 and GMD004899).

5.2.2 *In vivo* viral injections

Three healthy 9-month old Coopworth sheep (*Ovis aries*) were anaesthetised and prepared for neurosurgery as described in Section 3.2.2. Two sheep received unilateral parenchymal injections of 25 µl (containing 9 x 10^{11} vg) of AAV9-GFP into three sites. Co-ordinates for parenchymal structures were (from bregma): for the primary visual (occipital) cortex, 6 , 8 and 8 mm caudal to bregma, left of midline, and ventral to the pial surface respectively, for the thalamus -8, 8 and 27 mm and for the parietal cortex -8, 8 and 8 mm. The same drill hole was used for the thalamic and parietal injections but the needle was directed 10° rostral for the latter to avoid following the same needle track. For each injection, 2 µl of viral vector was infused over 30 seconds, the needle withdrawn 0.5 mm, and the process repeated until the full volume was discharged. The needle was left in position for a further 3 minutes before slow retraction. A third sheep received bilateral ICV injections of 450 µl AAV9-GFP (containing 1.62 x 10^{13} vg) infused at a rate of 0.1 mL/ min.

Treated animals were housed indoors, fed a mixed ration of chaffed lucerne and pelletised sheep feed concentrate (see Section 3.1.1). They were monitored daily for any adverse symptoms.

5.2.3 Tissue collection and immunohistochemistry

Procedures were performed as described in Section 3.7. Animals were euthanized and the brains perfusion-fixed *in situ* 4 weeks after AAV9 administration. Spinal cord samples (50 – 100 mm in length) were also collected from the lumbar, thoracic and cervical regions, fixed in 10% formalin for 5 days and then processed with the brains (Section 3.7). Serial sagittal brain sections and coronal spinal cord samples (50 µm), cut on a freezing sliding microtome (MICROM International, Walldorf, Germany), were stored in cryoprotectant in 96-well plates at -20°C.

GFP immunohistochemistry was performed as previously described (Linterman *et al*., 2011). In brief, floating sections were pre-incubated in 1% H_2O_2 , 30 min, blocked with 10% normal goat serum (Life Technologies, Carlsbad, CA, USA) in 0.3% Triton X-100 in phosphate-buffered saline (PBS), 2 h, followed by overnight incubation at 4°C with a rabbit polyclonal anti-GFP antibody (1:20,000; #ab290; Abcam, Cambridge, MA, USA), preblocked on normal sheep brains to remove non-specific antibodies. Immunoreactivity was detected with biotinylated goat anti-rabbit IgG (1:1000; B7389; Sigma-Aldrich, Castle Hill, NSW, Australia), 2 h, followed by ExtrAvidin peroxidase (1:1000; E2886; Sigma- Aldrich), 2 h, and staining with 0.5 mg ml-1 3, 3'-diaminobenzadine (DAB; D5637; Sigma-Aldrich) and 0.01% H_2O_2 in PBS. Sections were mounted in 0.5% gelatine and 0.05% chromium potassium sulphate on glass slides, air dried, dehydrated with 100% ethanol, cleared with xylene and coverslips mounted with DPX (BDH, Poole, England). No staining was observed in any negative control sections in which either the primary or secondary antibodies were omitted.

Parallel series of sections were double-labelled with GFP and either glial fibrillary acidic protein, GFAP (1:1000; DAKO Z0334; Carpinteria, CA, USA) or the fluorescent Nissl dye, NeuroTrace (1:150; Life Technologies N21482) as markers of transduced glial cells and neurons, respectively (Section 3.8, Linterman *et al*., 2011). Fluorescent sections were mounted in 0.5% gelatine and 0.05% chromium potassium sulphate on glass slides, air dried, coverslipped using glycerol and imaged on a Zeiss LSM710 confocal microscope.

A standard Nissl (cresyl violet) counterstain, and GFAP or biotinylated α-D galactose specific isoelectin I-B4 from *Griffonia simplicifolia* (1;500; GSB4; Vector Laboratories, Peterborough, UK) immunohistochemistry (see Section 3.8), was performed on adjacent sections around the injection sites, which were examined for signs of injection-related pathology.

5.3 Results

Sheep showed no adverse effects to the surgery, recovery from anaesthesia was uneventful and all resumed normal eating within 12 h. Rectal temperatures, growth rates, body condition and behaviour remained normal during the subsequent four-week observation period, after which the sheep were euthanized. Expression of GFP in the CNS was then compared for the two delivery routes using immunohistochemistry (Figure 5.1).

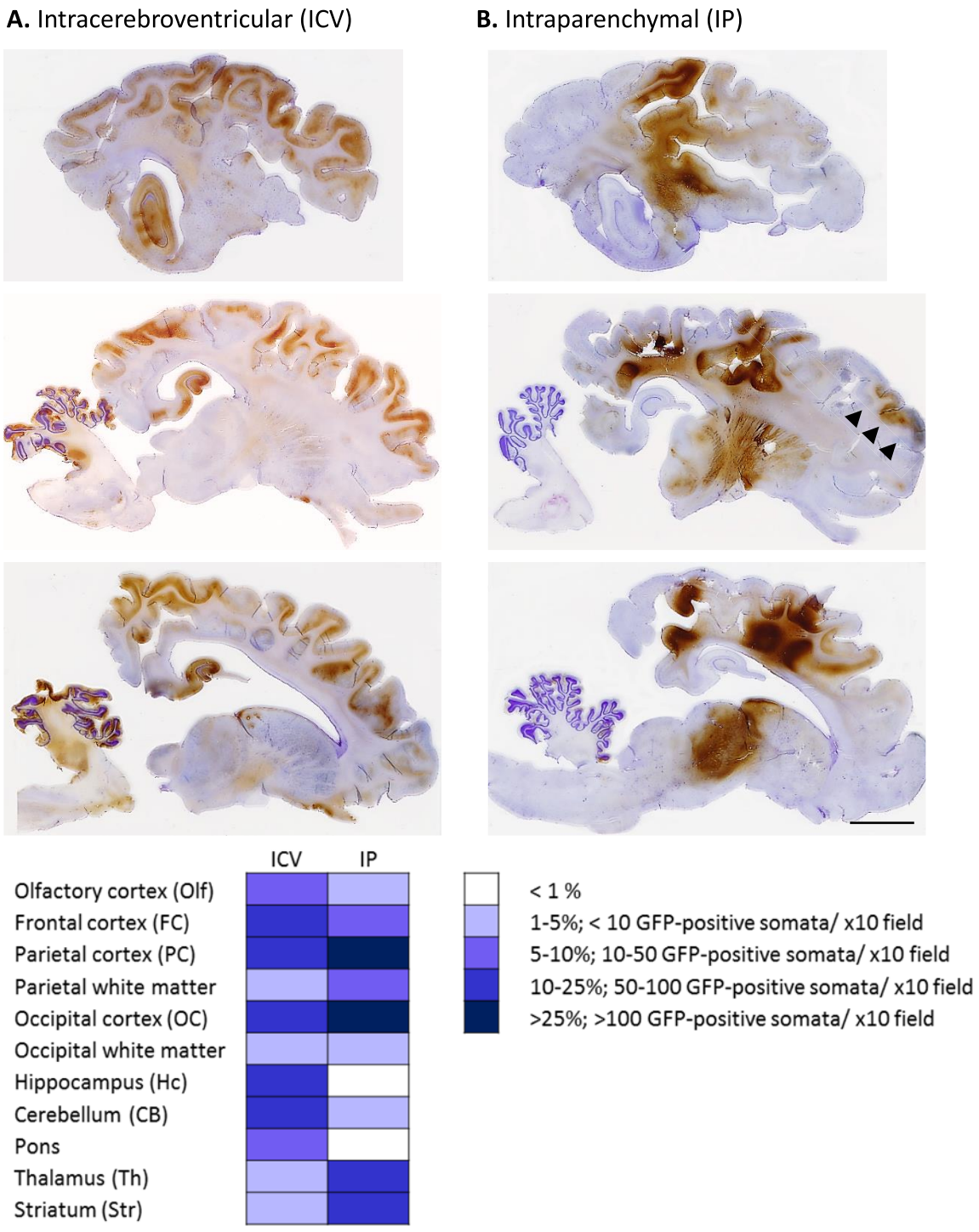

Figure 5.1 Comparative AAV9 transduction efficiency via two delivery routes in the sheep brain
Healthy, juvenile sheep received AAV9 vector encoding for the GFP marker, and transgene expression was evaluated in representative sagittal brain sections one month post-injection by immunohistochemistry. Sections were counterstained with cresyl violet. **A.** Widespread CNS transgene distribution was evident in the sheep brain after bilateral intracerebroventricular (ICV) delivery of a total dose of 3.24 x 10^{13} vg AAV9-GFP. **B.** Unilateral intraparenchymal (IP) delivery of a total dose of 2.7 x 10^{12} vg AAV9-GFP predominantly resulted in focal expression at the three injection sites (thalamus, parietal and occipital cortices), but with evidence of distal targeting (indicated by the arrowheads). **C.** Transduction in different brain regions by the two injection routes was compared through quantification of the GFP signal intensity in 3 images per region per sheep. Colour coding corresponds to % of positive area. Scale bar represents 1 cm.

5.3.1 ICV delivery of AAV9-GFP mediates widespread CNS transduction

GFP immunohistochemistry one-month post-ICV AAV9 delivery revealed widespread transduction in each hemisphere (Figure 5.1A,C), indicative of effective viral transport within the circulating CSF and vector penetration from the CNS surface to deeper regions. The broad transgene distribution extended through all cortical lobes and respective white matter tracts. Large clusters of GFP-positive cells were visible through most cortical laminae, particularly the layer V projection neurons of the occipital, parietal and frontal lobes (Figure 5.2A-C), extending up to 600 µm along multiple dendritic and axonal processes. Hilar, dentate gyrus and CA3 cells of the hippocampus were intensely stained as were cuboidal ependymal cells lining the lateral ventricle, extending right through to the rostral ventricular pole in all mediolateral sections analysed (Figure 5.2E). Additionally, scattered transduced subependymal cells were observed, at least 350 µm from the ventricular surface.

Subcortical GFP expression was more diffuse, although a band of stained puncta was evident in the superficial grey layers of the thalamus (Figure 5.2G) and the rostral and caudal colliculi. Clusters of immunopositive cells were present in the more superficial thalamic nuclei and the hypothalamus (Figure 5.2H) but transduction in the caudate nucleus and striatum was limited to the ventral surface regions. Transduction favoured cells of neuronal morphology, including olfactory bulb neurons and cerebellar Purkinje cells whose dendritic trees ramified in a single plane into the molecular layer (Figure 5.2F, J). Occasional transduced protoplasmic astrocytes were seen in the grey matter of the occipital cortex (Figure 5.2K).

GFP-positive cells were also seen along the extent of the spinal cord, from cervical to lumbar segments (Figure 5.3A). Transduced cell types ranged from interneurons of the intermediate spinal grey matter, scattered stellate cells in the ventral funiculi, columnar ependymal cells lining the CSF-filled central canal to the uni-, bi- and multipolar sensory neurons of the dorsal horn and ventral horn motor neurons with large (25 - 40 µm) diameter somata (Figure 5.3B). GFP was expressed along the thickened branched processes of the sensory neurons and the long thin extensions of the motor neurons, up to 350 µm from the cell soma.

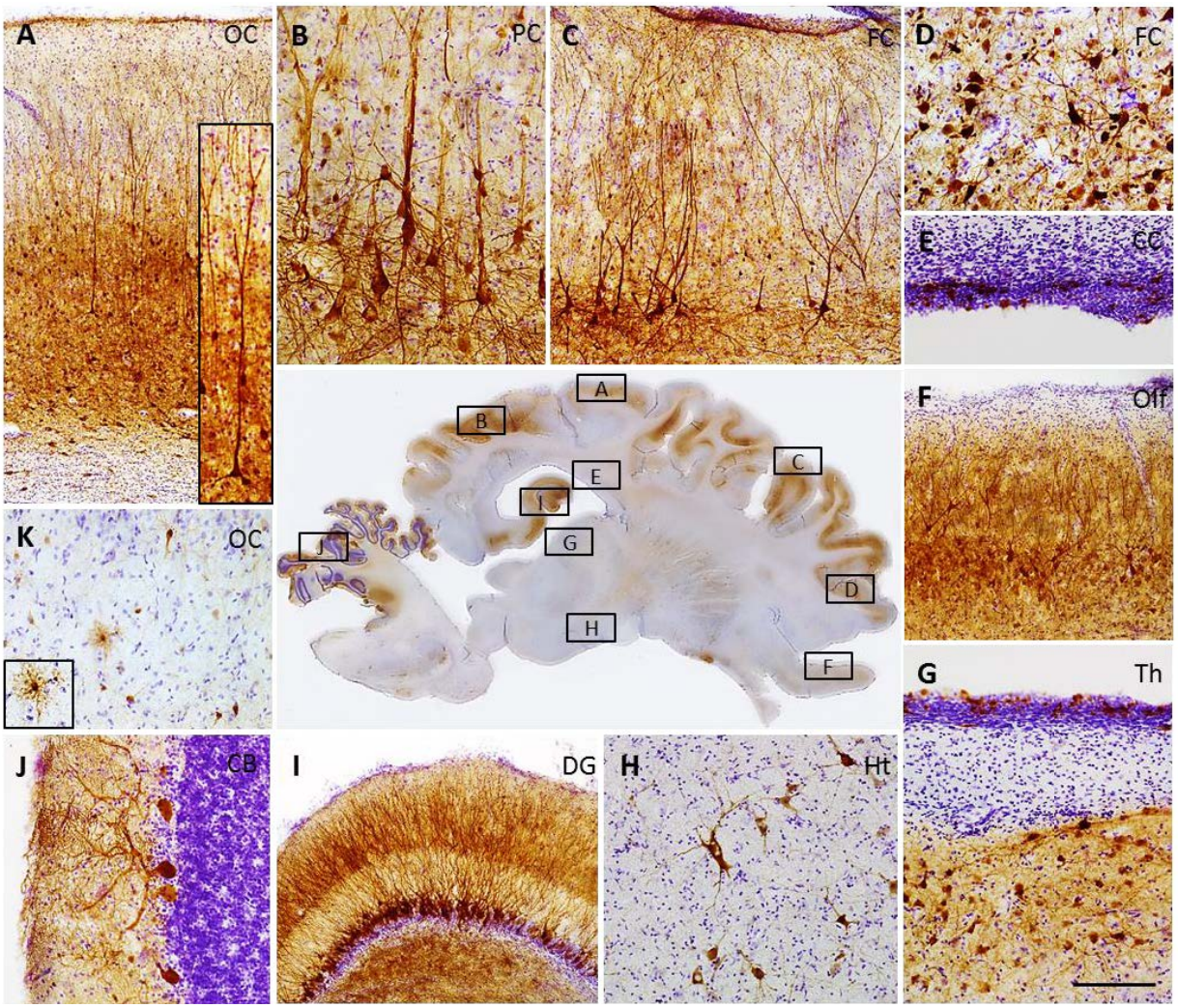

Figure 5.2 Robust CNS transduction profile of the sheep brain after ICV delivery of AAV9-GFP

A total dose of 1.62 x 10^{13} viral genomes of AAV9-*GFP* vector was injected into the lateral ventricles of a healthy 9 month old sheep, with necropsy a month later. Shown are high-magnification images of CNS cell transduction, with insets, and their corresponding locations in a representative mid-sagittal sheep brain section. Robust widespread transduction was observed with large numbers of transduced cells evident in all cortical lobes one month after delivery (**A – D, F**), which were typically neuronal in morphology. Strong GFP expression was seen in the ependymal cells lining the ventricles (**E, G**), as well as the granule cell layer of the dentate gyrus (**I**) and the hilus of the hippocampus. Subcortical transduction was less pronounced; GFP-positive cell clusters were concentrated in the superficial layers of the striatum, thalamus (**G**), colliculi and caudate nucleus adjacent to the ventricles, or closer to the ventral surface of lower brain structures including the hypothalamus (**H**), substantia nigra and cerebellum (**J**). Occasional transduced cells had stellate morphology, reminiscent of astrocytes (**K**). Scale bar represents 500 μm for **A,C,F,I** and 100 μm for **B,D,E,G,H,J,K**. Abbreviations: **CB** Cerebellum; **CC** corpus callosum and dorsal lateral ventricle; **DG** dentate gyrus; **Ht** hypothalamus; **FC** frontal cortex; **OC** occipital cortex; **Olf** olfactory cortex; **Th** thalamus and ventral lateral ventricle; **PC** parietal cortex.

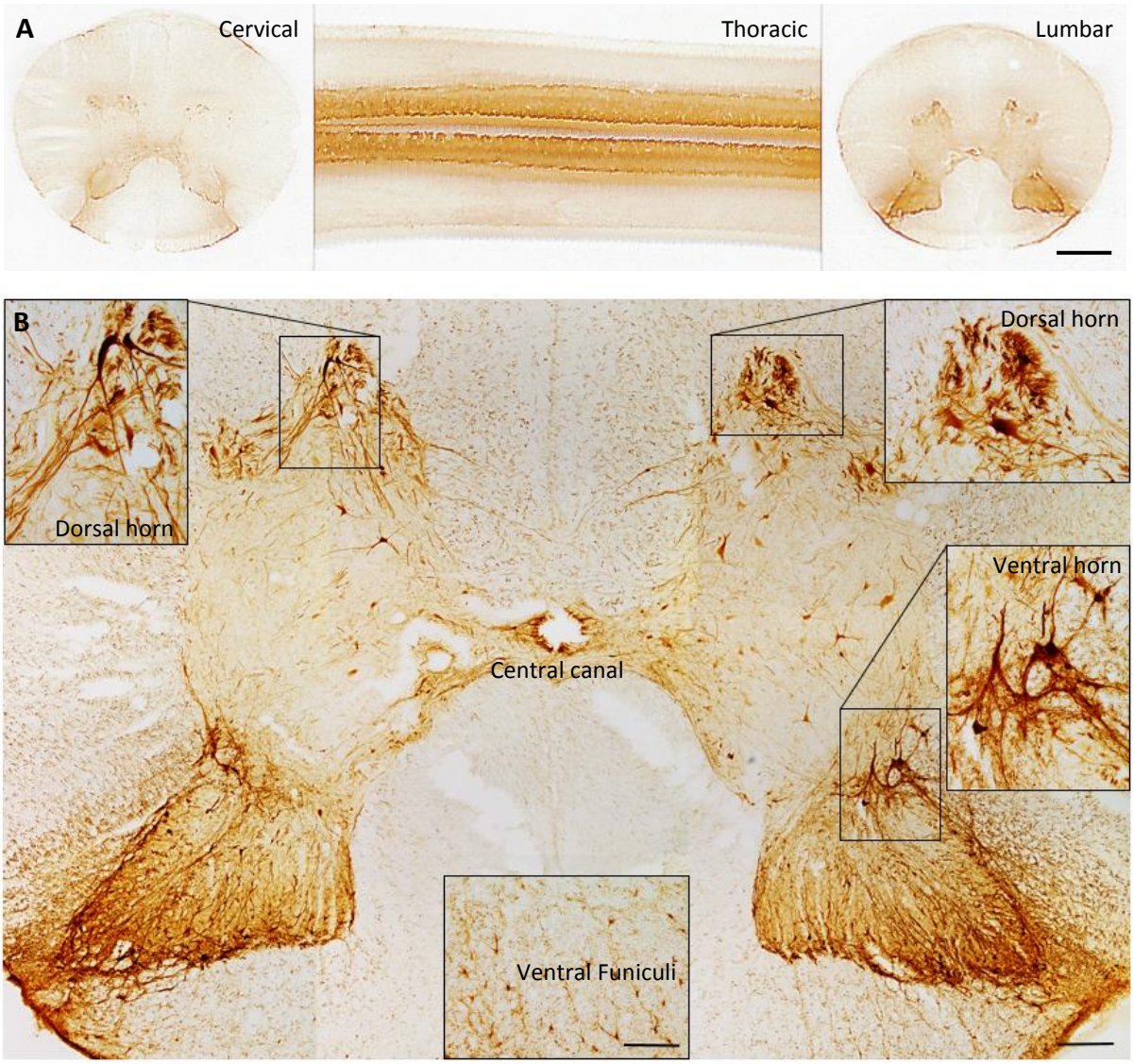

Figure 5.3 Robust transduction of the sheep spinal cord after ICV AAV9-*GFP* administration

Robust transduction of the spinal cord was also evident one month after delivery of 1.62 x 10^{13} vg of AAV9-*GFP* into the lateral cerebral ventricles. **A.** Low-magnification images of cervical, thoracic, and lumbar spinal cord revealed the presence of GFP-positive cells at all levels. **B.** A representative image of a lumbar spinal cord section, with high-magnification of the boxed areas showing immunopositive sensory and motor neurons of the dorsal and ventral horns respectively as well as transduced stellate cells in the ventral funiculi. Scale bar represents 0.2 cm in **A**, 200 μm in **B** and insets 100 μm.

5.3.2 IP delivery of AAV9-*GFP* results in localised and distal transduction

Immunohistochemistry a month after IP injection of AAV9-*GFP* revealed the highest density of GFP-positive cells proximal to the injection sites (Figure 5.1B), and some distal targeting (arrowheads). Dense GFP neuropil immunoreactivity was observed along the needle tracks in the occipital and parietal lobe cortical grey matter (Figure 5.4A,C), but declined further away from the centre of injection (Figure 5.4B). Lateral spread from the needle tracts was considerable, with GFP-positive soma spanning an area up to 12 mm rostrocaudal and 18 mm mediolateral from the injection column, indicating diffusion through the parenchyma. Injection into the thalamus, the largest relay centre for both sensory and motor modalities, resulted in robust transgene expression through most thalamic nuclei (Figure 5.4J) and distribution to motor and sensory cortical regions distal from the injection sites. AAV9 transduced a heterogeneous population of neurons, with immunopositive bi- and multipolar neurons, including the layer V projection neurons of the ipsilateral frontal association and motor cortices (Figure 5.4D,E). Neuronal somata were intensely stained, with GFP expression through the axonal hillock extending up to 500 µm along axonal and dendritic extensions. Cuboidal ependymal cells were transduced through multiple layers (Figure 5.4L), but not along the full extent of the ventricular surface. The cortical columnar delivery stratagem was designed to inject vector into the subventricular zone (SVZ) at its greatest depth but to avoid leakage into the ventricle. Transduced ependyma were therefore located near the base of the cortical injection sites, and sporadic GFP-positive subependymal cells with multiple processes extending vertically into the SVZ were evident. Very few hippocampal cells were transduced (less than five GFP-positive somata per field analysed).

There was modest AAV9 transduction in the non-injected hemisphere, typically concentrated in homotopic regions contralateral to the injection sites such as the parieto-occipital cortex and the thalamic ventricular surfaces (Figure 5.4F), but extending to sporadically transduced cells in the grey matter of the frontal association and motor cortices. Notably GFP-positive cells were detected in the non-injected hemisphere over 20 mm mediolateral from the closest injection site, suggesting antero- and/or retrograde transport of the protein or vector through axons or dendrites.

Examination of the sub-cortical regions of the IP injected brains revealed transduced olfactory bulb neurons (Figure 5.4G), striatal cells (Figure 5.4H), Purkinje cells of the cerebellum (Figure 5.4K) and caudal brainstem cells, which also indicated long-distance axonal transport of the AAV9 vector or protein.

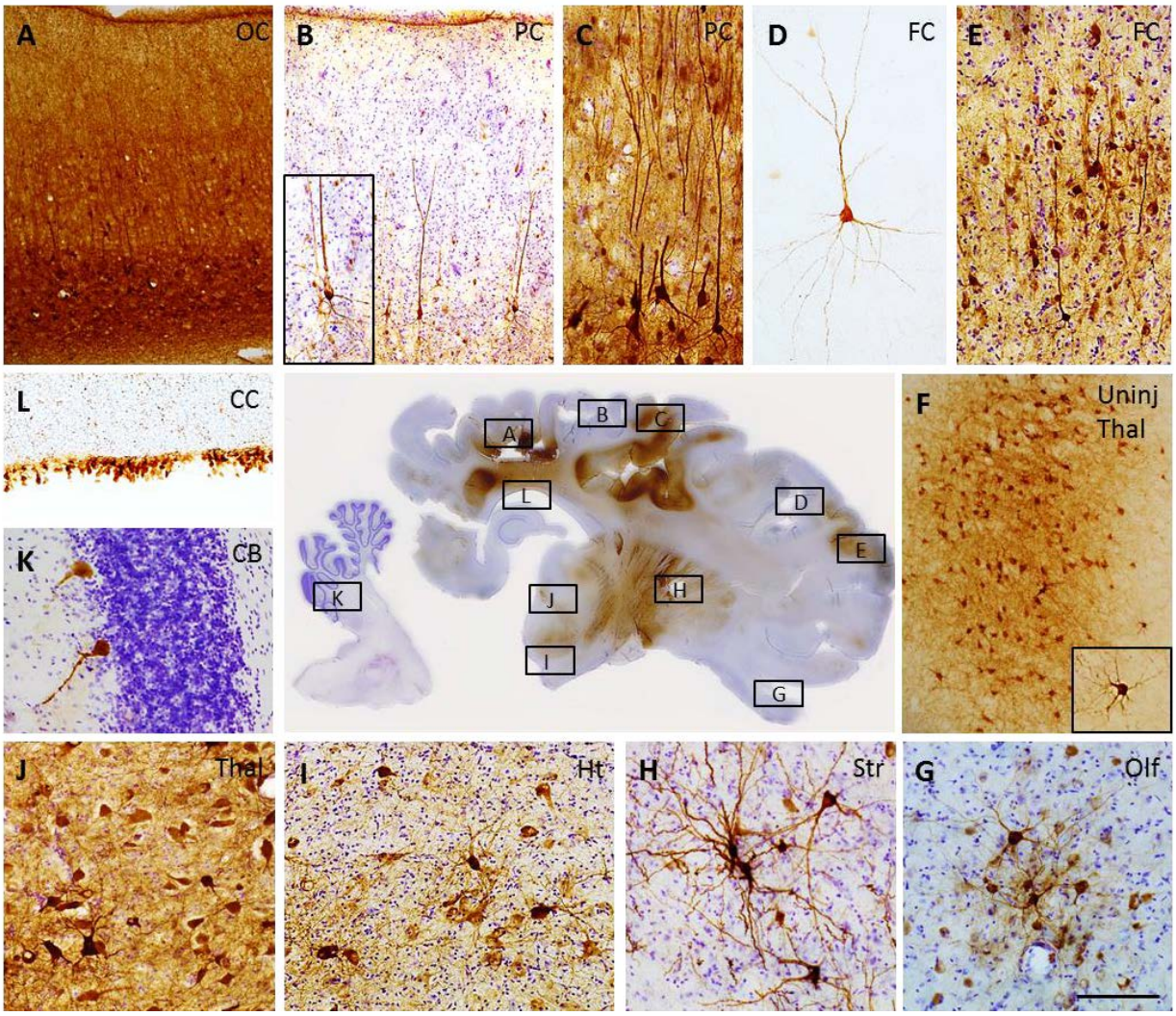

Figure 5.4 Localised CNS transduction profile of the sheep brain after IP delivery of AAV9-GFP
Two healthy 9 month old sheep received unilateral columnar injections of 9 x 10^{11} vg of AAV9-GFP into three parenchymal sites (the thalamus, parietal and occipital cortices, total dose 2.7 x 10^{12} vg). GFP distribution was analysed one month later by immunohistochemistry. Scale bar represents 500 μm for **A,B,G** and 100 μm for **C-F,H-L**. Abbreviations: **CB** Cerebellum; **CC** corpus callosum and dorsal lateral ventricle; **Ht** hypothalamus; **FC** frontal cortex; **OC** occipital cortex; **Olf** olfactory cortex; **Str** striatum; **Th** thalamus; **PC** parietal cortex; **Uninj Thal** uninjected thalamus.

5.3.3 Both ICV and IP delivery of AAV9-GFP result in predominantly neurotropism

AAV9 tropism was assessed in representative brain sections labelled with antibodies against GFP and cell specific phenotypic markers. GFP expression was strongest in cells with neuronal morphology, confirmed by confocal colocalisation of the neuronal marker NeuroTrace and GFP (Figure 5.5A,B). Multipolar NeuroTrace-positive neurons expressed GFP throughout spheroid cell somata and over 300 μm along multiple dendritic and axonal processes. Although scattered astrocytic profiles were seen using histochemical staining (Figure 5.2K), these were not detected using confocal co-labelling with GFAP antibodies (Figure 5.5C).

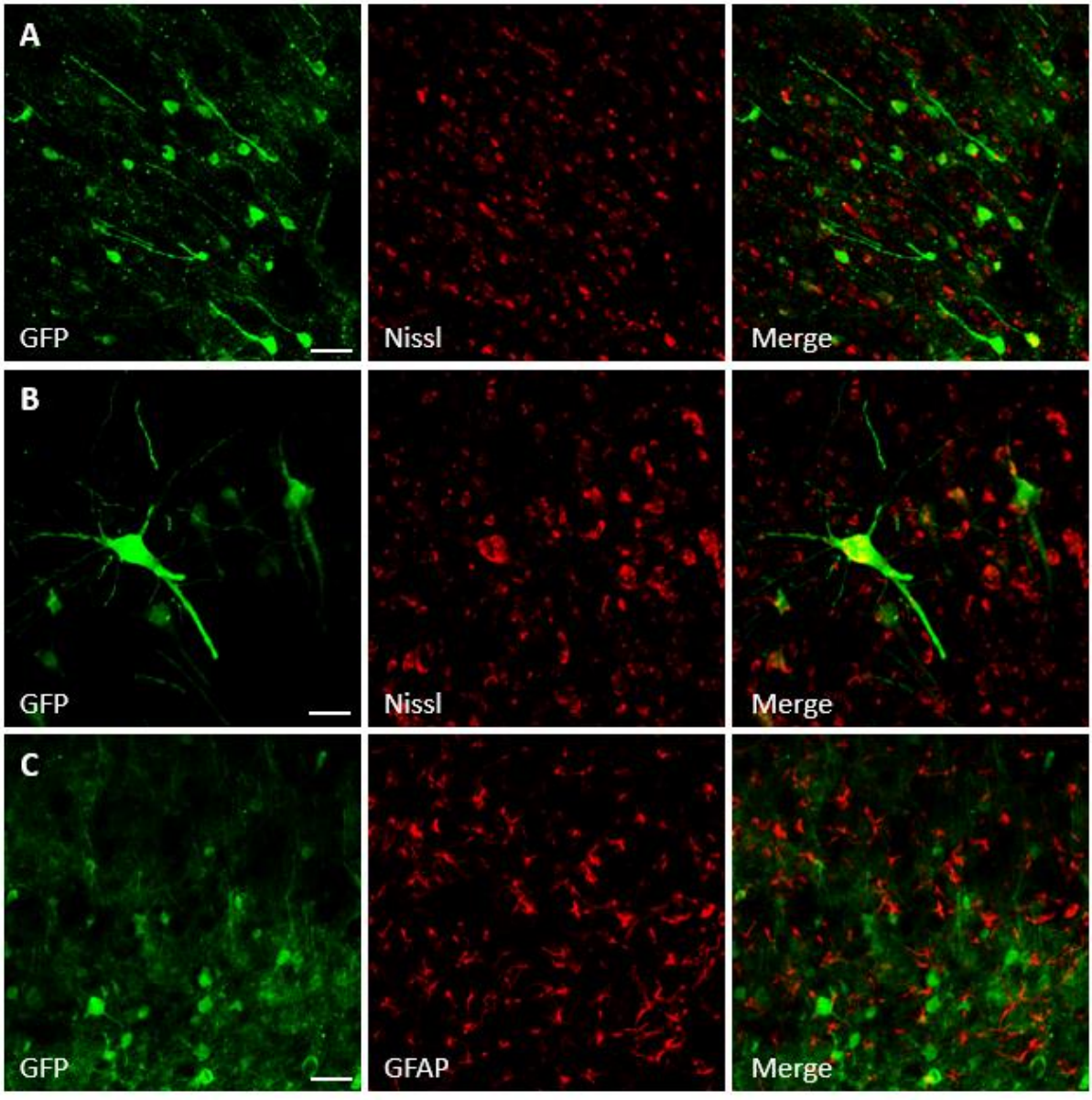

Figure 5.5 Dominant neurotropism of the AAV9-GFP vector in the healthy adult sheep brain
Representative images of brain sections stained with antibodies against GFP, **A-B**, Nissl, NeuroTrace (neurons) or **C.** GFAP (an astrocytic marker). Both ICV and IP infusion resulted in preferential neuronal transduction and low transduction of astrocytes. Scale bar represents 50 μm.

5.3.4 IP delivery of AAV9-GFP triggers an inflammatory response

Examination of GFAP, GSB4 (a microglial marker) and GFP/Nissl counterstained sheep sections indicated no signs of inflammation or other pathology in the ICV injected hemispheres and the GFP-expressing cells retained healthy morphologies typical of their type (Figure 5.6A,C,E). Gliosis was not evident and no adverse effects were detected within the vasculature. Elongated flattened GSB4-positive perivascular cells were observed, as they were in non-injected control brains.

Conversely, a localised lymphocytic inflammatory and focal glial response was evident around the needle tracks in the IP injected sheep. This was confirmed by GSB4 and GFAP immunohistochemistry, which revealed activated astroglia and microglia, possessing large soma and thickened retracted processes, in the parenchymal regions of highest transduction (Figure 5.6B,D) but typical quiescent ramified glial cells throughout the rest of the brain. Perivascular cuffs of macrophages and microglial infiltrates were observed in the white matter at the cortical IP injection sites (Figure 5.6F) accompanied by an incipient reactive astrocytosis. There was no indication of a brain-wide immune response or cell death resulting from these IP injections or in regions with high GFP expression mediated through retrograde vector transport.

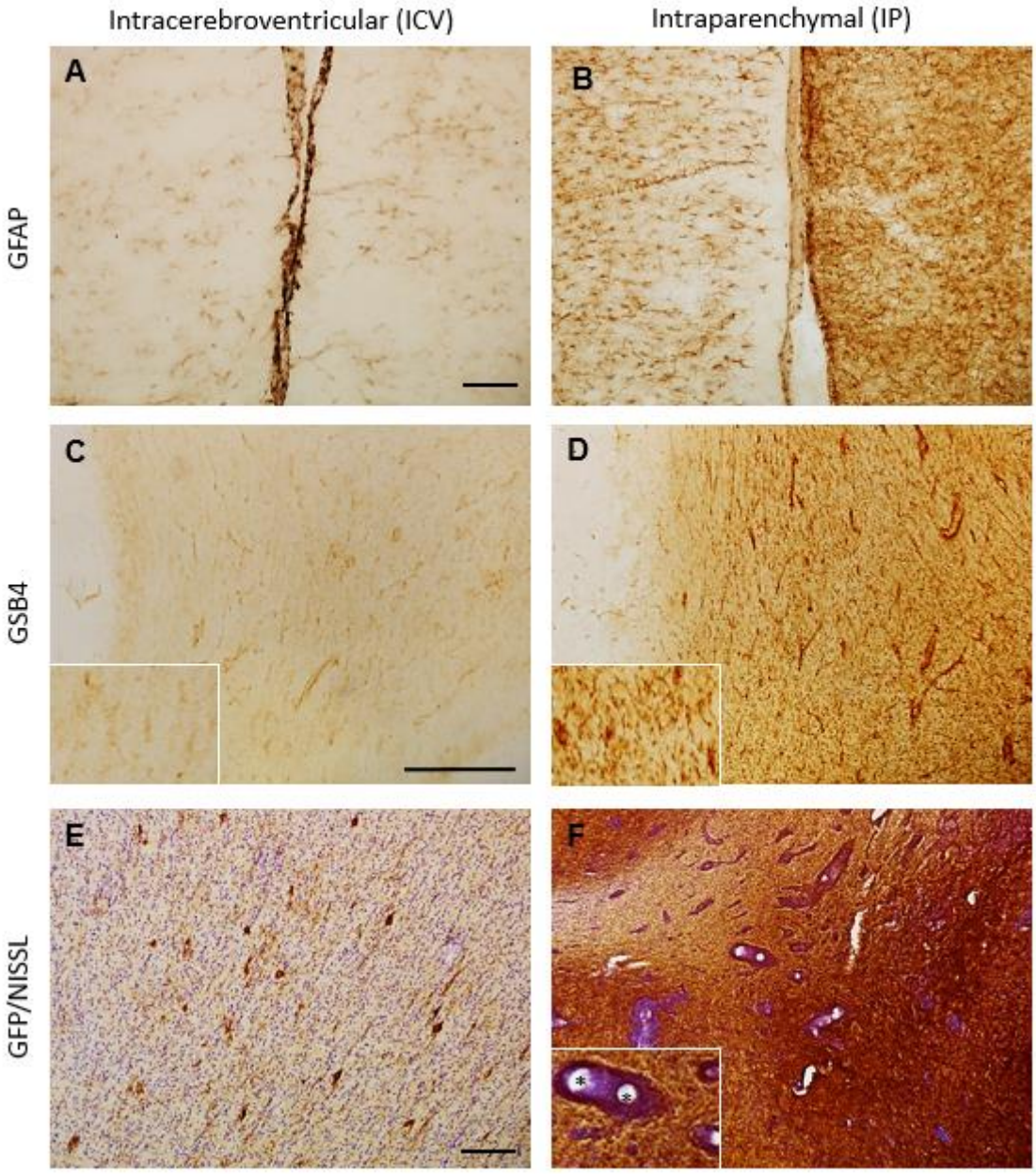

Figure 5.6 Differential inflammatory responses following ICV and IP injection of AAV9-GFP

Sagittal sheep brain sections were stained against **A,B** an astrocytic marker (GFAP), **C,D** a microglial marker (GSB4) and **E,F** GFP with Nissl (cresyl violet) counterstain. No neuroinflammatory response was found one-month after ICV administration (**A,C,E**) whereas inflammatory marker reactivity and perivascular cuffing was apparent in the IP-injected brains (**B,D,F**) particularly near the cortical injection sites. The reactive astrocytosis evident at the occipital injection site and adjacent gyrus in the IP-injected brain (**B**) was not seen in the distal cortical regions. Activated microglia were localized to the white matter tracts in close proximity to the intracortical injection sites (**D**). No perivascular infiltration or luminal pathology was observed in the blood vessels after ICV delivery (**E**) however localized perivascular inflammatory foci were seen in the transduced cortical white matter (asterisks) on IP infusion (**F**). Scale bar represents 100 µm for **A,B,E,F** and 500 µm for **C,D**.

5.4 Discussion

This study aimed to test the ability of AAV9 to transduce neurons in the normal sheep brain by direct stereotactic delivery into the brain parenchyma or into the CSF of healthy, juvenile sheep. Vector administration by both routes was safe and well tolerated, with stable GFP expression evident one month post-injection. AAV9 injections into the sheep brains resulted in strong robust predominantly neuronal transduction. After IP delivery, this was localised with some distal targeting by diffusion and axonal transport but was much more widespread through the CNS after ICV administration, including the spinal cord (Figure 5.1). The neuronal preference with minimal tropism for astrocytes following either delivery route is similar to that seen in other animal models. Strong neuronal transduction has been observed after both ICV and IP delivery of AAV9-GFP into the dog brain (Haurigot *et al*., 2013; Swain *et al*., 2014), cortical neurons were specifically targeted after IP injections into mice (Aschauer *et al*., 2013) and striatal AAV9 injection into non-human primates resulted in a high tropism for neuronal cells, with low transduction of astrocytes (Masamizu *et al*., 2011).

Previously direct brain parenchymal injections of AAV vectors have been extensively explored in animals and extended into clinical trials for patients affected by neuropathic LSDs, such as Canavan disease (Janson *et al*., 2002; Leone *et al*., 2012), late infantile neuronal ceroid lipofuscinosis (Crystal *et al*., 2004; Worgall *et al*., 2008), mucopolysaccharidosis types IIIA (Tardieu *et al*., 2014) and metachromatic leukodystrophy (Zerah *et al*., 2015). Naturally occurring ovine models of other LSDs exist and represent ideal pre-clinical models to test the efficacy and long-term safety of gene therapy, and also validating other translational delivery approaches. However the use of AAV vectors in the sheep brain has not been previously documented but, consistent with findings in non-human primates and dogs (Masamizu *et al*., 2011; Swain *et al*., 2014), unilateral IP injections of AAV9 in this ovine study result in focal transduction, with greater diffusion through the brain parenchyma than was reported for lentiviral vectors (Linterman *et al*., 2011). The vector doses given to sheep were comparable to those used in human clinical trials (Crystal *et al*., 2004). There was evidence of neuronal transport of AAV9 along neural projections, with distal targeting of layer V projection neurons of the ipsilateral frontal association and motor cortices (Figure 5.4), and scattered clusters of transduced cells in the uninjected hemisphere. This is consistent with previous studies in mice, dogs and non-human primates which indicate AAV9 undergoes anterograde and/or retrograde axonal transport with spread of the transgene product along specific interconnected CNS pathways and to the contralateral hemisphere through axonal tracts (Cearley & Wolfe, 2006, 2007; Masamizu *et al*., 2011; Castle *et al*., 2014; Swain *et al*., 2014). Additionally Purkinje cells of the cerebellum and caudal brainstem cells were transduced, a finding not observed in the hind-brain of dogs injected intraparenchymally with AAV9-GFP (Swain *et al*., 2014).

In the current study, three parenchymal sites were targeted. Sheep and human brains are too large and complex to attempt repair of the whole brain as viral spread from IP-directed gene therapy is relatively limited, therefore careful targeting of selected regions and cell types is required for this approach to be successful. The thalamus represents a structure that harbours high levels of neural interconnectivity. It receives afferent input from many CNS structures and relays this information through corticothalamic projections to the cortex, from which it also receives reciprocal sensory signals. Thus widespread distribution of lysosomal enzymes through the mammalian CNS may be achieved via axonal retrograde transport by targeted correction of the thalamus. Evidence to support this comes from widespread enzyme distribution from the CNS and eye after targeted thalamic injections with AAV vectors in adult GM1- gangliosidosis mice (Baek *et al*., 2010) and cats (McCurdy *et al*., 2014). The distal targeting of AAV9-GFP to the ipsilateral ovine motor and frontal cortex seen in the current study may be attributed to the IP thalamic injection. Cortical injections into the sheep parietal and occipital lobes specifically targeted the ependyma and subependymal cells of the subventricular zone (SVZ), in an approach explored in sheep with lentiviral-mediated gene transfer (Linterman *et al*., 2011). The rationale behind choosing these parenchymal sites is that specific direction of the injection locale to the subventricular zone (SVZ) could correct the resident neural progenitor cells (NPCs) in this region, providing an *in situ* stem cell repair therapy. The robust focal transduction detected after IP delivery of AAV9 vector to the sheep brain demonstrates that stereotactic injections in sheep can target smaller neuronal populations with distinct functions.

The intraparenchymal approach is ideal for gene therapies targeted to selected cell populations or specific anatomical circuitry, such as in Parkinson's disease, or specific anatomical regions where neuropathology is localized. However many neurogenetic disorders require wide-scale CNS transduction which is more difficult and less practical to achieve by IP injection, as shown here and by others (Foust *et al*., 2009; Fu *et al*., 2011; Hinderer *et al*., 2014). Scaling up the dose requires greater injection volumes and more injection sites. Additionally there was evidence of a focal immune response at the IP injection sites (Figure 5.6), which may be against the viral capsid or the transgene product itself, or following mechanical trauma associated with the needle insertion and/or the volume injected. Despite evidence for naturally occurring antibodies to AAV9 in sheep (Tellez *et al*., 2013), a humoral immune response to the capsid seems unlikely in this scenario as no obvious clinical problems have occurred in sheep undergoing long-term combined ICV/IP AAV therapeutic treatment (see Chapter 6 and Chapter 7). AAV9-mediated CNS expression of non-self proteins, including GFP, has been reported to induce neuroinflammation and neurotoxicity in rat and non-human primate brains after IP and intra-CSF delivery (Ciesielska *et al*., 2013; Samaranch *et al*., 2014). For patients with null mutations in the endogenous gene or those previously exposed to AAV serotypes, a non-self transgene response could become a problem in gene therapy (Mingozzi & High,

2013), regardless of delivery mechanism. A similar gauge needle was used in the ICV delivery without an immune response, indicating that the volume of fluid injected may be the sole cause of the localised inflammation after IP injection. How long this immune response persists is yet to be determined.

Intracerebroventricular injection of AAV into the CSF represents an alternative approach to transduce the brain. Initial attempts with AAV serotypes 2, 4 and 5 in mice and mammalian brains were thwarted, albeit with successful transduction of ependymal cells lining the ventricles, as there was limited or no penetration of the deep brain parenchyma from the CSF spaces and a lack of neuronal transduction without the systemic addition of adjuvants, such as mannitol (Ghodsi *et al*., 1999; Davidson *et al*., 2000; Liu *et al*., 2005b; Fu *et al*., 2003). In contrast, this study shows that direct ICV injection into the lateral ventricles is an effective method for AAV9-mediated transduction of the sheep CNS, resulting in comprehensive and strong transduction of the CNS (Figure 5.2), and no significant neuroinflammatory response at the dose used (Figure 5.6). Ependymal cells were targeted but GFP expression was detected throughout the CNS. A similar result was seen through the central and peripheral nervous systems following ICV delivery and a titre-matched dose of AAV9-GFP vector into dogs (Haurigot *et al*., 2013). This contrasts a lack of widespread transduction following ICV injection into the rat (Gray *et al*., 2013), which may relate to the smaller size of the rodent CNS highlighting the translational limitations of these models. Recombinant protein expression in mice was restricted to upper spinal cord segments following direct ICV delivery in a previous study (Storkebaum *et al*., 2005), whereas ICV infusion of AAV9 results in strong transduction of the sensory and motor neuron pools throughout the ovine spinal cord. This is consistent with observations following intra-CSF delivery to cats, pigs, dogs and non-human primates (Bevan *et al*., 2011; Federici *et al*., 2012; Samaranch *et al*., 2012, 2013; Haurigot *et al*., 2013; Bucher *et al*., 2014) and systemic delivery in mice, cats and non-human primates (Duque *et al*., 2009; Bevan *et al*., 2011).

As mentioned, the efficacy of AAV9 transduction by alternative intra-CSF (intrathecal or intracisternal) delivery routes has been studied in other models systems. Doses in the range of 10^{10} - 10^{12} vg/ kg were sufficient to mediate widespread spinal cord expression but only variable brain parenchymal transduction. From a neuroanatomical point of view, ICV delivery should be effective for brain-directed genetic correction than other intra-CSF delivery routes. The CSF is produced through dialysis of the capillary blood by epithelial cells of the choroid plexus. These plexi lie adjacent to the ependymal cells lining the lateral ventricles and the roof of the third and fourth ventricles. Widespread parenchymal correction can be achieved by ICV directed AAV9 gene transfer but this route also offers the opportunity for targeted transduction of the ependymal cells lining the ventricle, with resultant secretion of the transgene product into the CSF and hence an ongoing global protein delivery mechanism. Freshly made CSF flows from the lateral ventricles via the foramen of

Monro into the third ventricle, and then into the fourth ventricle via the cerebral aqueduct in the brainstem. From there, it passes into the cisterna magnum and subarachnoid space, bathing the brain and spinal cord, before being returned to the circulation via the arachnoid villi. One might expect less vector would be available to target the brain and ventricular system after intracisternal, and especially intrathecal, delivery than by the ICV route, although this direct comparison has yet to be examined in sheep. Interestingly, there was no evidence of transduced cells in the brain, not even the ventricular ependyma, after injection of lentiviral vectors into the cisterna magnum of sheep (Linterman *et al*., 2011). In dogs, delivery of 2 x 10^{13} vg AAV9-GFP resulted in slightly greater GFP expression and vector distribution in the brain, spinal cord and peripheral nervous system after ICV delivery than through the intracisternal route (Haurigot *et al*., 2013). Limited distribution through the CNS has been achieved by the lumbar intrathecal approach. Preclinical data in pigs show vector penetration was restricted to the injection site after lumbar delivery and required three consecutive bolus injections into the cervical, thoracic and lumbar regions to achieve widespread spinal cord transduction (Federici *et al*., 2012). Moreover, intracisternal and intrathecal routes also resulted in contradictory tropism observations. For example, intracisternal injection of AAV9 resulted in both neuronal and astrocytic transduction in cats (Bucher *et al*., 2014) whereas cisterna magna delivery to non-human primates resulted in greater transduction of fibrous and protoplasmic astrocytes than of neurons (Samaranch *et al*., 2012).

In terms of clinical translation and practicality, lumbar intrathecal delivery is a relatively low risk procedure and the most clinically applicable however, with inefficient penetration of the CNS, it may be futile. Whilst cisternal entry is a routine procedure in veterinary medicine, it is not as practicable in paediatric clinical medicine because of the smaller size of the human cisterna magna and its close proximity to the vital cardiac, respiratory and vasomotor centres of the medulla (Haurigot *et al*., 2013; Hinderer *et al*., 2014). Surgical ICV delivery on the other hand is relatively straight-forward; ventriculosotomy being a routine diagnostic and therapeutic neurosurgical procedure in humans with more than 24, 000 procedures performed in the United States annually (Rosenbaum *et al*., 2014).

A third option, systemic intravenous (IV) injection of AAV9 vectors, is minimally invasive and offers global transgene delivery, however much larger vector doses would be required. For example doses of more than 10^{14} vg of AAV9 (in a maximum volume of 10 mL) were utilized in macaques (Bevan *et al*., 2011) with 10^{15} vg predicted for adult human treatment (Samaranch *et al*., 2012). With systemic IV delivery, the vector circulates through the entire body so is not restricted to the CNS and transduction of peripheral organs can occur. This can result in a loss of vector, off-target side effects and the increased risk of an immune response (Zincarelli *et al*., 2008; Xie *et al*., 2011). High titres of neutralising antibodies may block transduction of the target or peripheral tissues after IV delivery,

with a resultant lack of efficacy (Gray *et al*., 2011; Samaranch *et al*., 2012). Vector neurotropism after IV delivery is also reported to vary with age at injection. Peripheral, systemic injection of murine neonates resulted in widespread neuronal transduction, whilst adult mice exhibited a preferential astroglial tropism (Foust *et al*., 2009). AAV9 also targeted glial cells predominantly after intravascular administration to adult monkeys (Bevan *et al*., 2011; Samaranch *et al*., 2012). This age-dependent viral tropism has not been reported following ICV delivery, so the reduced vector dose and wide dissemination make it an advantageous alternative for neuronal transduction.

5.5 Conclusion

In summary, proof of therapeutic concept for AAV9-mediated transduction has been established in a sheep model following ICV or IP administration. Neurotropic global transgene expression was achieved by ICV delivery with no evidence of vector or procedural neuroinflammation or toxicity indicating that this route of administration may be simpler and more effective than multiple intraparenchymal injections. Recently, the ICV approach has proven efficacious in correcting somatic and neuropathology in diverse LSD animal models, with favourable phenotypic outcomes after AAV9 administration in MPS-IIIA and IIIB mice (Haurigot *et al*., 2013; Ribera *et al*., 2015), and AAV2 in a canine model of CLN2 NCL (Katz *et al*., 2015). Concurrent studies with AAV9-mediated ICV delivery of corrective genes to ovine models of CLN5 and CLN6 NCL show protection from pathologic phenotype and behavioural dysfunction (Chapter 6 and Chapter 7 in this thesis). Clinical development of the ICV route as a therapeutic approach is underway.

Chapter 6

Gene transfer to the CLN5 affected sheep

6.1 Introduction

The majority of NCL proteins are localised to the lysosome and affect its function. However the exact cellular and physiological functions of many NCL proteins are unknown; including the *CLN5* gene product, a soluble mannose-6-phosphate-tagged lysosomal protein (Holmberg *et al*., 2004; Sleat *et al*., 2005, 2006) which is mainly expressed in brain tissue, particularly in neurons and microglial cells (Schmiedt *et al*., 2012). The CLN5 protein is proteolytically cleaved in the ER, with the mature protein traficking to the lysosome (Schmeidt *et al*., 2010). Loss of CLN5 function leads to selective neurodegeneration and the specific accumulation of subunit c of the mitochondrial ATP synthase complex (Tyynelä *et al*., 1997). The human CLN5 disease typically manifests between 4 and 7 years of age and phenotypic features include loss of vision, mental and motor deterioration, seizures and premature death, usually during the second decade (Santavuori *et al*., 1982, 1991; Teixeira *et al*., 2003b; Bessa *et al*., 2006; Xin *et al*., 2010).

Deficiencies in soluble lysosomal enzymes or proteins underlie other forms of NCL, including CLN1, CLN2 and CLN10. Like CLN5, these forms are considered potentially amenable to *in vivo* viral-mediated gene therapy by the phenomenon known as 'cross-correction', whereby soluble lysosomal proteins are secreted from cells and endocytosed by adjacent or distal protein-deficient cells (Fratantoni *et al*., 1968; Neufeld & Fratantoni, 1970). With as little as 5 – 15% of normal protein levels purported to restore cellular function, genetic correction of only a subset of diseased cells may supply a permanent source of secreted functional protein sufficient to cross-correct the surrounding protein-deficient parenchyma (reviewed by Sands & Davidson, 2006). However to achieve sustainable therapeutic concentrations of protein throughout the CNS, successful gene therapy for the NCLs will likely require either targeted or widespread neurotropic gene delivery.

Historically lentiviral (LV) vectors have been widely used as gene transfer tools for the CNS manifestations seen in the LSDs, showing persistent transgene expression in small (Brooks *et al*., 2002; Haskell *et al*., 2003; Di Domenico *et al*., 2009; Lattanzi *et al*., 2010) and large animal models (Kordower *et al*., 2000; Jarraya *et al*., 2009), including sheep (Linterman *et al*., 2011) after intraparenchymal (IP) delivery. Preferential neuronal transduction by lentiviral vectors has been achieved through pseudotyping with the glycoprotein of vesicular stomatitis virus (VSV-G) and neuron-specific promoters (Jakobsson & Lundberg, 2006). More recently, recombinant AAV vectors have emerged as the *in vivo* gene transfer platform of choice, with their natural broader tropism,

efficacious results in the CNS of numerous murine and large animal models (Burger *et al*., 2004; Sondhi *et al*., 2005; Baek *et al*., 2010; Haurigot *et al*., 2013) and an excellent safety profile in non-human primate and initial human studies (Markakis *et al*., 2010; Bartus *et al*., 2013; Gray *et al*., 2013; Tardieu *et al*., 2014). Of the AAV serotypes, AAV9 has been used increasingly in the treatment of neurodegenerative disorders because of its efficient targeting of the brain when introduced into the parenchyma, systemic circulation or cerebrospinal fluid (CSF) (reviewed by Dayton *et al*., 2012). AAV9 has also been shown to mediate neurotropic gene delivery to the sheep brain after both IP and intra-CSF delivery (Chapter 5).

Promising results achieved with direct delivery of AAV vectors to the brain parenchyma in animal models (Hackett *et al*., 2005; Sondhi *et al*., 2005, 2007, 2012; Passini *et al*., 2006) have been extended to human clinical trials for late infantile NCL patients caused by mutations in the *CLN2* gene (see Section 1.6.4). However limited distribution from the point of injections required vector administration at multiple sites (Worgall *et al*., 2008) and specific surgical procedures (Souweidane *et al*., 2010), suggesting other vectors and delivery routes should be explored. Large disease-relevant animal models, such as sheep, serve as a valuable translational tool in which to test and expedite these approaches to the clinic.

The current study was instigated to test and compare the safety and efficacy of AAV9- and lentiviral vector-mediated delivery of ovine *CLN5* in a naturally occuring CLN5 NCL model in New Zealand Borderdale sheep. Affected sheep have a c.571+1G>A splice site mutation in the *CLN5* gene (Frugier *et al*., 2008), which results in the loss of function of an uncharacterised soluble lysosomal glycoprotein in human patients (Holmberg *et al*., 2004; Sleat *et al*., 2005, 2006). The ovine model recapitulates many of the clinical and neuropathological features of the human disease, including visual loss, progressive neurodegeneration and storage body accumulation (Jolly *et al*., 2002; Frugier *et al*., 2008). Clinical progression is remarkably stereotypical. Affected sheep initially develop visual loss at 10 - 11 months of age, with progressive neurodegeneration, reaching a humane endpoint typically before 22 months of age. It was hypothesised that pre-symptomatic viral-mediated gene transfer with the corrective *CLN5* transgene would attenuate the natural disease progression in CLN5 affected sheep. If so, this would provide some hope in the search for a treatment for this and other soluble forms of NCL.

6.2 Materials and methods

6.2.1 Study design

CLN5 affected Borderdale sheep received lentiviral- or AAV9-mediated gene therapy between 2.1 - 3.5 months of age, prior to the onset of neurological disease signs. Viral vectors were delivered bilaterally into the cerebral lateral ventricles (intracerebroventricular; ICV) and to two intraparenchymal (IP) (cortical) sites which have been shown to degenerate significantly in the affected sheep. Clinical, cognitive and behavioural tests were developed, in conjunction with quantitative CNS imaging techniques, to assess disease progression and monitor therapeutic correction longitudinally.

The study endpoint was initially defined as 18 months of age, equivalent to an advanced disease state in untreated affected sheep, at which age the treated sheep were to be euthanized and collected tissues evaluated for any pathological amelioration. Once it became apparent that the treatment was functionally efficacious, the study was continued and has not yet reached its final endpoint. Table 6.1 summarises the study design.

6.2.2 Animals

Borderdale sheep within the CLN5 research flock were bred, maintained and diagnosed at birth as described in Section 3.1(Frugier *et al*., 2008). Cohorts of homozygous affected (*CLN5-/-*; *n* = 4) and clinically normal heterozygous (*CLN5+/-*; *n* = 4) sheep were maintained under normal pastural conditions at the Research Farm, Lincoln University, and acted as untreated affected and normal controls. An additional six pre-symptomatic *CLN5-/-* sheep were weaned early, at 1.5 $\pm$ 0.1 (lentiviral cohort) or 2.2 $\pm$ 0.2 (AAV cohort) months of age, housed indoors and fed initally on calf start-mix (Reliance Feeds, Rolleston, New Zealand), chaffed lucerne and a pelletised lucerne feed concentrate (see Section 3.1.1) prior to *in vivo* gene injection therapy at 2.1 to 3.5 months of age. There was one sibling pair in the study (1105/13 and 1106/13), with one in each treatment cohort (Table 6.1). In November 2015, the New Zealand Environmental Protection Agency (EPA) indoor housing restrictions for the AAV9-treated sheep were relaxed and these animals were permitted to move to outdoor pasture for the remainder of the trial. One animal remains alive at 33 months of age in May 2016. Two sheep included in the gene therapy study (1106/13 and 1117/13) were ram lambs that had been castrated by elastration prior to 1 month of age. Pretherapy, the CLN5 genotype was reconfirmed from genomic DNA isolated from venous blood and this was repeated by an independent evaluator every six months and/or at *post mortem.*

6.2.3 Viral vectors

The ovine CLN5 coding sequence (GenBank accession number NM_001082595; Frugier *et al*., 2008) was amplified at Lincoln University by a hybrid polymerase chain reaction using CLN5-specific primers on sheep cDNA (unpublished PhD findings, Janet Boyu Xu, Lincoln University). The full length CDS was cloned into a pCR4 plasmid (Invitrogen, Carlsbad, CA, USA) and sent to the Otago Viral Vector Facility, University of Otago for sub-cloning and generation of lentiviral (LV) and recombinant AAV (serotype 9; AAV9) viral vectors expressing ovine CLN5, under the control of the myeloid sarcoma virus U3 element as described (see Section 3.2.1). Functional viral titres for the LV-MND-*CLN5* (hereafter referred to as LV-*CLN5*) were 1.1 x 10^{10} transducing units (TU)/mL. Genomic titres for AAV9-MND-*CLN5* (hereafter AAV9-*CLN5*) were 2.85 x 10^{12} ssDNA viral genomes (vg)/mL.

6.2.4 *In vivo* viral injections

The stereotactic surgical procedures are described in Section 3.2.2. LV-*CLN5* or AAV9-CLN5 vectors were injected bilaterally into the occipital and parietal cortices, and into the lateral cerebral ventricles of pre-symptomatic *CLN5-/-* sheep. One cohort of sheep (*n* = 3, mean age 2.2 $\pm$ 0.1 months) each received a total dose of 3.6 x 10^{9} TU of LV-*CLN5* (110 µl per ventricle; 26 µl per parenchymal site; vector titre 1.1 x 10^{10} TU/ml) through four 3 mm holes made in the skull at the following co-ordinates (in mm) relative to bregma: occipital cortex, anterior-posterior (AP) -4, mediolateral (ML) $\pm$7, dorsoventral (DV) -11 (from the meninges/pial surface); parietal cortex, AP +7, ML $\pm$7, DV -11.

The second cohort (*n* = 3, mean age 3.2 $\pm$ 0.2 months) each received a total dose of 3.1 x 10^{12} vg of AAV9-*CLN5* (500 µl per ventricle; 25 µl per parenchymal site; vector titre 3.1 x 10^{12} vg/ml). To accommodate for brain growth due to their older age at injection, co-ordinates were revised for this cohort to: occipital cortex, AP -6, ML $\pm$8, DV -12; parietal cortex, AP +8, ML $\pm$8, DV -12.

6.2.5 *In vivo* monitoring

Protocols were established for longitudinal *in vivo* assessment of therapeutic efficacy. Treated sheep were monitored at monthly intervals for a period of 24 months, from 3.9 months of age, and compared with age-matched cohorts of untreated *CLN5-/-* and *CLN5+/-* sheep. A number of behavioural, cognitive and neurological parameters were determined and quantitative CNS imaging carried out as described in Sections 3.3– 3.6.

Table 6.1 Treatment groups and clinical assessment at *post mortem* (or trial completion)

Sheep	Genotype	Treatment*	Gender†	Age (months)	Cause of death‡	Clinical score	Clinical description	Seizures	Brain weight (g) §
1103/13	*CLN5+/-*	-	M	18.4	-	5	Normal	-	-
1118/13	*CLN5+/-*	-	M	19	-	5	Normal	-	-
1121/13	*CLN5+/-*	-	M	18.7	-	5	Normal	-	-
1128/13	*CLN5-/-*	-	M	27	Completion of trial	5	Normal	-	-
1107/13	*CLN5-/-*	-	M	16.9	Completion of trial	1	Advanced disease, blind	-	75.77
1114/13	*CLN5-/-*	-	M	18.3	Completion of trial	2	Mild clinical disease, blind	-	74.31
1115/13	*CLN5-/-*	-	M	18.8	Completion of trial	1	Advanced disease, blind	+	61.03
1116/13	*CLN5-/-*	-	M	17	Completion of trial	1	Advanced disease, blind	+	76.54
1106/13	*CLN5-/-*	LV-MND-*CLN5*	W	26.9	Completion of trial	3	Loss of vision only	-	87.5
1117/13	*CLN5-/-*	LV-MND-*CLN5*	W	27.0	Completion of trial	3	Loss of vision only	-	92.9
1126/13	*CLN5-/-*	LV-MND-*CLN5*	F	27.1	Completion of trial	3	Loss of vision only	-	84
1105/13	*CLN5-/-*	AAV9-MND-*CLN5*	F	27.1	Completion of trial	3	Mild visual deficits only	-	88.5
1109/13	*CLN5-/-*	AAV9-MND-*CLN5*	F	33+	Alive	5	Loss of vision only	-	-
1120/13	*CLN5-/-*	AAV9-MND-*CLN5*	F	26.4	Completion of trial	3	Loss of vision only	-	71

* LV, lentiviral vector; AAV9, adeno-associated viral vector serotype 9; MND (myeloproliferative sarcoma virus enhancer, negative control region deleted, dl587rev primer-binding site substituted) promoter

† M, male; F, female; W, wether (castrated male)

‡ Sheep were euthanized at clinical humane endpoint or trial completion. AAV9-*CLN5* injected sheep 1109/13 is still alive at 33 months of age in May 2016, with the only clinical sign being loss of vision

§ Fresh brain weight values for untreated animals; post-fixation brain weights for treated animals (boxed)

6.3 Results

Six *CLN5-/-* Borderdale sheep were treated, before the average age of clinical disease onset, by bilateral intracerebroventricular (ICV) and intraparenchymal (IP) injections with lentiviral or AAV9 vectors expressing ovine CLN5 under the control of a constitutive viral MND. Because sufficient affected ewe lambs were not available, two castrated ram lambs were included in the lentiviral cohort. All of the animals treated with either vector showed functional efficacy for two years after a single neurosurgical gene transfer session. Five of the treated sheep were euthanised at around 27 months of age, when the only clinical sign of disease was a delayed visual deficit, thus exceeding the normal life expectancy of ~22 months for untreated *CLN5-/-* sheep. Neuropathological analyses from these animals are outside the scope of this thesis but are underway. One AAV9-*CLN5* treated animal (1109/13) remains alive at 33 months of age, albeit with visual loss but is otherwise phenotypically indistinguishable from heterozygous controls. This ewe in maintained on outdoor pasture, interacting well with its untreated flockmates and is in excellent condition. The loss of vision is only detectable when it is physically isolated from the flock, travelling down a straight lane-way, whereby it will collide with fences. Within the field or within the flock, this deficit is not apparent. Any systemic manifestation will be monitored in this sheep over its extended lifespan resulting from its improved neurological function.

6.3.1 Confirmation of genotype

Affected animals were identified by reverse transcription PCR and sequencing of the c.571+1G>A splice site mutation at birth and a fortnight prior to gene transfer surgery (Frugier *et al*., 2008) (Figure 6.1). Genotype analyses on serial blood samples collected every six months revealed a consistent homozygous result for the mutant allele (*CLN5-/-*) over the life span of all treated animals., showing that no inadvertant animal substitutions had taken place nor was there an integration of the viral vector cargo into the host cell genome.

6.3.1.1 Safety and tolerability of LV-*CLN5* and AAV9-*CLN5* administration in sheep

All six sheep recovered well from surgery, despite their young age and within 90 minutes post-anaesthesia were standing up and eating. General safety was assessed in the three week observation period after vector administration. Rectal temperatures, pulse rates and respiratory rates remained normal during this time and no overt behavioural changes or clinical signs of an immune response occurred.

Over the course of the study, only one adverse event was reported. An AAV9-*CLN5* treated ewe (1120/13) had a recurrent vaginal prolapse, first seen at 5.7 months of age (2.9 months post-

surgery), which required suturing but with full recovery. This incident was not directly attributable to the vector, anaesthesia, surgical or administration procedure *per se* but rather to the housing constraints and resultant long-term concentrate feeding of the sheep. No other adverse clinical or biochemical events were observed.

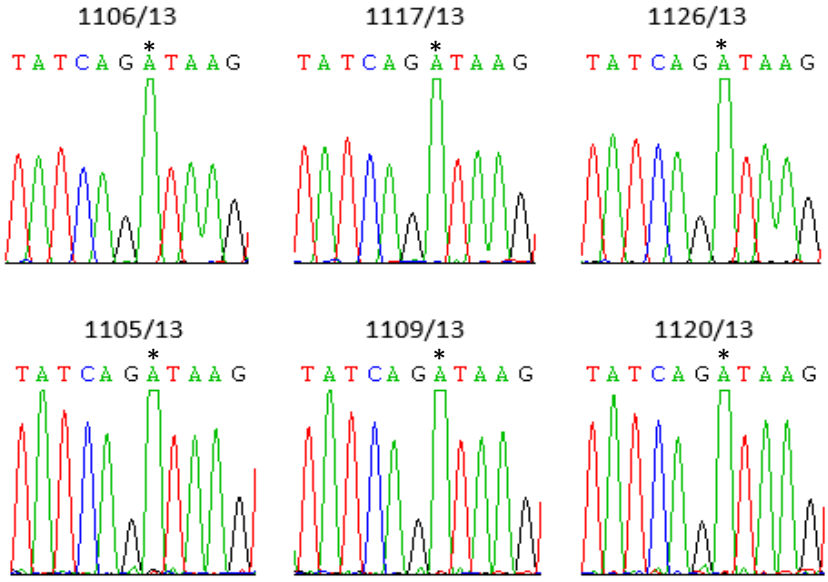

Figure 6.1 Confirmation of the affected genotype in the six gene therapy sheep subjects
CLN5-/- status was verified in the treated animals using PCR and sequencing (Frugier *et al*., 2008). Representative chromatographs show the c.571+1G>A (*) substitution in all six animals, confirming their CLN5 homozygosity.

6.3.1.2 Growth rate

Treated sheep continued to gain weight during the course of the study. Direct live weight comparisons were not possible between the treated and untreated cohorts, as untreated control sheep were maintained on pasture whilst treated sheep received a daily feed ration indoors. However linear regression of increases in live weight of the treated sheep and CLN5 heterozygous and affected animals from a previous trial, similarly housed and rationed, agreed, revealing comparable growth rates for all three genotype groups (3.0 kg/ month for *CLN5+/-*, 2.37 kg/ month for untreated *CLN5-/-* and 2.43 kg/ month for treated *CLN5-/-* sheep) (Figure 6.2).

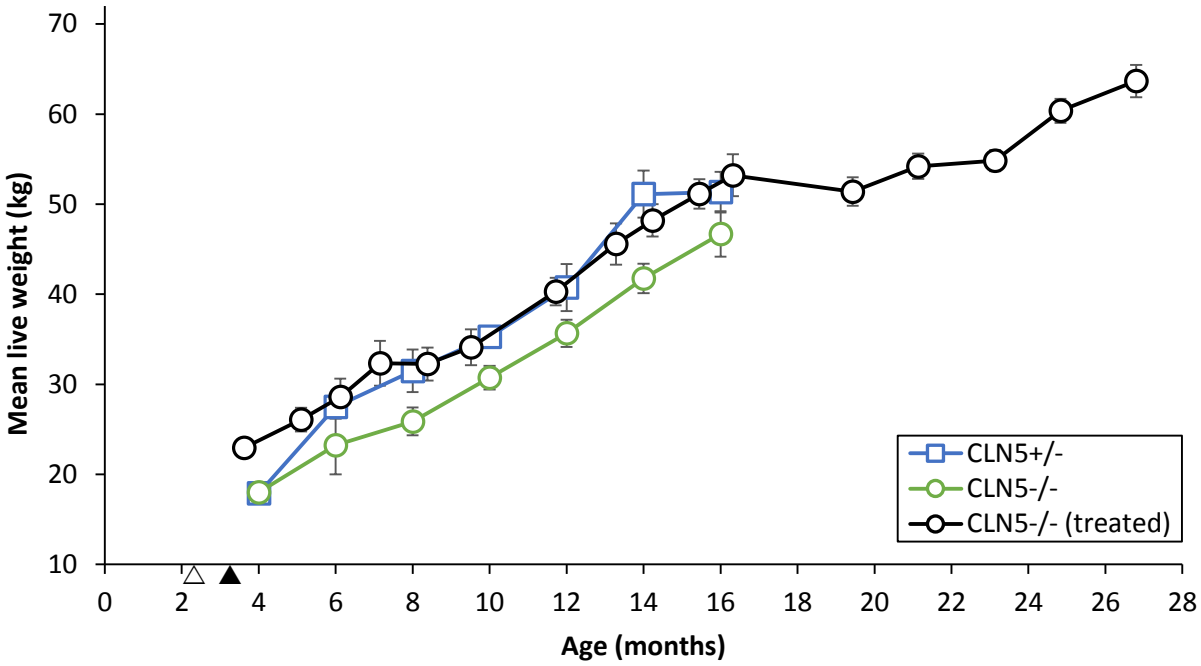

Figure 6.2 Mean live weight increases following viral-mediated *CLN5* gene transfer in sheep
Changes in the mean (± SEM) live weights of the treated CLN5 deficient (*CLN5-/-*, *n* = 6) sheep during the course of the experiment, compared with untreated CLN5 heterozygous (*CLN5+/-*, *n* = 6) and *CLN5-/-* (*n* = 6) sheep housed and fed similarly on a separate indoor trial. Animals in both trials were housed indoors and received a daily maintenance ration of lucerne pellets, chaffed lucerne and hay. Composite live weights were plotted for the LV-*CLN5* and AAV9-*CLN5* treated sheep as there was no significant difference between the two treatment groups. △ ▲ denote the time of treatment for LV-*CLN5* and AAV9-*CLN5* respectively.

6.3.2 *In vivo* assessment of therapeutic efficacy

6.3.2.1 Clinical staging of ovine CLN5

To assess any long-term clinical benefit in treated *CLN5-/-* sheep robustly, it was first necessary to characterise the natural disease history in untreated *CLN5-/-* sheep. Criteria were established for assessing neurological, behavioural, motor and visual function in the treatment groups and untreated Borderdale controls, based on historical observations on NCL ovine models (Westlake *et al*., 1985; Cook *et al*., 2002; Jolly *et al*., 2002). A clinical rating scale (Table 3.1, see Section 3.3), encompassing the multifocal nature of this disease, was developed to assess deviation from healthy function. Clinical rating scores (CRS) decreased from 5 (normal function) to 0 (progressive disease with spontaneous manifest seizures) as animals became more debilitated from the disease. Routine physical and neurological examinations were performed monthly, with concurrent open- and closed-field behavioural observation, beginning on average at 3.9 months of age.

As expected for a recessive disease, CLN5 heterozygous sheep were phenotypically normal throughout this study, with no functional deficits and consistently scored 5 on the rating scale (Figure 6.3). In contrast, stereotypical disease progression began at 5.7 $\pm$ 0.3 months of age in untreated *CLN5-/-* sheep. Manifestations included walking with their heads held low, crouching and/or baulking with occasional stumbling when in shadows, passing through gateways or negotiating steps (CRS 4). From 10.9 $\pm$ 0.2 months of age all untreated *CLN5-/-* animals were functionally blind (CRS 3), with an asymmetric reduction or bilateral absence in menace (blink) response, loss of visual tracking and decreased acoustic startle. Affected sheep at this age shared a diminished herding instinct and tended to self-segregate, grazing alone in the field. Clinical symptoms progressed with deterioration of cranial nerve reflexes, motor, behavioural and cognitive (reduced mentation, increased somnolence) deficits by 14.2 $\pm$ 1.8 months (CRS 2). Motor and proprioceptive dysfunction was evidenced by ataxia which was more severe in the pelvic limbs, stumbling, dragging of the feet, and intermittent episodes of localised muscle tremors particularly of the ears, eyelids, lips, and hind limbs. Behavioural changes from this age included a reduced awareness of surroundings, repetitive actions, such as aimless circling and teeth grinding, and feeding abnormalities, including dribbling and inefficient or sham eating. Affected CLN5 sheep in the advanced disease phase (15.2 $\pm$ 1.1 months, CRS 1) demonstrated low mentation, extended periods of somnolence, non-responsiveness to a variety of stimuli; including loud noise, pushing, flashing light and human presence, and loss of body condition with or without manifest seizure activity. Tetanic spasms, elicited by stress or handling, began in one CLN5 affected animal at 13.2 months. However there was significant individual variation in onset and severity with another of the affected animals not showing inducible manifest seizures, even at advanced disease at 18 months of age.

A.

Score	Clinical phenotype	Clinical status *	Age (months)
5	Normal	Normal	<5.7 ± 0.3
4	Pre-clinical	Low head carriage Propensity to crouch, baulk and stumble	5.7 ± 0.3
3	Blind	Head tilt/stargazing Visual deficits Decreased or lost menace (blink) response Reduced herding	10.9 ± 0.2
2	Overt/neurological	Behavioural, cognitive and proprioceptive deficits Decreased startle to auditory stimuli Wide stance	14.2 ± 1.8
1	Advanced	Progressive disease +/- induced tetanic seizures	15.2 ± 1.1
0	Terminal	Spontaneous tetanic seizures	Not observed

* Onset of inducible mild tremors in individual sheep began as early as 13.2 months; Spontaneous convulsive seizures have not been observed in any *CLN5-/-* sheep, even in animals carefully nursed to 24 months of age.

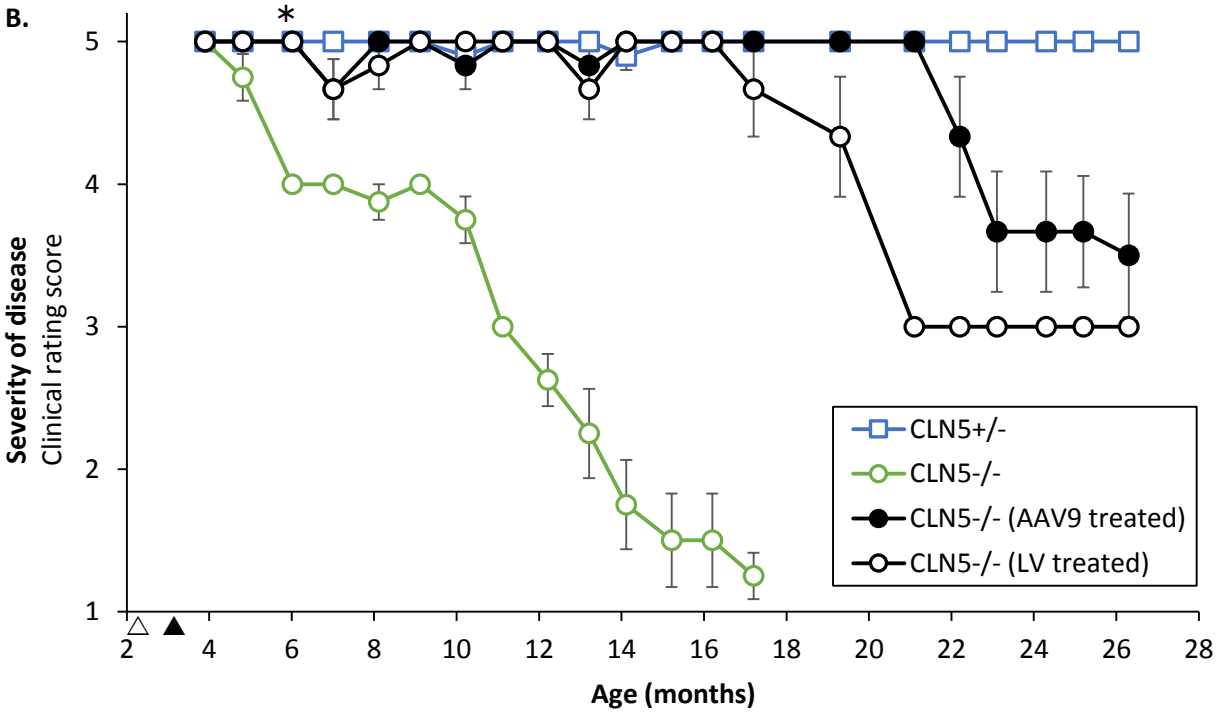

Figure 6.3 Attenuation of stereotypical clinical progression following viral-mediated *CLN5* delivery
Sheep were scored monthly after treatment using a clinical rating scale based on the natural course of disease progression in ovine NCL models. **A.** Ages of symptom onset are shown for untreated *CLN5-/-* sheep, with initial deficits at 5.7 ± 0.3 months of age. **B.** Composite clinical rating scores for *CLN5+/-* control (*n* = 4), untreated *CLN5-/-* (*n* = 4) and treated *CLN5-/-* sheep (*n* = 3 in each vector cohort). Treated sheep were clinically normal until 20.5 ± 0.6 months of age (LV cohort) and 24.1 ± 1.5 months of age (AAV9 cohort), when late-onset visual deficits developed. No further neurological decline was observed. All data are shown as the mean ± SEM (vertical bars). △ ▲ denote the time of treatment for LV-*CLN5* and AAV9-*CLN5* respectively, * marks the age from which differences between the treatment groups and untreated *CLN5-/-* sheep become significant ($P < 0.05$).

6.3.2.2 Clinical status in treated *CLN5-/-* sheep

The quality of life for treated *CLN5-/-* sheep was dramatically improved compared with untreated *CLN5-/-* animals. No overt disease onset or progression was documented for any of the treated sheep apart from a much delayed loss of vision relative to untreated affected controls. At the initial pre-determined study endpoint of 18 months of age, all of the treated sheep remained alive with no overt disease onset and negligible neurological signs. At this point, there was no discernible difference in therapeutic benefit between the LV and AAV9 cohorts, whose composite clinical rating scores were 4.7 ($\pm$ 0.3) and 5.0 ($\pm$ 0.0) respectively. The delineation from normal observed at this age in the LV cohort arose from one animal (1106/13), which developed a distinctive, yet non-attributable, head tilt at 17.2 months of age, that progressed to a myoclonic head jerk (dyskinesia) in photopic conditions by 18.5 months with complete loss of vision and reflex function by 19 months, but with no other stereotypical behaviour. In contrast, by 17.2 months of age, untreated *CLN5-/-* sheep obtained a score of only 1.25 ($\pm$ 0.2) on the rating scale, with three out of four animals showing advanced disease, including subtle tremors to whole-body handling and/or stress induced seizures, which defined their humane endpoint. Graphical review of the fitted curves at 18 months (Figure 6.3) revealed treated sheep were clinically indistinguishable from the heterozygote controls, such that the 16-month post-treatment experimental endpoint was suspended and the trial duration was extended.

Funduscopic examination at ~18 months of age, conducted by an independent veterinary ophthalmologist, revealed tapetal hyperreflectivity and severe generalised blood vessel attenuation in the clinically blind untreated *CLN5-/-* animals, compared with *CLN5+/-* controls, whilst treated sheep had intermediary indicators of retinal damage yet retained visual functionality. Despite signs of retinal pathology, the onset of blindness was significantly delayed ($P < 0.0001$) in the treated animals compared with untreated CLN5 deficient sheep that were functionally blind by 10.9 $\pm$ 0.2 months. Blindness developed in the other two animals in the lentiviral cohort by 21 months of age, whilst two of the three AAV9-treated animals began to lose vision from 22 months, with complete loss by 2 years of age. The AAV9-treated sheep that is still alive, 1109/13, did not show visual deficits until 27 months of age.

6.3.2.3 Maze testing as a biomarker of functional correction

The impact of LV-*CLN5* and AAV9-*CLN5* vector administration on vision, cognitive function and general locomotor activity was assessed monthly by closed-field maze testing. Time taken to traverse the maze was recorded, as was any time spent in the error zone, a cul-de-sac which deviated from the correct path through the maze (Figure 6.4). A simple maze rating scale was developed to describe each sheep's passage through the maze (Figure 6.5). At baseline (3.9 months of age) there was no significant difference between the mean traverse times of the cohorts but at all subsequent testing

intervals, the untreated *CLN5-/-* sheep were significantly slower at passing through the maze than the treated and heterozygous control sheep (Figure 6.4A). Untreated sheep showed a progressive navigational decline through the maze, with a propensity to stumble initially, and later a reduced awareness of their surroundings, behavioural phenotype and increased error scores (Figure 6.4 – 6.5). When induced to enter the maze by gentle pushing, affected sheep would move in a guarded manner with a tendency to circle. Under photopic conditions, untreated *CLN5-/-* sheep shied away from shadows and became increasingly unable to negotiate the ramp which led onto the maze testing arena without assistance. Despite functional blindness from 10.9 $\pm$ 0.2 months, untreated affected sheep were generally able to negotiate the maze for another few months and notably they did not tend to hit any of the obstacles but rather would pull up short and fail to find a way around. However by 16 months of age, they were so severely affected as to be akinesic. This defined the humane endpoint for this test.

In contrast, delivery of either LV-*CLN5* or AAV9-*CLN5* to preclinical CLN5 deficient lambs reversed the cognitive dysfunction, with no discernible difference in performance between the treated sheep and healthy heterozygous control sheep for some months after untreated *CLN5-/-* sheep reached the end stage of disease (Figure 6.4- 6.5). Treated sheep walked or ran through the maze with their heads held high, scarcely pausing yet avoiding the obstacles and error zone and mean transit times were significantly faster than those of the heterozygotes at some time points. From 23 and 25 months respectively, the LV-treated and then AAV9-treated sheep began to show the effects of their delayed visual loss, colliding with obstacles, often with force, as they ran through the maze (Figure 6.5) and the testing was hence terminated for humane reasons.

Nevertheless, treated sheep in both vector cohorts prior to euthanasia were neurologically sound. At 27 months of age, they were alert and responsive to their environment and auditory cues. They interacted with farm staff and each other both inside and during their outdoor testing times, through vocalisation and physical contact, and immediately detected the presence of foreign sheep or humans. Clinically, they were indistinguishable from heterozygous controls whilst grazing in the open field, with no evidence of the stereotypical wide stance, manifest hindlimb paresis or localised tremors seen in the overt neurological and advanced disease stages of CLN5 ovine NCL.

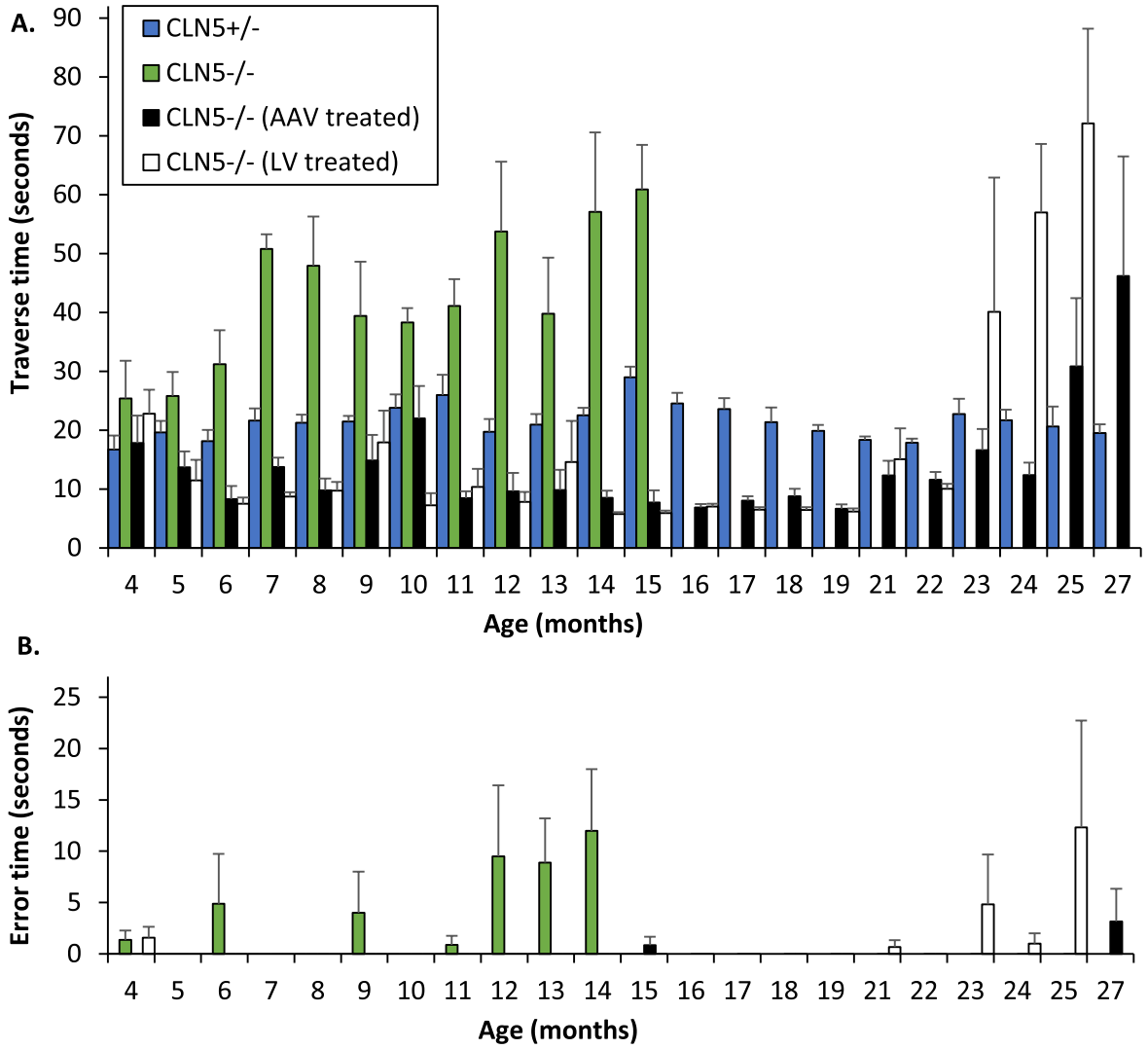

Figure 6.4 Sustained performance in a closed-field maze test after viral-mediated *CLN5* delivery

A. Mean maze traverse times for LV-*CLN5* (*n* = 3), AAV-*CLN5* (*n* = 3) treated *CLN5-/-* sheep, unaffected *CLN5+/-* control (*n* = 4) and untreated *CLN5-/-* (*n* = 4) sheep were recorded monthly. Statistical comparisons were performed between the individual treatment cohorts and untreated *CLN5-/-* at each age using Student's *t* test. The performances of the LV- and AAV9-treated *CLN5-/-* sheep were significantly better ($P \leq 0.05$) than untreated *CLN5-/-* sheep until 23 and 25 months of age respectively, when visual deficits became profound enough to hinder their passage.

B. Mean error times during maze passage for the groups recorded in **A** over the same period. Error times increased as sheep within each cohort approached the humane endpoint of the maze test. All data are shown as the mean ± SEM (vertical bars); *n* = 3 - 4 animals per group with 2 runs per animal at each timepoint.

A.

Score	Maze assessment	Age (months)
5	Traverse with no problems	< 4.3 ± 1.8
4	Traverse with small pauses	4.3 ± 1.8
3	Traverse but with obvious behavioural phenotype (+/- hits obstacles)	7.2 ± 2.4
2	Traverse with or without pauses but misses entry	12.9 ± 0.9
1	Traverse with errors	14.4 ± 1.4
0	Fail - requires assistance to traverse	15.7 ± 0.9

B.

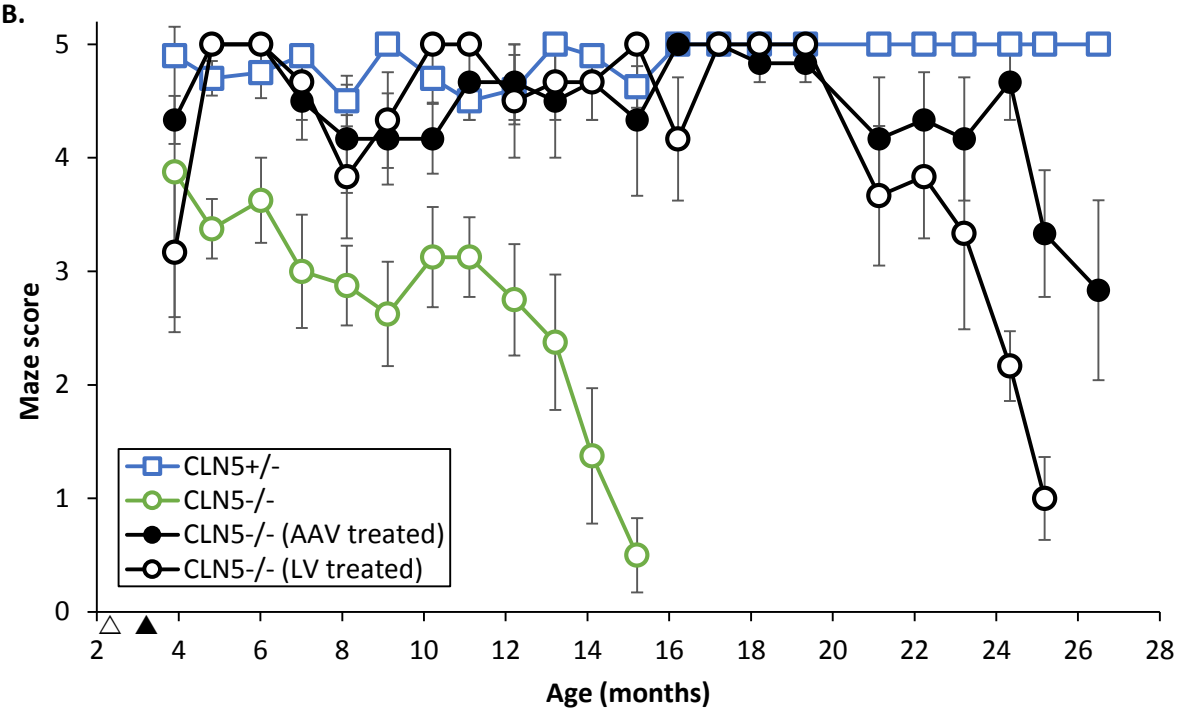

Figure 6.5 Prolonged visual acuity and maze navigational ability after viral-mediated *CLN5* delivery
A. Sheep were scored for every passage through a closed-field maze at monthly intervals, with scores ranging from 5 (normal traverse) to 0 (failure to traverse without assistance). Ages of onset for each stage are shown for untreated *CLN5-/-* sheep. Initial phenotypic deficits were observed from 7.2 ± 2.4 months of age. These included low head carriage, crouching, baulking, stumbling or 'self-spooking' at obstacles. **B.** Composite scores for the four cohorts showing that *CLN5+/-* sheep traversed the maze with no or small pauses, consistently scoring 5 whilst untreated *CLN5-/-* found the maze progressively harder to traverse without errors or assistance. In contrast, sheep in the LV and AAV treatment cohorts traversed the maze as normal until 23 and 25 months of age respectively, when late-onset visual deficits began to affect their performance. All data are expressed as the mean ± SEM; *n* = 3 - 4 animals per group, 2 runs per animal at each timepoint, △ ▲ denote the time of treatment for LV-*CLN5* and AAV9-*CLN5* respectively.

6.3.2.4 Disease progression assessed by CNS imaging

The characteristic brain atrophy that defines NCL was monitored by longitudinal computed tomography (CT) scanning. Intracranial volumes were used as an *in vivo* measure of brain atrophy and hence disease progression. Scans were performed every second or third month on treated animals from 5 months of age and the rates of change compared against longitudinal data previously recorded from untreated CLN5 deficient and heterozygous sheep (Figure 6.6A,B). At three months of age, the mean intracranial volumes were similar for untreated *CLN5-/-* and *CLN5+/-* animals but with time, these became disparate with affected animals losing about 0.7 mL/month of intracranial volume compared with a heterozygote gain of 0.7 mL/month. Three-dimensional reconstructions of the cranium and ventricles demonstrated a marked regional atrophy in the diseased brain, particularly in the occipital and parietal cortices, with secondary ventricular enlargement, widening subarachnoid CSF spaces and sulcal prominence (Figure 6.6– 6.8). By contrast, the cerebellum was similarly sized in CLN5 deficient and heterozygous animals, with well-preserved morphology.

The cranial volume loss and ventricular enlargement seen in sheep with CLN5 disease was attenuated in the treated animals (Figure 6.6A,B), intracranial volume and three-dimensional measurements being within the ranges recorded for heterozygous controls. This phenomenon was observed in all subjects, regardless of vector. Although mean intracranial volume increases were calculated as 0.5 mL/month and 0.2 mL/month respectively for the LV and AAV9 treated cohorts, this difference only reached statistical significance ($P < 0.04$) at 27 months of age. The initial cranial volumes and subsequent rates of change varied dramatically between individuals, with increases of between 3.8 mL (1105/13) and 13.6 mL (1117/13) from 5 to 27 months of age. One AAV9-*CLN5* treated animal (1120/13) exhibited a volumetric plateau, with a consistent cranial volume of 96.1 $\pm$ 0.2 mL over most of the study period, until 19 months when the intracranial volume began to decline at 0.5mL/month. This animal also had the lightest brain at *post mortem* of all the treated animals (Table 6.1).

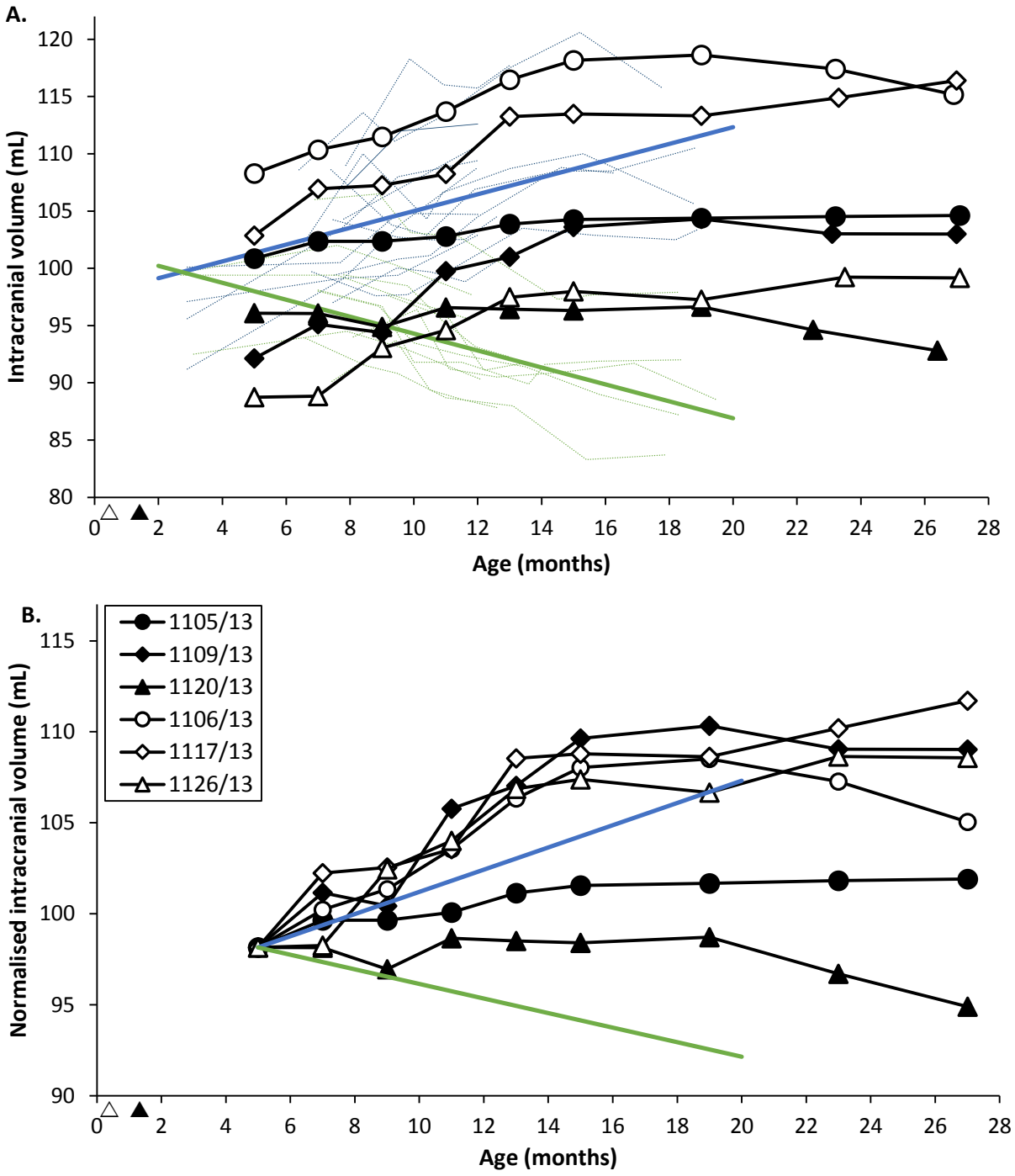

Figure 6.6 Attenuation of intracranial volume loss after viral-mediated *CLN5* delivery

A. Shown is longitudinal intracranial volume data for untreated *CLN5+/-* and *CLN5-/-* control sheep against LV (unfilled markers) and AAV9 (filled markers) treated sheep. Thin blue (*CLN5+/-*) and green (untreated *CLN5-/-*) lines represent historic individual volume changes over time; thick blue and green lines indicate respective volumetric trend lines. All treated *CLN5-/-* sheep demonstrated intracranial plateaux or growth over time, but not the atrophic loss seen in untreated *CLN5-/-* animals. **B.** Normalised intracranial volume trajectories further demonstrate the functional efficacy of gene therapy in CLN5 deficient sheep. Volumes were normalised to compensate for the differences in intracranial volumes at baseline. △ ▲ denote the time of treatment for LV-*CLN5* and AAV9-*CLN5* respectively.

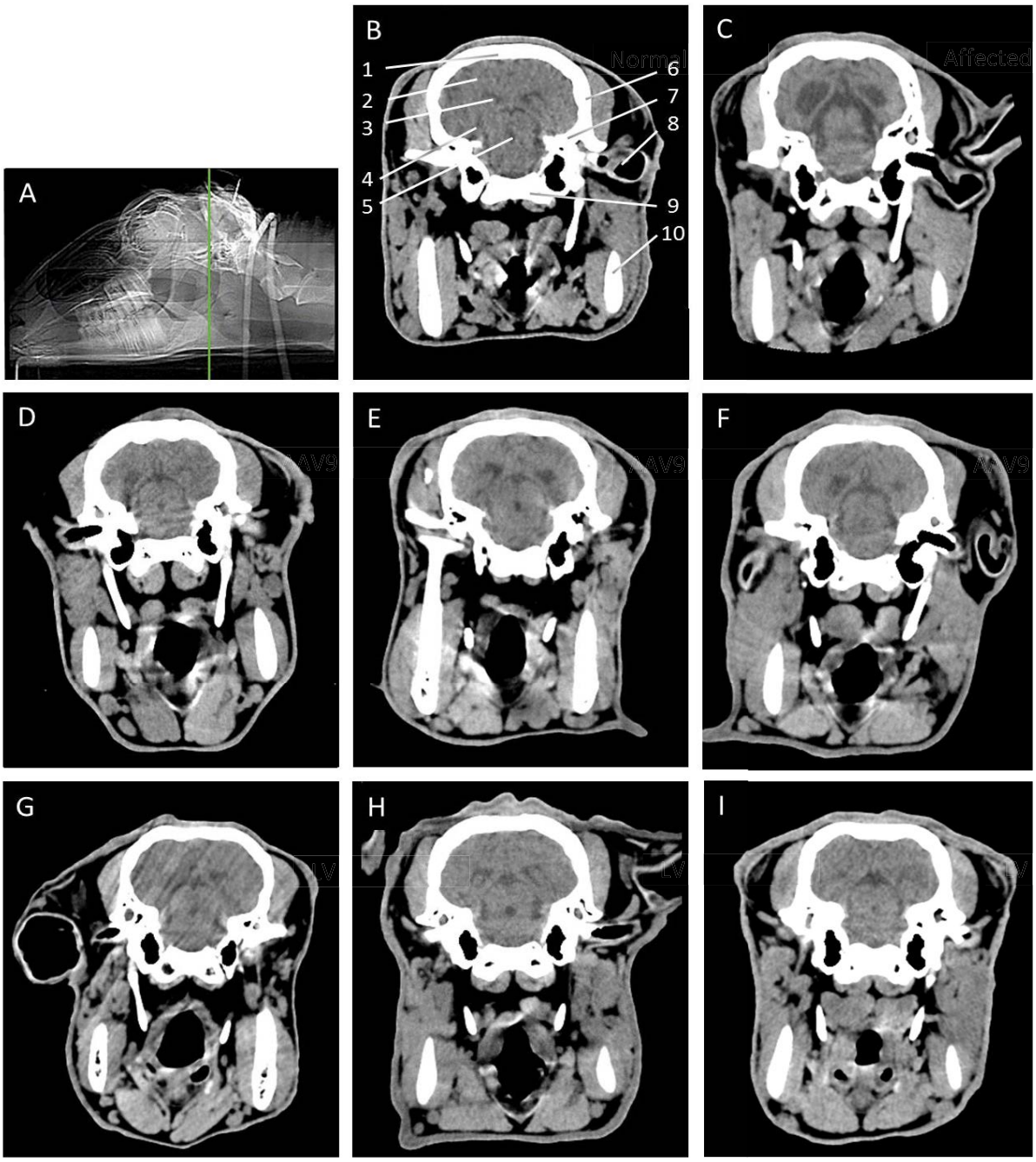

Figure 6.7 Preservation of brain structure in LV-*CLN5* and AAV9-*CLN5* treated sheep

Computer tomography (CT) images show the enlarged ventricles and atrophic changes in the untreated CLN5 deficient sheep brain at 12 months, compared with the relative structural normality in age-matched animals that received viral-mediated gene therapy. **A.** Lateral view of a sheep head showing the position of sections depicted in the other images (green line). **B.** CT image of a transverse section of the 12 month old clinically normal CLN5 heterozygous sheep brain at the level of the parieto-occipital cortex (equivalent to coronal section MSU#1280 from the Michigan State University Sheep brain atlas; https://www.msu.edu/~brains/brains/sheep/index.html). Brain and bone structures are indicated: 1, frontal bone; 2, parieto-occipital cortex; 3, lateral ventricle; 4, temporal cortex; 5, cerebral aqueduct; 6, parietal bone; 7, temporal bone; 8, external ear canal; 9, occipital bone; 10, mandible. **C**. Gross changes in the size of the lateral ventricles can be seen by 12 months in the untreated CLN5 affected sheep brain. **D – F**. AAV9-*CLN5* treated sheep 1105, 1109 and 1120/13 respectively. **G – I.** LV-*CLN5* treated sheep 1106, 1117, 1126/13 respectively.

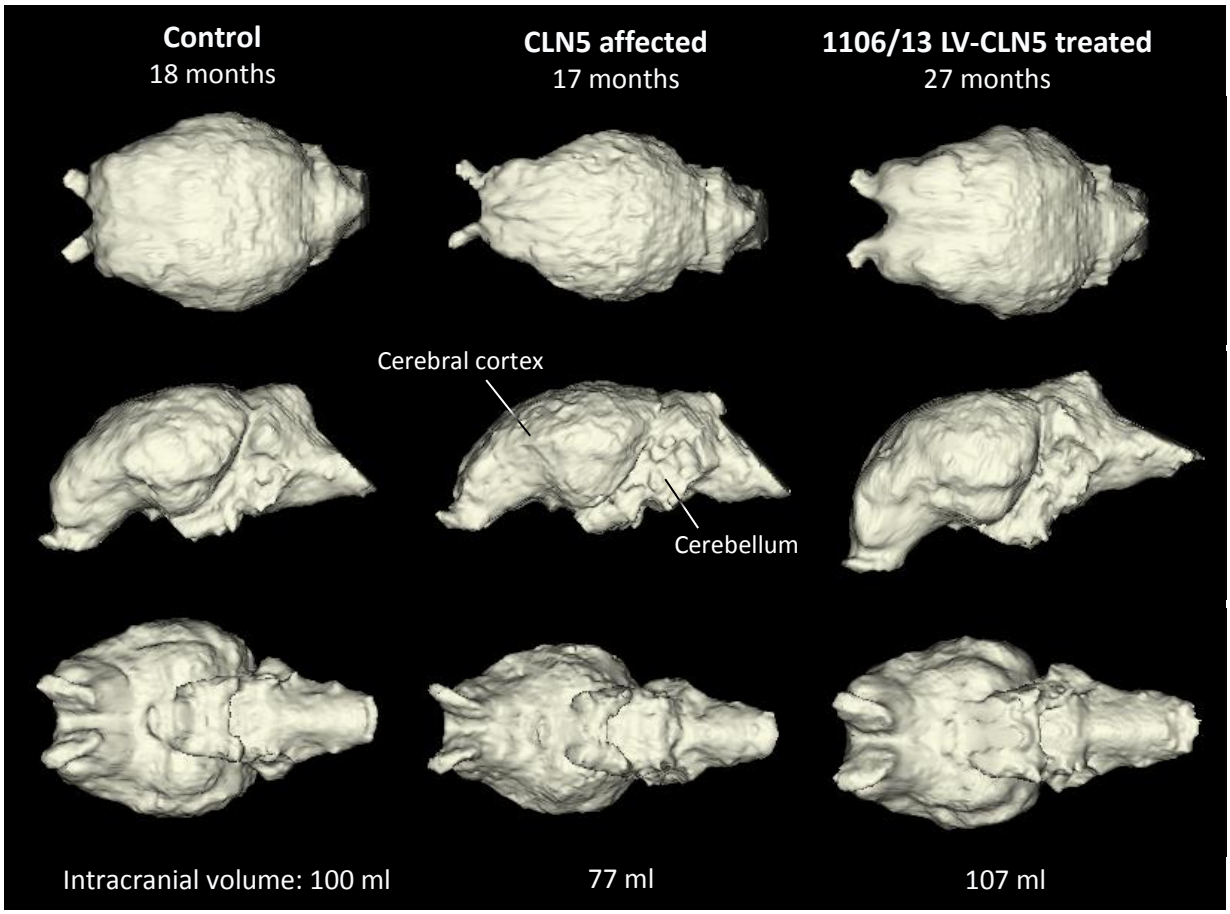

Figure 6.8 Retention of intracranial volume after *CLN5* delivery

Representative three-dimensional models of intracranial volumes from an 18 month old *CLN5+/-* control sheep (left), a 17 month old untreated *CLN5-/-* sheep (middle), and a 27 month old LV-treated *CLN5-/-* sheep (right) reconstructed from axial CT slices. Note the pronounced atrophic targeting of the cerebral cortex with relative sparing of the cerebellum in the untreated CLN5 deficient brain. In comparison, the gross anatomy of the treated brains is indiscernible from a healthy *CLN5+/-* control. The treated animal was blind but otherwise clinically normal at the time of imaging. Images were prepared by Katharina Russell (Lincoln University) as part of her PhD study.

Magnetic resonance imaging (MRI) confirmed the CT findings. MRI images of treated sheep at 25 months of age showed that the overall brain structure and architecture was normal (Figure 6.9), with no obvious degenerative changes. Together the CNS imaging showed that the stereotypical brain atrophy and ventricular enlargement is ameliorated in treated sheep and the brain white and grey matter structures are preserved after gene therapy.

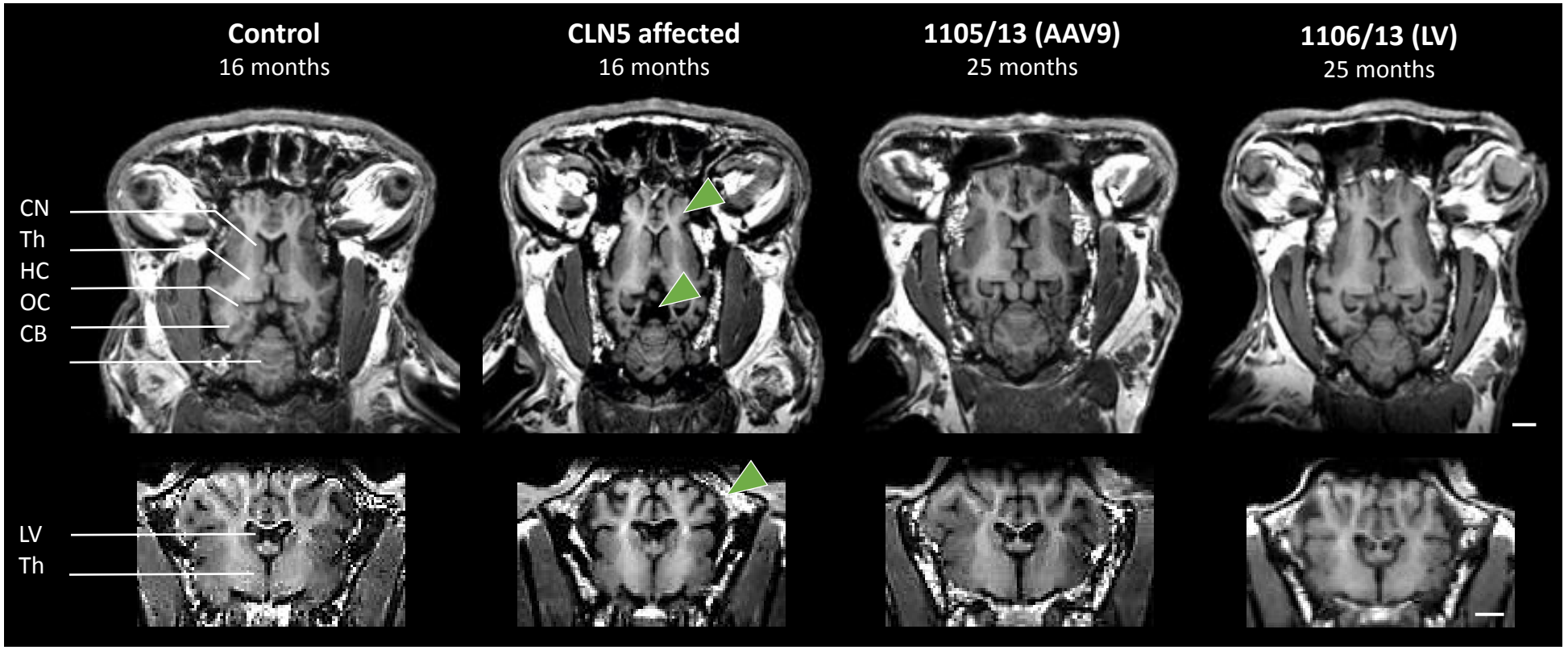

Figure 6.9 Normalisation of sheep brain structure after viral-mediated *CLN5* delivery

Representative MRI (T2) sections in the horizontal (top) and coronal (bottom) views of a typical 16 month unaffected control and CLN6 affected sheep, compared with 25 month old CLN5 affected sheep which have received AAV9 (1105/13) and lentiviral (1106/13) mediated *CLN6* gene therapy. Profound atrophy is apparent in the untreated affected sheep cortex (upper arrow), as is prominent ventricular enlargement (middle arrow) and cranial thickening (lower arrow). Treatment with either lentiviral or AAV9 vectors expressing ovine *CLN5* normalised the brain structure and protected against atrophy. Scale bar represents 1 cm. Abbreviations: **CB** cerebellum, **CN** caudate nucleus, **HC** hippocampus, **LV** lateral ventricle, **OC** occipital cortex, **Th** thalamus.

6.4 Discussion

Like most neuropathic lysosomal storage diseases resulting in premature death, the NCLs lack effective therapies beyond supportive treatment. Promising results have been achieved with direct delivery of AAV vectors to the brain parenchyma in CLN2 rodent and non-human primate models (Hackett *et al*., 2005; Sondhi *et al*., 2005, 2007, 2012; Passini *et al*., 2006). These have been extended to human clinical trials (Crystal *et al*., 2004; Worgall *et al*., 2008) however no treatment options or clinical testing are available for NCL patients bearing the *CLN5* mutation. Studies assessing the safety and efficacy of CLN5 gene therapy in large animal models of the disease are critical for potential clinical development of this strategy. To this end, results from the experiments described in this chapter document sustained functional and structural efficacy in pre-symptomatically treated CLN5 sheep via two different gene delivery platforms, lentiviral and AAV9 vectors carrying the therapeutic ovine *CLN5* gene, through just four burr holes in a single neurosurgical procedure lasting less than 90 minutes.

CLN5 affected lambs were weaned early and treatment was administered at 2.2 – 3.2 months, before the onset of clinical signs. Two years post-administration, five of the six treated sheep were euthanised at 27 months of age, exceeding the typical humane endpoint for untreated CLN5 deficient animals of 22 months of age. Surprisingly clinical outcomes were similar for both of the viral vector platforms tested; lentiviruses, currently in use in human clinical trials for a number of LSDS and neurodegenerative diseases (Cavazzana-Calvo *et al*., 2000; Biffi *et al*., 2013; Palfi *et al*., 2014), and AAV9, a newer AAV serotype which has shown promise in the treatment of neuropathic LSDs (Fu *et al*., 2011; Ribera *et al*., 2015; Walia *et al*., 2015). The treated sheep were disease-free, apart from delayed-onset visual deficits. They benefitted from a profound improvement in quality of life, preservation of cognitive and neurological function, and normalisation of intracranial volume and brain structure, compared to untreated animals.

Longitudinal studies of non-invasive biomarkers were used to assess the efficacy of lentiviral and AAV-based therapeutics in sheep *in vivo*. Monthly neurological examination and clinical scoring using a sheep-specific rating scale revealed the long-lasting functional efficacy of treatment, treated animals being clinically indistinguishable from untreated heterozygous controls until 20.5 $\pm$ 0.6 months and 24.1 $\pm$ 1.5 months for the lentiviral and AAV9 cohorts respectively, when they begin to show effects of their visual deficits (Figure 6.3). Aside from this loss of vision, at 27 months of age treated sheep were still highly interactive with their environment. They showed a willingness to engage with new stimuli (*e.g.* environmental enrichment items, including chains hanging from the ceiling, balls, plastic bottles or chewing bars in pens which were introduced to prevent oral stereotypies) and developed strong social attachments within their cohort and with animal care

personnel. In contrast, signs of clinical dysfunction in untreated CLN5 affected sheep developed progressively from 5.7 months of age. They were functionally blind by 11 months, isolated and in an advanced diseased state with differing degrees of inducible seizure activity by 14 - 16 months and were euthanized for humane reasons between 16.9 and 18.8 months of age.

Photopic behavioural maze testing was able to detect cognitive decline early in the course of NCL in affected sheep as well as the functional efficacy of viral-mediated gene transfer. Assessments in a relatively simple maze were highly informative. As the clinical signs of the disease developed, traverse and error times for the untreated CLN5 deficient sheep became significantly greater than for heterozygous and treated sheep and the testing was terminated when they became too akinesic to participate (Figure 6.4). Longitudinal subjective grading of sheep through the maze (Figure 6.5) provided graphical plots that mirrored the clinical rating data. Treated sheep retained the ability to navigate the maze well after this point and regularly outperformed the clinically normal heterozygotes with respect to maze passage and times taken.

Maze testing has been used previously in sheep for a number of different applications (Peirce *et al*., 2001; Shamir *et al*., 2010; Hunter *et al*., 2015; McBride *et al*., 2015), including the assessment of efficacy of intraocular AAV5 gene therapy in an ovine model of achromatopsia (Banin *et al*., 2015) as well as in ovine spatial learning and memory studies (Lee *et al*., 2006). These published maze studies and the current study rely on the natural flocking instinct of sheep, using conspecifics in the goal area to motivate movement through the maze. Under normal circumstances sheep have a strong compulsion to flock, particularly when they are wary (Lynch *et al*., 1992; King *et al*., 2012). However the Biosafety Level 2 containment that was required in the current study required treated sheep to be housed indoors in individual pens and this resulted in behavioural adaptation. Treated sheep became habituated to frequent human contact and handling, developing strong social bonds with animal care personnel, and losing their wariness. Sheep are gregarious by nature, requiring contact with other sheep to maintain well-being and normative physiology (Reinhardt & Reinhardt, 2002). Despite having uninterrupted visual, auditory, olfactory and tactile contact with their neighbours, treated sheep showed a reduction in their natural flocking behaviour – a phenomenon that has previously been reported in sheep held in confinement in small groups for several weeks (Fell *et al*., 1991; Degabriele & Fell, 2001). Food therefore had to be used as a further motivator for the maze testing, which may explain the faster traverse times seen with the treated animals. Additionally, because of the progressive debilitating nature of CLN5 NCL, it was not possible to blind investigators to the treatment status of the sheep during this *in vivo* testing. To limit observer bias, all subjective measurements (clinical rating scores, maze and behavioural assessments) were performed by two independent investigators, either at the time of testing or from retrospective video analysis and scores were then averaged.

CNS imaging (CT and MRI data) provided objective *in vivo* clinical measures of CNS atrophy in untreated CLN5 deficient sheep whilst demonstrating structural integrity in treated brains. Computed tomography (CT) images were generated by passing an x-ray beam through the skull and measuring the attenuation of the x-ray beam through the different tissues (*e.g.* brain, bone, CSF). Quantitative measurements of atrophy and ventricular dilatation are possible by this scanning technique. Longitudinal intracranial and ventricular volume estimates were obtained from a series of CT scans for each sheep using the Cavalieri principle (Graham Kay, personal communication) and, alongside three-dimensional (3D) reconstructions (Figure 6.8), served as excellent measures of disease progression. MRI scanning at the conclusion of the trial confirmed preservation of brain architecture following treatment (Figure 6.9). The typical cranial volume loss and ventricular enlargement seen in CLN5 disease was attenuated in the treated animals (Figure 6.6), that had volume measurements within range of heterozygous controls. On average, LV-treated and AAV-treated sheep showed intracranial volume increases of 0.5 and 0.2 mL/month respectively over the study, in line with rates of change for untreated CLN5 heterozygous sheep of 0.6mL/month whilst untreated CLN5 affected sheep lost 0.4 mL/month. Because the initial cranial volumes and subsequent rates of change varied between individuals, baseline volumes were normalised for the two treatment groups. Doing this clarified the comparative longitudinal changes for each vector. LV-treated animals maintained higher intracranial volumes than AAV9-treated ones through the study. This could be caused by a number of factors. Firstly there were two wethers in the LV cohort which would affect results if sexual dimorphism influences brain size. The larger brains and thus volumes of the LV-treated wethers was consistent with their larger body size. However a recent MRI study of healthy Merino sheep demonstrated that the volume of brain tissue did not differ between wethered rams and ewes (Nitzsche *et al*., 2015), conflicting with a report for humans which suggested that male brain volumes are typically larger than females (Allen *et al*., 2002; Lüders *et al*., 2002). Secondly, one animal in the AAV cohort (1120/13) had a plateau of intracranial volume from 5 to 19 months and, interestingly, lost 3.8 mL of intracranial volume in the last seven months of the trial (from 19 to 26 months of age). At *post mortem* the brain of this individual was considerably lighter than that of other treated animals, being more comparable to advanced disease-stage untreated CLN5 deficient animals (Table 6.1). The cause of this late-stage decline in intracranial volume is yet to be determined but neuropathological analysis may be enlightening.

Late-onset loss of vision was the only clinical sign presented by treated sheep from both vector treatment groups, with earlier deficits seen in the lentiviral cohort than in the AAV cohort. This visual loss experienced by the treated animals differed from that seen during natural disease progression. Despite being functionally blind by 10.9 ± 0.2 months, the untreated CLN5 affected sheep did not collide with fences or obstacles, rather they pulled up short or failed to find a path through an

opening. Their menace reflexes were generally absent or reduced at this age but pupillary light reflexes were intact. Positive ERG traces could be recorded from similarly aged CLN5 affected animals in a later trial (unpublished PhD findings, Katharina Russell, Lincoln University), confirming retinal functionality and demonstrating that blindness is likely due to a visual cortex lesion at this age. Cortical (or central) blindness presents with partial or total loss of vision, however the eye and retina are normal (Cassin & Rubin, 2011). Such patients may be able to distinguish light/dark and shapes (Cummings & Trimble, 1995) which may explain why the affected sheep here could avoid collisions during early clinical disease. *Post mortem* neuropathological studies have confirmed significant neurodegeneration in the ovine CLN5 affected visual cortex by 9 months of age, with the cortical thickness of this region being reduced to half that of normal at this age (Chapter 5). Not until late in the CLN5 disease progression, when the cortical blindness is compounded with the retinal degeneration (measured by negative ERG responses), do CLN5 affected sheep actually hit obstacles. This has been noted whilst moving affected Borderdale sheep between paddocks over the past decade (Nadia Mitchell, personal observation). However, as delayed-onset visual deficits began in treated sheep from 21-22 months of age, they started to run directly into obstacles, often with force. They would collide with fences, even in a straight laneway. Funduscopic examination from 18 months on showed the anterior and posterior segments of the treated eyes were normal except for a mild vascular attenuation. Menace responses diminished from 21-22 months of age, whilst the pupillary light response was sluggish but retained. ERG measurements at a single timepoint (27 months) were unrecordable, indicating retinal dysfunction. This suggests the pathophysiological cascade causing the visual disturbances in the treated sheep is different from the progressive visual cortex abnormalities and later retinal degeneration seen in untreated CLN5 affected animals. *Post mortem n*europathological studies of the brains and histological analysis of the eyes of treated sheep are underway to confirm this.

This delayed visual loss seen in the treated sheep likely reflects insufficient retinal penetration by the CLN5 protein for prevention of degeneration after intracranial gene therapy. In fact, the retention of eyesight for so long after intracranial gene delivery was remarkable given that no intraocular therapy was attempted. Similar findings were recently published for a dog model of CLN2 NCL after ICV AAV2-mediated delivery of TPP1, which encodes the soluble lysosomal enzyme tripeptidyl peptidase 1 (Katz *et al*., 2015). Like the sheep, diseased dogs had an extended lifespan after treatment, with protection from cognitive decline and delayed disease onset and progression. Visual abnormalities were also the first clinical signs in the treated dogs. Elevated levels of the recombinant TPP1 protein were detected throughout the brain parenchyma but not in the retinal pigmented epithelium or photoreceptor cells, indicating there was insufficient retinal penetration to preserve structure and function. Both the current study and the CLN2 dog findings suggest that adjunct ocular gene therapy may preserve vision in treated NCL patients for a longer time.

Due to the successful correction of phenotype in the treated sheep, *post mortem* CLN5 expression and neuropathological studies, looking for pathological correction, were not possible during the timeframe of this doctoral study. Brain, spinal cord, eye and peripheral tissue samples collected from the five euthanised animals are being processed as part of a collaborative initiative with Prof. Jon Cooper (Kings College, London UK) in 2016. Thick (50 μm) brain sections will be analysed for *CLN5* transgene expression, attenuation in neuropathology (neuronal loss, cortical atrophy, astrocytosis, microgliosis, storage) and any potential adverse events (inflammation, neurotoxicity). One can only theorise as to how and why the gene therapy was effective in the CLN5 sheep model. Based on previous findings in sheep (Chapter 5) (Linterman *et al*., 2011) and the literature (Liu *et al*., 2005a; Haurigot *et al*., 2013; Katz *et al*., 2015; Ribera *et al*., 2015), it is hypothesised that targeted ICV-mediated delivery of lentiviral and/or AAV9 vector to the ependymal cells, lining the brain ventricular system, with resultant secretion of the CLN5 transgene product into the CSF circulation has acted as a useful global protein delivery mechanism in the treatment of CLN5 NCL. Additionally columnar IP injections may have corrected the resident neural progenitor cells (NPCs) of the subventricular zone (Linterman *et al*., 2015), shown to migrate radially to the degenerating cortex in the diseased CLN5 sheep brain (Section 4.3.5), providing an alternative *in situ* stem cell repair therapy.

In conjunction with neuropathological studies, vector biodistribution will be determined through the CNS and peripheral tissues by quantitative PCR with primers specific for ovine *CLN5*. Blood serum samples, collected through the study from pre-injection to time of sacrifice, will be tested commercially for the prevalence of neutralising antibodies against the injected capsid and transgene product. Given the degree of functional and structural efficacy seen in the treated animals, one would expect low serum anti-vector and anti-*CLN5* titres, however it is possible a humoral response may explain the reduced duration of intracranial volume correction in the AAV9-treated animal 1120/13. Eyes have also been collected from the treated sheep and sent to Massey University for expert pathological analysis. This is particularly pertinent given the differing aetiology of the blindness exhibited by the treated and untreated *CLN5* deficient sheep.

In November 2015, the New Zealand Environmental Protection Agency (EPA) determined that sheep injected with AAV vectors at Lincoln University were no longer to be regarded as new organisms (genetically modified) under the Hazardous Substances and New Organisms (HSNO) Act 1996. This has given clearance for the one remaining AAV9-treated animal, 1109/13, to be maintained on pasture outdoors under normal husbandry conditions with untreated sheep. As such, this ewe will be kept alive unless otherwise indicated to assess the long-term and systemic effects of AAV therapeutics in a CLN5 affected sheep. It will be interesting to see if any non-CNS pathology becomes clinical in this sheep.

The timing of therapeutic intervention is likely to be a very important factor when predicting outcomes in human patients. The vast majority of children are not diagnosed with NCL prior to symptom onset whereas in the present study CLN5 deficient sheep were treated pre-symptomatically. Whilst there is evidence of regional reactive astrocytosis from birth in the pre-symptomatic CLN5 affected brain, loss of cortical neurons and overt brain atrophy do not commence until later, from four and six months of age respectively (Chapter 5). Whilst viral-mediated delivery of gene therapy pre-symptomatically in this study has shown functional and structural efficacy, it is unlikely to be as efficacious at delaying clinical symptoms and pathology when administered later in the disease course. To test this in a more clinically relevant scenario, post-symptomatic gene transfer to CLN5 affected sheep will be evaluated. A trial comprising six CLN5 deficient sheep injected with AAV9-*CLN5* at nine months of age is already underway and a further six affected sheep were injected at seven months of age in May 2016. Subretinal delivery of AAV9-*CLN5* will also be attempted in the latter cohort as a means to target degeneration within the eyes (see Section 8.3.3).

6.5 Conclusion

The tolerance, safety and efficacy of lentiviral and AAV based therapeutics was tested in pre-clinical affected CLN5 deficient sheep. Diseased sheep, treated pre-symptomatically with a single administration of either lentiviral or recombinant adeno-associated virus expressing ovine *CLN5*, showed protection from stereotypical disease onset and progression, retention of cognitive function, sustained normalisation of brain structure and intracranial volume, and an extended lifespan. The only disease manifestation seen in the treated sheep was a very delayed-onset visual deficit. *Post mortem* analysis of the CLN5 treated sheep will determine the exactitudes by which the intracranial gene therapy was able to correct neuropathology. The robust pre-clinical data of the safety and long-term biological efficacy of pre-clinical AAV- and LV-based gene therapy used here to treat the CNS pathology in the CLN5 sheep model is likely to expedite advancement of this methodology to the clinic.

Chapter 7

Gene transfer to the CLN6 affected sheep brain

7.1 Introduction

As described previously, a promising treatment modality for the NCLs is viral-mediated gene therapy with the corrective gene product. However one caveat for the treatment of disorders resulting from defective transmembrane proteins, such as CLN3, CLN6, CLN7, CLN8 and CLN12, is that *in vivo* gene therapy approaches are unlikely to benefit from cross-cell correction (Neufeld & Fratantoni, 1970). Vector-driven expression is likely to correct only those cells directly transduced by the viral vector, and not neighbouring cells (Sands & Davidson, 2006) and since the CNS manifestation of the NCL disease is widespread, an effective gene therapy strategy must transduce a high proportion of cells to restore protein function to a large portion of the brain.

Despite the intracellular nature of the CLN6 protein, studies in an ovine form of CLN6 NCL have suggested that *in vivo* intercellular correction may still be possible. CLN6 affected sheep develop clinical signs from 10 – 14 months of age, namely loss of vision and progressive psychomotor decline due to severe cortical atrophy, particularly of the occipital lobe, and loss of photoreceptor cells in the retina (Mayhew *et al*., 1985; Jolly *et al*., 1989), and usually die prematurely before 24 months. The course of neuropathology in these sheep closely mimics than in affected children, with progressive neurodegeneration, neuroinflammation and accumulation of subunit c of mitochondrial ATP synthase in lysosome-derived organelles in most cells (Palmer *et al*., 1989, 1992; Oswald *et al*., 2005). However despite the widespread intralysosomal accumulation in ovine CLN6, the cellular degeneration is primarily confined to the CNS with regional specificity (Oswald *et al*., 2005). Location and connectiviy, not phenotype, appear to determine neuron survival (Oswald *et al*., 2008), indicating some degree of intercellular interaction.

Studies of chimeric sheep also support this hypothesis. Sheep chimeras, produced by the aggregation of blastomeres from unaffected normal and CLN6 affected embryos, retained normal neuronal architecture and neurogenic capability, and showed no evidence of neurodegeneration or disease-associated glial activation, despite having varied ratios of normal to affected tissue composition (Barry, 2011). Chimeric sheep surpassed the typical life expectancy of affected sheep and retained their vision long after terminal disease in affected animals (Barry, 2011). These findings indicate that the CLN6 defect is cell extrinsic and given the correct environmental milieu affected and newly generated cells can survive and are potentially amenable to correction by unaffected normal cells.

Importantly for gene therapy studies, not all cells needed to be 'corrected' for disease amelioration to be achieved.

Also propitious for CLN6 gene therapy was evidence of extended neurogenesis in the CLN6 affected sheep (Dihanich *et al*., 2009) (see Section 1.5.4). Immunohistochemistry revealed a prominent band of neurogenic cells and fibres along the subventricular zone (SVZ) of affected sheep brains, which migrate to form large clusters of newly generated neurons in the cortical laminae undergoing degeneration. This observation has since been confirmed in human CLN6 patients and has been proposed as an intrinsic attempt at cell replacement within the diseased brain (Dihanich *et al*., 2012). As such, the SVZ represents an accessible site for targeted viral-mediated gene correction of neural stem and progenitor cells. Intraparenchymal injection of lentiviral vectors into the SVZ has shown targeted transduction of the ependymal and subependymal cells along the extent of the ventricular surface in sheep (Linterman *et al*., 2011). Transduced cells included type B astrocytic cells, thought to be the *bona fide* adult neural stem cells (Doetsch *et al*., 1999), which have the ability to perform lifelong migration, differentiation and repopulation of functionally defined regions in the brain (Alvarez-Buylla & 2004; Lim & Alvarez-Buylla, 2014). If targeted early enough in the pathogenic cascade, whilst the rate of cell loss is still low and the microenvironment is still conducive to cell maturation and survival, corrected neuroblasts and their progeny could migrate rostrally, as well as radially to the outer cortex, allowing cross-correction of diseased neurons.

There is likely to be a threshold minimum percentage of cells necessary to be corrected to observe functional amelioration and/or impede disease progression but it is anticipated that either widespread or specific targeting will benefit the gene therapy strategy for the CLN6 disease. Over the past 7 years, much effort within BARN has concentrated on optimising strategies to maximise delivery. On this basis, *in vivo* gene therapy was attempted on pre-symptomatic CLN6 affected sheep comparing the capability of AAV9 and lentiviral vector platforms to effectively deliver ovine *CLN6* and prevent disease development in these sheep. Based on the findings described in Chapter 4 and the Linterman study (2011), it was hypothesised that the AAV9 vector would provide greater spread of transgenic protein through the CLN6 affected sheep brain, whilst targeting the migratory neural progenitor cells with the lentiviral vector could facilitate broad transduction within the diseased brain via migraton.

7.2 Materials and methods

7.2.1 Study design

Pre-symptomatic CLN6 affected sheep were treated with lentiviral or AAV vectors containing ovine *CLN6* and then phenotypically compared with untreated CLN6 affected and clinically normal heterozygous controls (Table 7.1). On trial completion, *post mortem* CNS tissues from treated sheep were examined for evidence of disease amelioration, specifically looking for any attenuation in the cortical thinning and severe neurodegeneration, glial activation, and storage body accumulation documented for untreated CLN6 affected sheep (Chapter 4, Oswald *et al*., 2005).

7.2.2 Animals

South Hampshire sheep were bred, maintained and diagnosed at birth as described in Section 3.1 (Tammen *et al*., 2006). Cohorts of CLN6 homozygous affected (*CLN6-/-*; *n* = 9) and clinically normal heterozygous (*CLN6+/-*; *n* = 3) sheep were maintained under normal pastural conditions at the Research Farm, Lincoln University, and acted as untreated affected and normal controls. An additional six pre-symptomatic CLN6-/- sheep were weaned early, at 1.8 $\pm$ 0.1 months of age, and moved indoors prior to *in vivo* gene therapy at 3 to 4 months of age (see Section 3.1.1). There were two sibling pairs, with one pair in each treatment cohort (1001/13 and 1002/13; 1026/13 and 1027/13). Pretherapy, the CLN6 genotype was reconfirmed from genomic DNA isolated from venous blood (see Section 3.1.2.2) and this was repeated by an independent evaluator every six months and/or at *post mortem.*

7.2.3 Viral vectors

The ovine CLN6 coding sequence (GenBank accession number NM_001040289; Tammen *et al*., 2006) was generated using the polymerase chain reaction with *CLN6*-specific primers on sheep cDNA by the author in 2005. The full-length CDS was cloned into a pcDNA3.1D TOPO plasmid (Invitrogen, Carlsbad, CA, USA) and sent to Otago University where lentiviral (LV) and recombinant AAV (serotype 9; AAV9) viral vectors expressing ovine *CLN6*, under the control of the myeloid sarcoma virus U3 element were produced at the Otago Viral Vector Facility as described in Chapter 3 (Section 3.2.1). Functional viral titres for the LV-MND-*CLN6* (hereafter referred to as LV-*CLN6*) ranged from 7.5 to 8.1 x 10^9 TU/mL. Genomic titre for the AAV9-MND-*CLN6* (hereafter AAV9-*CLN6*) vector was 2.36 x 10^{12} ssDNA vg/mL.

Table 7.1 Treatment groups and clinical assessment at *post mortem* (or trial completion)

Sheep	Genotype	Treatment*	Gender†	Age (months)	Cause of death‡	Clinical score	Clinical description	Seizures	Brain weight (g) ¶
1007/13	*CLN6+/-*	-	M	18.4	-	5	Normal	-	-
1012/13	*CLN6+/-*	-	M	18.3	-	5	Normal	-	-
1022/13	*CLN6+/-*	-	M	18.1	-	5	Normal	-	-
1003/13	*CLN6-/-*	-	M	17.6	Completion of trial	2	Clinical disease, blind	-	77
1005/13	*CLN6-/-*	-	M	19.2	Completion of trial	1	Advanced disease, blind	-	64.72
1011/13	*CLN6-/-*	-	M	17.4	Completion of trial	2	Clinical disease, blind	-	77.79
1013/13	*CLN6-/-*	-	M	12.6	Disease-related	1	Advanced disease, blind	-	n.t. #
1015/13	*CLN6-/-*	-	M	19	Completion of trial	1	Advanced disease, blind	-	61.03
1017/13	*CLN6-/-*	-	M	17.3	Completion of trial	1	Advanced disease, blind	-	71.34
1021/13	*CLN6-/-*	-	M	17.2	Completion of trial	1	Advanced disease, blind	-	74.47
1028/13	*CLN6-/-*	-	M	13.4	Misadventure	1	Advanced disease, blind	+	n.t. #
1041/13	*CLN6-/-*	-	M	13.4	Indeterminable §	1	Advanced disease, blind	+	51.4
1001/13	*CLN6-/-*	LV-MND-*CLN6*	F	16.7	Completion of trial	3	Clinical disease, blind	-	67.32
1002/13	*CLN6-/-*	LV-MND-*CLN6*	F	14.8	Copper toxicosis	3.5	Onset of disease, losing vision	-	66.8
1004/13	*CLN6-/-*	LV-MND-*CLN6*	F	14.1	Copper toxicosis	3	Onset of disease, losing vision	-	66.22
1025/13	*CLN6-/-*	AAV9-MND-*CLN6*	F	13.8	Age-match for 1004/13ψ	2.5	Clinical disease, blind	-	69.34
1026/13	*CLN6-/-*	AAV9-MND-*CLN6*	F	16.2	Completion of trial	2	Advanced disease, blind	-	63.14
1027/13	*CLN6-/-*	AAV9-MND-*CLN6*	F	26.2	Completion of trial	5	Normal	-	84.9

* LV lentiviral vector; AAV9 adeno-associated viral vector serotype 9; MND (myeloproliferative sarcoma virus enhancer, negative control region deleted, dl587rev primer-binding site substituted) promoter

† M male; F female

‡ Sheep were euthanised at a clinical humane endpoint or trial completion

§ Presentation of symptoms similar to Listeriosis. A veterinary *post mortem* and examination of tissues by Gribbles Veterinary Pathology failed to confirm this diagnosis. Death was likely attributable to advanced NCL

¶ Fresh brain weight values for untreated animals; post-fixation brain weights for treated animals (boxed)

n.t not tested

ψ1025/13 was euthanised with clinical symptoms as an AAV9 age-match comparison to 1004/13 (LV)

7.2.4 *In vivo* viral injections

Pre-symptomatic *CLN6-/-* sheep received bilateral parenchymal (occipital and parietal cortices) and intracerebroventricular (ICV) injections as described in Section 3.2.2. For the lentiviral (LV) cohort, four 3 mm holes were made in each skull at the following co-ordinates (in mm) relative to bregma: occipital cortex, anterior-posterior (AP) -4, mediolateral (ML) ±7, dorsoventral (DV) -11 (from the meninges/ pial surface); parietal cortex, AP +7, ML ±7, DV -11. Each sheep (*n* = 3, aged 2.7 months) received a total dose of 2.3 x 10^9 TU of LV-*CLN6* (110 µl per ventricle; 26 µl per parenchymal site).

A month later, the second cohort (*n* = 3, aged 3.7 months) each received a total dose of 2.6 x 10^{12} vg of AAV9-*CLN6* (500 µl per ventricle; 25 µl per parenchymal site). To accommodate brain growth due to their older age at injection, co-ordinates were revised for this cohort to: occipital cortex, AP -6, ML ±8, DV -12; parietal cortex, AP +8, ML ±8, DV -12.

7.2.5 *In vivo* monitoring

Treated *CLN6-/-* sheep were monitored for *in vivo* assessment of therapeutic efficacy for a period of 24 months, from 4.3 months of age, and compared with age-matched cohorts of untreated *CLN6+/-* and *CLN6-/-* sheep using the parameters and CNS imaging described in Sections 3.3– 3.6.

7.2.6 Tissue collection and immunohistochemistry

Injected animals were euthanised by exsanguination at 13.8 to 26.2 months of age, and the brains perfusion fixed as described in Section 3.8. Spinal cord and visceral tissue samples, including liver, lung, spleen, adrenal gland, bladder, oesophagus, pancreas, lymph nodes, kidney, gastrointestinal tract, skeletal and cardiac muscles were either snap-frozen in liquid nitrogen for retrospective RNA isolation and quantitative real-time PCR-based biodistribution studies or fixed in formyl saline, equilibrated in cryoprotectant, frozen at -80 °C, and sectioned at 50 µm (see Section 3.8). Eye globes were enucleated at *post mortem,* fixed in 10 % formalin for at least 2 h, and sent to Gribbles Veterinary Pathology (Christchurch, New Zealand) for post-fixation in Bouin's solution (HT10132; Sigma-Aldrich, St. Louis, MO, USA) for 4 h, wax-embedding and sectioning at 5 µm.

Brain hemispheres from the injected animals were analysed for CLN6 and CLN5 expression, cortical thickness and neuronal loss, neurogenesis, storage body accumulation and glial activation with different histological and immunostains (Section 3.9).

7.3 Results

CNS-directed gene therapy was performed on pre-clinical *CLN6-/-* animals at 2.7 (LV-*CLN6*; *n* = 3) and 3.7 months of age (AAV9-*CLN6*; *n* = 3). Of the six animals treated, three were euthanised during the study period at 12 months post-treatment, whilst the remaining three survived to study completion. *In vivo* monitoring showed that five of the six treated sheep developed stereotypical CLN6 disease, which was confirmed by *post mortem* neuropathology studies. This group will hereafter be referred to as the unsuccessful treatment cohort. However, one AAV9-treated animal (1027/13) maintained phenotypic correction through the two year follow up period and was euthanised at 26.2 months of age to allow assessment of CLN6 transgene expression and neuropathological assessment of treatment-dependent modulation of lysosomal storage pathology, glial activation, and neuronal loss.

7.3.1 Confirmation of genotype

The genotype of each treated sheep was determined from restriction fragment length polymorphic analysis of a silent substitution in *CLN6* exon 7 at birth and a fortnight prior to surgery (Figure 7.1) with confirmation by sequencing. A consistent homozygous result for the mutant allele (*CLN6-/-*) was observed from serial blood samples collected every 6 months over the life span of all treated animals.

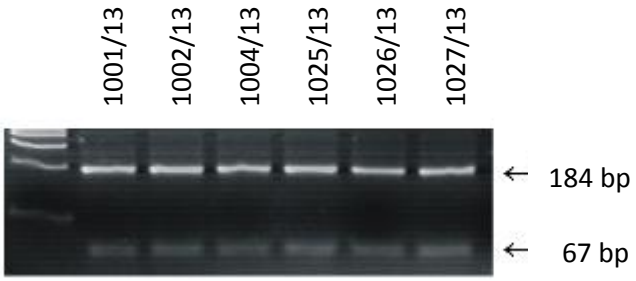

Figure 7.1 Confirmation of the affected genotype in the six gene therapy sheep subjects
CLN6-/- status was verified in the six treated animals using the disease-associated A/G polymorphism (Tammen *et al*., 2006). Shown is a representative agarose gel of the affected banding pattern from the six treated *CLN6-/-* animals after *Hae* II digestion of a 251 bp PCR product from exon 7 of ovine *CLN6* (refer to Figure 3.1). Lane 1 contains a size standard with 400, 300, 200 and 100 bp bands visible.

7.3.1.1 Safety and tolerability of LV-*CLN6* and AAV9-*CLN6* administration to sheep

The neurosurgical *CLN6* gene transfer procedure was well tolerated by the CLN6 deficient sheep. They had an uneventful post-operative course with no neurobehavioural changes, alteration in health status, or clinical signs of an immune response - as indicated by normal rectal temperatures.

Over the course of the study, five adverse events were reported (Table 7.2). None of these were directly attributable to the vector, anaesthesia, surgical or administration procedure *per se* but most likely resulted from the housing constraints and resultant long-term concentrate feeding of the sheep.

Table 7.2 Reported adverse events following viral-mediated CLN6 gene therapy in sheep

Level of severity	Number of events	Description of event	Outcome
Serious	2	Copper toxicosis	Fatal (euthanasia)
Non-serious	1	Lip piercing	Non-fatal, self-resolving
	1	Contagious ecthyma	Self-limiting
	1	Stereotypical behaviour	Required intervention

7.3.1.1.1 Chronic copper toxicosis

The most serious adverse event was the development of fatal copper toxicoses in two of the lentiviral- injected sheep ~12 months post-treatment. The first sheep, 1004/13, presented with haematuria (haemoglobinuria), fever, anorexia and reduced activity. An initial veterinary diagnosis of urinary tract calculi was made. Although a 5 day course of intramuscular antibiotic (Alamycin 10, Norbrook NZ Ltd, Auckland New Zealand) and oral drenching with ammonium chloride (7 g per day) resolved the fever and haematuria, the sheep remained lethargic, with depression, loss of appetite and repetitive teeth grinding, indicative of ongoing pain. A decision was made to euthanise on humane grounds. A veterinary *post mortem* examination showed pathological changes typical of a haemolytic crisis. There was marked jaundice through all the tissues. The liver was swollen, with rounded edges and was pale yellow in appearance. The kidneys were enlarged with a dark 'gun-metal' appearance. Histological examination of the liver by Gribbles Veterinary Pathology identified hepatocyte megalocytosis with mild multifocal apoptosis and cholestasis, compatible with chronic copper toxicity. Kidney lesions were consistent with haemoglobinuric nephrosis. The copper concentrations in the kidney confirmed this diagnosis, measuring 510 µmol/kg, well above the adequate healthy range for sheep of 0 – 157 µmol/kg.

Three weeks later, a second sheep, 1002/13, presented with similar symptoms and was also euthanised. The pathology report confirmed chronic copper toxicity, with intravenous haemolysis detected and widespread apoptotic and mitotic hepatocytes indicative of progressive liver damage.

Trace copper concentrations in the kidney and liver again well exceeded the normal range (906 µmol/kg and 5000 µmol/kg respectively; normal liver range 95 – 3000 µmol/kg).

Extra supplementation was added to the diet. Ammonium molybdate (50 mg) and sodium thiosulphate (0.5 g) were added daily for three week-long periods as a preventative measure to reverse the copper overload. Copper levels in the concentrate lucerne pellet feed, lucerne chaff and hay chaff were found to be low; 9, 7 and 6 parts per million respectively (Gribbles Veterinary Pathology). Levels from the water supply to the sheep holding facility were found to be 2 parts per billion and below detection respectively in the two samples sites tested (Analytical Services, Lincoln University).

Despite the introduction of supplementation to reduce copper absorption, the copper concentration in the livers of all of the other treated sheep were excessively high at euthanasia (>3000 µmol/kg), indicating this to be an ongoing problem for sheep maintained long-term indoors on lucerne-based concentrate feed.

7.3.1.1.2 Other adverse events

During the gene therapy trial, three other adverse incidents were reported. One sheep (1027/13) pierced its lip on the metal mesh surrounding its cage. Regular treatment with saline solution prevented infection and the piercing closed over within a month. Another sheep (1001/13) developed a large purulent papule on its upper lip, with no other systemic symptoms. This was identified as contagious ecthyma (Orf disease, scabby mouth), a pustular form of dermatitis. The animal was isolated, no further cases developed in the other similarly housed animals and the pustule self-resolved in 3 weeks. The third incident occurred early in the trial and involved stereotypic “wool biting” behaviour, with one animal (1002/13) pulling strands of wool from the fleece of her subordinate sibling (1001/13), who became substantially denuded in patches. Environmental enrichment was increased, including hanging chains from the ceiling, balls, plastic bottles or chewing bars in the pens, and these were rotated biweekly to stimulate investigative behaviour. Long-strand fibre (chaffed hay) was also added to the diet, to increase the roughage content, with the resultant cessation of the behaviour.

7.3.1.2 Growth rate

Despite injected sheep being weaned early and maintained indoors on a daily feed ration during the course of the trial, growth rates for treated sheep were steady (1.91 kg/month) and comparable with age-matched untreated *CLN6-/-* (1.46 kg/month) and *CLN6+/-* cohorts (2.25 kg/month) maintained on pasture (Figure 7.2). Rates were also consistent with those documented for animals similarly housed indoors on a long-term pharmaceutical trial, being 1.7 kg/month for CLN6-/- sheep and 2.1 kg/month for CLN6+/- sheep (Kay & Palmer, 2013).

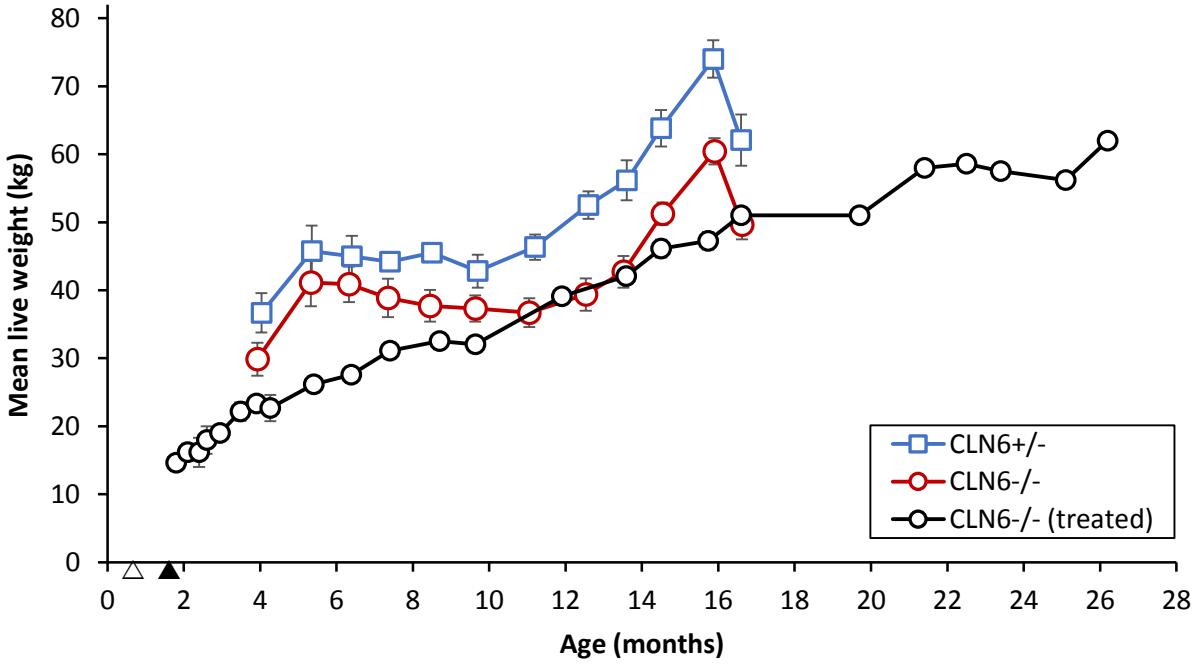

Figure 7.2 Mean live weight increases following viral-mediated *CLN6* gene transfer in sheep
Mean live weight changes in outdoor housed untreated heterozygous (*CLN6+/-*) and CLN6 affected (*CLN6-/-*) cohorts reflect normal seasonal fluctuations, whilst treated *CLN6-/-* animals were weaned early at 1.8 months, housed indoors after their gene transfer neurosurgery (△ LV-*CLN6*, ▲ AAV9-*CLN6*) and received a daily maintenance ration of feed, reflected in their steady weight gains. Composite live weights were plotted for the treated sheep as there was no significant difference between the two viral vector treatment groups. Vertical bars depict ±SEM.

7.3.2 *In vivo* assessment of gene therapy efficacy

7.3.2.1 Clinical staging of ovine CLN6

Determining the natural progression of disease was essential for evaluating therapeutic success in the gene therapy study. As in the CLN5 gene therapeutic study, sheep in the treatment and control cohorts were assessed for neurological, behavioural, motor and visual function based on an ovine-specific clinical rating scale (Table 3.1, see Section 3.3). Clinical rating scores (CRS) decreased from 5 (normal function) to 0 (progressive disease with spontaneous tetanic seizures, defined as the humane end-point) as animals became more debilitated from the disease. Routine monthly physical and neurological examinations were performed, with concurrent open- and closed-field behavioural observation, beginning on average at 4.3 months of age.

CLN6 heterozygous sheep were clinically normal throughout the study period, consistently scoring 5 on the rating scale (Figure 7.3) and exhibited no functional deficits. In comparison, clinical signs of CLN6 disease in homozygous affected (*CLN6-/-*) sheep developed slowly and progressively from 7 $\pm$ 0.9 months of age. They initially presented with low head carriage, which was especially apparent when they were passing through gates, races, a maze (see Section 7.3.2.4) and in shadows (CRS 4). From 9 months of age, individual sheep began to show visual deficits with an overt head tilt, thereby extending their visual field, and depressed visual reflexes, namely the menace (eye preservation), pupillary light and dazzle responses. By 10 to 12 months *CLN6-/-* sheep were smaller and had less condition than their heterozygous counterparts; this coincided with the onset of winter, when grazing was limited. Despite the difference in live weights at this timepoint, the subsequent growth rate of the *CLN6-/-* cohort mirrored that of the *CLN6+/-* cohort (Figure 7.2). From 12.6 $\pm$ 1.0 months, all untreated *CLN6 -/-* sheep were functionally blind (CRS 3).

An overt neurological disease phenotype (CRS 2) was detected in the remainder of the affected South Hampshire sheep from 15.4 $\pm$ 1.0 months of age, with reduced mentation and spontaneous episodes of head nodding and facial twitches, particularly of the eyelids, ears and lips. There was however significant variation in the disease onset and progression in the *CLN6-/-* cohort. Three untreated *CLN6-/-* sheep died naturally, but prematurely with advanced disease symptoms, during the study (Table 7.1). 1013/12 died at 12.6 months, with disease-related pathology observed *post mortem*. Another animal (1028/13) developed stress-induced tremors at 12.7 months and died of misadventure (falling into a ditch) at 13.4 months. A second sheep (1041/13) also developed severe inducible tremors, with a circling tendency resembling encephalitic listeriosis, and was euthanised at 13.4 months. Thus the sample size of the untreated *CLN6-/-* cohort decreased with age prior to trial completion.

After 17.2 ± 0.8 months, *CLN6-/-* sheep exhibited progressively more obvious changes in sensation (blindness), mental state (behavioural changes), and posture or movement (motor deficits), termed the advanced disease state (CRS 1). Menace and dazzle responses were absent and pupillary reflexes were diminished. Affected sheep self-segregated from the flock, showed a reduced awareness of their surroundings and performed repetitive activities, such as inefficient or sham eating, aimless walking and compulsive circling in a confined space. Sheep showed a higher propensity to stumble, and when they stood still often adopted a wide stance with more manifest hindlimb paresis and localised tremors. Spontaneous seizure activity was not evident in the *CLN6-/-* cohort during this study, however this manifestation of the disease usually presents from 18 months of age and only occurs in a minority of the affected sheep (Palmer and Mitchell, personal observation). Despite affected South Hampshire sheep having lived up to 29 months with extensive nursing, all *CLN6-/-* sheep in this study were euthanised by 19.2 months for humane reasons with varying degrees of clinical disease (Table 7.1).

A.

Score	Clinical phenotype	Clinical status *	Age (months)
5	Normal	Normal	<7.0 ± 0.9
4	Pre-clinical	Low head carriage Propensity to crouch, baulk and stumble	7.0 ± 0.9
3	Blind	Head tilt/stargazing Visual deficits Decreased or lost menace (blink) response Reduced herding	12.6 ± 1.0
2	Overt/neurological	Motor, cognitive and proprioceptive deficits Decreased startle to auditory stimuli Wide stance	15.4 ± 1.0
1	Advanced	Progressive disease +/- induced tetanic seizures	18.1 ± 0.9
0	Terminal	Spontaneous tetanic seizures	Not observed

* Onset of inducible mild tremors in individual sheep began as early as 12.7 months. Spontaneous convulsive seizures were not reported for the *CLN6*$^{-/-}$ sheep in this study but have been observed previously in the field in animals approaching or into their second year of life.

B.

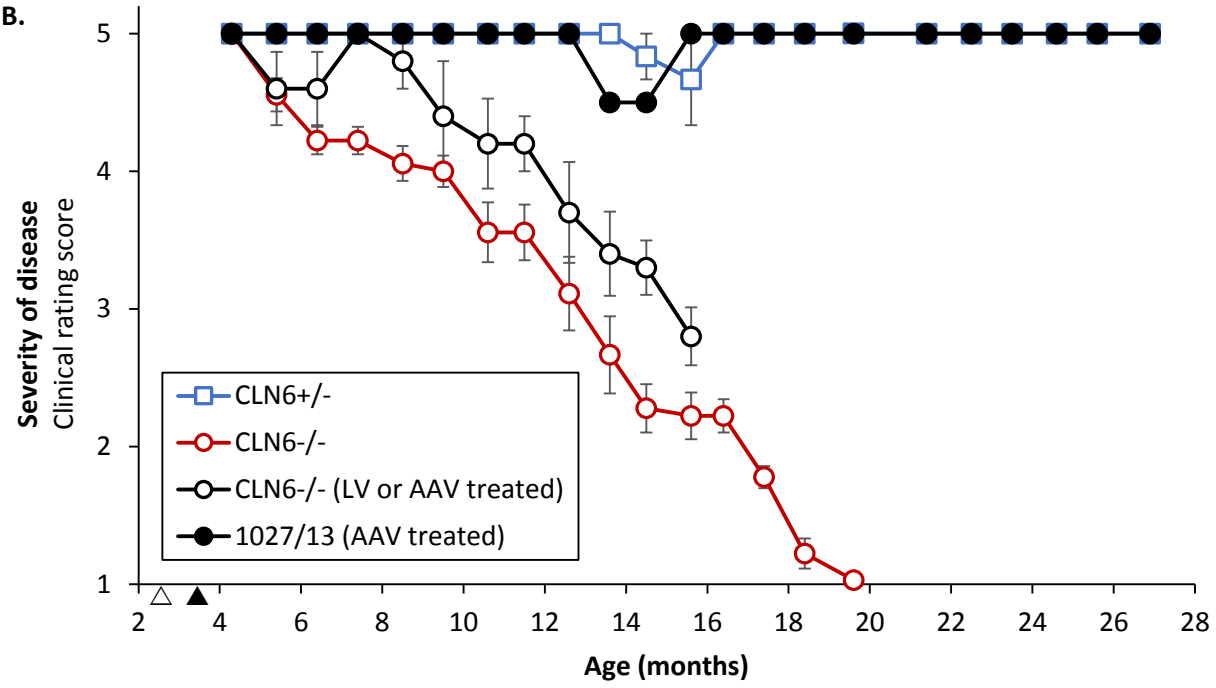

Figure 7.3 Clinical progression of CLN6 deficient sheep following viral-mediated CLN6 gene transfer
Treated sheep were followed for 24 months after treatment (△ LV-CLN6,▲ AAV9-CLN6) and monitored against disease progression in untreated *CLN6-/-* sheep. **A.** Ages of symptom onset are shown for untreated *CLN6-/-* sheep (mean ± SEM, *n* = 9). The scale is based on multi-focal neurological and motor defects, with initial behavioural deficits at 7 ± 0.9 months of age. **B.** One animal (1027/13) responded robustly to the treatment showing clinical scores consistent with untreated *CLN6+/-* controls, whereas the remaining five treated animals responded less favourably, developing behavioural deficits from 12.7 ± 0.6 months and loss of vision and other clinical symptoms from 14 ± 0.8 months of age.

7.3.2.2 Clinical status in treated *CLN6-/-* sheep

At baseline (4.3 months), no neurological abnormalities were detected in the study animals with all cohorts scoring 5 (Figure 7.3). The treated cohort could be divided into two groups: one animal (1027/13) responded so favourably to AAV9-*CLN6* treatment that it was indistinguishable clinically from the untreated *CLN6+/-* cohort over the duration of the study whereas the same level of therapeutic efficacy was not achieved by the other five treated animals. At the pre-determined study endpoint of 18 months of age, sheep 1027/13 showed no clinical evidence of ovine NCL disease symptoms and, with a CRS of 5, the trial was extended to gain an insight into the persistence of efficacy.

At 26.2 months of age (23.9 months post-treatment), 1027/13 was euthanised. The only clinicopathological indication of NCL detected in this animal was low level retinal damage, described below, which did not impact her visual functionality. Bilateral funduscopic examination at 18 months of age, conducted by an independent veterinary ophthalmologist, revealed a degree of tapetal hyperreflectivity and mild attenuation of the retinal vasculature in 1027/13 compared with untreated *CLN6+/-* controls. Electroretinography (ERG) and funduscopy performed on 1027/13 just prior to euthanasia corroborated this finding. ERG waveforms in both eyes of untreated *CLN6-/-* animals began to decrease from 12 - 15 months of age, becoming extinguished (flatline) in some individuals from 18 months (Katharina Russell, personal communication), confirming retinal dysfunction in the ovine model. However a- and b-waveforms were detected for 1027/13 at 26 months of age, although the amplitude of the a-wave was slightly reduced compared with fully sighted heterozygous controls (Figure 7.4). Only a single ERG episode was recorded for 1027/13, hence no longitudinal data are available. At this age, the menace response and pupillary light reflexes were still intact. Mild vascular attenuation was confirmed in the tapetal and non-tapetal fundus, but this was much less marked than in younger untreated *CLN6-/-* animals (Katharina Russell, personal communication).

Although the other five treated *CLN6-/-* animals did not show the same degree of functional correction, disease onset was delayed in them by a few months on average (Figure 7.3). These sheep were clinically normal until 12.7 $\pm$ 0.6 months of age, when they began to baulk at obstacles, shadows and their cohorts (CRS4). The presentation of a head tilt in some animals and reduced menace reflexes indicated the onset of visual deficits, with functional blindness reported at 14 $\pm$ 0.8 months (CRS 3). During this early-clinical stage, animals 1004/13 and 1002/13 were euthanised due to the cumulative effects of copper toxicity. A third sheep (1025/13) was also euthanised early, at 13.8 months, because of overt clinical signs of NCL, which included blindness, confusion and circling. Animals 1001/13 and 1026/13 saw the trial to completion, but were functionally blind from 15.6 and 12.6 months respectively, and developed an overt clinical phenotype prior to euthanasia.

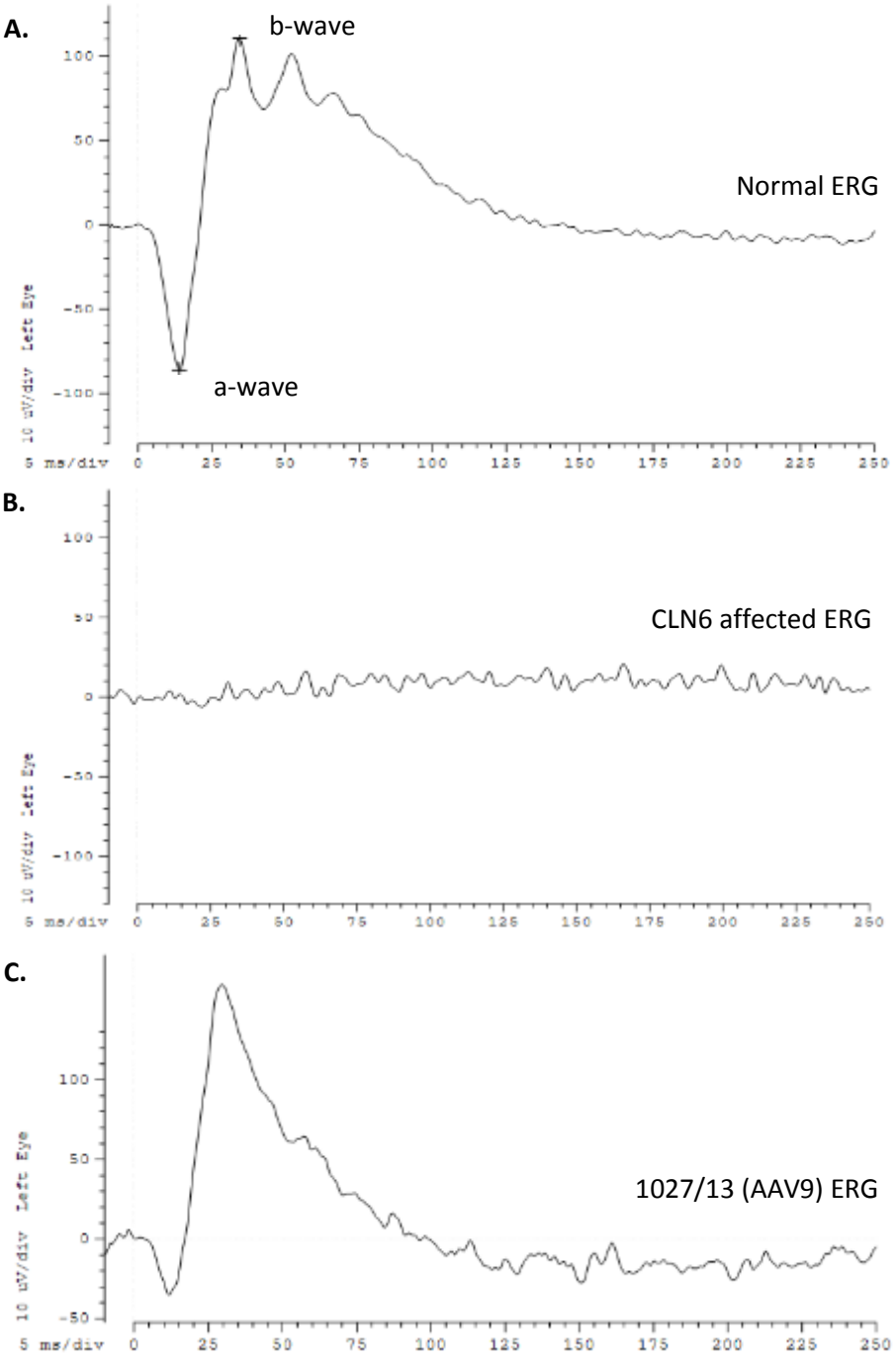

Figure 7.4 Electroretinography (ERG) as an indicator of retinal damage

A. Scotopic electroretinogram from the left fundus of an 18.8 month old *CLN6+/-* sheep with normal retinal function. A negative deflection (a-wave) and larger positive deflection (b-wave) can be seen.

B. A flatline response, in the left fundus of a 18.3 month untreated *CLN6-/-* sheep, with complete ablation of the a- and b-waves, indicative of retinal dysfunction.

C. A response, albeit with decreased a-wave amplitude, is detected from the left fundus of the treated *CLN6-/-* sheep, 1027/13, at 26.2 months of age, almost 24 months after AAV9-*CLN6* delivery. This suggests CNS-directed gene therapy afforded sufficient protection to the retina to maintain vision and elicit an ERG response. Electroretinogram traces were provided by Katharina Russell (PhD student, Lincoln University).

7.3.2.4 Maze testing as a biomarker of functional correction

Functional efficacy of *CLN6* gene transfer was assessed monthly in a closed-field maze test (see Section 3.4). Total mean maze traverse times for the treatment groups and untreated *CLN6-/-* and *CLN6+/-* cohorts are shown in Figure 7.5A. There was no detectable difference between the four groups at baseline (4.3 months of age) but a significant ($P < 0.05$) treatment effect became apparent from 5.4 months as untreated *CLN6-/-* sheep took progressively more time to navigate the maze. Despite being functionally blind from 12.6 $\pm$ 1 months, they were still able to traverse the maze without assistance until 15.4 months of age. Maze testing was abandoned for humane reasons for untreated *CLN6-/-* sheep from that timepoint because of generalised akinesia and the risk of stress-induced tremor activity. Treated sheep could be divided into two groups: one AAV9-treated animal, 1027/13, required less than 10 seconds on average to traverse the maze for most testing intervals, whereas the remainder of the LV- and AAV9-treated sheep ($n = 5$) did not show the same level of functional correction. This unsuccessful treatment cohort were initially faster through the maze than untreated controls, but from 9 months of age their mean transit times matched untreated heterozygotes and then they became increasingly slower.

Figure 7.5B is a graphical plot of the mean error times per month. Although five of the nine untreated *CLN6-/-* sheep spent time in the error zone during the first testing episode, this was not an increasing trend. Heterozygous sheep never entered the error zone, a cul-de-sac which deviated from the correct path through the maze, instead running through the maze rapidly with few pauses. Subjective grading of each sheep's individual negotiation of the maze demonstrated this, and also showed the increasing gap in performance and the developing behavioural phenotype in the untreated *CLN6-/-* sheep and the unsuccessful treatment cohort with time (Figure 7.6). Despite retaining visual acuity to 14 $\pm$ 0.8 months, the unsuccessful treatment cohort demonstrated non-quantifiable NCL phenotypic signs in the final testing sessions, including confusion and pacing back and forth in front of an obstacle, bleating and lowering the head in search of olfactory cues, similar to that seen earlier by untreated *CLN6-/-* sheep.

In contrast, the AAV9-*CLN6* treated sheep, 1027/13, was clinically indistinguishable from healthy heterozygous control sheep, showing no discernible difference in maze performance to them. It ran through the maze arena with its head held high, avoiding obstacles easily, showing no visual problems. It was alert and responsive to visual, auditory and environmental cues, such as wind, pasture, and food rewards, as well as wary of foreign humans or sheep. There was no evidence of the hindlimb ataxia, stereotypical wide stance or localised manifest tremors previously reported for untreated *CLN6-/-* sheep at end-stage disease (~24 months of age).

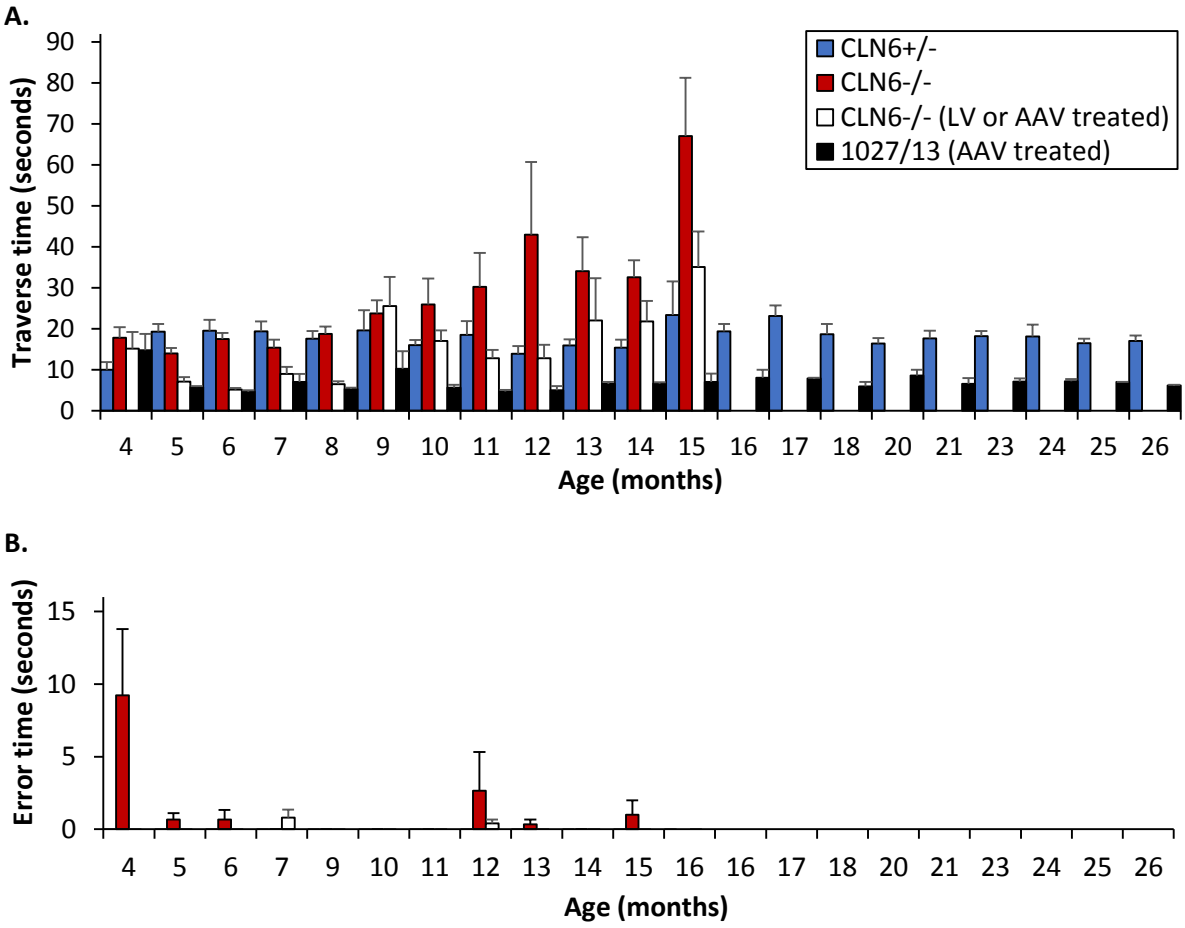

Figure 7.5 Performance in a close-field maze test after viral-mediated *CLN6* delivery

A. Mean traverse times for LV-*CLN6* (*n* = 3) or AAV9-*CLN6* (*n* = 3) treated *CLN6-/-* sheep were compared with unaffected *CLN6+/-* control (*n* = 3) and untreated *CLN6-/-* (*n* = 9) sheep over a period of almost 2 years. The performance of treated sheep was initially significantly better ($P \leq 0.05$) than untreated *CLN6-/-* sheep but with time five of the treated animals began to take progressively longer to traverse the maze. However one AAV9-treated animal, 1027/13, maintained long-term functional correction, with significantly faster traverse times ($P \leq 0.05$).

B. Mean error times during maze passage for the groups in **A** recorded over the same period. Error times do not reflect the changes in performance as efficiently as the average traverse time plot. However the only animals to enter the error zone in the maze were the untreated *CLN6-/-* sheep and later the five sheep who did not respond so favourably to the viral-mediated *CLN6* treatment.

Data are shown as the mean + SEM (vertical bars); *n* = 3 - 4 animals per group, 2 runs per animal at each time point.

A.

Score	Maze assessment	Age (months)
5	Traverse with no problems	< 5.7 ± 0.7
4	Traverse with small pauses	5.7 ± 0.7
3	Traverse but with obvious behavioural phenotype (+/- hits obstacles)	9.8 ± 1.1
2	Traverse with or without pauses but misses entry	13.6 ± 0.7
1	Traverse with errors	15.2 ± 0.4
0	Fail - requires assistance to traverse	Not seen

B.

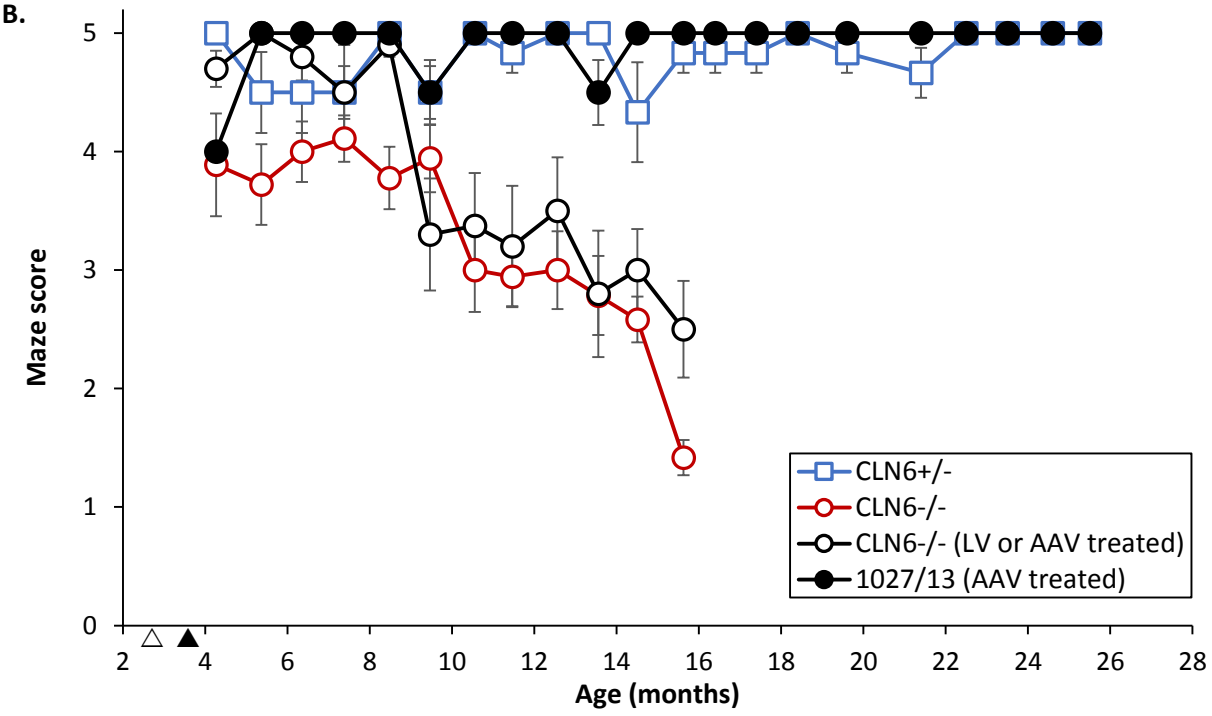

Figure 7.6 Grading of maze navigational ability after viral-mediated *CLN6* delivery

Subjective grading of individual sheep traverses through a closed-field maze were performed at monthly intervals. **A.** Sheep were scored for every maze passage, with scores ranging from 5 (normal traverse) to 0 (failure to traverse without assistance). Ages of onset are shown for seven untreated *CLN6-/-* sheep. Initial phenotypic deficits were detected from 9.8 ± 1.1 months of age and included low head carriage, crouching, baulking, stumbling or 'self-spooking' at obstacles. **B.** Composite scores for the four cohorts show that untreated *CLN6+/-* sheep traversed the maze with no or small pauses, consistently scoring 5 whilst untreated *CLN6-/-* found the maze progressively harder to traverse without errors or assistance. Five of the lentiviral or AAV9- treated sheep traversed the maze with only pauses until 13 months of age when they began to show a behavioural phenotype. The onset of visual deficits then began to affect their performance in line with the untreated *CLN6-/-* sheep. However, one AAV9-*CLN6* treated sheep demonstrated prolonged visual acuity, maze navigational ability and cognitive function, being indistinguishable from untreated *CLN6+/-* controls at 26 months of age. All data are expressed as the mean ± SEM (vertical bars); *n* = 3 - 9 animals per group, 2 runs per animal at each timepoint. △ ▲ denotes the time of treatment for LV- and AAV9-*CLN6* respectively.

7.3.2.5 Disease progression assessed by CNS imaging

Treated animals were CT scanned every two months, intracranial volumes determined and the rates of change calculated from the raw data. At the first scan at 5 months of age, the intracranial volume for treated sheep ranged from 84.1 to 89.0 mL (mean 86.4 ± 0.8 mL; median 86.6 mL), exceeding the mean anticipated for an affected CLN6 animal of the same age (83.0 mL). However for five of the treated sheep, the measured rates of decline in volume after the first scan were faster than those seen from historical data for untreated *CLN6-/-* animals (Figure 7.7, Table 7.3). In contrast, the AAV9-*CLN6* treated animal (1027/13) demonstrated a positive rate of change over the study, equivalent to an increase in intracranial volume of 0.61 mL/month until 15 months of age, then plateauxed at 91 mL. A similar plateau at >100 mL would be expected for a normal adult sheep, based on the literature (Nitzsche *et al*., 2015) and personal observation.

Brain structure was also examined by MRI. A single imaging session performed on 1027/13 at 25 months of age demonstrated long-term normalisation of the brain structure after AAV9-*CLN6* gene transfer (Figure 7.8). Ventricles were of similar size to those of an untreated control animal and there was no evidence of the overt brain atrophy and cranial bone thickening seen in a much younger untreated affected animal.

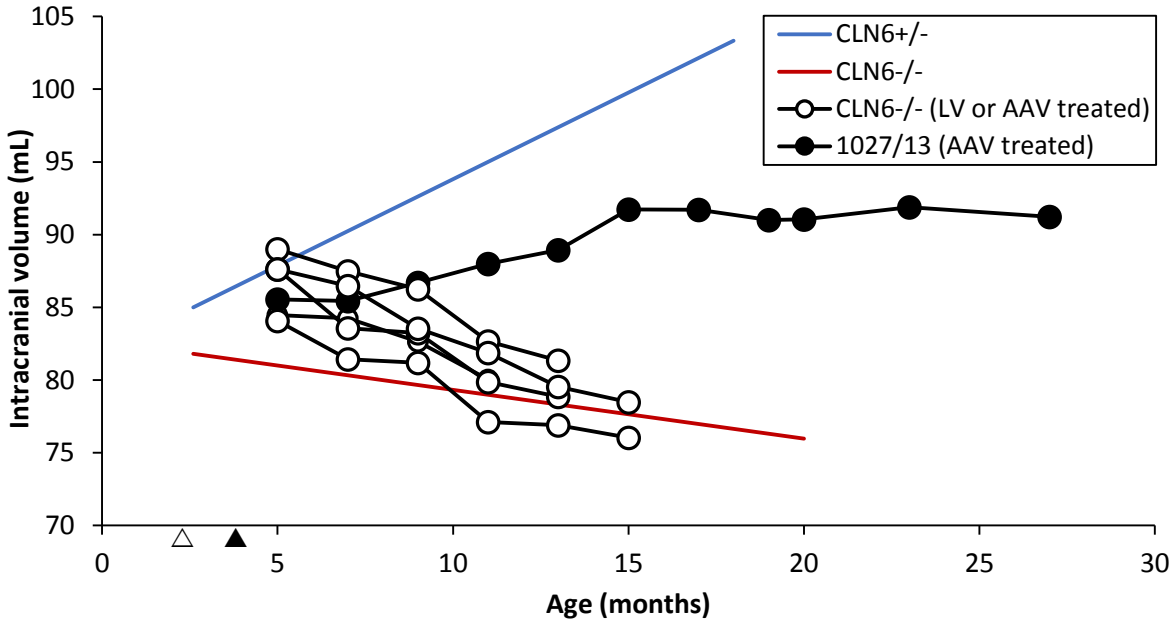

Figure 7.7 Prevention of brain atrophy in 1027/13 after AAV9-mediated *CLN6* delivery
Longitudinal changes in the intracranial volume profile of treated CLN6-/- sheep were compared with average volumetric changes observed in untreated control CLN6+/- and CLN6-/- animals in previous studies. Whilst five treated animals showed a decline in intracranial volume over time to mirror that seen in untreated CLN6 affected sheep, one AAV9-*CLN6* treated sheep maintained volume for an extended period of time. △ ▲ denote the time of treatment for LV-*CLN6* and AAV9-*CLN6* respectively.

Table 7.3 Average intracranial volume changes in treated and untreated sheep over time

Animal	Treatment	Average volume change (mL/month)
CLN6-/-	None	+ 1.19
CLN6+/-	None	- 0.34
1001/13	LV-*CLN6*	- 0.97
1002/13	LV-*CLN6*	- 1.06
1004/13	LV-*CLN6*	- 0.74
1025/13	AAV9-*CLN6*	- 1.01
1026/13	AAV9-*CLN6*	- 0.83
1027/13	AAV9-*CLN6*	+ 0.61

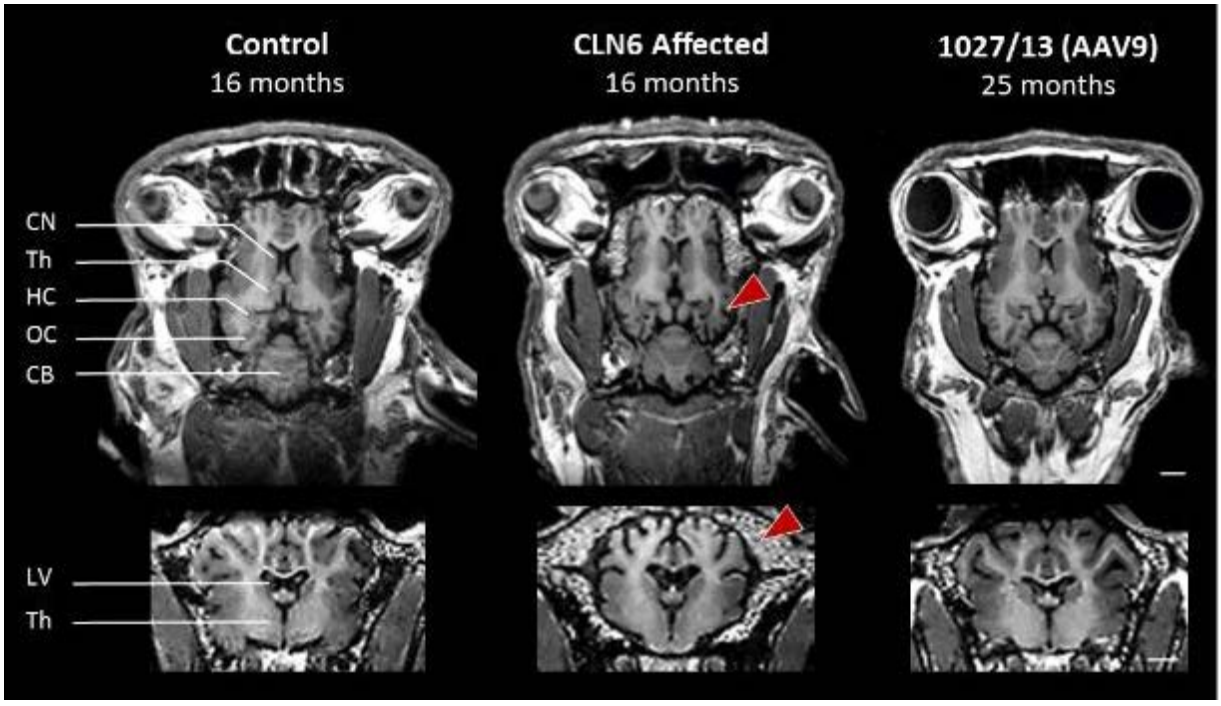

Figure 7.8 Normalisation of brain structure in 1027/13 after AAV9-mediated *CLN6* delivery

MRI sections (T1) of a 16 month unaffected control (left) and untreated CLN6 affected sheep (middle) were compared with a 25 month old CLN6 affected sheep (right) which received pre-clinical AAV9-mediated *CLN6* gene therapy. The upper horizontal slices of the midbrain are at the level of the eyes. The lower coronal view aligns with section #0800 of the Michigan State University sheep brain atlas (https://www.msu.edu/~brains/brains/sheep/index.html).

Significant brain atrophy is evident in the untreated affected sheep, particularly in the occipital cortex (upper arrow), with concomitant enlargement of the ventricles and CSF spaces and compensatory thickening of the cranial bones (lower arrow). Pre-clinical treatment with AAV9-*CLN6* prevented the stereotypical disease-associated brain atrophy and normalised the brain structure. Scale bar represents 1 cm. Abbreviations: **CB** cerebellum, **CN** caudate nucleus, **HC** hippocampus, **LV** lateral ventricle, **OC** occipital cortex, **Th** thalamus.

7.3.3 *Post mortem* analysis of CLN6 gene therapy efficacy

Sheep treated with LV and AAV-*CLN6* were euthanised for analysis of transgene expression and morphological assessment of neuropathology from 13.8 – 26.2 months of age. The two treated hemispheres were analysed individually. However, since no statistical significant differences were found, results are presented as an average of the two.

7.3.5.1 CLN6 Transgene expression

Vector-driven CLN6 expression and distribution was assessed in sagittal sections of the brain by immunohistochemical staining using the anti-sheep CLN6 antibody (Figure 7.9). Specificity has been demonstrated by the absence of staining in untreated *CLN6-/-* sheep tissue (Figure 4.15). In all treated sheep, clusters of CLN6-expressing cells were detected in multiple brain regions, particularly near the targetted parenchymal locations in the occipital and parietal cortices. There was intense, punctate staining of the periphery or the entire cell soma, and along proximal neuritic processes extending up to 150 µm. Transduced cells from both vectors were typically neuronal in morphology, although there was considerable heterogeneity with multi- and bipolar cells expressing CLN6. Some LV-transduced cells resembled protoplasmic astrocytes morphologically (Figure 7.9C).

A high density of CLN6-positive cells was evident for up to 7 mm along the extent of the cortical needle tracks in the lentiviral-treated brains. Transduced cells were detected in the brain parenchyma up to 4 mm rostro-caudal and lateral to the injection sites as revealed by DAB staining. The circular spatial pattern of the staining appeared to reflect the 2 µl bolus and withdrawal nature of the injection strategy (Figure 7.9B). Cuboidal ependymal cells at the ventricular surface were also transduced along the entire rostro-caudal extent (Figure 7.9D). In one LV-treated animal (1004/13) transduced cells extended into the rostral migratory stream leading to the main olfactory bulb (Figure 7.9E). Occasional Purkinje cerebellar cells were also CLN6-positive but little CLN6 expression was detected elsewhere either cortically or subcortically.

AAV9-mediated delivery of *CLN6* resulted in a more widespread distribution of transduced cells, predominantly with neuronal morphology. Pockets of expression, through all cortical layers and spanning up to 6 mm, were noted near the two parenchymal injection sites. Additionally sporadic transduced cells were detected in the cerebellum, hipppocampus of all AAV-treated brains and in the striatum of 1027/13. No ependymal transduction was observed. A higher density of tranduced cells was apparent in 1027/13 than in the other two AAV9-treated sheep.

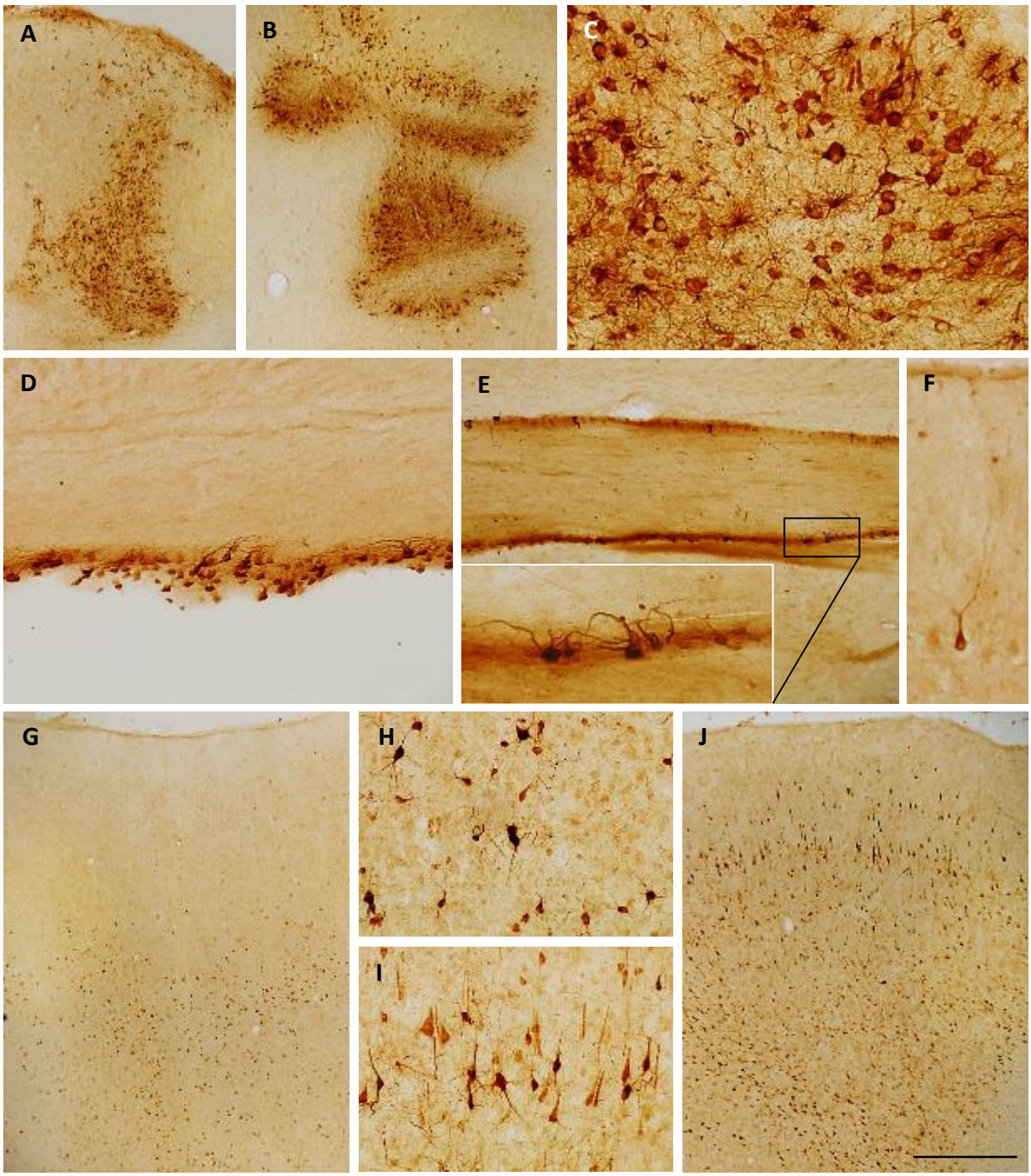

Figure 7.9 Lentiviral and AAV9-mediated *CLN6* transfer to the CLN6 affected sheep brain

DAB staining showing CLN6 positive transduced cells within the brain parenchyma of CLN6 affected sheep after lentiviral (LV) and AAV9-mediated *CLN6* transfer. Potent lentiviral infection was restricted to the brain parenchyma proximal to the occipital (**A**) and parietel (**B**, inset **C**) cortex injection sites or along the entire rostro-caudal extent of the ependyma lining the lateral ventricle (**D**). Transduced cells were mainly neuronal in morphology with punctate staining through the cytosol and along neural extensions, although CLN6 was also expressed in astroglia. Immunopositive cells were also detected along the rostral migratory stream in one LV-treated animal (**E**, inset), and sparsely in the cerebellum (**F**). AAV9 delivery of *CLN6* resulted in pockets of cortical expression (**G,** inset **H**) with greater intensity in 1027/13, the only animal to show functional and structural efficacy(**J**, inset **I**). Transduced cells were predominantly neuronal. Scale bar represents 500 μm in **A-B,G,J**; 200 μm in **E**; 100 μm in **D,F,H,I**; 50 μm in **C,E inset**.

7.3.5.2 Neurodegeneration

The impact of pre-clinical CLN6 gene therapy on neurodegeneration was analysed by measuring cortical thickness in Nissl stained sections. Measurements were made from the pia to the easily identifiable boundary between the white and grey matter in three cortical regions differentially affected by the disease. Individual hemispheres from the treated sheep brains were analysed in three groups against age-matched untreated CLN6-/- and CLN6+/- controls; three animals (1002/13, 1004/13 and 1025/13) were compared with a 13.8 month old *CLN6-/-* control, and two animals (1001/13 and 1026/13) were assessed against 16 month old controls. The final surviving sheep (1027/13) was euthanised at a much later age and its brain histology was compared with 24 month old control brains (Figure 7.10).

As expected, there was no apparent loss of neurons in the unaffected control brains, and the typical laminar distribution of cells was observed through all cortical regions. However marked atrophy was seen in all regions of the cerebral cortex of the CLN6 affected sheep brains, with associated neuronal loss and progressive thinning of the cortical layers (Figure 7.10, Table 7.4). This atrophy was most pronounced in the affected visual cortex, where the cortical thickness was reduced from 55 % at 13.8 months to 37 % of normal by 24 months of age. Concurrently, individual layer boundaries became less discernible, with clusters of cellular aggregates observed at the layer I/II boundary throughout the affected cortical mantle but not in the control brain.

Five of the treated brains, excluding 1027/13, displayed reduced definition of the cortical layers and very distinct layer I/II cellular clusters, similar to a 13.8 month old CLN6 affected brain (Figure 7.10, representative images). Cortical thickness measurements reinforced these findings (Table 7.4). Mean thicknesses for each cortical region examined (visual, motor and parieto-occipital) were not significantly different between these 5 treated sheep and an untreated 13.8 month old CLN6 affected brain. Although treated sheep measurements were significantly greater ($P < 0.019$) than an untreated 16 month old CLN6 affected sheep across all cortical regions, pre-clinical CLN6 gene transfer appeared to have no, or only a mild, neuroprotective effect in five of the six treated sheep.

In comparison, a distinct laminar structure was seen across the cortical mantle of one AAV9-CLN6 treated brain (1027/13), and no overt loss of neurons was observed although sporadic clusters were seen in the layer I/II boundary of the visual and parieto-occipital cortices. The cortical thicknesses were reduced compared with an untreated control brain, ranging from 94 % of normal thickness in the motor cortex, 76 % in the parieto-occipital cortex, to 70 % in the visual cortex. However all thicknesses were significantly greater than those of a 24 month old untreated CLN6-/- animal ($P < 0.0001$) (Table 7.4, grey box), demonstrating some correction of disease-associated atrophy and neurodegeneration by AAV9-mediated delivery of *CLN6* cDNA to the sheep CNS.

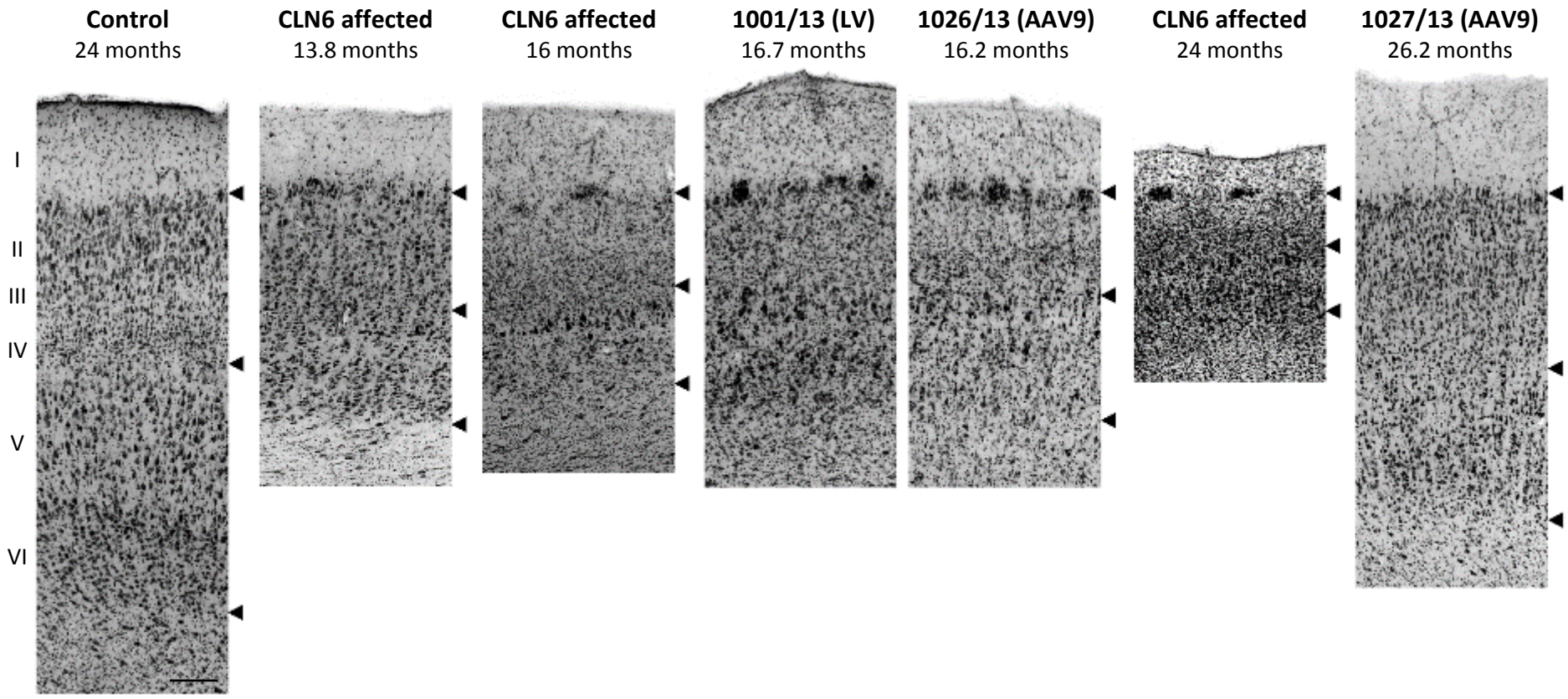

Figure 7.10 Qualitative assessment of neurodegeneration after lentiviral- and AAV9-mediated *CLN6* gene transfer to preclinical *CLN6* deficient sheep

Nissl staining demonstrates progressive atrophy of the visual cortex in untreated CLN6 affected sheep, with associated disruption of the cortical cytoarchitecture and aggregation of cells at the lamina I/II boundary. The lentiviral treated (1001/13) and AAV9 treated (1026/13) brains, which are representative of other treated sheep (1002/13, 1004/13 and 1026/13), resemble a 13.8 month old untreated CLN6 affected brain, with dense cellular clusters and thinning of the cortex. In contrast, a more normal laminar distribution of cells and no clusters are evident in one AAV9-*CLN6* treated sheep (1027/13). Although the cortical thickness of this animal was reduced compared with an untreated normal control, it was significantly greater than an untreated CLN6 deficient sheep brain of similar age ($P < 0.0001$). Upper arrows mark the layer I/II boundary, middle arrows indicate the layer IV/V boundary whilst lower arrows denote the layer VI/white matter boundary. Scale bar represents 200 µm.

Table 7.4 Quantitative assessment of neurodegeneration after viral-mediated *CLN6* gene transfer to preclinical *CLN6* deficient sheep

Cortex (Layers I-VI)	Mean thickness of layers (µm ± SEM)*										
	Affected Untreated 13.8 m	**1025/13 AAV-*CLN6*** 13.8 m	**1004/13 LV-*CLN6*** 14.1 m	**1002/13 LV-*CLN6*** 14.8 m	**Affected Untreated** 16 m	**1026/13 AAV-*CLN6*** 16.2 m	**1001/13 LV-*CLN6*** 16.7 m	**Normal Untreated** 16 m	**Affected Untreated** 24 m	**1027/13 AAV-*CLN6*** 26.2 m	**Normal Untreated** 24.6 m
Visual	912 ± 12	981 ± 18	908 ± 16	942 ± 19	802 ± 32	906 ± 19	1010 ± 23	1668 ± 56	621 ± 37	1178 ± 21	1694 ± 43
Parieto-occipital	1081 ± 14	1050 ± 17	1022 ± 14	1016 ± 16	889 ± 28	965 ± 19	1071 ± 32	1772 ± 39	614 ± 20	1335 ± 23	1765 ± 34
Motor	1539 ± 13	1584 ± 19	1549 ± 23	1583 ± 24	1485 ± 31	1553 ± 27	1564 ± 23	1795 ± 29	1109 ± 44	1702 ± 15	1806 ± 44

*25 measurements per cortical region

7.3.5.3 Glial activation

Glial activation precedes neurodegeneration during pathogenesis in the ovine CLN6 model (Chapter 4; Oswald *et al*., 2005) hence any amelioration in this response due to gene therapy was evaluated. Activation was assessed by immunohistochemistry using the astrocytic marker GFAP, and GSB4-lectin histochemistry to detect activated microglia in normal, CLN6 affected and treated brains.

7.3.5.3.1 GFAP

In the normal cerebral cortex, GFAP reactivity was predominantly detected in protoplasmic astrocytes, with short, fine highly branched processes that were distributed uniformly across all cortical layers and regions. Ramified fibrous astrocytes were detected along white matter tracts, often associated with the capillary vasculature, or at the pial surface with weakly labelled glial processes (Figure 7.11A). Conversely, a dense meshwork of hypertrophic astrocytes formed in the untreated CLN6 affected brains across the upper cortical layers (Figure 7.11A). Reactivity in the visual cortex was more pronounced compared with parieto-occipital and motor cortices.

GFAP staining in the five unsuccessfully treated brains, excluding 1027/13, was similar to that in the brain from the untreated affected control animal. A dense glial meshwork was apparent in the upper cortical layers and immunoreactive astrocytes shared the same hypertrophic morphology with thickened intensely immunostained processes (Figure 7.11A). Quantitative threshold analysis of the intensity of GFAP immunoreactivity confirmed that the gene therapy had no effect on astrocytosis in these five animals (Figure 7.11B). Immunoreactivity across the cortical layers (I-VI) of the visual cortex was 22.8 $\pm$ 1.5 % for the 16 month old untreated CLN6 affected animal and ranged from 19.2 $\pm$ 0.9 % (1025/13) to 24.9 $\pm$ 1.5 % (1002/13) for the treated sheep, indicative of a similar astrocytic response in these animals. No significant differences were observed between normal, untreated and treated CLN6 affected animals in subcortical or cerebellar regions.

In contrast, there was a significant amelioration in disease-associated astrocytic activation in the AAV9-treated animal, 1027/13. White matter astrocytes were fibrous whereas astrocytes throughout the cortical grey matter in this animal were protoplasmic, being highly branched with numerous processes. Both astroglial morphologies resembled those seen in the untreated normal control brain (Figure 7.11A). Quantitative analysis revealed that the total immunoreactivity across the grey matter layers of the visual cortex was 2.6 $\pm$ 0.5 % for 1027/13, which was not significantly different to the control brain (P = 0.017) but markedly less than that of a representative untreated CLN6 affected animal (27.8 $\pm$ 0.2 %), P < 0.0001, (Figure 7.11B).

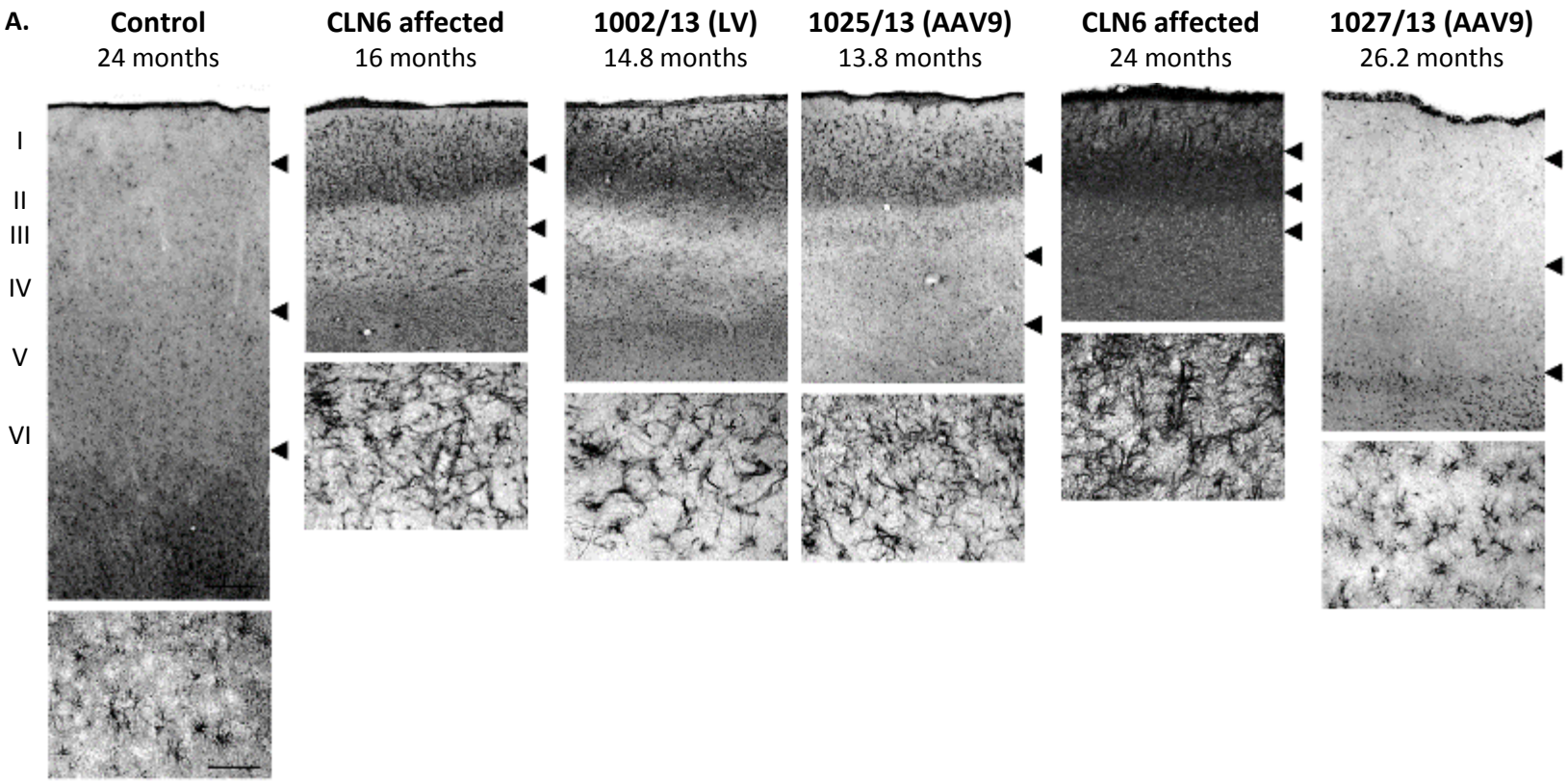

Figure 7.11 Effects of viral-mediated *CLN6* gene transfer upon astrocytosis

A. Immunostaining for GFAP reveals the extent of astrocytosis in the untreated normal control and CLN6 affected sheep visual cortices compared with those from CLN6 affected sheep treated pre-clinically with lentiviral- and AAV9-mediated *CLN6* gene transfer. Compared with scattered protoplasmic astrocytes present throughout the normal sheep brain, widespread upregulation of astrocytosis was observed in the untreated CLN6 affected brain, where intensely stained astrocytes with thickened processes and hypertrophied cell soma formed a dense glial meshwork. Hypertrophic astrocytes were also seen in the five unsuccessfully treated brains (1001/13, 1002/13, 1004/13, 1025/13 and 1026/13), forming a prominent band in the upper cortical laminae. In contrast, one AAV9-*CLN6* treated sheep (1027/13) displayed GFAP-positive protoplasmic astrocytes, similar to the untreated control, with no evidence of astroglial activation. Note images of 1002/13 and 1025/13 are representative of the other lentiviral and AAV9 treated sheep. Scale bar represents 200 µm (upper) and 50 µm (lower).

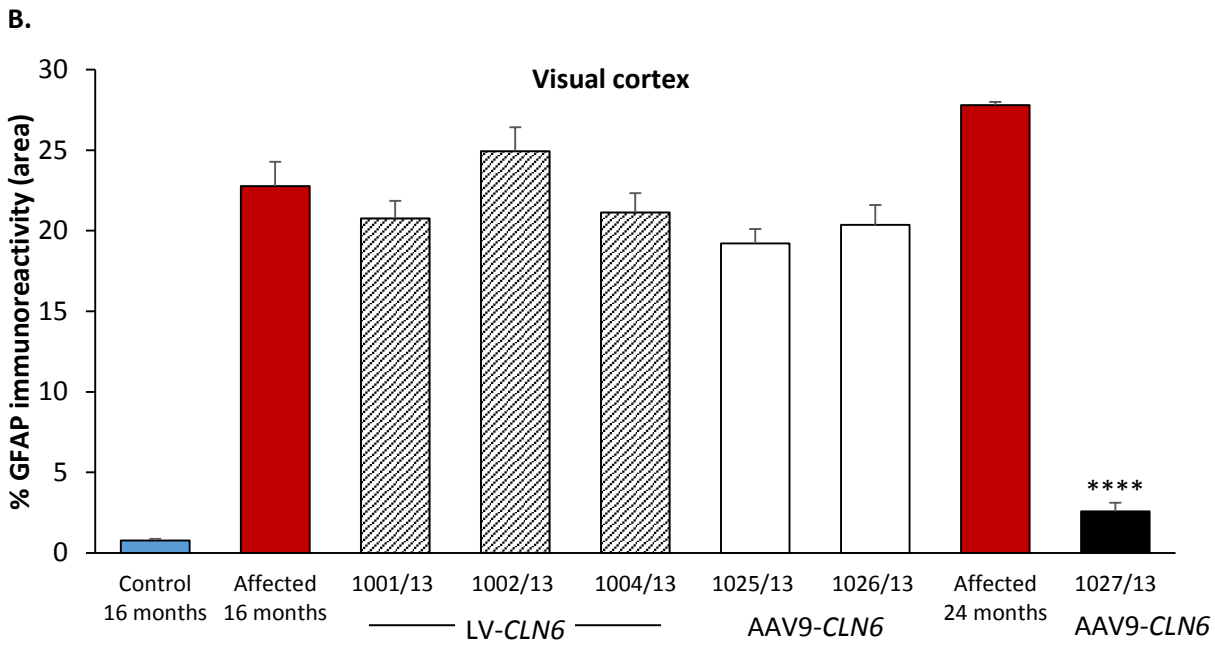

Figure 7.11 Effects of viral-mediated *CLN6* gene transfer upon astrocytosis (cont.)

B. A histogram of the mean area of immunoreactivity per field (%) obtained by thresholding image analysis of GFAP immunostaining in the visual cortex. These data confirm the progressive disease-associated astrocytosis in the CLN6 affected visual cortex, as described previously (Oswald *et al*., 2005) and show that lentiviral- (shaded) and AAV9- (white) mediated CLN6 gene transfer did not prevent astrocytic activation in five CLN6 affected sheep. However pre-clinical AAV9-*CLN6* administration significantly decreased the level of GFAP immunoreactivity in one treated animal, to levels similar to the untreated control sheep. **** $P < 0.0001$, one way ANOVA. Vertical bars represent + SEM.

7.3.5.3.2 GSB4

Little staining was seen in the normal control brain with the neuroinflammatory marker, GSB4-lectin. GSB4 reactivity was limited to meningeal and flattened elongated perivascular macrophages with no parenchymal microglia detected in any cortical layer or region (Figure 7.12). In contrast, there was a marked and progressive increase in reactivity in the CLN6 affected brain, with intense staining in the grey matter and subcortical nuclei. Clusters of GSB4 positive microglia and brain macrophages, with hypertrophic cell bodies and retracted thickened processes, merged to form two conspicuous bands within layers II-III and V-VI of the parieto-occipital and visual cortices from 13.8 months (Figure 7.12). The width of these bands decreased with age as the cortex atrophied. Ramified microglia clustered at the white and grey matter boundaries, with strong staining in all white matter tracts.

There was no indication that CLN6 gene therapy reduced microglial-related neuroinflammation in five of the treated sheep brains. Similar dense clusters of activated amoeboid microglia and hypertrophied cells, reminiscent of brain macrophages, were detected in the cortical grey matter and these were also concentrated into the two bands seen in the age-matched untreated CLN6 affected brains (Figure 7.12). The widths of the upper GSB4 positive band in three cortical regions (visual, motor and parieto-occipital) were not statistically different between the untreated and these treated brains (Table 7.5). Moreover, these five unsuccessfully treated animals had staining intensities within white matter tracts and subcortical nuclei comparable to those in the untreated CLN6 affected brain.

Conversely, examination of the 26.2 month old AAV-*CLN6* treated brain from animal 1027/13 revealed a distinct lack of GSB4-positive cells in the cortical grey matter (Figure 7.12) which was indistinguishable from the untreated control cortex (Table 7.5, grey box).

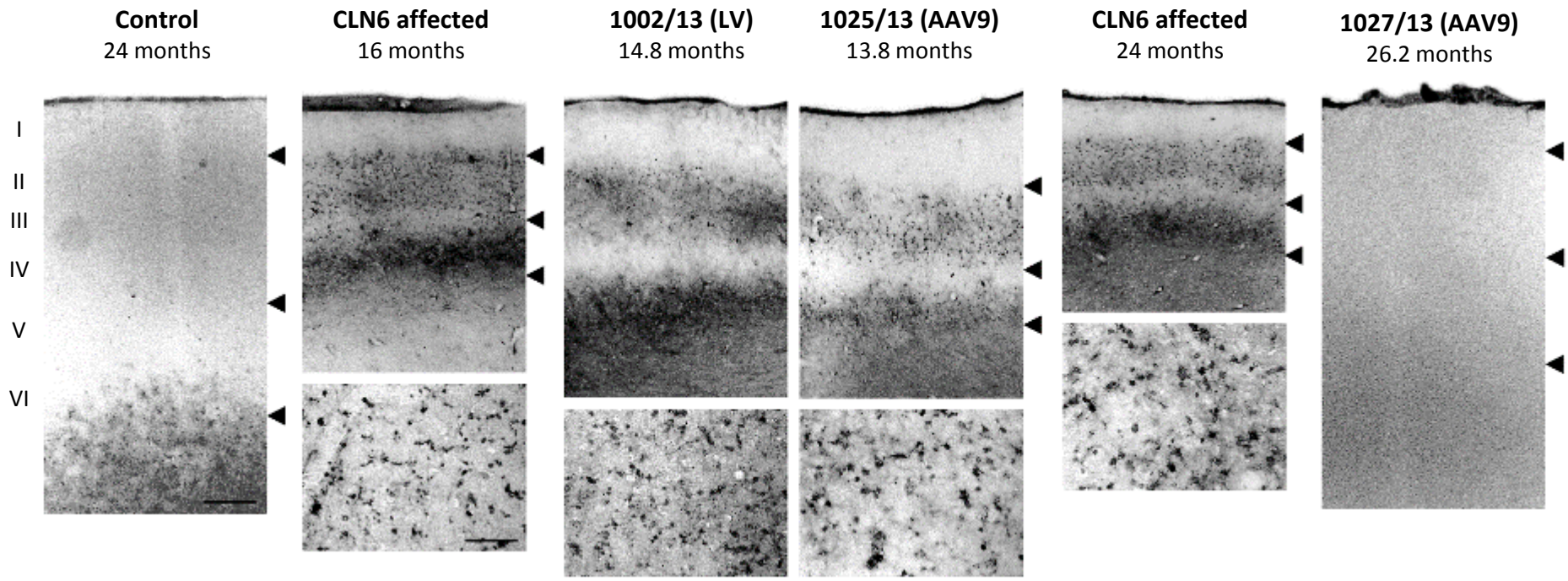

Figure 7.12 Effects of viral-mediated CLN6 gene transfer upon microglial activation

GSB4-lectin histochemistry reveals the extent of microgliosis in the untreated normal control and CLN6 affected sheep visual cortices compared with those from CLN6 affected sheep treated pre-clinically with lentiviral- and AAV9-mediated CLN6 gene transfer. No reactivity was detected in the cortical grey matter of the normal sheep brain, whereas activated microglia were apparent throughout the affected visual cortex. Staining was particularly intense in the superficial laminae II - III and in deeper laminae V – VI, where prominent bands of reactivity were seen. GSB4 positive cells were ramified and clustered together or had hypertrophied cell bodies and thickened retracted processes, typical of brain macrophages. Comparable staining morphologies, intensities and distribution were observed in five of the treated brains (1001/13, 1002/13, 1004/13, 1025/13 and 1026/13), indicating viral-mediated *CLN6* transfer had little therapeutic effect on microglial activation in these animals. In contrast, no GSB4-positive cells were detected in the cortical grey matter of one AAV9-*CLN6* treated sheep (1027/13) indicating therapeutic inhibition of disease-associated microglial activation. Note images of 1002/13 and 1025/13 are representative of the other lentiviral and AAV9 treated sheep. Scale bar represents 200 µm (upper) and 50 µm (lower).

Table 7.5 Quantitation of microglial activation in the cortex after viral-mediated *CLN6* gene transfer to preclinical *CLN6* deficient sheep

	Mean thickness of GSB-positive band width* (µm ± SEM)†										
Cortex (Layers II-III)	**Affected Untreated** 13.8 m	**1025/13 AAV-*CLN6*** 13.8 m	**1004/13 LV-*CLN6*** 14.1 m	**1002/13 LV-*CLN6*** 14.8 m	**Affected Untreated** 16 m	**1026/13 AAV-*CLN6*** 16.2 m	**1001/13 LV-*CLN6*** 16.7 m	**Normal Untreated** 16 m	**Affected Untreated** 24 m	**1027/13 ‡ AAV-*CLN6*** 26.2 m	**Normal Untreated** 24.6 m
Visual	241 ± 8	223 ± 8	215 ± 7	249 ± 8	290 ± 7	200 ± 7	269 ± 13	-	138 ± 3	-	-
Parieto-occipital	285 ± 8	297 ± 5	283 ± 3	277 ± 5	313 ± 8	267 ± 9	262 ± 7	-	151 ± 8	-	-
Motor	232 ± 9	185 ± 7	225 ± 7	249 ± 6	240 ± 12	200 ± 8	202 ± 7	-	165 ± 8	-	-

* GSB4, biotinylated α-D-galactose-specific isolectin I-B4 from *Griffonia simplicifolia* (microglial marker)

† 25 measurements per cortical region

‡ No parenchymal microglia were detected in any cortical regions for this animal

m = months

7.3.5.4 Storage body accumulation

To assess the accumulation of storage bodies in the brain, sections from treated sheep were analysed for the presence of fluorescent storage material (Figure 7.13). No storage bodies were identified in the normal sheep brain. Conversely, punctate globular storage body deposits were densely packed into the cortical neurons and glial-like cells of the untreated CLN6 deficient sheep brain, as well as the perikarya of cerebellar Purkinje cells. Consistent with this observation, similar levels of storage material were also seen throughout neocortical, subcortical and cerebellar regions of five unsuccessfully treated CLN6 deficient sheep. However the AAV9-treated brain from animal 1027/13 was phenotypically normal, with minimal storage body accumulation in all brain regions.

A brief examination of thin (5 μm) wax-embedded sections of liver and mesenteric lymph node from this animal revealed some storage body accumulation in these tissues, confirming the CLN6-/- (affected) genotype. Not all hepatocytes or lymphatic cells had storage body accumulation, suggesting that the AAV9-mediated gene therapy was capable of correcting not only the lysosomal storage defect in the brain but also some of the peripheral pathology (Figure 7.14).

Figure 7.13 Effects of viral-mediated *CLN6* gene transfer upon storage body accumulation

Fluorescent microscopy of storage material (450-490 nm excitation, 510 nm emission) in 50 μm brain sections of normal, untreated and treated CLN6 affected cerebral cortex. Storage bodies are not present in the 16 month old normal sheep brain (**A**) but cytoplasmic inclusions are present peripherally in the age-matched CLN6 affected cell soma (**B**). A comparable distribution of fluorescent storage material was observed in all of the lentiviral-treated brains at 14 -16 months of age (**C**). Two of the three AAV9-*CLN6* treated brains also showed no reduction in lysosomal storage burden at this same age (**D**). However storage body accumulation was significantly reduced in the third AAV9-treated animal (1027/13) at 26.2 months of age (**E**) when compared with the other treated brains and a 24 month old untreated CLN6 affected brain (**F**). A histogram of the mean area of fluorescence per field (%) obtained by thresholding image analyses in the visual cortices (**G**) confirms viral-mediated *CLN6* transfer had little therapeutic effect on lysosomal storage in five of the treated animals but significantly reduced the storage burden in 1027/13, **** $P < 0.0001$, one way ANOVA. Vertical bars denote ± SEM. Scale bar represents 50 μm.

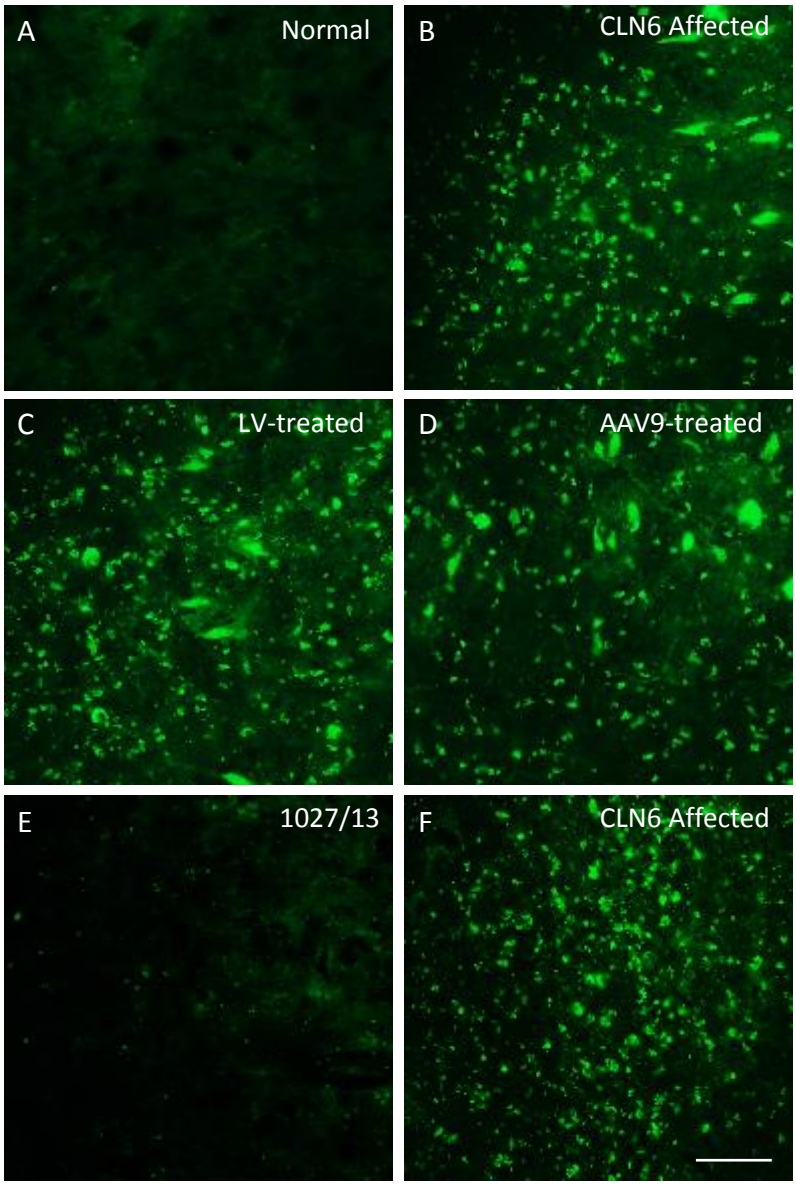
A
Normal
B
CLN6 Affected
C
LV-treated
D
AAV9-treated
E
1027/13
F
CLN6 Affected

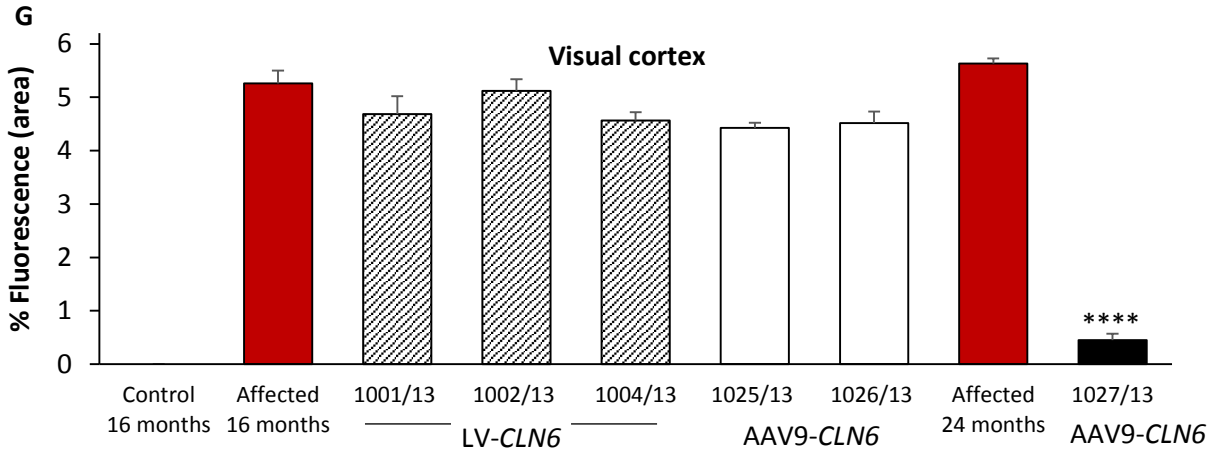
G
Visual cortex
% Fluorescence (area)
0
1
2
3
4
5
6
****
Control 16 months
Affected 16 months
1001/13
1002/13
1004/13
LV-CLN6
1025/13
1026/13
AAV9-CLN6
Affected 24 months
1027/13
AAV9-CLN6

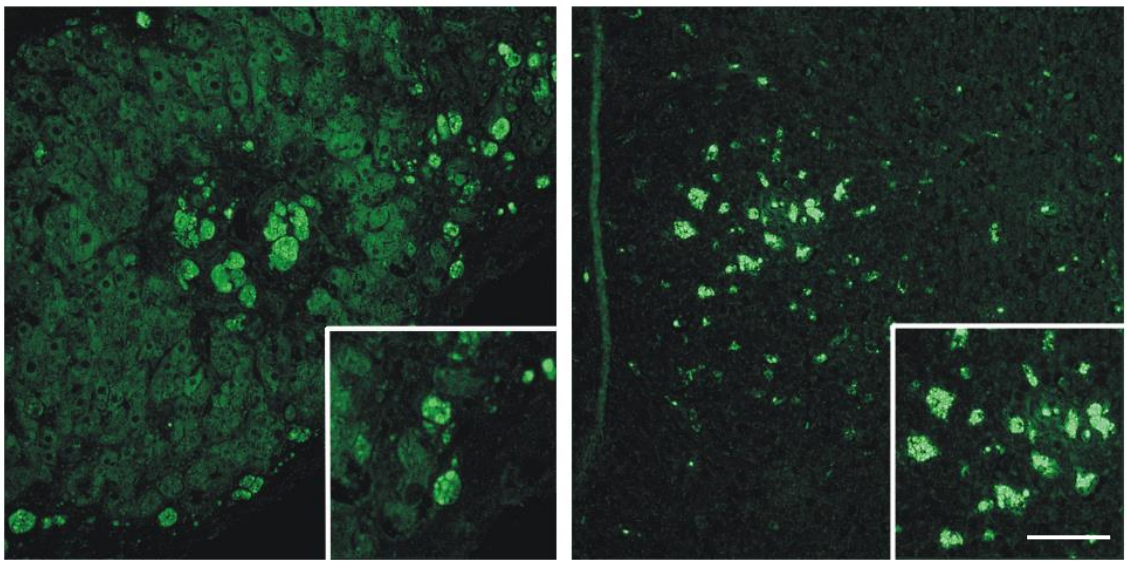

Figure 7.14 Evidence of peripheral storage body accumulation in 1027/13
Thin 5 μm sections of liver (left) and lymph node (right) from the AAV9-*CLN6* treated sheep 1027/13 confirmed the presence of storage material in some cells. Scale bar represents 50 μm, and 25 μm for insets.

7.3.5.5 Injection related pathology

For the unsuccessful treatment cohort, Nissl staining showed the site of injection in 6 out of 10 hemispheres, but without any other noticeable neuropathological changes to the brain parenchyma. However staining with the neuroinflammatory markers, GFAP for astrocytes and GSB4 for macrophages and activated microglia, showed injection-site-specific infiltration. Obvious needle tracks with localised GFAP immunoreactvity and GSB4 reactivity in the vicinity of the injection area were detected over 11 months after vector administration. These correlated with the locales of greatest transgene expression.

In contrast, no noticeable neuropathological changes were found in the successfully treated brain (1027/13), indicating the treatment in this animal did not induce damage to or an inflammatory response in the brain parenchyma.

7.3.5.6 Eye pathology

Histopathology of the retina from the successfully treated sheep (1027/13) was compared with that of untreated normal controls (Figure 7.15). Atrophy was apparent in the untreated CLN6 affected retina at 17 months, with compression of the outer retinal layers. There was degeneration of the photoreceptor layer, with particular dystrophy of the outer segments of the rods and cones, whilst the outer nucler layer was reduced to a double row of nuclei, reflecting loss of photoreceptor cell bodies. The bipolar cells of the inner nuclear layer appeared distended, as did the ganglion cells near the vitreal surface, however other retinal layers were attenuated.

Although the number of nuclei in both the inner and outer nuclear layers appeared reduced and less densely packed, the retina from 1027/13 more closely resembled the normal phenotype than that of an untreated affected sheep. There was little compression across the retina in this successfully treated animal and the inner and outer photoreceptor segments retained their uniformity. Despite some degenerative changes, the animal maintained its vision.

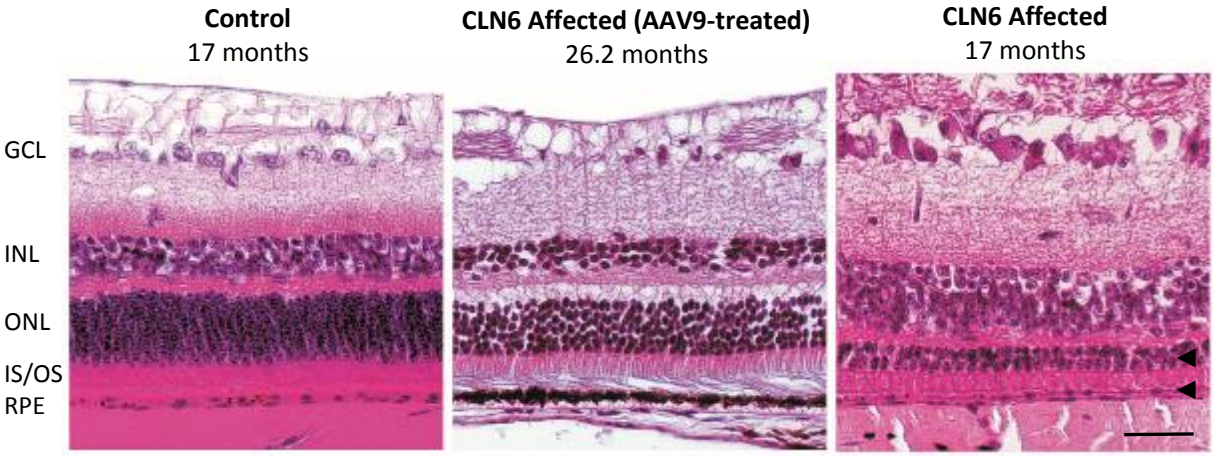

Figure 7.15 Effect of AAV9-mediated CLN6 gene therapy on the retina

Haematoxylin and eosin stained retinal sections from 17 month old CLN6 heterozygous control (left) and a CLN6 affected sheep (right), compared with that of a 26 month old CLN6 affected sheep (1027/13) which successfully responded to pre-clinical brain-directed *CLN6* gene therapy (middle). The typical ovine retinal pattern was evident for the clinically normal heterozygous animal. The age-matched CLN6 affected animal was functionally blind and histopathology shows degeneration of rod and cone photoreceptors in the affected OS and ONL (arrows). In contrast, AAV9-mediated delivery of *CLN6* to a pre-symptomatic CLN6 affected lamb largely prevented this cell loss, attenuating the retinal atrophy and protecting against the onset of blindness. Some of the different retinal layers are marked: **GCL** ganglion cell layer; **INL** inner nuclear layer; **ONL** outer nuclear (photoreceptor cell body) layer; **IS** inner segment; **OS** outer segment; **RPE** retinal pigment epithelium. Scale bar represents 25 µm.

7.4 Discussion

Some forms of NCL present a greater therapeutic challenge than others. They result from defective, intracellular proteins (*e.g.* CLN3, CLN6, CLN7, CLN8) that are not secreted and thus cannot benefit from extracellular cross-correction. There is suggestion that some of these proteins may regulate the secretion of other factors allowing cross-correction to still occur (Barry, 2011; Sondhi *et al*., 2014). The present study sought to test the impact of lentiviral (LV) and AAV9-mediated gene therapy in an ovine model of CLN6. Pre-clinical CNS administation of viral vectors expressing the ovine *CLN6* cDNA prevented the CLN6 phenotype in one AAV9-treated animal, whilst the other five developed stereotypical disease. In the successfully treated animal, inhibition of the NCL neurobehavioural dysfunction and normalisation of brain structure was prolonged, lasting longer than 2 years. This is the first report of successful correction of neurobehavioural dysfunction and the pathologic phenotype in NCL caused by a defective CLN6 membrane protein. Importantly, NCL disease hallmarks such as neurodegeneration, glial activation and storage pathology were significantly attenuated and no neurotoxic or inflammatory responses associated with AAV9-driven *CLN6* expression were seen.

7.4.1 Phenotypic assessment of *CLN6* gene transfer

On the basis of clinical disease symptoms and *in vivo* biomarkers of therapeutic efficacy, the six treated sheep could be split into two groups; five sheep showed a three month delay in clinical presentation but ultimately succumbed to the disease, whilst one AAV9-*CLN6* treated animal (1027/13) displayed phenotypic correction, with a significantly improved quality of life and survival. In these experiments, untreated (heterozygous and CLN6 affected) and treated cohorts were assessed monthly by neurological examination and maze testing. From 7 months, a clear distinction could be made between CLN6 affected and heterozygous sheep, who were phenotypically normal. As anticipated based on the literature (Mayhew et al., 1985; Jolly et al., 1989) the diseased sheep began to show behavioural symptoms on examination and shortly thereafter in maze testing. They were functionally blind from 12 - 13 months of age and progressively declined as an overt neurological phenotype, with reduced mentation, disorientation, akinesia and hindlimb ataxia, became more established. Five of the treated sheep showed a similar decline, albeit delayed. They were clinically normal until 12 - 13 months, then began to show a stereotypical neurobehavioral phenotype. Functional blindness was established by 14 $\pm$ 0.8 months, yet onset ranged from 12.6 months in an AAV9-treated individual to 15.6 months for a lentiviral-treated sheep. The adverse complications related to copper toxicity and indoor housing (see Section 8.2.4) prompted the premature euthanasia of three of the treated sheep prior to their reaching the akinesic disease state, however this was after it became apparent that therapeutic efficacy had not been fully realised.

In contrast, one AAV9-treated animal (1027/13) displayed remarkable functional and structural correction throughout the study. It was clinically indistinguishable from age-matched heterozygotes on neurological examination, in the open field and during maze-testing. It was alert and responsive to visual, auditory and tactile stimuli, including mirrors, environmental enrichment toys, claps, bleats, wind and loud noises, and developed a strong social attachment with animal care personnel and similarly treated Borderdale CLN5 cohorts. Despite ophthalmoscopic and ERG studies indicating some degenerative changes in the retina, there was no clinical evidence of visual deterioration. Neuro-opthalmic reflexes were intact, including the menace response which was suggestive of a functioning visual cortex.

CNS neuroimaging confirmed the structural functionality of the brain of 1027/13. MR imaging of the sheep brain is becoming more common as ovine models gain popularity in translational neuroscientific research (Amorim *et al*., 2015; Ella & Keller, 2015; Lee *et al*., 2015; Nitzsche *et al*., 2015; Sawiak *et al*., 2015). An MRI performed on 1027/13 at 25 months of age showed none of the cortical atrophy or ventricular enlargement associated with ovine NCL (Figure 7.8). Only a single MRI session occurred and voxel-based morphometry was not performed however the data could later be compared with that collected during a longitudinal MRI study in CLN6 South Hampshire sheep at end-stage disease (Sawiak *et al*., 2015). Intracranial brain volumes were calculated through the study from CT images. These demonstrated an initial steady increase for 1027/13 to plateau during adulthood at 91 mL. This equates to approximately 82 % of normal adult volume (Figure 7.7). CLN6 affected sheep brains develop normally for the first 4 months of life, offering an ideal temporal window for optimum therapeutic efficacy, before commencing regionally specific neurodegeneration with concomitant cortical atrophy (Chapter 4, Oswald *et al*., 2005). Typically by 18 months of age, normal and affected intracranial volumes differ by at least 30 mL, with normal volumes exceeding 100 mL and CLN6 affected volumes under 80 mL. Interestingly in this study, all treated sheep had intracranial volumes at baseline (5 months of age) above that expected for age-matched untreated CLN6 deficient animals. It may be that the treatment initially allowed normal growth of the brain but, as efficacy wore off from 5 months of age, volume loss and subsequent atrophic changes became evident in the five unsuccessfully treated sheep.

7.4.2 Histological impact of *CLN6* gene transfer

The accumulation of fluorescent storage material within the lysosome, coupled with neuron loss and gliosis, characterises the NCLs, including those in sheep (Oswald *et al*., 2005; Mole *et al*., 2011). To show the definitive impact of treatment on phenotype, these *post mortem* neuropathological parameters were used as a measure of therapeutic efficacy. The five unsuccessfully treated sheep displayed little reduction in the pathological hallmarks of NCL previously reported for untreated

affected controls (Jolly *et al*., 1989; Oswald *et al*., 2001, 2005, 2008). Conversely, the AAV9-mediated expression of *CLN6* in one sheep (1027/13) successfully resulted in widespread neuropathological correction.

As described above, sheep received treatment at 2.7 (LV) or 3.7 (AAV9) months of age – a pre-clinical window of time deemed likely to be efficacious. Prenatal lysosomal storage has been reported in South Hampshire sheep (Jolly *et al*., 1989). Storage bodies are generalised, yet sparse, through the brain in the first few months of life, but they progressively accumulate (Chapter 4, Oswald *et al*., 2005). Reactive astrocytosis has been described in the CLN6 affected brain as early as 40 days before birth, whilst microglial activation is apparent at birth (Kay *et al*., 2006). Both precede neurodegeneration, which becomes regionally established in the early post-natal period (Chapter 4, Oswald *et al*., 2005), and the onset of clinical symptoms from 7 - 13 months (this study, Mayhew *et al*., 1985). Despite treatment early in the pathogenic cascade, the level of storage burden was not reduced for five out of six treated sheep. Nissl staining revealed densely packed cellular aggregates in the upper neocortex and a reduction in cortical thicknesses for these five treated animals (Figure 7.10, Table 7.4). Comparable patterns of astrocytosis and gliosis were detected (Figure 7.11- Figure 7.12), with widepread staining of brain macrophages, representative of end-stage microglial activation (Streit, 1990). Collectively these five animals displayed findings similar to those of affected controls, indicating that *CLN6* gene transfer did not impact favourably on them for any extended period.

However pre-clinical AAV9-*CLN6* administration had a significant neuroprotective effect in one sheep, demonstrating significant neuropathological correction for NCL caused by a defective CLN6 membrane protein for the first time. *Post mortem* analysis corroborated the CT volumetric data with the brain weight of 1027/13 at 26.2 months of age about 80 % of normal. Preliminary neuropathological analysis revealed a degree of cortical thinning in the brain of 1027/13, ranging from 94 % of normal thickness in the motor cortex to 70 % in the visual cortex. By comparison, cortical thicknesses in the best matched untreated CLN6 affected brain were 65 to 55 % of normal for the same regions at 24 months (Table 7.4). The laminar distribution of neurons was retained across the cortical mantle in 1027/13 and very few cellular aggregates were evident. There was a distinct lack of glial activation, even at 26.2 months of age, in contrast to affected animals in which astrocytosis and gliosis were profound well before this age (Figure 7.11 - Figure 7.12). Similarly minimal storage body accumulation was seen in the brain, however there was evidence of lysosomal storage in some peripheral tissues, albeit significantly reduced (Figure 7.13). This suggests that either some, as yet unknown, form of cross-cell correction has occurred or there has been transduction of a significant proportion of cells. However when CLN6 expression within the treated brains was examined by immunohistochemistry with a sheep-specific CLN6 polyclonal antibody, only

a slight greater transduction of cells in 1027/13 was noted compared with the unsuccessfully treated animals (Figure 7.9).

There was strong evidence for transduction of the ependyma lining the lateral ventricles in the LV-treated brains, similar to that documented in sheep with the reporter green fluorescent protein (Linterman *et al*., 2011), and even in the rostral migratory stream of one animal (Figure 7.9) but apparently this was insufficient to provide therapeutic efficacy. Despite ependymal transduction in other animal models after AAV-mediated gene delivery to the ventricular system (Liu *et al*., 2005b; Haurigot *et al*., 2013; Katz *et al*., 2015; Ribera *et al*., 2015), this was not apparent in the AAV-treated brains in this study. Why therapeutic efficacy was seen in 1027/13 and not in the other treated sheep is still to be elucidated. Whilst immunohistochemistry suggested the level of CLN6 expression in the brain of 1027/13 was relatively limited, a biodistribution study in CNS and peripheral tissues will follow with detection at the mRNA level as this method may prove to be above the threshold for detection by immunohistochemical means.

Studies in sheep and mice models of CLN6 and CLN3 respectively suggest these proteins may regulate the secretion of other factors allowing some level of cross-correction to occur (Barry, 2011; Sondhi *et al*., 2014). As described above, studies by Barry (2011) determined that the CLN6 defect is cell extrinsic and that the presence of unaffected normal cells had a corrective effect on neighbouring affected cells in chimeric sheep. Like CLN6, the *CLN3* gene product is a hydrophobic, intracellular protein that is not secreted yet neonatal administration of an AAV serotype rh.10 vector expressing the human *CLN3* cDNA to a *Cln3*$^{\Delta ex7/8}$ knock-in mouse model of juvenile NCL resulted in partial correction of phenotype (Sondhi *et al*., 2014). Treated mice demonstrated safe, long-term expression of the *CLN3* transgene with reduced storage material burden, decreased gliosis and some attentuation of neuronal loss after targeted injections into the hippocampus, striatum and cerebellum. Taken together with the results from the current study, it is envisaged that for NCL subtypes with defective intracellular proteins, correction of some cells can have a neuroprotective effect on adjacent uncorrected cells and this may be sufficient to correct phenotype.

A particularly interesting observation from this study was the retention of eyesight in 1027/13. The retina was not normal (Figure 7.15) yet retained long-term functionality. This contrasted the late-onset loss of vision in similarly treated CLN5 deficient animals (Chapter 6). Based on CSF circulation, it would be anticipiated that only the ganglion cells of the retina should take up either circulating vector at administration or some neurotrophic factor secreted into the CSF by corrected cells. This is due to their close proximity to the meninges ensheathing the optic nerve. CLN6 expression in the retina has not yet been performed but will provide information on the retinal transduction profile.

A number of factors still need to be determined, which may extend the success of future treatments to all animals. Firstly, the pathogenicity and cell toxicity of AAV9-*CLN6* delivery has not been explored fully. There appears to be a mild change in density of Nissl stained cells in cortical regions of the successfully treated brain (1027/13) although quantification of the number of neurons and interneurons in specific brain regions will be required to confirm this. However Nissl staining revealed no alteration in tissue near or at the injection sites in the occipital and parietal cortices and negligible injection-related neuroinflammation was observed. This contrasted with the results from the unsuccessfully treated sheep, which had obvious needle tracks with localised GFAP immunoreactvity and GSB4 reactivity in the vicinity of the injection area over 11 months after vector administration. Similarly, whilst the immunogenicity of AAV vectors is low, there can be a high prevalence of neutralising antibodies (NAbs) against various AAV serotypes in human (Calcedo *et al*., 2009; Boutin *et al*., 2010) and sheep (Rapti *et al*., 2012; Tellez *et al*., 2013) populations. Studies have shown that anti-AAV NAbs do not appear to affect focal brain parenchymal delivery of AAV vectors (Kaplitt *et al*., 2007), but transduction efficiency after delivery to the CSF is partially affected (Gray *et al*., 2011; Haurigot *et al*., 2013). Analysis of collected serum samples for any viral capsid-driven or CLN6-driven host immune response may be helpful in determining the potential to improve therapeutic outcome.

7.5 Conclusion

Under field conditions, CLN6 affected sheep are not expected to live beyond two years of age. Here data are presented that shows pre-clinical administration of an AAV9 viral vector encoding the therapeutic *CLN6* transgene to CLN6 deficient sheep reverted the pathologic phenotype and prevented disease onset and behavioural dysfunction for over 26 months in one out of six treated animals. The longevity of the AAV9-mediated transgene expression was encouraging, given that CLN6 NCL results from an intrinsic transmembrane protein deficiency. Some questions remain as to how this approach can be improved upon to correct all animals under treatment, paving the way for translation to therapy in the human clinic.

Chapter 8

Summary and General Discussion

8.1 Thesis summary and significance

8.1.1 Comparative neuropathology in CLN5 and CLN6 ovine forms of NCL

The neuronal ceroid lipofuscinoses (NCLs; Batten disease) are a group of fatal neurodegenerative lysosomal storage diseases which are caused by mutations in up to 13 distinctly different genes. They are commonly grouped together by the near-ubiquitous accumulation of lysosome-derived storage bodies and regionally specific neurodegeneration and neuroinflammation, with resultant severe brain atrophy (Mole *et al*., 2011). Animal models of most of the human NCL subtypes exist (Shacka, 2012; Bond *et al*., 2013) and a CLN6 form of NCL in New Zealand South Hampshire sheep has been particularly informative in identifying some of the pathogenic aspects that underlie this group of diseases (see Section 1.5). Findings in sheep have subsequently been extended to other animal models and human patients. However, despite their well-defined pathophysiology and the extensive research on NCL disease mechanisms, no effective therapies for the NCLs exist.

Gene therapy represents a promising treatment strategy for the monogenic NCLs. With their large complex human-like gyrencephalic brain and recapitulation of the key molecular, pathological and clinical features of the human NCL phenotype, sheep with naturally occurring NCLs are ideal pre-clinical subjects for gene therapy studies. Thus the first aim of the studies described in this thesis was to elucidate the timeline of progression of pathological changes within the ovine NCL brain over the two year disease course and to define windows in which to best attempt therapeutic intervention. The ovine CLN6 disease pathology has been well characterised previously (Oswald *et al*., 2005; Kay *et al*., 2006). Chapter 4 describes a comparative neuropathological study of the ovine CLN5 and CLN6 disease models and provides the first detailed description of progressive pathological changes in the CLN5 affected sheep. Importantly, the two forms in sheep represent the two distinct NCL protein subclasses: CLN5 being a soluble lysosomal glycoprotein whilst CLN6 is predicted to be a transmembrane protein. The disease-causing mutation in ovine *CLN5* is a single base substitution at a consensus splice site, which excises exon 3 and results in a truncated putative protein (Frugier *et al*., 2008). In contrast, a 402bp deletion and 1bp insertion in *CLN6* which leads to the deletion of the ATG start codon and the whole of exon 1 is predicted to cause the ovine CLN6 form in South Hampshire sheep (Mohd Ismail, 2014). Given the large differences between the mutated CLN5 and CLN6 gene products and their subcellular localisation, one might expect quite different pathological and/or clinical phenotypes in the two disease models.

This was not the case. The pathogenic cascades were remarkably similar for CLN5 and CLN6 affected sheep (Table 8.1, Table 8.2). Focal astrocytosis and activation of microglia, the resident macrophages of the CNS, was evident from birth or in early perinatal stages in both models (this study; Oswald *et al*., 2005; Kay *et al*., 2006). Despite precocious glial activation being the earliest described manifestation of the disease, it is still unclear what causes the initial gliosis in NCL. Regardless, targeted suppression of neuroinflammation will likely be an important adjunct to any therapy (see Section 8.3.4).

Markedly regional neuron loss and cerebral atrophy became detectable at 4 and 6 months of age for the CLN5 and CLN6 affected sheep respectively and followed the same pattern as the glial activation. Layer II-III neurons were specific and early targets of the disease (Figure 4.4). Cortical atrophy commenced and progressed faster in the primary visual and parieto-occipital regions than in other cortices and the development of pathology in subcortical structures was relatively delayed whilst the affected cerebellum was spared (Figure 4.5).

The specific lysosomal storage of subunit c of mitochondrial ATP synthase was first identified in the CLN6 ovine model (Palmer *et al*., 1989; Fearnley *et al*., 1990) and subsequently in the majority of human forms of NCL (Palmer, 2015). Ovine CLN5 is also a subunit c storage disease (Jolly *et al*., 2002; Frugier *et al*., 2008) yet, unlike the selective regionality of neurodegeneration and neuroinflammation, fluorescent storage bodies were uniformly distributed throughout the diseased brains of both genotypes in the current study (Figure 4.13) and many neurons accumulated large amounts of storage material with no overt signs of degeneration. Thus despite its ubiquity, a causative role for storage body accumulation in neurodegeneration in ovine NCL is not plausible.

Overt clinical signs of disease were not seen until at least 10 months of age in either ovine NCL model, well after neuropathology was established. The earlier onset of both neuroinflammation and neurodegeneration in the CLN5 model correlated with the earlier onset of clinical symptoms in the CLN5 sheep. The predominant involvement of the primary visual cortex in both disease models also is in agreement with the first overt clinical symptom, being visual failure in ovine NCL. The delayed motor and thalamic involvement in pathogenesis is likely to be responsible for the later presentation of manifest seizures and motor dexterity issues in the disease course. Interestingly, motor, proprioceptive and cognitive dysfunction are more pronounced in the CLN5 deficient sheep than in their CLN6 affected counterparts and this is reflected by the greater atrophy in the CLN5 frontal lobe (Figure 4.5).

Concurrent with the neuronal loss was evidence of continued endogenous neurogenesis in the subventricular zone of both ovine NCL models (Figure 4.14). This suggests a regenerative response by the diseased brain early in the pathogenic cascade. It also represents a target site for therapeutic

correction of neural progenitor cells which could replace affected cells lost in neurodegeneration. Thus therapeutic interventions, such as gene transfer technologies, would likely be most efficacious if delivered early in the disease, before irreparable damage was done (see Section 8.2.1).

Systematic neuropathological analyses, such as used in the current study, are simply not feasible in humans. Using established techniques, a spatio-temporal survey of the whole sheep brain is possible. Multiple comparisons can be made between brain regions within the same sagittal section, on adjacent sections or between genotypes. These are highly informative for the human disease, in which small non-specific *post mortem* brain biopsy samples are often all that is available. Additionally, a large number of unstained sections from control and CLN5 and CLN6 deficient brains have been catalogued and are available for future investigations.

Table 8.1 Summary of clinical and neuropathological changes in CLN5 Borderdale sheep

Age *	Mean brain weight (g) †	Neuropathological findings					Clinical phenotype
		Neuronal loss	Astrocytosis	Microgliosis	Storage	Neurogenesis	
E70	~3.5 Smooth surface		ND	ND	ND	ND	
E90	~14 g		ND	ND	ND	ND	
E150 Birth	~55 g (55%)	Normal except in V1	Foci in laminae II/ III of V1 and POC	Foci in laminae II/ III of V1 and POC	Sparse, only neuronal cells	SVZ, HC and CB	Normal
4 m	~ 82 g (89%) Peak brain weight	V1, POC, S1	Laminae II/ III of V1 and POC	Laminae II/ III of V1 and POC	ND	ND	Normal
6 m	~80 g (89%) Cortical atrophy first evident	V1, POC, S1	Laminae II/ III of V1, POC and M1	Laminae II/ III of V1, POC and M1	Widespread, mainly neuronal	Prominent in SVZ, cortical laminae II/III	**Preclinical:** Low head carriage Propensity to baulk, crouch, stumble
9 m	~78 g (85%)	V1, POC, S1, FA	Laminae II/ III of V1, POC and M1	Laminae II/ III of V1, POC and M1	ND	ND	
10- 11 m							**Blind:** Visual deficits, head tilt/stargazing Decreased or lost menace response, depressed PLR, dazzle response and ERG Reduced herding
12 m	~78 g (81%)	V1, POC, S1, FA, Ent	Spread to laminae VI-VI, BG and Th	Spread to laminae VI-VI, BG and Th	Neuronal and non-neuronal	SVZ, cortical laminae II/III	
14 m							**Overt/Neurological:** Motor, cognitive and proprioceptive deficits, including ataxia, wide stance, reduced mentation, decreased acoustic startle
15 m	~76 g	V1, POC, S1, FA, Ent, M1	Widespread through cortex, less in subcortex	Widespread through cortex, less in subcortex	ND	ND	**Advanced:** Progressive disease +/- induced tetanic seizures Inefficient eating/drinking, compulsive circling
18 m	~71 g (73%)	Few cortical neurons remain	Widespread through brain	Widespread through brain	Mostly non-neuronal/ brain macrophages	Prominent in SVZ, cortical laminae II/III	
24 m	~62 g (58%) Very atrophied but CB normal	Few cortical neurons remain	Widespread through brain	Widespread through brain	Widespread through brain	Much less prominent	**Terminal:** Progressive disease +/- spontaneous seizures

Table 8.2 Summary of clinical and neuropathological changes in CLN6 South Hampshire sheep

Age *	Mean brain weight (g) †	Neuropathological findings					Clinical phenotype
		Neuronal loss	Astrocytosis	Microgliosis	Storage	Neurogenesis	
E60 ‡	~2 g (2%) Smooth surface				Sparse		
E80 ‡	~8 g				Sparse		
E100 ‡	~20 g Gyri evident				Sparse		
E110 ‡	~30 g		Cortical WM		Sparse		
E130 ‡	~45 g		Foci in laminae II/ III of V1 and POC		Sparse		
E150 Birth ‡	~50 g (50%)		Foci in laminae II/ III of V1	Foci in laminae II/ III of V1	Sparse, only neuronal cells	SVZ, HC and CB	Normal
12 d ‡	~60 g		Laminae II/ III of V1, S1 and POC	Laminae II/ III of V1, S1 and POC	Sparse, only neuronal cells	ND	Normal
2 m	~70 g (95%)	V1, POC	Reduced	Reduced	ND	ND	Normal
4 m	~ 75 g (81%) Peak brain weight	V1, POC	Laminae II/ III of V1 and POC	Laminae II/ III of V1 and POC	ND	ND	Normal
6 m	~70 g (79%) Cortical atrophy first evident	V1, POC	Laminae II/ III of V1 and POC	Laminae II/ III of V1 and POC	Widespread, mainly neuronal	Prominent in SVZ, cortical laminae II/III	Normal
7m							**Preclinical:** Low head carriage Propensity to baulk, crouch, stumble
9 m	~68 g (74%)	V1, POC, S1	Laminae II/ III of V1, POC	Laminae II/ III of V1, POC	ND	ND	
12 m	~68 g (69%)	V1, POC, S1, Ent, FA	Spread to laminae VI-VI, M1, BG and Th	Spread to laminae VI-VI, M1, BG and Th	Neuronal and non-neuronal	Prominent in SVZ, cortical laminae II/III	**Blind:** Visual deficits, head tilt/stargazing Decreased or lost menace response, depressed PLR, dazzle response and ERG Reduced herding

Age *	Mean brain weight (g) †	Neuropathological findings					Clinical phenotype
		Neuronal loss	Astrocytosis	Microgliosis	Storage	Neurogenesis	
15 m							**Overt/Neurological:** Motor, cognitive and proprioceptive deficits, including ataxia, wide stance, reduced mentation, decreased acoustic startle Some spontaneous facial tics
18 m	~66 g (67%) Very atrophied but CB normal	V1, POC, S1, FA, Ent, M1	Widespread through cortex, less in subcortex	Widespread through cortex, less in subcortex	Mostly non-neuronal/ brain macrophages	ND	**Advanced:** Progressive disease +/- induced tetanic seizures Inefficient eating/drinking, compulsive circling Extinct ERG waveforms in most
24 m	~58 g (54%)	Few cortical neurons remain	Widespread through brain	Widespread through brain	Widespread through brain	Prominent in SVZ, cortical laminae II/III	**Terminal:** Progressive disease +/- spontaneous seizures

Figure legend for Tables 8.1 and 8.2:

* Age in embryonic day (E), days (d) or months (m)

† Percentage mean brain weight of normal

‡ Results from previous studies (Oswald *et al.,* 2005; Kay *et al.,* 2006)

Abbreviations: **BG** basal ganglia; **CB** cerebellum; **Ent** entorhinal cortex; **ERG** electroretinography; **FA** frontal association cortex; **HC** hippocampus; **m** months; **M1** primary motor cortex; **ND** not determined; **POC** parieto-occipital cortex; **PLR** pupillary light reflex; **S1** somatosensory cortex; **SVZ** subventricular zone; **Th** thalamus; **V1** primary visual cortex; **WM** white matter

8.1.2 Gene transfer to the sheep brain

In an initial proof of concept study, the efficacy and tropism of adeno-associated virus serotype 9 (AAV9) as a gene transfer vector was tested in the normal sheep brain (Chapter 5). This vector has successfully mediated gene delivery to non-dividing or terminally differentiated post-mitotic cells in many animal models of LSDs, with broad long-term gene expression and minimal associated inflammation or toxicity (Liu *et al*., 2005a; Sondhi *et al*., 2005, 2012; Fu *et al*., 2011; Haurigot *et al*., 2013). Only the use of AAV serotype 1 has been documented in the sheep brain in gene knockdown experiments (Dufourny *et al*., 2008). In the current study, naïve, juvenile sheep received injections of AAV9 expressing a reporter gene (green fluorescent protein; GFP) into either the brain parenchyma or the lateral cerebral ventricles and GFP expression through the CNS was analysed a month later. Stable neurotropic expression of the transgene was achieved by both delivery routes (Figure 5.5). However the spread was better after intracerebroventricular delivery (Figure 5.1- Figure 5.2), and there was no evidence of vector or procedural neuroinflammation or toxicity (Figure 5.6), indicating that this simpler route may be the one of greater translational benefit.

Chapter 6 and Chapter 7 describe successful viral-mediated gene therapy in pre-clinical CLN5 and CLN6 affected sheep respectively. As described above, no specific treatment is available for NCL. Preclinical experiments in murine models of CLN1, CLN2 and CLN3 NCL have shown that gene therapy can significantly slow disease progression (Griffey *et al*., 2004, 2006; Hackett *et al*., 2005; Sondhi *et al*., 2005, 2007, 2012, 2014; Passini *et al*., 2006) and safety and efficacy clinical trials are underway for the CLN2 form (see Section 1.6.4). The current study provides the first evidence of therapeutic and functional efficacy in large animal models of NCL. CLN5 deficient sheep, treated pre-symptomatically with a single administration of brain-directed gene therapy, showed protection from stereotypical disease onset and progression. Two viral vector platforms were tested: lentiviruses which have previously proven efficacious in sheep (Linterman *et al*., 2010) and AAV9 which showed promise in Chapter 5. Surprisingly, both vectors afforded similar therapeutic benefit. The only disease manifestation seen in the treated sheep was a delayed onset visual deficit. Monthly clinical assessment and maze testing revealed retention of neurological and cognitive function (Figure 6.3-Figure 6.5), whilst CNS imaging demonstrated sustained normalisation of brain structure and intracranial volume (Figure 6.7– Figure 6.8). Quality of life was profoundly improved for the treated sheep and this was evident in their extended lifespan. In fact, one AAV9-treated sheep is still alive at 32 months of age in May 2016, well exceeding the typical humane endpoint for untreated CLN5 deficient sheep of 22 months of age. CLN5 transgene expression and neuropathological attenuation of the lysosomal storage pathology, glial activation, and neuronal loss will be examined in the *post mortem* treated brains but the *in vivo* results look particularly encouraging for clinical translation of *CLN5* gene therapy.

The efficacy of *CLN5* gene transfer was not entirely unforeseen, given that the CLN5 disease results from a soluble lysosomal protein deficiency and thus was expected to be amenable to 'cross-correction' if sufficient cells were corrected. However the fact that one CLN6 deficient animal treated pre-clinically with AAV9-*CLN6* (1027/13) also demonstrated phenotypic correction was a surprising finding. As CLN6 is a membrane-bound protein, gene therapy approaches for this form were deemed not likely to benefit from 'cross-correction' (Sands & Davidson, 2006). Only cells directly transduced by the AAV vector were thought capable of correction, yet the lysosomal storage defect, disease-associated neuropathology and behavioural dysfunction was prevented or reversed in this one AAV9-treated animal. At 26 months of age, 1027/13 was clinically indistinguishable from age-matched control animals and exceeded the maximum life expectancy of 24 months for CLN6 deficient sheep. Unlike the similarly treated CLN5 deficient sheep, 1027/13 retained vision although the retina was not entirely normal in appearance (Figure 7.15). Neuroimaging confirmed the structural integrity of the brain (Figure 7.8) and this was corroborated in subsequent neuropathological analyses. Lysosomal storage was significantly diminished after AAV9-mediated *CLN6* transfer to 1027/13 at the pre-clinical age of 3.7 months (Figure 7.13) and a partial correction of disease-associated atrophy and neurodegeneration was also noted (Figure 7.10; Table 7.4). Importantly, the treatment had a profound therapeutic effect on the already established glial activation in the brain (Figure 7.11-Figure 7.12). Why one CLN6 deficient sheep benefitted from the treatment whilst the others did not is yet to be determined. However previous studies on chimeric sheep, produced by the aggregation of blastomeres from normal and CLN6 affected embryos, indicated that the CLN6 disease may not be cell-autonomous and that corrected cells may release factors which promote the survival of diseased cells (Barry, 2011). This may well be the case in the one successfully treated CLN6 deficient sheep and merits exploration of CLN6 gene transfer in children.

In fact, a Phase I/II CLN6 clinical trial (ClinicalTrials.gov identifier: NCT02725580) was just announced in April 2016. Interest in establishing a human trial was sparked after personal communication with the Gray Foundation detailing the ovine CLN6 results presented in Chapter 7. Subsequent unpublished safety and efficacy studies were performed by Dr. Brian Kaspar and colleagues at the Nationwide Children's Hospital (Columbus, Ohio, U.S.A) on a murine form of CLN6. Gene transfer has since been attempted in 2 CLN6 patients with a further 4 to enrol, using a one-time intrathecal delivery by lumbar puncture with a self-complementary AAV9 vector (see Section 8.3.1) carrying the human *CLN6* gene. Efficacy will be assessed by MRI, cognitive testing, electroencephalography, and ERG or optical coherence tomography (OCT).

8.2 Clinical translation

The results presented in this thesis provide a strong rationale for the clinical translation of viral-mediated gene transfer to human patients with both soluble and membrane-bound forms of NCL. On the whole, treatment of pre-symptomatic lambs prevented stereotypical NCL disease onset and progression. The literature suggests that corrective gene therapies for human neurodegenerative diseases may be restorative if intervention is delivered early in the disease process, otherwise therapeutic benefit is more likely to be achieved by simply halting further disease progression (Waddington *et al*., 2005). Sheep with well-characterised naturally occurring NCLs are ideal models in which to test if recombinant viral vectors can revert the pathological phenotype and established behavioural dysfunction in clinically symptomatic animals. Gene transfer to affected sheep at different ages will be useful for testing different temporal windows of therapeutic intervention for translation to humans and future studies will focus on this. Delivery prior to disease onset will always be an important objective but optimising the method of delivery and using gene transfer vectors that diffuse through the CNS most effectively will likely optimise efficacy.

8.2.1 Timing of therapeutic intervention in the NCL sheep model

In the absence of newborn genetic screening for all forms of NCL, the majority of human patients are diagnosed after the onset of symptoms. Early diagnosis occurs only when an older sibling has already presented with the disease. However there is no doubt that in progressive neurodegenerative disorders in children, like NCL, that better therapeutic advantage is afforded if treatment is administered early in the disease progression. For example, several NCL murine studies have shown that administration of gene therapy earlier in life is more advantageous than when administered to older animals (Griffey *et al*., 2006; Cabrera-Salazar *et al*., 2007; Sondhi *et al*., 2008). The rationale is that early administration gives both higher density and more widespread distribution of the gene therapy vector into the smaller, less mature neonatal brain and aims to prevent disease development rather than trying to reverse established disease (Waddington *et al*., 2004; Bostick *et al*., 2007; Sondhi *et al*., 2008).

Early intervention likely underlies the success of the treated sheep in the current study. Pre-clinical gene therapy was administered to the sheep between 2 and 4 months of age. Examination of the ovine CLN5 and CLN6 neuropathological cascades indicated that these treatments were administered prior to the onset of neurodegeneration and brain atrophy (Chapter 4). For both ovine models, despite the presence of localised glial activation from birth, neonatal brains appear normal and grow within the normal weight range to 4 months of age. Although focal gliosis and slight compression of the upper laminae of the visual and parieto-occipital cortices is evident in this early pre-clinical stage (Figure 4.5, Figure 4.8 and Figure 4.11), the pathological effects are regionally limited and it is quite

probable any damage is reversible if the therapy is targeted and fast-acting (Chapter 6 and Chapter 7).

Between 4 and 6 months of age, both the CLN5 and CLN6 affected brains cease to grow and regional atrophy begins. Significant neuronal loss and reactive gliosis are evident in the visual and parieto-occipital cortices in both models by 6 months. Using brain weight as a measure of atrophy, the CLN5 and CLN6 affected brains weigh 89% and 78% of normal respectively (Table 8.1, Table 8.2). At this stage, CLN6 affected sheep are phenotypically indistinguishable from normal sheep however CLN5 affected sheep exhibit mild 'pre-clinical' signs of NCL, which include a low head carriage and a propensity to stumble, baulk or crouch when travelling through gates or races. Although the neuropathology is more advanced than at 4 months of age, it is still restricted to localised cortical regions and there is evidence of a strong neurogenic 'self-repair' response in affected sheep (Figure 4.14), which suggests the diseased brain at this stage is likely to be amenable to corrective gene therapy.

The disparity between the normal and affected sheep brains becomes increasingly apparent with age, as neuroinflammation and cortical atrophy are more established. By nine months of age, both CLN5 and CLN6 affected brains weigh significantly less than normal brains (Table 4.2). Cortical thinning has spread to further regions, particularly the frontal cortex of the CLN5 affected sheep brain and the somatosensory cortex of the CLN6. The CLN6 affected sheep demonstrate a pre-clinical phenotype (described above for CLN5) from 7 months of age, whilst CLN5 sheep begin to lose vision at 10 - 11 months of age. The visual impairment seen in NCL affected sheep has both a central (cerebral) and a peripheral (retinal) component (Mayhew *et al*., 1985). The former is likely to be responsible for the early loss of vision, given the CLN5 and CLN6 affected visual cortices are reduced to 51% and 60% of normal thickness respectively by 9 months of age (Figure 4.3), whilst obvious differences were not detected in ERG recordings of diseased and normal sheep (unpublished PhD findings, Katharina Russell).

Affected sheep at 6 – 10 months of age represent an early-symptomatic stage in NCL disease, correlating well with those children who receive an early NCL diagnosis on presentation of symptoms. As such, testing whether treatment to early-symptomatic sheep would be efficacious warrants further investigation. To this end, during the course of the present studies, six CLN5 affected sheep received bilateral intracerebroventricular delivery of 3.5×10^{14} vg (total dose) of AAV9-*CLN5* at 9 months of age. These sheep have been assessed by the author, using the same *in vivo* monitoring regime detailed in Chapters 6 and 7, through to euthanasia on trial completion at/before 19 months of age. *Post mortem* neuropathological analyses are underway but the results

of this trial are not included in this thesis. A second cohort of sheep was similarly injected with ICV AAV9-*CLN5* at 7 months of age in May 2016.

Unfortunately, an NCL diagnosis in children can often take some time after presentation of symptoms (Batten Disease Family Association, UK). Although clinically relevant, the impact of intervention on well-established mid-stage disease remains unclear. Injections into affected sheep from 12 months of age may be informative for this. By this age, neuronal loss is pronounced across the cortical mantle. Sheep have established disease signs, namely loss of vision and the onset of proprioceptive, motor and cognitive deficits, which are more pronounced in the CLN5 Borderdales (Figure 6.3). Neuroimaging reveals overt cortical atrophy, enlargement of the ventricles and intracranial ossification in both NCL sheep models. It is likely that the damage to the brain at this stage would be irreversible and the best therapeutic outcome of treatment at this stage may be a halt in disease progression. Although this is not a 'cure' *per se*, this would be a considerable advance on the currently inevitable decline to premature death.

A paradigm that is possible but that has not yet been explored in ovine NCL is prenatal gene therapy. This method offers several potential advantages: a smaller brain size thus a beneficial vector-to-cell ration, transduction of stem and progenitor cells during a time when neurogenesis and gliogenesis is still occurring, immune tolerance to the vector and expressed protein, and intervention before irreversible damage is done. Prenatal gene transfer studies in rodents and rabbits have demonstrated the feasibility of *in utero* gene therapy (Baumgartner *et al*., 1999; Rahim *et al*., 2012; Roybal *et al*., 2012). However, the small size of these animal models and substantial differences in their embryonic development compared with humans limit their utility. Large animal models, such as sheep, represent a more accurate model of human embryonic development and pregnancy, as well as being a less costly alternative to primates (Themis *et al*., 1999; Tran *et al*., 2001; David *et al*., 2003; Pebbles *et al*., 2004; Porada *et al*., 2004). Certain fecund sheep breeds have multiple births (SanCristobal *et al*., 2001), thus providing siblings as uninjected experimental controls for such studies. Intraperitoneal injection of AAV vectors into early and late gestation foetal sheep is possible and results in systemic spread of the vector through the foetal tissues (David *et al*., 2011), which may prove advantageous in the treatment of LSDs. Whilst *in utero* gene therapy in humans remains controversial (Coutelle, 2008), for recessive diseases like the NCLs, pre-natal treatment could be possible currently in a minority of cases where a family history has been established or neonatally in the future as newborn screening programmes for all NCL genes become more widely available.

8.2.2 Optimising CNS gene delivery routes in sheep for human translation

CNS-directed gene therapy has already entered clinical testing for several LSDs. Intraparenchymal (IP) delivery of AAV vectors have been used in patients affected by Canavan disease (Janson *et al*., 2002; Leone *et al*., 2012), late infantile NCL (CLN2) (Crystal *et al*., 2004; Worgall *et al*., 2008), metachromatic leukodystrophy (Zerah *et al*., 2015) and mucopolysaccharidoses type IIIA and B (Tardieu *et al*., 2014). However one of the greatest limitations of this approach is the restricted diffusion of the vector, limiting transgene expression to the vicinity of the injection site. It has been estimated that 50 to 350 injection tracts would be required for complete transduction of the entire human infant brain, with each injection risking oedema or infection (Ojala *et al*., 2015). Alternative routes of vector administration need to be explored.

Intracerebroventricular administration of AAV encoding therapeutic transgenes has recently proven efficacious in correcting LSD (neuro)pathology in diverse animal models (this study; Rafi *et al*., 2012; Haurigot *et al*., 2013; Katz *et al*., 2015; Ribera *et al*., 2015). ICV delivery is less invasive than multiple intraparenchymal injections, it avoids systemic vector dissemination and has been shown to transduce ependymal cells and/or the choroid plexi, which serve as a 'biological reservoirs' for the continual secretion of recombinant protein into the CSF for distribution across the brain parenchyma (Passini *et al*., 2003; Liu *et al*., 2005a, 2005b; Yamazaki *et al*., 2014; Katz *et al*., 2015; Hironaka *et al*., 2015). Additionally the ICV route is considered safe in humans, with ventricular access to the CSF through the lateral cerebral ventricles a routine diagnostic and therapeutic neurosurgical procedure in humans (Rosenbaum *et al*., 2014). Plans for clinical translation of this approach are underway (Biffi, 2015). Whilst bilateral ICV delivery has been employed in most studies, Katz *et al* (2015) demonstrated therapeutic benefit in a canine model of CLN2 NCL after a single unilateral injection of AAV2 expressing the canine *TPP1* enzyme. ICV delivery is relatively simple to perform in sheep. Accessing only one ventricle would be less invasive and even faster and should be attempted.

Intrathecal delivery, into the lumbar cistern or cisterna magna, also provides a simple alternative approach and has proven efficacious in other disease models, particularly those with motoneuron loss (Wang *et al*., 2014; Duque *et al*., 2015; Meyer *et al*., 2015). However limited distribution was seen in the porcine CNS after delivery via the lumbar intrathecal route (Federici *et al*., 2012) and no transduction was observed after intracisternal (IC) lentiviral-mediated delivery of GFP in sheep (linterman *et al*., 2011). The latter may be related to the vector dosage used (1×10^9 TU) and further investigation of these delivery routes with AAV vectors is warranted in sheep. Nevertheless, intracisternal injections are uncommon in the clinic due to the risks of complications derived from the proximity of the cisterna magna to vital cardiac, respiratory and vasomotor centres of the medulla, especially in children. Also, as vector spread after intrathecal delivery is reportedly limited to the caudal regions of the brain, it is rarely used in humans in preference to the ICV route (Wolf *et*

al., 2015). Interestingly though, this was the delivery route chosen for the recent Phase I/II CLN6 clinical trial (NCT02725580).

For NCLs with transmembrane protein deficiencies, convection enhanced delivery (CED) via multiple intraparenchymal microcatheters may have potential for treating the global brain pathology. This technique has been employed for delivery of drugs to the brain in animal models of Alzheimer and Parkinson's disease (Barua *et al*., 2012, 2014, 2015). It uses a pressure gradient at the tip of the infusion catheter to induce convective flow of the vector through the interstital fluid spaces of the brain, which results in a greater spread than diffusion alone (Bankiewicz *et al*., 2000; Nguyen *et al*., 2001). The technique has already been attempted in sheep for AAV-GFP based therapeutics (van der Bom *et al*., 2013a, 2013b) however no reports of expression, tropism or neuropathological outcomes have been published from these studies. CED of the reporter (green fluorescent protein; GFP) and therapeutic proteins will be assessed in sheep, in collaboration with colleagues from the University of Manchester, using the cranial navigation software Brainlab (Munich, Germany), in October 2016. It is hoped that this technique will prove beneficial for widespread gene delivery to the brain for those LSDs with defective transmembrane proteins, like the NCL protein CLN6 or heparan sulfate acetyl-CoA: α-glucosaminide N-acetyltransferase (HGSNAT), the missing enzyme in mucopolysaccharidosis type III C under study by the Manchester group.

8.2.3 Optimising gene expression in the sheep brain for human translation

The current study is one of the first to perform a side-by-side comparison of AAV and lentiviral-mediated gene transfer. AAV vectors are currently considered the best platform for CNS-directed gene therapy, because of their broad spread and viral tropism, and are in advanced clinical development and testing (Fu *et al*., 2011; Bartus *et al*., 2013; Rafii *et al*., 2014; Ribera *et al*., 2015; Walia *et al*., 2015). However lentiviral-mediated gene transfer in LSD brains has shown promising results in terms of transgene biodistribution, safety and therapeutic efficacy in small (Consiglio *et al*., 2001; Di Domenico *et al*., 2009; Lattanzi *et al*., 2010, 2014) and large animal models (Kordower *et al*., 2000; Jarraya *et al*., 2009). Moreover, the first clinical trial using a lentivirus to deliver dopaminergic genes in Parkinson's patients showed safety and indications of efficacy in all treated patients (Palfi *et al*., 2014).

Surprisingly clinical outcomes were similar in CLN5 affected sheep with both viral vector platforms that were tested here (Chapter 6). Late-onset loss of vision was the only clinical sign presented by treated sheep from both vector treatment groups, with earlier deficits seen in the lentiviral cohort than in the AAV cohort. Studies are underway to compare CLN5 transgene expression, vector tropism and neuropathological assessment of treatment-dependent modulation of lysosomal storage pathology, glial activation, and neuronal loss. In comparison, AAV9 proved to be more efficacious in

the treatment of ovine CLN6 disease than a lentiviral vector (Chapter 7). Whilst there was strong evidence for transduction of the ependyma lining the lateral cerebral ventricles in the lentiviral-treated CLN6 sheep brains, this did not show sufficient therapeutic benefit to prevent disease onset and progression. Lentiviral vectors transduce both astrocytes and neurons in the normal and CLN6 affected sheep brain (Linterman *et al*., 2011, Figure 7.9), whilst AAV9 has a predominant neurotropism (Figure 5.5). Similar findings have been published recently for the cynomolgus monkey brain, although lentivirus shows a greater tropism for astrocytes over neurons (An *et al*., 2016). The cellular tropism of the two vectors in the affected sheep brain may prove enlightening and suggest which vector is better suited for delivery to neurons.

One of the limitations of using lentiviral vectors for ovine gene therapy studies in New Zealand relates to the genetically-modified status of the treated sheep. During the therapy trials described in Chapters 6 and 7, a successful application was made to the New Zealand Environmental Protection Agency to reclassify AAV-treated sheep as not 'genetically modified' under the Hazardous Substances and New Organisms (HSNO) Act (1996). This was made on the premise that the genome of the host (sheep) was not sufficiently altered or modified by treatment with an AAV vector to constitute a risk. AAVs lack integrative capacity, remaining episomal in the host cell nucleus *in vivo* (see Section 1.6.3.2). Unfortunately a similar case could not be established for sheep treated with lentiviruses as these vectors do integrate into the host genome (see Section 1.6.3.1). The outcome of this reclassification was that AAV-treated sheep were released from the indoor Physical Containment 2 sheep facility and could be maintained under normal pastoral conditions at Lincoln University. Hence, due to their greater efficacy, and the problems associated with long-term indoor housing of sheep (see Section 8.2.4), AAV vectors are the preferred vector platform for future sheep studies. They are also the vectors of choice for human NCL gene therapy studies (Crystal *et al*., 2004; Worgall *et al*., 2008; Crystal, 2014), thus making translation of this work to human medicine more straightforward.

The current study used traditional single stranded (ss) AAV vectors. A rate-limiting step which can affect the efficiency of single stranded vectors is the speed and ability with which infected cells perform viral genome second strand synthesis before initiation of transgene expression. Faster gene expression can be achieved with self-complementary (sc) AAV vectors and a 10- to 100-fold increase in transduction efficiency has been reported compared with ssAAVs (McCarty *et al*., 2001, 2003; Yang *et al*., 2002; Gray *et al*., 2011). Upon infection, an scAAV vector is not reliant on cell mediated second strand synthesis but rather folds back on itself through intramolecular base pairing to create a duplex, which is immediately ready for transcription (McCarty *et al*., 2001, 2003). Caveats associated with scAAV constructs are their reduced packaging capacity of ~2.3 kB, compared with ~4.5 kB for ssAAV (Wu *et al*., 2007), and reports that scAAV elicit a more potent transgene-specific immune response than ssAAV (Wu *et al*., 2012). The former is not an issue for the *CLN5* and *CLN6* cDNAs

(1086 and 933 bp respectively). The robust gene expression of scAAV warranted their inclusion in ovine NCL gene therapy trials in an attempt to improve expression and efficacy. Codon-optimised scAAV9-*CLN6* vector was sourced from the University of North Carolina Vector Core in collaboration with Dr. Steven Gray (Chapel Hill, North Carolina, U.S.A.) and injected into pre-clinical CLN6 South Hampshire sheep in December 2015. Therapeutic efficacy is being assessed using the *in vivo* parameters described in this thesis. Additionally the codon-optimisation will allow *post mortem* quantitative measures of transgene-specific expression.

8.2.4 Detrimental effects of long-term indoor confinement of sheep

An external factor which negatively impacted on this study was the long-term indoor confinement of the treated sheep. During the trial, two lentiviral-treated animals were euthanised due to acute haemolysis caused by chronic copper poisoning. Of the ruminants, sheep are particularly susceptible to this, and it is exacerbated in animals housed indoors on pelleted feeds (Hogan *et al*., 1968; Lewis *et al*., 1997), because of their reduced copper requirement (Bostwick, 1982). Generally, sheep require about 5 ppm of copper in their total diet however acute toxicity can occur at levels above 25 ppm (Kahn & Line, 2014). Excess copper is stored in the lysosomes within hepatocytes (Kumaratilake & Howell, 1987) and when retained there it does not cause any tissue damage. However it can be released spontaneously or at times of stress (*e.g.* shearing, extreme weather, transportation, exertion) (Bostwick, 1982). Once released into the circulation, copper causes acute oxidative injury to haemoglobin, preventing the binding of oxygen and carbon dioxide. The red blood cell membrane is concomitantly disturbed, resulting in haemolysis (a haemolytic crisis) and anaemia. Hepatic necrosis and renal failure result from the massive release of haemoglobin and death usually occurs within four days (Bostwick, 1982).

The onset of symptoms in both treated sheep in this trial correlated with or occurred in the days shortly after completion of their maze testing. The general literature suggests that sheep breeds of British origin are particularly stress-prone (*e.g.* Suffolk, Texel and the crossbred South Hampshires) and thus are especially vulnerable to copper poisoning. This may explain why the toxicity remained sub-clinical in the more docile Borderdale sheep that were similarly housed (Chapter 6). Although the concentrate feed was relatively low in copper content, excessive levels in the sheep tissues at *post mortem* suggested a cumulative effect of low level copper ingestion over the year. Serum concentrations of the enzymes aspartate transaminase (AST) and gamma glutamyl transpeptidase (gGT) have been reported as predictive indicators of hepatic copper accumulation (Lewis *et al*., 1997). Routine haematological screening for these enzymes in the current study was insufficient to detect elevated levels prior to the haemolytic crisis and subsequent euthanasia of the two treated sheep.

Long-term indoor confinement of sheep can also be extremely detrimental to their wellbeing (Reinhardt & Reinhardt, 2002). Combined with a reduced feeding time per day and the inability to exercise or perform simple natural behaviours (*e.g.* graze on grass), classic stereotypical behaviours can manifest. These include repetitive actions or body movements, such as head butting or nosing, aggression, increased vocalisation, pacing, pawing, or oral stereotypies (*e.g.* wool pulling, teeth grinding or chewing bar fixtures) (Sambraus, 1985; Hinch & Lynch, 1997; Vasseur *et al*., 2006). Given their similarity to the clinical signs of NCL, it was necessary to eliminate/minimise any chance of stereotypy in this trial to assess neurological efficacy accurately. The experimental design included environmental enrichment - sensory (playing music), social interaction, exercise and new objects/ toys to explore - to counter boredom and stereotypy. The provision of a rich and stimulating environment has previously been shown to induce neuronal changes that have a protective role, ameliorating functional deficits associated with various degenerative disorders and brain trauma (Horner & Gage, 2000; van Dellen *et al*., 2000; Johnson *et al*., 2013). During the current study, the enrichment appeared to be successful with the only behavioural pathology exhibited being wool-biting for a short period of time (~1 month). The provision of fibre, in the form of chaffed hay, redirected this oral stereotypy whilst also increasing the bulkiness of the feed, time spent feeding and rumination.

8.3 Future directions

8.3.1 *In vivo* monitoring of disease progression and therapeutic efficacy

The current study demonstrated the value of sheep as an alternative neurotherapeutic translational model to non-human primates and other domestic animals, and the utility of longitudinal *in vivo* behavioural and neurological function testing and neuroimaging techniques in the assessment of efficacy. It is particularly encouraging to see that similar efficacy parameters currently used or planned in sheep (Chapters 6 and 7; Sections 8.3.1and 8.3.3; Katharina Russell (unpublished PhD findings, Lincoln University); Perentos *et al*., 2015) are also applicable in human clinical trials. However there is potential to improve many of the *in vivo* parameters used to assess therapeutic efficacy in ovine NCL. Firstly, the slow and insidious onset of clinical signs in ovine NCL under field conditions make clinical staging of disease progression, especially in the early disease stages, difficult. Neurological dysfunction was assessed subjectively in the current study by a sheep-specific clinical neurologic examination (Passler *et al*., 2012); components of which included open- and closed-field behavioural observation (mentation, gait, head carriage and postural traits, as well as manifest tremor or seizure onset) and cranial nerve (optic II, oculomotor III, trigeminal V and facial VII) evaluation. Sheep were subjectively assessed by two independent investigators on a basic clinical

rating scale in the current study however this scale could be honed for better assessment of therapeutic efficacy in future trials.

The unified Batten disease rating scale (UBDRS) is used to measure physical impairment and severity of disease-associated symptoms in human NCL (Marshall *et al*., 2005). Patients are scored from 0 to 4 (normal to abnormal) for each of 27 items, which include vision, speech, tone, bulbar and motor function and the presence of abnormal movements. Higher scores reflect greater dysfunction. Based on the current study, specific components could be singled out for categorical grading in a similar method to the UBDRS, permitting a more in-depth rating scale for future sheep therapy trials.

Although the maze used to assess therapeutic efficacy in the current study was relatively basic, it was sensitive enough to detect neurologic impairment. Sheep perform well in maze tests (Peirce *et al*., 2001; Lee *et al*., 2006; Shamir *et al*., 2010; Banin *et al*., 2015; Hunter *et al*., 2015; McBride *et al*., 2015), which indicates that they have good cognition and spatial memory – traits that allow them to graze with optimum efficiency (Bailey *et al*., 1996; Howery *et al*., 1999). To improve the quality of the data collected from maze testing, a computerised global positioning system (GPS) tracking set-up could be developed in conjunction with computational methods to codify spatio-temporal data. Similar methodology has been used to measure the flocking behaviour of CLN5 Borderdale sheep in naturalistic settings (Furmston *et al*., 2015).

In vivo neuroimaging procedures used to assess efficacy in ovine gene transfer trials are also continually improving. Due to the increasing popularity of ovine models in translational neuroscience, many reports detailing MR imaging of the sheep brain have been published recently (Amorim *et al*., 2015; Ella & Keller, 2015; Lee *et al*., 2015; Nitzsche *et al*., 2015; Sawiak *et al*., 2015) . Longitudinal MRI studies of treated sheep should be possible. To complement this, quantitative measures and three-dimensional modelling of intracranial and ventricular volumetric changes in the neurodegenerating sheep brain have been developed from CT images (unpublished PhD data, Katharina Russell, Lincoln University) and MRI studies have begun with Dr. Tracy Melzer at the New Zealand Brain Research Institute (Christchurch, New Zealand).

8.3.2 Other considerations for human translation

Neuropathological studies will provide an important efficacy endpoint for the pre-clinical CLN5 trial (Chapter 6). These are underway in collaboration with BARN colleagues at Kings College London (United Kingdom). If amelioration of NCL disease hallmarks is noted then dose reduction studies could be easily conducted in sheep. A major obstacle in translating therapies from pre-clinical animal trials to a human clinical application is the need to produce large titres of highly concentrated viral vectors (Clement *et al*., 2009). Determining the lowest dose in sheep that provides full therapeutic benefit would be important for clinical translation and would minimise the risk of immunotoxicity.

One of the greatest limitations to successful viral-mediated gene therapy relates to immunotoxicity. Despite the removal of the replicative and pathogenic ability of viral vectors, administration can lead to a harmful innate or adaptive host immune response to either the vector or the transgene product, resulting in decreased efficiency of gene transfer or elimination of the transduced cells over time. Lentiviruses possess an intrinsic low immunogenicity and a mild proinflammatory profile, being well tolerated by the host immune system (Abordo-Adesida *et al*., 2005; Annoni *et al*., 2007). Whilst the immunogenicity of AAV is also low, a high prevalence of neutralising antibodies (NAbs) against various AAV serotypes has been detected in human (Calcedo *et al*., 2009; Boutin *et al*., 2010) and sheep (Rapti *et al*., 2012; Tellez *et al*., 2013) populations. There was no clinical evidence of an immune response in any of the treated sheep through the current study. CSF and serum were routinely collected from the treated sheep through the therapeutic trials and can be used in neutralising titre studies to detect potential sub-clinical immune responses to the viral capsid and/or transgene product if these data are required.

8.3.3 Intraocular gene therapy

Despite its peripheral location, the retina is actually part of the CNS. However brain-directed *CLN5* and *CLN6* delivery delayed, but did not prevent, the natural retinal dysfunction seen in ovine NCL (see Sections 6.3.3.2 and 7.3.3.2). Other retinal degenerative disorders, such as Leber's congenital amaurosis type 2, have been successfully treated in intraocular gene therapy clinical trials (Bainbridge *et al*., 2008; Cideciyan *et al*., 2009). This approach may hold promise as an adjunct therapy to preserve vision in treated sheep and NCL patients.

Retinopathy in NCL results from the degeneration of rod and cone photoreceptor cells (Figure 8.1B) (Goebel *et al*., 1977; Goebel 1992). These lie several hundred microns deep within the human (and sheep) retina and thus represent a challenging target cell type. Intravitreal injection offers a relatively non-invasive readily accessible delivery route to the eye (Figure 8.1A). However, when administered intravitreally, most viral vectors do not transduce the retina. Transduction by those that do, such as AAV2, is mainly restricted to retinal ganglion and Müller cells of the middle retina (Stieger *et al*., 2011; Trapani *et al*. 2015). This is unlikely to be sufficient to protect against degeneration in NCL. For example, intravitreal AAV2-mediated delivery of palmitoyl protein thioesterase (PPT1/CLN1) to a murine model of infantile NCL specifically transduced ganglion cells (Griffey *et al*., 2005). Enzyme levels in the eye were elevated to above normal but only a partial improvement in retinal architecture and function was reported. Also, despite evidence of inner retinal transduction after intravitreal AAV2 delivery to the macaque in one study (Yin *et al*., 2011), similar success was not achieved in rodents with AAV serotypes 2, 7, 8 or 9 (Dalkara *et al*., 2009; Pang *et al*., 2008).

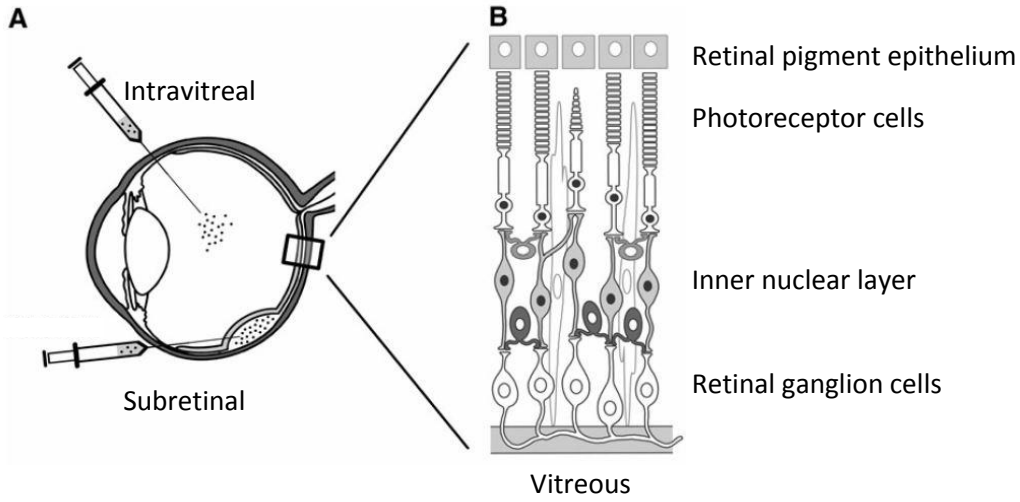

Figure 8.1 Schematic representation of intraocular injection routes (A) and some retinal layers (B). Amended from Trapani *et al*., 2015

By comparison, subretinal injection of various viral vectors (Figure 8.1A) has been shown to transduce both photoreceptors and retinal pigment epithelium of mice effectively (Pang *et al*., 2008; Puppo *et al*., 2014). AAV5 restored vision in canine and ovine models of congenital achromatopsia (Komáromy *et al*., 2010; Banin *et al*., 2015). Phenotypic rescue has also been achieved by subretinal AAV gene transfer in several lysosomal storage diseases, including a feline model of mucopolysaccharidosis (MPS) V (Ho *et al*., 2002) and MPS VII mice (Hennig *et al*., 2004). However delivery by this route can be technically challenging. Injection into the subretinal space results in a transient retinal detachment which can be detrimental to retinas already undergoing degeneration, therefore early intervention is likely to be important.

Ethical approval has been granted to perform ocular gene therapy in NCL sheep, using a subretinal strategy already tested in sheep (Banin *et al*., 2015). A veterinary ophthalmologist will inject one eye with an AAV9 vector encoding the corrective *CLN* gene, with the other eye being an internal control. Therapeutic efficacy will be objectively examined over time using established techniques including ophthalmic observations, fundus photography and electroretinography (Katharina Russell, PhD student, Lincoln University). The sheep eye is an excellent ophthalmic candidate for human studies, sharing a similar axial length, and equatorial and vitreous cavity diameter to humans (Mohammadi *et al*., 2011). A novel technique, optical coherence tomography, which has proven successful in efficacy studies in human NCL (Angela Schulz, personal communication) will be trialled in sheep and histopathology will follow at *post mortem*.

8.3.4 Combination therapy

Despite a strong record of success, limitations still exist with gene therapies. These include gene silencing or phenotoxicity, immunotoxicity, insertional mutagenesis and commercial viability

(Mingozzi & High, 2011), and it is likely that no single treatment for the NCLs will suffice in many cases but rather a combination of therapies will be required. Many clinical gene therapy protocols currently employ transient immunosuppressant drugs (Sack & Herzog, 2009) however there is no mention of these in the Phase I/II CLN2 or CLN6 clinical trials underway. The evidence presented in the current study and by others (Oswald *et al*., 2005; Pontikis *et al*., 2005; Kay *et al*., 2006; Kielar *et al*., 2007) of precocial activation of non-neuronal cells highlights the important mediatory role of glial cells in early-stage NCL pathogenesis. As a chronic inflammatory response can be detrimental to both neuronal survival and neurogenesis (Raivich *et al*., 1999; Stoll & Jander, 1999; Streit *et al*., 2004; Whitney *et al*., 2009; Lyman *et al*., 2014; Lee & MacLean, 2015), early suppression of inflammation may be a valuable adjunctive treatment to gene therapy. Macauley *et al*. (2014) investigated the therapeutic value of a small molecule anti-neuroinflammatory drug as co-therapy to CNS-directed, AAV5-mediated gene therapy in a CLN1/PPT1 mouse model. Whilst the drug (MW151) alone decreased seizure susceptibility, the combination therapy did not significantly improve therapeutic efficacy over AAV-mediated *PPT1* gene transfer alone. However like the *PPT-/-* mice, the human CLN1 disease typically has a rapid clinical course, affecting the brain in its entirety (Haltia 2003). Clinical improvement with gene therapies, which target the primary genetic defect, complemented with pharmocological neuro-inflammatory agents, that target dysregulated glia, may be synergistically greater in NCL subtypes that have a more protracted disease course.

8.4 Conclusion

Together the neuronal ceroid lipofuscinoses (Batten disease) are the most common degenerative brain diseases in childhood (Schulz *et al*., 2013). On average, four New Zealand families receive an NCL diagnosis each year imposing a huge burden on family life and relationships at an estimated cost of $60,000-$100,000 per annum per patient (Lysosomal Diseases New Zealand). Presently there are no effective treatment options for any forms of NCL, other than palliative care.

The results presented in this thesis provide a strong rationale for the clinical translation of viral-mediated gene transfer to human patients with CLN5 and CLN6 disease. Delivery of viral vectors encoding therapeutic NCL genes to pre-symptomatic lambs protected against stereotypical disease onset and progression. Treated CLN5 deficient sheep retained cognitive function and a normal brain structure and intracranial volume, and demonstrated an extended lifespan. The only clinical sign of NCL was a delayed-onset loss of vision. Neuropathological analyses of efficacy are pending. One AAV9-treated CLN6 deficient sheep demonstrated sustained functional efficacy and vision, and the treatment reversed the established neuropathology.

This study poses a number of questions. How efficacious will gene therapy be when administered later in the disease course? At what stage is the neuropathology too advanced to reduce any

likelihood of therapeutic outcome? Whilst the successful gene transfer in CLN5 deficient sheep likely benefits from 'cross-correction', accounting for the amelioration of disease phenotype in one AAV9-treated CLN6 deficient sheep is harder to explain. Is the CLN6 protein involved in the processing of some soluble factor, which itself is secreted and endocytosed to correct functionality of neighbouring cells? What can be done to increase the efficacy of *CLN6* gene transfer to ensure therapeutic benefit for all treated animals? These questions warrant further investigation, but do not detract from the value of studies presented in this thesis which demonstrate that viral-mediated gene therapy of the CLN5 and CLN6 forms of NCL is possible and that NCL sheep provide excellent large animal neurotherapeutic models to expedite the translation of these findings to the clinic.

'*sometimes the best answer a scientist could want is more questions*'

Richard Panek, 2000

Appendix A

Sheep Neurological Test

NEUROLOGICAL EXAMINATION OF SHEEP

DATE: **ANIMAL NO:**

AGE: **BREED:**

SEX: **RECORDED BY:**

GENERAL EXAMINATION:

1. Body Weight	kg				
2. Body Condition Score	1	2	3	4	5
3. Blood Sample taken:	Y / N				

4. Rectal temperature: ° C Normal range 38.3–39.9° C

5. Heart rate: beats/minute Normal range 60-90 beats/minute

6. Respiration rate: breaths/minute Normal range 12-20 breaths/minute

7. Hydration level: Normal to Dehydrated

8. Ruminal contractions: Normal / Decreased / Absent

9. Mucous membranes: Normal (pink/red) / Abnormal (white)

GENERALISED BEHAVIOUR AND MOVEMENT:

Describe in detail if abnormal

10. Posture when approached	**Standing**	**Sitting sternal**	**Other**
11. Behaviour/mentation	**Resting:**	**Approached:**	**Handled:**

BEHAVIOUR / MOVEMENT	**Normal**	**Abnormal**	**Exaggerated**
12. Posture/ Head Carriage	Head high	Head low	
13. Gait		Ataxia	
14. Walking upstairs/ flat surface		Difficulty on stairs	
15. Abnormal behaviour	Absent	Circling	
16. Abnormal movements/ tremors/ tics/ seizures	Absent		

CRANIAL NERVE FUNCTION AND REFLEXES:

FACE / NECK	**Normal**	**Decreased**	**Absent**
17. Menace response (medial) (Optic nerve)	Eyelid blink/ head aversion		No response
18. Menace response (lateral) (Optic nerve)	Eyelid blink/ head aversion	Absent (unilateral)	Absent (bilateral)

CRANIAL NERVE FUNCTION AND REFLEXES:

FACE / NECK	**Normal**	**Decreased**	**Absent**
19. Pupillary light reflex (direct) (Oculomotor nerve)	Direct pupil constriction	Absent (unilateral)	Absent (bilateral)
20. Pupillary light reflex (consensual) (Oculomotor nerve)	Consensual pupil constriction	Absent (unilateral)	Absent (bilateral)
21. Dazzle reflex (Oculomotor, optic, facial nerves)	Blink/head aversion on bright light		No response
22. Corneal reflex (Trigeminal, facial nerves)	Blink on touching cornea	Absent (unilateral)	Absent (bilateral)
23. Palpebral reflex (Trigeminal, facial nerves)	Blink on touching canthi	Absent (unilateral)	Absent (bilateral)
23. Visual tracking (Optic nerve)	Follow visual stimulus		Not follow visual stimulus
23. Startle response (Facial nerve, hearing)	Startle on loud noise		No response to loud noise

OTHER HEAD ABNORMALITIES	**Normal**	**Abnormal**	**Exaggerated**
24. Ears (position/touch)		Droop	
25. Lips (symmetry/touch)		Droop	
26. Nose (movement/touch)			
27. Mouth/jaw (salivation/tone)		Dribbling	
28. Eating/drinking		Sham	

29. Skin lesions: **Y / N** List areas and types*/ draw below*

30. Any other abnormalities: **Y / N** List areas and types*/ draw below*

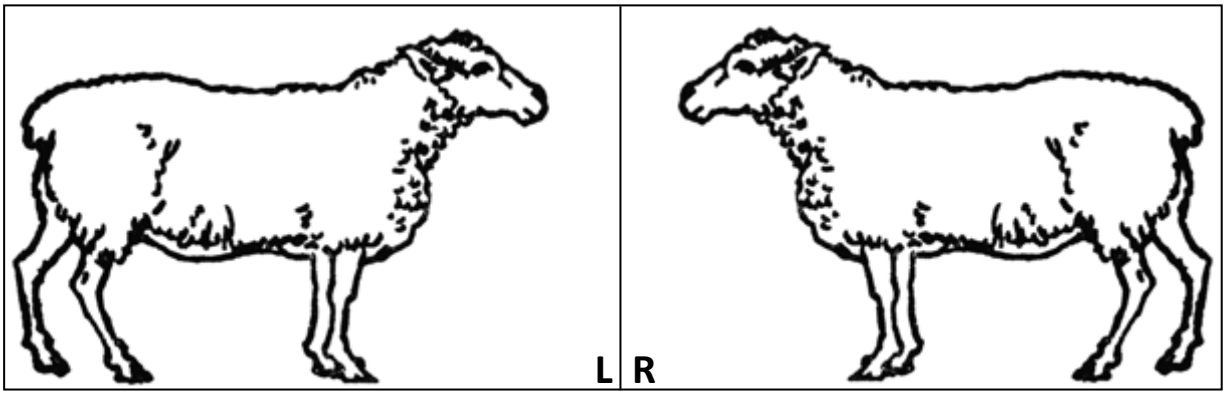

Recording:

Still photo taken:	**Y** Describe	**N**
Video taken:	**Y** Describe	**N**

References

Abordo-Adesida, E., Follenzi, A., Barcia, C., Sciascia, S., Castro, M. G., Naldini, L., & Lowenstein, P. R. (2005). Stability of lentiviral vector-mediated transgene expression in the brain in the presence of systemic antivector immune responses. *Human Gene Therapy*, *16*(6), 741–751.

Achord, D. T., Brot, F. E., Bell, C. E., & Sly, W. S. (1978). Human beta-glucuronidase: in vivo clearance and in vitro uptake by a glycoprotein recognition system on reticuloendothelial cells. *Cell*, *15*(1), 269–278.

Ahern-Rindell, A. J., Prieur, D. J., Murnane, R. D., Raghavan, S. S., Daniel, P. F., McCluer, R. H., Walkley, S. U., & Parish, S. M. (1988). Inherited lysosomal storage disease associated with deficiencies of beta-galactosidase and alpha-neuraminidase in sheep. *American Journal of Medical Genetics*, *31*(1), 39–56.

Aigner, B., Renner, S., Kessler, B., Klymiuk, N., Kurome, M., Wünsch, A., & Wolf, E. (2010). Transgenic pigs as models for translational biomedical research. *Journal of Molecular Medicine*, *88*(7), 653–664.

Allen, J. S., Damasio, H., & Grabowski, T. J. (2002). Normal neuroanatomical variation in the human brain: an MRI-volumetric study. *American Journal of Physical Anthropology*, *118*(4), 341–358.

Alvarez-Buylla, A., & Lim, D. A. (2004). For the long run: maintaining germinal niches in the adult brain. *Neuron*, *41*(5), 683–686.

Amorim, I. S., Mitchell, N. L., Palmer, D. N., Sawiak, S. J., Mason, R., Wishart, T. M., & Gillingwater, T. H. (2015). Molecular neuropathology of the synapse in sheep with CLN5 Batten disease. *Brain and Behavior*, *5*(11), e00401.

An, H., Cho, D.-W., Lee, S. E., Yang, Y.-S., Han, S.-C., & Lee, C. J. (2016). Differential cellular tropism of lentivirus and adeno-associated virus in the brain of cynomolgus monkey. *Experimental Neurobiology*, *25*(1), 48–54.

Anderson, P. D., Parton, K. H., Collett, M. G., Sargison, N. D., & Jolly, R. D. (1999). A lower motor neuron disease in newborn Romney lambs. *New Zealand Veterinary Journal*, *47*(3), 112–114.

Andrade, D. M., Paton, T., Turnbull, J., Marshall, C. R., Scherer, S. W., & Minassian, B. A. (2012). Mutation of the CLN6 gene in teenage-onset progressive myoclonus epilepsy. *Pediatric Neurology*, *47*(3), 205–208.

Annoni, A., Battaglia, M., Follenzi, A., Lombardo, A., Sergi-Sergi, L., Naldini, L., & Roncarolo, M.-G. (2007). The immune response to lentiviral-delivered transgene is modulated in vivo by transgene-expressing antigen-presenting cells but not by CD4+CD25+ regulatory T cells. *Blood*, *110*(6), 1788–1796.

Arsov, T., Smith, K. R., Damiano, J., Franceschetti, S., Canafoglia, L., Bromhead, C. J., Andermann, E., Vears, D. F., Cossette, P., Rajagopalan, S., McDougall, A., Sofia, V., Farrell, M., Aguglia, U., Zini, A., Meletti, S., Morbin, M., Mullen, S., Andermann, F., Mole, S. E., Bahlo, M., & Berkovic, S. F. (2011). Kufs disease, the major adult form of neuronal ceroid lipofuscinosis, caused by mutations in CLN6. *American Journal of Human Genetics*, *88*(5), 566–573.

Arvidsson, A., Collin, T., Kirik, D., Kokaia, Z., & Lindvall, O. (2002). Neuronal replacement from endogenous precursors in the adult brain after stroke. *Nature Medicine*, *8*(9), 963–970.

Aschauer, D. F., Kreuz, S., & Rumpel, S. (2013). Analysis of transduction efficiency, tropism and axonal transport of AAV serotypes 1, 2, 5, 6, 8 and 9 in the mouse brain. *PLoS ONE*, *8*(9), e76310.

Atchison, R. W., Casto, B. C., & Hammon, W. M. (1965). Adenovirus-associated defective virus particles. *Science*, *149*(3685), 754–756.

Autti, T., Hämäläinen, J., Mannerkoski, M., Van Leemput, K. Van, & Aberg, L. E. (2008). JNCL patients show marked brain volume alterations on longitudinal MRI in adolescence. *Journal of Neurology*, *255*(8), 1226–1230.

Autti, T., Raininko, R., Launes, J., Nuutila, A., & Santavuori, P. (1992). Jansky-Bielschowsky variant disease: CT, MRI, and SPECT findings. *Pediatric Neurology*, *8*(2), 121–126.

Azizieh, R., Orduz, D., Van Bogaert, P., Bouschet, T., Rodriguez, W., Schiffmann, S. N., Pirson, I., & Abramowicz, M. J. (2011). Progressive myoclonic epilepsy-associated gene KCTD7 is a regulator of potassium conductance in neurons. *Molecular Neurobiology*, *44*(1), 111–121.

Baek, R. C., Broekman, M. L. D., Leroy, S. G., Tierney, L. a, Sandberg, M. a, d'Azzo, A., Seyfried, T. N., & Sena-Esteves, M. (2010). AAV-mediated gene delivery in adult GM1-gangliosidosis mice corrects lysosomal storage in CNS and improves survival. *PloS One*, *5*(10), e13468.

Bailey, D. W., Gross, J. E., Laca, E. A., Rittenhouse, L. R., Coughenour, M. B., Swift, D. M., & Sims, P. L. (1996). Mechanisms that result in large herbivore grazing distribution patterns. *Journal of Range Management*, *49*(5), 386–400.

Bainbridge, J. W. B., Smith, A. J., Barker, S. S., Robbie, S., Henderson, R., Balaggan, K., Viswanathan, A., Holder, G. E., Stockman, A., Tyler, N., Petersen-Jones, S., Bhattacharya, S. S., Thrasher, A. J., Fitzke, F. W., Carter, B. J., Rubin, G. S., Moore, A. T., & Ali, R. R. (2008). Effect of gene therapy on visual function in Leber's congenital amaurosis. *The New England Journal of Medicine*, *358*(21), 2231–2239.

Banin, E., Gootwine, E., Obolensky, A., Ezra-Elia, R., Ejzenberg, A., Zelinger, L., Honig, H., Rosov, A., Yamin, E., Sharon, D., Averbukh, E., Hauswirth, W. W., & Ofri, R. (2015). Gene augmentation therapy restores retinal function and visual behavior in a sheep model of CNGA3 Achromatopsia. *Molecular Therapy*, *23*(9), 1423–1433.

Bankiewicz, K. S., Eberling, J. L., Kohutnicka, M., Jagust, W., Pivirotto, P., Bringas, J., Cunningham, J., Budinger, T. F., & Harvey-White, J. (2000). Convection-enhanced delivery of AAV vector in parkinsonian monkeys; in vivo detection of gene expression and restoration of dopaminergic function using pro-drug approach. *Experimental Neurology*, *164*(1), 2–14.

Barry, L. A. (2011). *Neuroinflammation and defining gene therapy approaches for ovine CLN6 Batten disease*. PhD thesis, Lincoln University, Lincoln, New Zealand.

Bartus, R. T., Baumann, T. L., Brown, L., Kruegel, B. R., Ostrove, J. M., & Herzog, C. D. (2013). Advancing neurotrophic factors as treatments for age-related neurodegenerative diseases: developing and demonstrating "clinical proof-of-concept" for AAV-neurturin (CERE-120) in Parkinson's disease. *Neurobiology of Aging*, *34*(1), 35–61.

Barua, N. U., Bienemann, A. S., Woolley, M., Wyatt, M. J., Johnson, D., Lewis, O., Irving, C., Pritchard, G., & Gill, S. (2015). Convection-enhanced delivery of MANF-volume of distribution analysis in porcine putamen and substantia nigra. *Journal of the Neurological Sciences*, *357*(1-2), 264–269.

Barua, N. U., Gill, S. S., & Love, S. (2014). Convection-enhanced drug delivery to the brain: therapeutic potential and neuropathological considerations. *Brain Pathology* , *24*(2), 117–127.

Barua, N. U., Miners, J. S., Bienemann, A. S., Wyatt, M. J., Welser, K., Tabor, A. B., Hailes, H. C., Love, S., & Gill, S. S. (2012). Convection-enhanced delivery of neprilysin: a novel amyloid-β-degrading therapeutic strategy. *Journal of Alzheimer's Disease* , *32*(1), 43–56.

Baudry, M., Yao, Y., Simmons, D., Liu, J., & Bi, X. (2003). Postnatal development of inflammation in a murine model of Niemann-Pick type C disease: immunohistochemical observations of microglia and astroglia. *Experimental Neurology*, *184*(2), 887–903.

Bauer, H. J., & Monreal, G. (1986). Herpesviruses provide helper functions for avian adeno-associated parvovirus. *The Journal of General Virology*, *67*((Pt 1)), 181–185.

Baumgartner, T. L., Baumgartner, B. J., Hudon, L., & Moise, K. J. (1999). Ultrasonographically guided direct gene transfer in utero: successful induction of beta-galactosidase in a rabbit model. *American Journal of Obstetrics and Gynecology*, *181*(4), 848–852.

Bell, P., Moscioni, A. D., McCarter, R. J., Wu, D., Gao, G., Hoang, A., Sanmiguel, J. C., Sun, X., Wivel, N. A., Raper, S. E., Furth, E. E., Batshaw, M. L., & Wilson, J. M. (2006). Analysis of tumors arising in male B6C3F1 mice with and without AAV vector delivery to liver. *Molecular Therapy*, *14*(1), 34–44.

Bell, P., Wang, L., Lebherz, C., Flieder, D. B., Bove, M. S., Wu, D., Gao, G. P., Wilson, J. M., & Wivel, N. A. (2005). No evidence for tumorigenesis of AAV vectors in a large-scale study in mice. *Molecular Therapy*, *12*(2), 299–306.

Bennett, M. J., & Rakheja, D. (2013). The neuronal ceroid-lipofuscinoses. *Developmental Disabilities Research Reviews*, *17*(3), 254–259.

Benussi, L., Binetti, G., Sina, E., Gigola, L., Bettecken, T., Meitinger, T., & Ghidoni, R. (2008). A novel deletion in progranulin gene is associated with FTDP-17 and CBS. *Neurobiology of Aging*, *29*(3), 427–435.

Berns, K. I., Byrne, B. J., Flotte, T. R., Gao, G., Hauswirth, W. W., Herzog, R. W., Muzyczka, N., VandenDriessche, T., Xiao, X., Zolotukhin, S., & Srivastava, A. (2015). Adeno-associated virus type 2 and hepatocellular carcinoma? *Human Gene Therapy*, *26*(12), 779–781.

Bessa, C., Teixeira, C. A. F., Mangas, M., Dias, A., Sá Miranda, M. C., Guimarães, A., Ferreira, J. C., Canas, N., Cabral, P., & Ribeiro, M. G. (2006). Two novel CLN5 mutations in a Portuguese patient with vLINCL: insights into molecular mechanisms of CLN5 deficiency. *Molecular Genetics and Metabolism*, *89*(3), 245–253.

Bevan, A. K., Duque, S., Foust, K. D., Morales, P. R., Braun, L., Schmelzer, L., Chan, C. M., McCrate, M., Chicoine, L. G., Coley, B. D., Porensky, P. N., Kolb, S. J., Mendell, J. R., Burghes, A. H., & Kaspar, B. K. (2011). Systemic gene delivery in large species for targeting spinal cord, brain, and peripheral tissues for pediatric disorders. *Molecular Therapy*, *19*(11), 1971–1980.

Bible, E., Gupta, P., Hofmann, S. L., & Cooper, J. D. (2004). Regional and cellular neuropathology in the palmitoyl protein thioesterase-1 null mutant mouse model of infantile neuronal ceroid lipofuscinosis. *Neurobiology of Disease*, *16*(2), 346–359.

Biffi, A. (2015). Gene therapy for lysosomal storage disorders: a good start. *Human Molecular Genetics*, *25*(R1), R65–R75.

Biffi, A., Montini, E., Lorioli, L., Cesani, M., Fumagalli, F., Plati, T., Baldoli, C., Martino, S., Calabria, A., Canale, S., Benedicenti, F., Vallanti, G., Biasco, L., Leo, S., Kabbara, N., Zanetti, G., Rizzo, W. B., Mehta, N. A. L., Cicalese, M. P., Casiraghi, M., Boelens, J. J., Del Carro, U., Dow, D. J., Schmidt, M., Assanelli, A., Neduva, V., Di Serio, C., Stupka, E., Gardner, J., von Kalle, C., Bordignon, C., Ciceri, F., Rovelli, A., Roncarolo, M. G., Aiuti, A., Sessa, M., & Naldini, L. (2013). Lentiviral hematopoietic stem cell gene therapy benefits metachromatic leukodystrophy. *Science*, *341*(6148), 1233158.

Bildfell, R., Matwichuk, C., Mitchell, S., & Ward, P. (1995). Neuronal ceroid-lipofuscinosis in a cat. *Veterinary Pathology*, *32*(5), 485–488.

Block, M. L., & Hong, J.-S. (2005). Microglia and inflammation-mediated neurodegeneration: Multiple triggers with a common mechanism. *Progress in Neurobiology*, *76*(2), 77–98.

Blömer, U., Naldini, L., Kafri, T., Trono, D., Verma, I. M., & Gage, F. H. (1997). Highly efficient and sustained gene transfer in adult neurons with a lentivirus vector. *Journal of Virology*, *71*(9), 6641–6649.

Blumkin, L., Kivity, S., Lev, D., Cohen, S., Shomrat, R., Lerman-Sagie, T., & Leshinsky-Silver, E. (2012). A compound heterozygous missense mutation and a large deletion in the KCTD7 gene presenting as an opsoclonus-myoclonus ataxia-like syndrome. *Journal of Neurology*, *259*(12), 2590–2598.

Bond, M., Holthaus, S.-M. K., Tammen, I., Tear, G., & Russell, C. (2013). Use of model organisms for the study of neuronal ceroid lipofuscinosis. *Biochimica et Biophysica Acta*, *1832*(11), 1842–1865.

Bosch, A., Perret, E., Desmaris, N., Trono, D., & Heard, J. M. (2000). Reversal of pathology in the entire brain of mucopolysaccharidosis type VII mice after lentivirus-mediated gene transfer. *Human Gene Therapy*, *11*(8), 1139–1150.

Bosch, M. E., & Kielian, T. (2015). Neuroinflammatory paradigms in lysosomal storage diseases. *Frontiers in Neuroscience*, *9*, 417.

Bostick, B., Ghosh, A., Yue, Y., Long, C., & Duan, D. (2007). Systemic AAV-9 transduction in mice is influenced by animal age but not by the route of administration. *Gene Therapy*, *14*(22), 1605–1609.

Bostwick, J. L. (1982). Copper toxicosis in sheep. *Journal of the American Veterinary Medical Association*, *180*(4), 386–387.

Bourke, C. A., Carrigan, M. J., & Dent, C. H. (1993). Chronic locomotor dysfunction, associated with a thalamic-cerebellar neuropathy, in Australian merino sheep. *Australian Veterinary Journal*, *70*(6), 232–233.

Boutin, S., Monteilhet, V., Veron, P., Leborgne, C., Benveniste, O., Montus, M. F., & Masurier, C.

(2010). Prevalence of serum IgG and neutralizing factors against adeno-associated virus (AAV) types 1, 2, 5, 6, 8, and 9 in the healthy population: implications for gene therapy using AAV vectors. *Human Gene Therapy*, *21*(6), 704–712.

Braak, H., & Goebel, H. H. (1979). Pigmentoarchitectonic pathology of the isocortex in juvenile neuronal ceroid-lipofuscinosis: axonal enlargements in layer IIIab and cell loss in layer V. *Acta Neuropathologica*, *46*(1-2), 79–83.

Bradley, R., & Terlecki, S. (1977). Muscle lesions in hereditary “daft lamb” disease of Border Leicester sheep. *The Journal of Pathology*, *123*(4), 225–236.

Bras, J., Verloes, A., Schneider, S., Mole, S., & Guerreiro, R. (2012). Mutation of the parkinsonism gene ATP13A2 causes neuronal ceroid-lipofuscinosis. *Human Molecular Genetics*, *21*(12), 2646–2650.

Bronson, R. T., Donahue, L. R., Johnson, K. R., Tanner, A., Lane, P. W., & Faust, J. R. (1998). Neuronal ceroid lipofuscinosis (nclf), a new disorder of the mouse linked to chromosome 9. *American Journal of Medical Genetics*, *77*(4), 289–297.

Bronson, R. T., Lake, B. D., Cook, S., Taylor, S., & Davisson, M. T. (1993). Motor neuron degeneration of mice is a model of neuronal ceroid lipofuscinosis (Batten’s disease). *Annals of Neurology*, *33*(4), 381–385.

Brooks, A. I., Stein, C. S., Hughes, S. M., Heth, J., McCray, P. M. J., Sauter, S. L., Johnston, J. C., Cory-Slechta, D. A., Federoff, H. J., & Davidson, B. L. (2002). Functional correction of established central nervous system deficits in an animal model of lysosomal storage disease with feline immunodeficiency virus-based vectors. *Proceedings of the National Academy of Sciences of the United States of America*, *99*(9), 6216–6221.

Broom, M. F., Zhou, C., Broom, J. E., Barwell, K. J., Jolly, R. D., & Hill, D. F. (1998). Ovine neuronal ceroid lipofuscinosis: a large animal model syntenic with the human neuronal ceroid lipofuscinosis variant CLN6. *Journal of Medical Genetics*, *35*(9), 717–721.

Brus, M., Meurisse, M., Franceschini, I., Keller, M., & Lévy, F. (2010). Evidence for cell proliferation in the sheep brain and its down-regulation by parturition and interactions with the young. *Hormones and Behavior*, *58*(5), 737–746.

Brus, M., Meurisse, M., Gheusi, G., Keller, M., Lledo, P. M., & Lévy, F. (2013). Dynamics of olfactory and hippocampal neurogenesis in adult sheep. *The Journal of Comparative Neurology*, *521*(1), 169–188.

Bucher, T., Dubreil, L., Colle, M.-A., Maquigneau, M., Deniaud, J., Ledevin, M., Moullier, P., & Joussemet, B. (2014). Intracisternal delivery of AAV9 results in oligodendrocyte and motor neuron transduction in the whole central nervous system of cats. *Gene Therapy*, *21*(5), 1–7.

Buller, R. M., Janik, J. E., Sebring, E. D., & Rose, J. A. (1981). Herpes simplex virus types 1 and 2 completely help adenovirus-associated virus replication. *Journal of Virology*, *40*(1), 241–247.

Burger, C., Gorbatyuk, O. S., Velardo, M. J., Peden, C. S., Williams, P., Zolotukhin, S., Reier, P. J., Mandel, R. J., & Muzyczka, N. (2004). Recombinant AAV viral vectors pseudotyped with viral capsids from serotypes 1, 2, and 5 display differential efficiency and cell tropism after delivery to different regions of the central nervous system. *Molecular Therapy*, *10*(2), 302–317.

Cabrera-Salazar, M. a, Roskelley, E. M., Bu, J., Hodges, B. L., Yew, N., Dodge, J. C., Shihabuddin, L. S., Sohar, I., Sleat, D. E., Scheule, R. K., Davidson, B. L., Cheng, S. H., Lobel, P., & Passini, M. a. (2007). Timing of therapeutic intervention determines functional and survival outcomes in a mouse model of late infantile Batten disease. *Molecular Therapy*, *15*(10), 1782–1788.

Calcedo, R., Vandenberghe, L. H., Gao, G., Lin, J., & Wilson, J. M. (2009). Worldwide epidemiology of neutralizing antibodies to adeno-associated viruses. *The Journal of Infectious Diseases*, *199*(3), 381–390.

Cannelli, N., Garavaglia, B., Simonati, A., Aiello, C., Barzaghi, C., Pezzini, F., Cilio, M. R., Biancheri, R., Morbin, M., Dalla Bernardina, B., Granata, T., Tessa, A., Invernizzi, F., Pessagno, A., Boldrini, R., Zibordi, F., Grazian, L., Claps, D., Carrozzo, R., Mole, S. E., Nardocci, N., & Santorelli, F. M. (2009). Variant late infantile ceroid lipofuscinoses associated with novel mutations in CLN6. *Biochemical and Biophysical Research Communications*, *379*(4), 892–897.

Cassin, B., & Rubin, M. L. (Eds.). (2011). *Dictionary of Eye Terminology* (6th Edition). Gainesville, Florida, USA: Triad Publishing Company.

Castle, M. J., Gershenson, Z. T., Giles, A. R., Holzbaur, E. L. F., & Wolfe, J. H. (2014). Adeno-associated virus serotypes 1, 8, and 9 share conserved mechanisms for anterograde and retrograde axonal transport. *Human Gene Therapy*, *25*(8), 705–720.

Cattoglio, C., Facchini, G., Sartori, D., Antonelli, A., Miccio, A., Cassani, B., Schmidt, M., von Kalle, C., Howe, S., Thrasher, A. J., Aiuti, A., Ferrari, G., Recchia, A., & Mavilio, F. (2007). Hot spots of retroviral integration in human CD34+ hematopoietic cells. *Blood*, *110*(6), 1770–1778.

Cavazzana-Calvo, M., Hacein-Bey, S., de Saint Basile, G., Gross, F., Yvon, E., Nusbaum, P., Selz, F., Hue, C., Certain, S., Casanova, J. L., Bousso, P., Deist, F. L., & Fischer, A. (2000). Gene therapy of human severe combined immunodeficiency (SCID)-X1 disease. *Science*, *288*(5466), 669–672.

Cearley, C. N., & Wolfe, J. H. (2006). Transduction characteristics of adeno-associated virus vectors expressing cap serotypes 7, 8, 9, and rh10 in the mouse brain. *Molecular Therapy*, *13*(2), 528–537.

Cearley, C. N., & Wolfe, J. H. (2007). A single injection of an adeno-associated virus vector into nuclei with divergent connections results in widespread vector distribution in the brain and global correction of a neurogenetic disease. *The Journal of Neuroscience*, *27*(37), 9928–9940.

Cenik, B., Sephton, C. F., Kutluk Cenik, B., Herz, J., & Yu, G. (2012). Progranulin: a proteolytically processed protein at the crossroads of inflammation and neurodegeneration. *The Journal of Biological Chemistry*, *287*(39), 32298–32306.

Cesta, M. F., Mozzachio, K., Little, P. B., Olby, N. J., Sills, R. C., & Brown, T. T. (2006). Neuronal ceroid lipofuscinosis in a Vietnamese pot-bellied pig (Sus scrofa). *Veterinary Pathology*, *43*(4), 556–560.

Cetin, A., Komai, S., Eliava, M., Seeburg, P. H., & Osten, P. (2006). Stereotaxic gene delivery in the rodent brain. *Nature Protocols*, *1*(6), 3166–3173.

Chang, R., Liu, X., Li, S., & Li, X.-J. (2015). Transgenic animal models for study of the pathogenesis of Huntington's disease and therapy. *Drug Design, Development and Therapy*, *9*, 2179–2188.

Chen, J. Z. (2016). *A molecular dissection of neuroinflammation in ovine Batten disease*. PhD thesis, Lincoln University, Lincoln, New Zealand.

Cideciyan, A. V, Hauswirth, W. W., Aleman, T. S., Kaushal, S., Schwartz, S. B., Boye, S. L., Windsor, E. A. M., Conlon, T. J., Sumaroka, A., Pang, J.-J., Roman, A. J., Byrne, B. J., & Jacobson, S. G. (2009). Human RPE65 gene therapy for Leber congenital amaurosis: persistence of early visual improvements and safety at 1 year. *Human Gene Therapy*, *20*(9), 999–1004.

Ciesielska, A., Hadaczek, P., Mittermeyer, G., Zhou, S., Wright, J. F., Bankiewicz, K. S., & Forsayeth, J. (2013). Cerebral infusion of AAV9 vector-encoding non-self proteins can elicit cell-mediated immune responses. *Molecular Therapy*, *21*(1), 158–166.

Clark, K.R., Liu, X., McGrath, J.P & Johnson, P.R. (1999). Highly purified recombinant adeno-associated virus vectors are biologically active and free of detectable helper and wild-type viruses. *Human Gene Therapy,10*(6), 1031-1039.

Clément, N., Knop, D. R., & Byrne, B. J. (2009). Large-scale adeno-associated viral vector production using a herpesvirus-based system enables manufacturing for clinical studies. *Human Gene Therapy*, *20*(8), 796–806.

Consiglio, A., Quattrini, A., Martino, S., Bensadoun, J. C., Dolcetta, D., Trojani, A., Benaglia, G., Marchesini, S., Cestari, V., Oliverio, A., Bordignon, C., & Naldini, L. (2001). In vivo gene therapy of metachromatic leukodystrophy by lentiviral vectors: correction of neuropathology and protection against learning impairments in affected mice. *Nature Medicine*, *7*(3), 310–316.

Conway, J. E., Zolotukhin, S., Muzyczka, N., Hayward, G. S., & Byrne, B. J. (1997). Recombinant adeno-associated virus type 2 replication and packaging is entirely supported by a herpes simplex virus type 1 amplicon expressing Rep and Cap. *Journal of Virology*, *71*(11), 8780–8789.

Cook, R. W., Jolly, R. D., Palmer, D. N., Tammen, I., Broom, M. F., & McKinnon, R. (2002). Neuronal ceroid lipofuscinosis in Merino sheep. *Australian Veterinary Journal*, *80*(5), 292–297.

Cooper, J. D. (2010). The neuronal ceroid lipofuscinoses: the same, but different? *Biochemical Society Transactions*, *38*(6), 1448–1452.

Cooper, J. D., Messer, A., Feng, A. K., Chua-Couzens, J., & Mobley, W. C. (1999). Apparent loss and hypertrophy of interneurons in a mouse model of neuronal ceroid lipofuscinosis: evidence for partial response to insulin-like growth factor-1 treatment. *The Journal of Neuroscience*, *19*(7), 2556–2567.

Cooper, J. D., Russell, C., & Mitchison, H. M. (2006). Progress towards understanding disease mechanisms in small vertebrate models of neuronal ceroid lipofuscinosis. *Biochimica et Biophysica Acta*, *1762*(10), 873–889.

Cordy, D. R., Richards, W. P., & Bradford, G. E. (1967). Systemic neuroaxonal dystrophy in Suffolk sheep. *Acta Neuropathologica*, *8*(2), 133–140.

Cotman, S. L., Karaa, A., Staropoli, J. F., & Sims, K. B. (2013). Neuronal Ceroid Lipofuscinosis: Impact of recent genetic advances and expansion of the clinicopathologic spectrum. *Current Neurology and Neuroscience Reports*, *13*(8), 366.

Coutelle, C. (2008). Why bother? Is in utero gene therapy worth the effort? *Molecular Therapy*, *16*(2),

219–220.

Cronin, J., Zhang, X.-Y., & Reiser, J. (2005). Altering the tropism of lentiviral vectors through pseudotyping. *Current Gene Therapy*, *5*(4), 387–398.

Crystal, R. G. (2014). Gene therapy for the CNS manifestations of the lysosomal storage disorders. 14th International Conference on Neuronal Ceroid Lipofuscinoses (Batten disease). Hotel Sheraton, Cordoba, Argentina, 22 Oct 2014 - 26 Oct 2014, *Medicina*, *74*(Suppl II, L-5), 12.

Crystal, R. G., Sondhi, D., Hackett, N. R., Kaminsky, S. M., Worgall, S., Stieg, P., Souweidane, M., Hosain, S., Heier, L., Ballon, D., Dinner, M., Wisniewski, K., Kaplitt, M., Greenwald, B. M., Howell, J. D., Strybing, K., Dyke, J., & Voss, H. (2004). Clinical protocol. Administration of a replication-deficient adeno-associated virus gene transfer vector expressing the human CLN2 cDNA to the brain of children with late infantile neuronal ceroid lipofuscinosis. *Human Gene Therapy*, *15*(11), 1131–1154.

Cudeiro, J., & Sillito, A. M. (2006). Looking back: corticothalamic feedback and early visual processing. *Trends in Neurosciences*, *29*(6), 298–306.

Cummings, J. L., & Trimble, M. R. (Eds.). (1995). *Concise Guide to Neuropsychiatry and Behavioral Neurology* (2nd Edition). Washington DC, USA: American Psychiatric Publishing Inc.

Curtis, M. A., Penney, E. B., Pearson, A. G., van Roon-Mom, W. M. C., Butterworth, N. J., Dragunow, M., Connor, B., & Faull, R. L. M. (2003). Increased cell proliferation and neurogenesis in the adult human Huntington's disease brain. *Proceedings of the National Academy of Sciences of the United States of America*, *100*(15), 9023–9027.

Curtis, M. A., Penney, E. B., Pearson, J., Dragunow, M., Connor, B., & Faull, R. L. M. (2005). The distribution of progenitor cells in the subependymal layer of the lateral ventricle in the normal and Huntington's disease human brain. *Neuroscience*, *132*(3), 777–788.

Dahl, M., Doyle, A., Olsson, K., Månsson, J.-E., Marques, A. R., Mirzaian, M., Aerts, J. M., Ehinger, M., Rothe, M., Modlich, U., Schambach, A., & Karlsson, S. (2015). Lentiviral gene therapy using cellular promoters cures type 1 Gaucher disease in mice. *Molecular Therapy*, *23*(5), 835–844.

Dalkara, D., Kolstad, K. D., Caporale, N., Visel, M., Klimczak, R. R., Schaffer, D. V, & Flannery, J. G. (2009). Inner limiting membrane barriers to AAV-mediated retinal transduction from the vitreous. *Molecular Therapy*, *17*(12), 2096–2102.

Dalley, J. W., Cardinal, R. N., & Robbins, T. W. (2004). Prefrontal executive and cognitive functions in rodents: neural and neurochemical substrates. *Neuroscience & Biobehavioral Reviews*, *28*(7), 771–784.

David, A., Cook, T., Waddington, S., Peebles, D., Nivsarkar, M., Knapton, H., Miah, M., Dahse, T., Noakes, D., Schneider, H., Rodeck, C., Coutelle, C., & Themis, M. (2003). Ultrasound-guided percutaneous delivery of adenoviral vectors encoding the beta-galactosidase and human factor IX genes to early gestation fetal sheep in utero. *Human Gene Therapy*, *14*(4), 353–364.

David, A. L., McIntosh, J., Peebles, D. M., Cook, T., Waddington, S., Weisz, B., Wigley, V., Abi-Nader, K., Boyd, M., Davidoff, A. M., & Nathwani, A. C. (2011). Recombinant adeno-associated virus-mediated in utero gene transfer gives therapeutic transgene expression in the sheep. *Human Gene Therapy*, *22*(4), 419–426.

Davidson, B. L., Stein, C. S., Heth, J. A., Martins, I., Kotin, R. M., Derksen, T. A., Zabner, J., Ghodsi, A., & Chiorini, J. A. (2000). Recombinant adeno-associated virus type 2, 4, and 5 vectors: transduction of variant cell types and regions in the mammalian central nervous system. *Proceedings of the National Academy of Sciences of the United States of America*, *97*(7), 3428–3432.

Dayton, R. D., Wang, D. B., & Klein, R. L. (2012). The advent of AAV9 expands applications for brain and spinal cord gene delivery. *Expert Opinion on Biological Therapy*, *12*(6), 757–766.

Degabriele, R., & Fell, L. R. (2001). Changes in behaviour, cortisol and lymphocyte types during isolation and group confinement of sheep. *Immunology and Cell Biology*, *79*(6), 583–589.

Di Domenico, C., Villani, G. R. D., Di Napoli, D., Nusco, E., Calì, G., Nitsch, L., & Di Natale, P. (2009). Intracranial gene delivery of LV-NAGLU vector corrects neuropathology in murine MPS IIIB. *American Journal of Medical Genetics*, *149A*(6), 1209–1218.

Dihanich, S., Palmer, D. N., Oswald, M. J., Barry, L. A., Elleder, M., Williams, B., & Cooper, J. D. (2012). Clusters of newly generated neurons in the cortex of sheep and human CLN6 deficiency. *13th International Conference on Neuronal Ceroid Lipofuscinoses (Batten Disease)*. London, UK 28 -31 Mar 2012 (O20).

Dihanich, S., Palmer, D. N., Oswald, M. J., Williams, B. P., Schwartz, H., Kay, G., & Cooper, J. D. (2009). In vivo and in vitro evidence for adult neurogenesis in CLN6 sheep. *Proceedings of the 27th International Australasian Winter Conference on Brain Research*. Queenstown, New Zealand. 29 Aug - 2 Sep 2009 (Vol. 27, 8.5).

Doetsch, F., Caillé, I., Lim, D. A., García-Verdugo, J. M., & Alvarez-Buylla, A. (1999). Subventricular zone astrocytes are neural stem cells in the adult mammalian brain. *Cell*, *97*(6), 703–716.

Dolezalova, D., Hruska-Plochan, M., Bjarkam, C. R., Sørensen, J. C. H., Cunningham, M., Weingarten, D., Ciacci, J. D., Juhas, S., Juhasova, J., Motlik, J., Hefferan, M. P., Hazel, T., Johe, K., Carromeu, C., Muotri, A., Bui, J., Strnadel, J., & Marsala, M. (2014). Pig models of neurodegenerative disorders: Utilization in cell replacement-based preclinical safety and efficacy studies. *The Journal of Comparative Neurology*, *522*(12), 2784–2801.

Donsante, A., Miller, D. G., Li, Y., Vogler, C., Brunt, E. M., Russell, D. W., & Sands, M. S. (2007). AAV vector integration sites in mouse hepatocellular carcinoma. *Science, 317*(5837), 477.

Dufourny, L., Migaud, M., Thiery, J.-C., & Malpaux, B. (2008). Development of an in vivo adeno-associated virus-mediated siRNA approach to knockdown tyrosine hydroxylase in the lateral retrochiasmatic area of the ovine brain. *Journal of Neuroscience Methods*, *170*(1), 56–66.

Duque, S. I., Arnold, W. D., Odermatt, P., Li, X., Porensky, P. N., Schmelzer, L., Meyer, K., Kolb, S. J., Schümperli, D., Kaspar, B. K., & Burghes, A. H. M. (2015). A large animal model of spinal muscular atrophy and correction of phenotype. *Annals of Neurology*, *77*(3), 399–414.

Duque, S., Joussemet, B., Riviere, C., Marais, T., Dubreil, L., Douar, A.-M., Fyfe, J., Moullier, P., Colle, M.-A., & Barkats, M. (2009). Intravenous administration of self-complementary AAV9 enables transgene delivery to adult motor neurons. *Molecular Therapy*, *17*(7), 1187–1196.

Edwards, J. F., Storts, R. W., Joyce, J. R., Shelton, J. M., & Menzies, C. S. (1994). Juvenile-onset neuronal ceroid-lipofuscinosis in Rambouillet sheep. *Veterinary Pathology*, *31*(1), 48–54.

Eikelenboom, P., Veerhuis, R., Scheper, W., Rozemuller, A. J. M., van Gool, W. A., & Hoozemans, J. J. M. (2006). The significance of neuroinflammation in understanding Alzheimer's disease. *Journal of Neural Transmission (Vienna, Austria : 1996)*, *113*(11), 1685–1695.

Ella, A., & Keller, M. (2015). Construction of an MRI 3D high resolution sheep brain template. *Magnetic Resonance Imaging*, *33*(10), 1329–1337.

Elleder, M., Franc, J., Kraus, J., Nevsímalová, S., Sixtová, K., & Zeman, J. (1997). Neuronal ceroid lipofuscinosis in the Czech Republic: analysis of 57 cases. Report of the "Prague NCL group". *European Journal of Paediatric Neurology*, *1*(4), 109–114.

Eriksson, P. S., Perfilieva, E., Björk-Eriksson, T., Alborn, A. M., Nordborg, C., Peterson, D. A., & Gage, F. H. (1998). Neurogenesis in the adult human hippocampus. *Nature Medicine*, *4*(11), 1313–1317.

Ezaki, J., Takeda-Ezaki, M., Koike, M., Ohsawa, Y., Taka, H., Mineki, R., Murayama, K., Uchiyama, Y., Ueno, T., & Kominami, E. (2003). Characterization of Cln3p, the gene product responsible for juvenile neuronal ceroid lipofuscinosis, as a lysosomal integral membrane glycoprotein. *Journal of Neurochemistry*, *87*(5), 1296–1308.

Ezaki, J., Takeda-Ezaki, M., & Kominami, E. (2000). Tripeptidyl peptidase I, the late infantile neuronal ceroid lipofuscinosis gene product, initiates the lysosomal degradation of subunit c of ATP synthase. *Journal of Biochemistry*, *128*(3), 509–516.

Fabritius, A.-L., Vesa, J., Minye, H. M., Nakano, I., Kornblum, H., & Peltonen, L. (2014). Neuronal ceroid lipofuscinosis genes, CLN2, CLN3 and CLN5 are spatially and temporally co-expressed in a developing mouse brain. *Experimental and Molecular Pathology*, *97*(3), 484–491.

Farfel-Becker, T., Vitner, E. B., & Futerman, A. H. (2011). Animal models for Gaucher disease research. *Disease Models & Mechanisms*, *4*(6), 746–752.

Faust, J. R., Rodman, J. S., Daniel, P. F., Dice, J. F., & Bronson, R. T. (1994). Two related proteolipids and dolichol-linked oligosaccharides accumulate in motor neuron degeneration mice (mnd/mnd), a model for neuronal ceroid lipofuscinosis. *The Journal of Biological Chemistry*, *269*(13), 10150–10155.

Fearnley, I. M., Walker, J. E., Martinus, R. D., Jolly, R. D., Kirkland, K. B., Shaw, G. J., & Palmer, D. N. (1990). The sequence of the major protein stored in ovine ceroid lipofuscinosis is identical with that of the dicyclohexylcarbodiimide-reactive proteolipid of mitochondrial ATP synthase. *The Biochemical Journal*, *268*(3), 751–758.

Federici, T., Taub, J. S., Baum, G. R., Gray, S. J., Grieger, J. C., Matthews, K. A., Handy, C. R., Passini, M. A., Samulski, R. J., & Boulis, N. M. (2012). Robust spinal motor neuron transduction following intrathecal delivery of AAV9 in pigs. *Gene Therapy*, *19*(8), 852–859.

Fell, L., Lynch, J., Adams, D., Hinch, G., Munro, R., & Davies, H. (1991). Behavioural and physiological effects in sheep of a chronic stressor and a parasite challenge. *Australian Journal of Agricultural Research*, *42*, 1335–1346.

Fernández-Chacón, R., Wölfel, M., Nishimune, H., Tabares, L., Schmitz, F., Castellano-Muñoz, M., Rosenmund, C., Montesinos, M. L., Sanes, J. R., Schneggenburger, R., & Südhof, T. C. (2004). The synaptic vesicle protein CSP alpha prevents presynaptic degeneration. *Neuron*, *42*(2), 237–251.

Finnie, J. W., Jerrett, I. V, Manavis, J., & Cave, J. (2014). Neuroaxonal dystrophy in Merino-Border Leicester × Polled Dorset lambs. *Australian Veterinary Journal*, *92*(10), 389–391.

Fiske, R. A., & Storts, R. W. (1988). Neuronal ceroid-lipofuscinosis in Nubian goats. *Veterinary Pathology*, *25*(2), 171–173.

Fossale, E., Wolf, P., Espinola, J. A., Lubicz-Nawrocka, T., Teed, A. M., Gao, H., Rigamonti, D., Cattaneo, E., MacDonald, M. E., & Cotman, S. L. (2004). Membrane trafficking and mitochondrial abnormalities precede subunit c deposition in a cerebellar cell model of juvenile neuronal ceroid lipofuscinosis. *BMC Neuroscience*, *5*, 57.

Foust, K. D., Nurre, E., Montgomery, C. L., Hernandez, A., Chan, C. M., & Kaspar, B. K. (2009). Intravascular AAV9 preferentially targets neonatal-neurons and adult-astrocytes in CNS. *Nature Biotechnology*, *27*(1), 59–65.

Fratantoni, J. C., Hall, C. W., & Neufeld, E. F. (1968). Hurler and Hunter syndromes: mutual correction of the defect in cultured fibroblasts. *Science*, *162*(3853), 570–572.

Frugier, T., Mitchell, N. L., Tammen, I., Houweling, P. J., Arthur, D. G., Kay, G. W., van Diggelen, O. P., Jolly, R. D., & Palmer, D. N. (2008). A new large animal model of CLN5 neuronal ceroid lipofuscinosis in Borderdale sheep is caused by a nucleotide substitution at a consensus splice site (c.571+1G>A) leading to excision of exon 3. *Neurobiology of Disease*, *29*(2), 306–315.

Fu, H., Dirosario, J., Killedar, S., Zaraspe, K., & McCarty, D. M. (2011). Correction of neurological disease of mucopolysaccharidosis IIIB in adult mice by rAAV9 trans-blood-brain barrier gene delivery. *Molecular Therapy*, *19*(6), 1025–1033.

Fu, H., Kang, L., Jennings, J. S., Moy, S. S., Perez, A., Dirosario, J., McCarty, D. M., & Muenzer, J. (2007). Significantly increased lifespan and improved behavioral performances by rAAV gene delivery in adult mucopolysaccharidosis IIIB mice. *Gene Therapy*, *14*(14), 1065–1077.

Fu, H., Muenzer, J., Samulski, R. J., Breese, G., Sifford, J., Zeng, X., & McCarty, D. M. (2003). Self-complementary adeno-associated virus serotype 2 vector: Global distribution and broad dispersion of AAV-mediated transgene expression in mouse brain. *Molecular Therapy 8*(6), 911–917.

Fuller, M, Meikle, P., & Hopwood, J. (Eds.). (2006). *Epidemiology of Lysosomal Storage Diseases: An overview*. Oxford, UK: Oxford PharmaGenesis.

Furmston, T., Morton, A. J., & Hailes, S. (2015). A significance test for inferring affiliation networks from spatio-temporal data. *PLoS ONE*, *10*(7), e0132417.

Gage, F. (2000). Mammalian neural stem cells. *Science*, *287*(5457), 1433–1438.

Gao, H., Boustany, R.-M. N., Espinola, J. A., Cotman, S. L., Srinidhi, L., Antonellis, K. A., Gillis, T., Qin, X., Liu, S., Donahue, L. R., Bronson, R. T., Faust, J. R., Stout, D., Haines, J. L., Lerner, T. J., & Macdonald, M. E. (2002). Mutations in a novel CLN6-encoded transmembrane protein cause variant neuronal ceroid lipofuscinosis in man and mouse. *American Journal of Human Genetics*, *70*(2), 324–335.

Gaspar, H. B., Parsley, K. L., Howe, S., King, D., Gilmour, K. C., Sinclair, J., Brouns, G., Schmidt, M., Von Kalle, C., Barington, T., Jakobsen, M. A., Christensen, H. O., Al Ghonaium, A., White, H. N.,

Smith, J. L., Levinsky, R. J., Ali, R. R., Kinnon, C., & Thrasher, A. J. (2004). Gene therapy of X-linked severe combined immunodeficiency by use of a pseudotyped gammaretroviral vector. *Lancet*, *364*(9452), 2181–2187.

Ghodsi, A., Stein, C., Derksen, T., Martins, I., Anderson, R. D., & Davidson, B. L. (1999). Systemic hyperosmolality improves beta-glucuronidase distribution and pathology in murine MPS VII brain following intraventricular gene transfer. *Experimental Neurology*, *160*(1), 109–116.

Gieselmann, V. (2008). Metachromatic leukodystrophy: genetics, pathogenesis and therapeutic options. *Acta Paediatrica*, *97*(457), 15–21.

Gilliam, D., Kolicheski, A., Johnson, G. S., Mhlanga-Mutangadura, T., Taylor, J. F., Schnabel, R. D., & Katz, M. L. (2015). Golden Retriever dogs with neuronal ceroid lipofuscinosis have a two-base-pair deletion and frameshift in CLN5. *Molecular Genetics and Metabolism*, *115*(2-3), 101–109.

Goebel, H. H. (1992). Retina in various animal models of neuronal ceroid-lipofuscinosis. *American Journal of Medical Genetics*, *42*(4), 605–608.

Goebel, H. H., Schochet, S. S., Jaynes, M., Brück, W., Kohlschütter, A., & Hentati, F. (1999). Progress in neuropathology of the neuronal ceroid lipofuscinoses. *Molecular Genetics and Metabolism*, *66*(4), 367–372.

Goebel, H. H., Zeman, W., & Damaske, E. (1977). An ultrastructural study of the retina in the Jansky-Bielschowsky type of neuronal ceroid-lipofuscinosis. *American Journal of Ophthalmology*, *83*(1), 70–79.

Gonçalves, M. A. F. V. (2005). Adeno-associated virus: from defective virus to effective vector. *Virology Journal*, *2*, 43.

Granger, R. H., & Hearn, R. A. (2007). Models of thalamocortical system. *Scholarpedia*, *2*(11), 1796.

Gray, S. J., Kalburgi, S. N., McCown, T. J., & Samulski, R. J. (2013). Global CNS gene gelivery and evasion of anti-AAV neutralizing antibodies by intrathecal AAV administration in non-human primates. *Gene Therapy*, *20*(4), 450–459.

Gray, S. J., Matagne, V., Bachaboina, L., Yadav, S., Ojeda, S. R., & Samulski, R. J. (2011). Preclinical differences of intravascular AAV9 delivery to neurons and glia: A comparative study of adult mice and nonhuman primates. *Molecular Therapy*, *19*(6), 1058–1069.

Gray, S. J., & Samulski, R. J. (2011). Vector design and considerations for CNS applications. In: *Gene Vector Design and Application to Treat Nervous System Disorders.* Glorioso, J. (Ed.), (pp. 1–9). Washington DC, USA: Society for Neuroscience.

Graydon, R. J., & Jolly, R. D. (1984). Ceroid-lipofuscinosis (Batten's disease). Sequential electrophysiologic and pathologic changes in the retina of the ovine model. *Investigative Ophthalmology & Visual Science*, *25*(3), 294–301.

Green, P. D., & Little, P. B. (1974). Neuronal ceroid-lipofuscin storage in Siamese cats. *Canadian Journal of Comparative Medicine*, *38*(2), 207–212.

Greig, L. C., Woodworth, M. B., Galazo, M. J., Padmanabhan, H., & Macklis, J. D. (2013). Molecular logic of neocortical projection neuron specification, development and diversity. *Nature Reviews Neuroscience*, *14*(11), 755–769.

Griffey, M. A., Bible, E., Vogler, C., Levy, B., Gupta, P., Cooper, J., & Sands, M. S. (2004). Adeno-associated virus 2-mediated gene therapy decreases autofluorescent storage material and increases brain mass in a murine model of infantile neuronal ceroid lipofuscinosis. *Neurobiology of Disease*, *16*(2), 360–369.

Griffey, M., Macauley, S. L., Ogilvie, J. M., & Sands, M. S. (2005). AAV2-mediated ocular gene therapy for infantile neuronal ceroid lipofuscinosis. *Molecular Therapy*, *12*(3), 413–421.

Griffey, M. A., Wozniak, D., Wong, M., Bible, E., Johnson, K., Rothman, S. M., Wentz, A. E., Cooper, J. D., & Sands, M. S. (2006). CNS-directed AAV2-mediated gene therapy ameliorates functional deficits in a murine model of infantile neuronal ceroid lipofuscinosis. *Molecular Therapy* , *13*(3), 538–547.

Hacein-Bey-Abina, S., Von Kalle, C., Schmidt, M., McCormack, M. P., Wulffraat, N., Leboulch, P., Lim, A., Osborne, C. S., Pawliuk, R., Morillon, E., Sorensen, R., Forster, A., Fraser, P., Cohen, J. I., de Saint Basile, G., Alexander, I., Wintergerst, U., Frebourg, T., Aurias, A., Stoppa-Lyonnet, D., Romana, S., Radford-Weiss, I., Gross, F., Valensi, F., Delabesse, E., Macintyre, E., Sigaux, F., Soulier, J., Leiva, L. E., Wissler, M., Prinz, C., Rabbitts, T. H., Le Deist, F., Fischer, A., & Cavazzana-Calvo, M. (2003). LMO2-associated clonal T cell proliferation in two patients after gene therapy for SCID-X1. *Science*, *302*(5644), 415–419.

Hackett, N. R., Redmond, D. E., Sondhi, D., Giannaris, E. L., Vassallo, E., Stratton, J., Qiu, J., Kaminsky, S. M., Lesser, M. L., Fisch, G. S., Rouselle, S. D., & Crystal, R. G. (2005). Safety of direct administration of AAV2(CU)hCLN2, a candidate treatment for the central nervous system manifestations of late infantile neuronal ceroid lipofuscinosis, to the brain of rats and nonhuman primates. *Human Gene Therapy*, *16*(12), 1484–1503.

Hafner, S., Flynn, T. E., Harmon, B. G., & Hill, J. E. (2005). Neuronal ceroid-lipofuscinosis in a Holstein steer. *Journal of Veterinary Diagnostic Investigation*, *17*(2), 194–197.

Hainsworth, D. P., Liu, G. T., Hamm, C. W., & Katz, M. L. (2009). Funduscopic and angiographic appearance in the neuronal ceroid lipofuscinoses. *Retina*, *29*(5), 657–668.

Haltia, M. (2003). The neuronal ceroid-lipofuscinoses. *Journal of Neuropathology and Experimental Neurology*, *62*(1), 1–13.

Haltia, M. (2006). The neuronal ceroid-lipofuscinoses: from past to present. *Biochimica et Biophysica Acta*, *1762*(10), 850–856.

Harper, P. A., Duncan, D. W., Plant, J. W., & Smeal, M. G. (1986). Cerebellar abiotrophy and segmental axonopathy: two syndromes of progressive ataxia of Merino sheep. *Australian Veterinary Journal*, *63*(1), 18–21.

Harper, P. A., & Morton, A. G. (1991). Neuroaxonal dystrophy in Merino sheep. *Australian Veterinary Journal*, *68*(4), 152–153.

Harper, P. A., Plant, J. W., Walker, K. H., & Timmins, K. G. (1991). Progressive ataxia associated with degenerative thoracic myelopathy in Merino sheep. *Australian Veterinary Journal*, *68*(11), 357–358.

Harper, P. A., Walker, K. H., Healy, P. J., Hartley, W. J., Gibson, A. J., & Smith, J. S. (1988). Neurovisceral ceroid-lipofuscinosis in blind Devon cattle. *Acta Neuropathologica*, *75*(6), 632–

636.

Haskell, R. E., Hughes, S. M., Chiorini, J. A., Alisky, J. M., & Davidson, B. L. (2003). Viral-mediated delivery of the late-infantile neuronal ceroid lipofuscinosis gene, TPP-I to the mouse central nervous system. *Gene Therapy*, *10*(1), 34–42.

Haurigot, V., Marcó, S., Ribera, A., Garcia, M., Ruzo, A., Villacampa, P., Ayuso, E., Añor, S., Andaluz, A., Pineda, M., García-Fructuoso, G., Molas, M., Maggioni, L., Muñoz, S., Motas, S., Ruberte, J., Mingozzi, F., Pumarola, M., & Bosch, F. (2013). Whole body correction of mucopolysaccharidosis IIIA by intracerebrospinal fluid gene therapy. *The Journal of Clinical Investigation*, *123*(8), 3254–3271.

Heine, C., Koch, B., Storch, S., Kohlschütter, A., Palmer, D. N., & Braulke, T. (2004). Defective endoplasmic reticulum-resident membrane protein CLN6 affects lysosomal degradation of endocytosed arylsulfatase A. *The Journal of Biological Chemistry*, *279*(21), 22347–22352.

Heine, C., Quitsch, A., Storch, S., Martin, Y., Lonka, L., Lehesjoki, A.-E., Mole, S. E., & Braulke, T. (2007). Topology and endoplasmic reticulum retention signals of the lysosomal storage disease-related membrane protein CLN6. *Molecular Membrane Biology*, *24*(1), 74–87.

Hennig, A. K., Ogilvie, J. M., Ohlemiller, K. K., Timmers, A. M., Hauswirth, W. W., & Sands, M. S. (2004). AAV-mediated intravitreal gene therapy reduces lysosomal storage in the retinal pigmented epithelium and improves retinal function in adult MPS VII mice. *Molecular Therapy*, *10*(1), 106–116.

Hinch, G., & Lynch, J. (1997). Comfortable quarters for sheep and goats. In: *Comfortable Quarters for Laboratory Animals.* Reinhardt, V. (Ed.), (pp. 94–100). Animal Welfare Institute, Washington DC, U.S.A.

Hinderer, C., Bell, P., Vite, C. H., Louboutin, J.-P., Grant, R., Bote, E., Yu, H., Pukenas, B., Hurst, R., & Wilson, J. M. (2014). Widespread gene transfer in the nervous system of cynomolgus macaques following delivery of AAV9 into the cisterna magna. *Molecular Therapy*, *1*, 14051.

Hironaka, K., Yamazaki, Y., Hirai, Y., Yamamoto, M., Miyake, N., Miyake, K., Okada, T., Morita, A., & Shimada, T. (2015). Enzyme replacement in the CSF to treat metachromatic leukodystrophy in mouse model using single intracerebroventricular injection of self-complementary AAV1 vector. *Scientific Reports*, *5*, 13104.

Ho, T. T., Maguire, A. M., Aguirre, G. D., Surace, E. M., Anand, V., Zeng, Y., Salvetti, A., Hopwood, J. J., Haskins, M. E., & Bennett, J. (2002). Phenotypic rescue after adeno-associated virus-mediated delivery of 4-sulfatase to the retinal pigment epithelium of feline mucopolysaccharidosis VI. *The Journal of Gene Medicine*, *4*(6), 613–621.

Hogan, K. G., Money, D. F. L., & Blayney, A. (1968). The effect of a molybdate and sulfate supplement on the accumulation of copper in the livers of penned sheep. *New Zealand Journal of Agricultural Research*, *11*, 435–444.

Holmberg, V., Jalanko, A., Isosomppi, J., Fabritius, A. L., Peltonen, L., & Kopra, O. (2004). The mouse ortholog of the neuronal ceroid lipofuscinosis CLN5 gene encodes a soluble lysosomal glycoprotein expressed in the developing brain. *Neurobiology of Disease*, *16*(1), 29–40.

Holmberg, V., Lauronen, L., Autti, T., Santavuori, P., Savukoski, M., Uvebrant, P., Hofman, I., Peltonen,

L., & Järvelä, I. (2000). Phenotype-genotype correlation in eight patients with Finnish variant late infantile NCL (CLN5). *Neurology*, *55*(4), 579–581.

Horner, P. J., & Gage, F. H. (2000). Regenerating the damaged central nervous system. *Nature*, *407*(6807), 963–970.

Houweling, P. J., Cavanagh, J. A. L., Palmer, D. N., Frugier, T., Mitchell, N. L., Windsor, P. A., Raadsma, H. W., & Tammen, I. (2006). Neuronal ceroid lipofuscinosis in Devon cattle is caused by a single base duplication (c.662dupG) in the bovine CLN5 gene. *Biochimica et Biophysica Acta*, *1762*(10), 890–897.

Howery, L. D., Bailey, D. W., & Laca, E. A. (1999). Impact of spatial memory on habitat use. In: *Grazing Behavior of Livestock and Wildlife.* Launchbaugh, K. L., Sanders, K. D. & Mosley, J. C. (Eds.), (pp. 91–100). Moscow, Idaho, USA: University of Idaho, Rangeland Ecology and Management.

Hughes, S. M., Hope, K. M., Xu, J. B., Mitchell, N. L., & Palmer, D. N. (2014a). Inhibition of storage pathology in prenatal CLN5-deficient sheep neural cultures by lentiviral gene therapy. *Neurobiology of Disease*, *62*, 543–550.

Hughes, S. M., Palmer, D. N., Schoderboeck, L., Mitchell, N. L., McIntyre, K., Haskell, R. E., Anderson, R.D., Wicky, H. E., & Xu, J. B. (2014b). New antibodies predict an interaction between CLN5 and CLN6. 14th International Conference on Neuronal Ceroid Lipofuscinoses (Batten disease). Hotel Sheraton, Cordoba, Argentina, 22 Oct 2014 - 26 Oct 2014, *Medicina, 74*(Supl II, O-49), 23.

Hunter, D. S., Hazel, S. J., Kind, K. L., Liu, H., Marini, D., Owens, J. A., Pitcher, J. B., & Gatford, K. L. (2015). Do I turn left or right? Effects of sex, age, experience and exit route on maze test performance in sheep. *Physiology & Behavior*, *139*, 244–253.

Innes, J. R. M., & MacNaughton, W. N. (1950). Inherited cortical cerebellar atrophy in Corriedale lambs in Canada identical with “daft lamb” disease in Britain. *The Cornell Veterinarian*, *40*(2), 127–135.

Isosomppi, J., Vesa, J., Jalanko, A., & Peltonen, L. (2002). Lysosomal localization of the neuronal ceroid lipofuscinosis CLN5 protein. *Human Molecular Genetics*, *11*(8), 885–891.

Jacobsen, J. C., Bawden, C. S., Rudiger, S. R., McLaughlan, C. J., Reid, S. J., Waldvogel, H. J., MacDonald, M. E., Gusella, J. F., Walker, S. K., Kelly, J. M., Webb, G. C., Faull, R. L. M., Rees, M. I., & Snell, R. G. (2010). An ovine transgenic Huntington’s disease model. *Human Molecular Genetics*, *19*(10), 1873–1882.

Jakobsson, J., Ericson, C., Jansson, M., Björk, E., & Lundberg, C. (2003). Targeted transgene expression in rat brain using lentiviral vectors. *Journal of Neuroscience Research*, *73*(6), 876–885.

Jakobsson, J., & Lundberg, C. (2006). Lentiviral vectors for use in the central nervous system. *Molecular Therapy*, *13*(3), 484–493.

Janson, C., McPhee, S., Bilaniuk, L., Haselgrove, J., Testaiuti, M., Freese, A., Wang, D.-J., Shera, D., Hurh, P., Rupin, J., Saslow, E., Goldfarb, O., Goldberg, M., Larijani, G., Sharrar, W., Liouterman, L., Camp, A., Kolodny, E., Samulski, J., & Leone, P. (2002). Clinical protocol. Gene therapy of Canavan disease: AAV-2 vector for neurosurgical delivery of aspartoacylase gene (ASPA) to the human brain. *Human Gene Therapy*, *13*(11), 1391–1412.

Järplid, B., & Haltia, M. (1993). An animal model of the infantile type of neuronal ceroid-lipofuscinosis. *Journal of Inherited Metabolic Disease*, *16*(2), 274–277.

Jarraya, B., Boulet, S., Ralph, G. S., Jan, C., Bonvento, G., Azzouz, M., Miskin, J. E., Shin, M., Delzescaux, T., Drouot, X., Hérard, A.-S., Day, D. M., Brouillet, E., Kingsman, S. M., Hantraye, P., Mitrophanous, K. A., Mazarakis, N. D., & Palfi, S. (2009). Dopamine gene therapy for Parkinson's disease in a nonhuman primate without associated dyskinesia. *Science Translational Medicine*, *1*(2), 2ra4.

Jeyakumar, M., Thomas, R., Elliot-Smith, E., Smith, D. A., van der Spoel, A. C., d'Azzo, A., Perry, V. H., Butters, T. D., Dwek, R. A., & Platt, F. M. (2003). Central nervous system inflammation is a hallmark of pathogenesis in mouse models of GM1 and GM2 gangliosidosis. *Brain*, *126*(Pt 4), 974–987.

Jian, J., Konopka, J., & Liu, C. (2013). Insights into the role of progranulin in immunity, infection, and inflammation. *Journal of Leukocyte Biology*, *93*(2), 199–208.

Jiang, Y., Xie, M., Chen, W., Talbot, R., Maddox, J. F., Faraut, T., Wu, C., Muzny, D. M., Li, Y., Zhang, W., Stanton, J.-A., Brauning, R., Barris, W. C., Hourlier, T., Aken, B. L., Searle, S. M. J., Adelson, D. L., Bian, C., Cam, G. R., Chen, Y., Cheng, S., DeSilva, U., Dixen, K., Dong, Y., Fan, G., Franklin, I. R., Fu, S., Fuentes-Utrilla, P., Guan, R., Highland, M. A., Holder, M. E., Huang, G., Ingham, A. B., Jhangiani, S. N., Kalra, D., Kovar, C. L., Lee, S. L., Liu, W., Liu, X., Lu, C., Lv, T., Mathew, T., McWilliam, S., Menzies, M., Pan, S., Robelin, D., Servin, B., Townley, D., Wang, W., Wei, B., White, S. N., Yang, X., Ye, C., Yue, Y., Zeng, P., Zhou, Q., Hansen, J. B., Kristiansen, K., Gibbs, R. A., Flicek, P., Warkup, C. C., Jones, H. E., Oddy, V. H., Nicholas, F. W., McEwan, J. C., Kijas, J. W., Wang, J., Worley, K. C., Archibald, A. L., Cockett, N., Xu, X., Wang, W., & Dalrymple, B. P. (2014). The sheep genome illuminates biology of the rumen and lipid metabolism. *Science, 344*(6188), 1168–1173.

Johnson, E. M., Traver, K. L., Hoffman, S. W., Harrison, C. R., & Herman, J. P. (2013). Environmental enrichment protects against functional deficits caused by traumatic brain injury. *Frontiers in Behavioral Neuroscience*, *7*, 44.

Johnstone, A. C., Johnson, C. B., Malcolm, K. E., & Jolly, R. D. (2005). Cerebellar cortical abiotrophy in Wiltshire sheep. *New Zealand Veterinary Journal*, *53*(4), 242–245.

Jolly, R. D., Arthur, D. G., Kay, G. W., & Palmer, D. N. (2002). Neuronal ceroid-lipofuscinosis in Borderdale sheep. *New Zealand Veterinary Journal*, *50*(5), 199–202.

Jolly, R. D., Gibson, A. J., Healy, P. J., Slack, P. M., & Birtles, M. J. (1992). Bovine ceroid-lipofuscinosis: pathology of blindness. *New Zealand Veterinary Journal*, *40*(3), 107–111.

Jolly, R. D., Hartley, W., Jones, B., Johnstone, A., Palmer, A., & Blakemore, W. (1994). Generalised ceroid-lipofuscinosis and brown bowel syndrome in Cocker spaniel dogs. *New Zealand Veterinary Journal*, *42*(6), 236–239.

Jolly, R. D., Janmaat, A., Graydon, R. J., & Clemett, R. S. (1982). Ovine ceroid-lipofuscinosis: The ovine model. In: *Ceroid Lipofuscinoses (Batten disease).* Armstrong, D., Koppang, N. & Rider J. A. (Eds.), (pp. 219–228). Amsterdam, The Netherlands: Elsevier Biomedical Press.

Jolly, R. D., Janmaat, A., West, D. M., & Morrison, I. (1980). Ovine ceroid-lipofuscinosis: a model of

Batten's disease. *Neuropathology and Applied Neurobiology*, *6*(3), 195–209.

Jolly, R. D., Shimada, A., Dopfmer, I., Slack, P. M., & Palmer, D. N. (1989). Ceroid-lipofuscinosis (Batten's disease): pathogenesis and sequential neuropathological changes in the ovine model. *Neuropathology and Applied Neurobiology*, *15*(4), 371–383.

Jolly, R. D., & West, D. M. (1976). Blindness in South Hampshire sheep: a neuronal ceroidlipofuscinosis. *New Zealand Veterinary Journal*, *24*(6), 123.

Kahn, C. M., & Line, S. (Eds.). (2014). *The Merck Veterinary Manual* (11th Edition). Merck & Co., Inc, Whitehouse Station, New Jersey, U.S.A.

Kaplan, A., Achord, D. T., & Sly, W. S. (1977). Phosphohexosyl components of a lysosomal enzyme are recognized by pinocytosis receptors on human fibroblasts. *Proceedings of the National Academy of Sciences of the United States of America*, *74*(5), 2026–2030.

Kaplitt, M. G., Feigin, A., Tang, C., Fitzsimons, H. L., Mattis, P., Lawlor, P. A., Bland, R. J., Young, D., Strybing, K., Eidelberg, D., & During, M. J. (2007). Safety and tolerability of gene therapy with an adeno-associated virus (AAV) borne GAD gene for Parkinson's disease: an open label, phase I trial. *Lancet*, *369*(9579), 2097–2105.

Karageorgos, L., Lancaster, M. J., Nimmo, J. S., & Hopwood, J. J. (2011). Gaucher disease in sheep. *Journal of Inherited Metabolic Disease*, *34*(1), 209–215.

Katz, M. L., Coates, J. R., Cooper, J. J., O'Brien, D. P., Jeong, M., & Narfström, K. (2008). Retinal pathology in a canine model of late infantile neuronal ceroid lipofuscinosis. *Investigative Ophthalmology & Visual Science*, *49*(6), 2686–2695.

Katz, M. L., Coates, J. R., Sibigtroth, C. M., Taylor, J. D., Carpentier, M., Young, W. M., Wininger, F. A., Kennedy, D., Vuillemenot, B. R., & O'Neill, C. A. (2014). Enzyme replacement therapy attenuates disease progression in a canine model of late-infantile neuronal ceroid lipofuscinosis (CLN2 disease). *Journal of Neuroscience Research*, *92*(11), 1591–1598.

Katz, M. L., Farias, F. H., Sanders, D. N., Zeng, R., Khan, S., Johnson, G. S., & O'Brien, D. P. (2011). A missense mutation in canine CLN6 in an Australian shepherd with neuronal ceroid lipofuscinosis. *Journal of Biomedicine & Biotechnology*, 198042.

Katz, M. L., Narfström, K., Johnson, G. S., & O'Brien, D. P. (2005). Assessment of retinal function and characterization of lysosomal storage body accumulation in the retinas and brains of Tibetan Terriers with ceroid-lipofuscinosis. *American Journal of Veterinary Research*, *66*(1), 67–76.

Katz, M. L., Tecedor, L., Chen, Y., Williamson, B. G., Lysenko, E., Wininger, F. A., Young, W. M., Johnson, G. C., Whiting, R. E. H., Coates, J. R., & Davidson, B. L. (2015). AAV gene transfer delays disease onset in a TPP1-deficient canine model of the late infantile form of Batten disease. *Science Translational Medicine*, *7*(313), 313ra180.

Kay, G. W., Hughes, S. M., & Palmer, D. N. (1999). In vitro culture of neurons from sheep with Batten disease. *Molecular Genetics and Metabolism*, *67*(1), 83–88.

Kay, G. W., Jay, N. P., & Palmer, D. N. (2011). The specific loss of GnRH-positive neurons from the hypothalamus of sheep with CLN6 neuronal ceroid lipofuscinosis occurs without glial activation and has only minor effects on reproduction. *Neurobiology of Disease*, *41*(3), 614–623.

Kay, G. W., & Palmer, D. N. (2013). Chronic oral administration of minocycline to sheep with ovine CLN6 neuronal ceroid lipofuscinosis maintains pharmacological concentrations in the brain but does not suppress neuroinflammation or disease progression. *Journal of Neuroinflammation*, *10*(1), 97.

Kay, G. W., Palmer, D. N., Rezaie, P., & Cooper, J. D. (2006). Activation of non-neuronal cells within the prenatal developing brain of sheep with neuronal ceroid lipofuscinosis. *Brain Pathology*, *16*(2), 110–116.

Kendrick, K. M., da Costa, A. P., Leigh, A. E., Hinton, M. R., & Peirce, J. W. (2001). Sheep don't forget a face. *Nature*, *414*(6860), 165–166.

Kessell, A. E., Finnie, J. W., Manavis, J., Cheetham, G. D., & Blumbergs, P. C. (2012). A Rosenthal fiber encephalomyelopathy resembling Alexander's disease in 3 sheep. *Veterinary Pathology*, *49*(2), 248–254.

Kielar, C., Maddox, L., Bible, E., Pontikis, C. C., Macauley, S. L., Griffey, M. A., Wong, M., Sands, M. S., & Cooper, J. D. (2007). Successive neuron loss in the thalamus and cortex in a mouse model of infantile neuronal ceroid lipofuscinosis. *Neurobiology of Disease*, *25*(1), 150–162.

King, A. J., Wilson, A. M., Wilshin, S. D., Lowe, J., Haddadi, H., Hailes, S., & Morton, A. J. (2012). Selfish-herd behaviour of sheep under threat. *Current Biology*, *22*(14), R561–562.

Klockars, T., Holmberg, V., Savukoski, M., Lander, E. S., & Peltonen, L. (1999). Transcript identification on the CLN5 region on chromosome 13q22. *Human Genetics*, *105*(1-2), 51–56.

Koie, H., Shibuya, H., Sato, T., Sato, A., Nawa, K., Nawa, Y., Kitagawa, M., Sakai, M., Takahashi, T., Yamaya, Y., Yamato, O., Watari, T., & Tokuriki, M. (2004). Magnetic resonance imaging of neuronal ceroid lipofuscinosis in a border collie. *The Journal of Veterinary Medical Science*, *66*(11), 1453–1456.

Kollmann, K., Uusi-Rauva, K., Scifo, E., Tyynelä, J., Jalanko, A., & Braulke, T. (2013). Cell biology and function of neuronal ceroid lipofuscinosis-related proteins. *Biochimica et Biophysica Acta*, *1832*(11), 1866–1881.

Komáromy, A. M., Alexander, J. J., Rowlan, J. S., Garcia, M. M., Chiodo, V. A., Kaya, A., Tanaka, J. C., Acland, G. M., Hauswirth, W. W., & Aguirre, G. D. (2010). Gene therapy rescues cone function in congenital achromatopsia. *Human Molecular Genetics*, *19*(13), 2581–2593.

Konold, T., Bone, G. E., Phelan, L. J., Simmons, M. M., González, L., Sisó, S., Goldmann, W., Cawthraw, S., & Hawkins, S. A. C. (2010). Monitoring of clinical signs in goats with transmissible spongiform encephalopathies. *BMC Veterinary Research*, *6*, 13.

Kopra, O., Vesa, J., von Schantz, C., Manninen, T., Minye, H., Fabritius, A. L., Rapola, J., van Diggelen, O. P., Saarela, J., Jalanko, A., & Peltonen, L. (2004). A mouse model for Finnish variant late infantile neuronal ceroid lipofuscinosis, CLN5, reveals neuropathology associated with early aging. *Human Molecular Genetics*, *13*(23), 2893–2906.

Kordower, J. H., Bloch, J., Ma, S. Y., Chu, Y., Palfi, S., Roitberg, B. Z., Emborg, M., Hantraye, P., Déglon, N., & Aebischer, P. (1999). Lentiviral gene transfer to the nonhuman primate brain. *Experimental Neurology*, *160*(1), 1–16.

Kordower, J. H., Emborg, M., Bloch, J., Ma, S., Chu, Y., Leventhal, L., McBride, J., Chen, E. Y., Palfi, S., Roitberg, B., Brown, W., Holden, J., Pyzalski, R., Taylor, M., Carvey, P., Ling, Z., Trono, D., Hantraye, P., Déglon, N., & Aebischer, P. (2000). Neurodegeneration prevented by lentiviral vector delivery of GDNF in primate podels of Parkinson's disease. *Science*, *290*(5492), 767–773.

Kornfeld, S. (1987). Trafficking of lysosomal enzymes. *Federation of American Societies for Experimental Biology Journal*, *77*(1), 462–468.

Kousi, M., Lehesjoki, A.-E., & Mole, S. E. (2012). Update of the mutation spectrum and clinical correlations of over 360 mutations in eight genes that underlie the neuronal ceroid lipofuscinoses. *Human Mutation*, *33*(1), 42–63.

Kumaratilake, J. S., & Howell, J. M. (1987). Histochemical study of the accumulation of copper in the liver of sheep. *Research in Veterinary Science*, *42*(1), 73–81.

Kuronen, M., Lehesjoki, A.-E., Jalanko, A., Cooper, J. D., & Kopra, O. (2012). Selective spatiotemporal patterns of glial activation and neuron loss in the sensory thalamocortical pathways of neuronal ceroid lipofuscinosis 8 mice. *Neurobiology of Disease*, *47*(3), 444–57.

Kyttälä, A., Ihrke, G., Vesa, J., Schell, M. J., & Luzio, J. P. (2004). Two motifs target Batten disease protein CLN3 to lysosomes in transfected nonneuronal and neuronal cells. *Molecular Bology of the Cell*, *15*(3), 1313–1323.

Lake, B. D., & Cavanagh, N. P. (1978). Early-juvenile Batten's disease--a recognisable sub-group distinct from other forms of Batten's disease. Analysis of 5 patients. *Journal of the Neurological Sciences*, *36*(2), 265–271.

Lattanzi, A., Neri, M., Maderna, C., di Girolamo, I., Martino, S., Orlacchio, A., Amendola, M., Naldini, L., & Gritti, A. (2010). Widespread enzymatic correction of CNS tissues by a single intracerebral injection of therapeutic lentiviral vector in leukodystrophy mouse models. *Human Molecular Genetics*, *19*(11), 2208–2227.

Lee, C., Colegate, S., & Fisher, A. D. (2006). Development of a maze test and its application to assess spatial learning and memory in Merino sheep. *Applied Animal Behaviour Science*, *96*, 43–51.

Lee, W., Lee, S. D., Park, M. Y., Foley, L., Purcell-Estabrook, E., Kim, H., & Yoo, S.-S. (2015). Functional and diffusion tensor magnetic resonance imaging of the sheep brain. *BMC Veterinary Research*, *11*, 262.

Lee, K. M., & MacLean, A. G. (2015). New advances on glial activation in health and disease. *World Journal of Virology*, *4*(2), 42–55.

Leone, P., Shera, D., McPhee, S. W. J., Francis, J. S., Kolodny, E. H., Bilaniuk, L. T., Wang, D.-J., Assadi, M., Goldfarb, O., Goldman, H. W., Freese, A., Young, D., During, M. J., Samulski, R. J., & Janson, C. G. (2012). Long-term follow-up after gene therapy for Canavan disease. *Science Translational Medicine*, *4*(165), 165ra163.

Lerchner, W., Corgiat, B., Der Minassian, V., Saunders, R. C., & Richmond, B. J. (2014). Injection parameters and virus dependent choice of promoters to improve neuron targeting in the nonhuman primate brain. *Gene Therapy*, *21*(3), 233–241.

Lewis, N. J., Fallah-Rad, A. H., & Connor, M. L. (1997). Copper toxicity in confinement-housed ram

lambs. *The Canadian Veterinary Journal*, *38*(8), 496–498.

Lim, D. A., & Alvarez-Buylla, A. (2014). Adult neural stem cells stake their ground. *Trends in Neurosciences*, *37*(10), 563–571.

Lin, L., & Lobel, P. (2001). Enzyme-replacement therapy in late infantile neuronal ceroid lipofuscinosis. *The Biochemical Journal*, *55*(Pt.1), 49–55.

Lin, S.-W., & Ertl, H. C. (2008). Safety of adeno-associated viral vectors. *Future Virology*, *3*(5), 491–503.

Linterman, K. S., Palmer, D. N., Kay, G. W., Barry, L. A., Mitchell, N. L., McFarlane, R. G., Black, M. A., Sands, M. S., & Hughes, S. M. (2011). Lentiviral-mediated gene transfer to the sheep brain: implications for gene therapy in Batten disease. *Human Gene Therapy*, *22*(8), 1011–1020.

Liu, G., Martins, I. H., Chiorini, J. A., & Davidson, B. L. (2005a). Adeno-associated virus type 4 (AAV4) targets ependyma and astrocytes in the subventricular zone and RMS. *Gene Therapy*, *12*(20), 1503–1508.

Liu, G., Martins, I., Wemmie, J. A., Chiorini, J. A., & Davidson, B. L. (2005b). Functional correction of CNS phenotypes in a lysosomal storage disease model using adeno-associated virus type 4 vectors. *The Journal of Neuroscience*, *25*(41), 9321–9327.

Lonka, L., Kyttälä, A., Ranta, S., Jalanko, A., & Lehesjoki, A. E. (2000). The neuronal ceroid lipofuscinosis CLN8 membrane protein is a resident of the endoplasmic reticulum. *Human Molecular Genetics*, *9*(11), 1691–1697.

Lonka, L., Salonen, T., Siintola, E., Kopra, O., Lehesjoki, A.-E., & Jalanko, A. (2004). Localization of wild-type and mutant neuronal ceroid lipofuscinosis CLN8 proteins in non-neuronal and neuronal cells. *Journal of Neuroscience Research*, *76*(6), 862–871.

Low, V. F., Faull, R. L. M., Bennet, L., Gunn, A. J., & Curtis, M. A. (2013). Neurogenesis and progenitor cell distribution in the subgranular zone and subventricular zone of the adult sheep brain. *Neuroscience*, *244*, 173–187.

Lüders, E., Steinmetz, H., & Jäncke, L. (2002). Brain size and grey matter volume in the healthy human brain. *Neuroreport*, *13*(17), 2371–2374.

Luiro, K., Kopra, O., Lehtovirta, M., & Jalanko, A. (2001). CLN3 protein is targeted to neuronal synapses but excluded from synaptic vesicles: new clues to Batten disease. *Human Molecular Genetics*, *10*(19), 2123–2131.

Lyly, A., von Schantz, C., Heine, C., Schmiedt, M.-L., Sipilä, T., Jalanko, A., & Kyttälä, A. (2009). Novel interactions of CLN5 support molecular networking between Neuronal Ceroid Lipofuscinosis proteins. *BMC Cell Biology*, *10*, 83.

Lyman, M., Lloyd, D. G., Ji, X., Vizcaychipi, M. P., & Ma, D. (2014). Neuroinflammation: the role and consequences. *Neuroscience Research*, *79*, 1–12.

Macauley, S. L., Wong, A. M. S., Shyng, C., Augner, D. P., Dearborn, J. T., Pearse, Y., Roberts, M. S., Fowler, S. C., Cooper, J. D., Watterson, D. M., & Sands, M. S. (2014). An anti-neuroinflammatory that targets dysregulated glia enhances the efficacy of CNS-directed gene therapy in murine infantile neuronal ceroid lipofuscinosis. *The Journal of Neuroscience*, *34*(39), 13077–13082.

Macauley, S. L., Wozniak, D. F., Kielar, C., Tan, Y., Cooper, J. D., & Sands, M. S. (2009). Cerebellar pathology and motor deficits in the palmitoyl protein thioesterase 1-deficient mouse. *Experimental Neurology*, *217*(1), 124–135.

Magavi, S. S., Leavitt, B. R., & Macklis, J. D. (2000). Induction of neurogenesis in the neocortex of adult mice. *Nature*, *405*(6789), 951–955.

Manktelow, B. W., & Hartley, W. J. (1975). Generalized glycogen storage disease in sheep. *Journal of Comparative Pathology*, *85*(1), 139–145.

McBride, S. D., Perentos, N., & Morton, A. J. (2014). Understanding the concept of a reflective surface: Can sheep improve navigational ability through the use of a mirror? *Animal Cognition*, *18*(1), 361-371.

McCarty, D. M., Fu, H., Monahan, P. E., Toulson, C. E., Naik, P., & Samulski, R. J. (2003). Adeno-associated virus terminal repeat (TR) mutant generates self-complementary vectors to overcome the rate-limiting step to transduction in vivo. *Gene Therapy*, *10*(26), 2112–2118.

McCarty, D. M., Monahan, P. E., & Samulski, R. J. (2001). Self-complementary recombinant adeno-associated virus (scAAV) vectors promote efficient transduction independently of DNA synthesis. *Gene Therapy*, *8*(16), 1248–1254.

McCarty, D. M., Young, S. M., & Samulski, R. J. (2004). Integration of adeno-associated virus (AAV) and recombinant AAV vectors. *Annual Review of Genetics*, *38*, 819–845.

McClure, C., Cole, K.L., Wulff, P., Klugmann, M & Murray, A.J. (2011). Production and titering of recombinant adeno-associated viral vectors. *Journal of Visualised Experiments, (57)*, e3348.

McCormack, M. P., & Rabbitts, T. H. (2004). Activation of the T-cell oncogene LMO2 after gene therapy for X-linked severe combined immunodeficiency. *The New England Journal of Medicine*, *350*(9), 913–922.

McCurdy, V. J., Johnson, A. K., Gray-Edwards, H. L., Randle, A. N., Brunson, B. L., Morrison, N. E., Salibi, N., Johnson, J. A., Hwang, M., Beyers, R. J., Leroy, S. G., Maitland, S., Denney, T. S., Cox, N. R., Baker, H. J., Sena-Esteves, M., & Martin, D. R. (2014). Sustained normalization of neurological disease After intracranial gene therapy in a feline model. *Science Translational Medicine*, *6*(231), 231ra48.

McCurdy, V. J., Rockwell, H. E., Arthur, J. R., Bradbury, A. M., Johnson, A. K., Randle, A. N., Brunson, B. L., Hwang, M., Gray-Edwards, H. L., Morrison, N. E., Johnson, J. A., Baker, H. J., Cox, N. R., Seyfried, T. N., Sena-Esteves, M., & Martin, D. R. (2015). Widespread correction of central nervous system disease after intracranial gene therapy in a feline model of Sandhoff disease. *Gene Therapy*, *22*(2), 181–189.

McGeer, E. G., & McGeer, P. L. (2007). The role of anti-inflammatory agents in Parkinson's disease. *CNS Drugs*, *21*(10), 789–797.

McIntyre, C., K Derrick-Roberts, A. L., Byers, S., & Anson, D. S. (2014). Correction of murine mucopolysaccharidosis type IIIA central nervous system pathology by intracerebroventricular lentiviral-mediated gene delivery. *The Journal of Gene Medicine*, *16*, 374–387.

Melville, S. A., Wilson, C. L., Chiang, C. S., Studdert, V. P., Lingaas, F., & Wilton, A. N. (2005). A

mutation in canine CLN5 causes neuronal ceroid lipofuscinosis in Border collie dogs. *Genomics*, *86*(3), 287–294.

Meyer, K., Ferraiuolo, L., Schmelzer, L., Braun, L., McGovern, V., Likhite, S., Michels, O., Govoni, A., Fitzgerald, J., Morales, P., Foust, K. D., Mendell, J. R., Burghes, A. H. M., & Kaspar, B. K. (2015). Improving single injection CSF delivery of AAV9-mediated gene therapy for SMA: a dose-response study in mice and nonhuman primates. *Molecular Therapy*, *23*(3), 477–487.

Meyerrose, T. E., Roberts, M., Ohlemiller, K. K., Vogler, C. A., Wirthlin, L., Nolta, J. A., & Sands, M. S. (2008). Lentiviral-transduced human mesenchymal stem cells persistently express therapeutic levels of enzyme in a xenotransplantation model of human disease. *Stem Cells*, *26*(7), 1713–1722.

Milne, E. M., & Schock, A. (1998). Cerebellar abiotrophy in a pedigree Charollais sheep flock. *The Veterinary Record*, *143*(8), 224–225.

Ming, G., & Song, H. (2005). Adult neurogenesis in the mammalian central nervous system. *Annual Review of Neuroscience*, *28*, 223–250.

Mingozzi, F., & High. (2011). Therapeutic in vivo gene transfer for genetic disease using AAV: progress and challenges. *Nature Reviews. Genetics*, *12*(5), 341–355.

Mingozzi, F., & High, K. A. (2013). Immune responses to AAV vectors: overcoming barriers to successful gene therapy. *Blood*, *122*(1), 23–36.

Mink, J. W., Augustine, E. F., Adams, H. R., Marshall, F. J., & Kwon, J. M. (2013). Classification and natural history of the neuronal ceroid lipofuscinoses. *Journal of Child Neurology*, *28*(9), 1101–1105.

Mitchison, H. M., Bernard, D. J., Greene, N. D., Cooper, J. D., Junaid, M. A., Pullarkat, R. K., de Vos, N., Breuning, M. H., Owens, J. W., Mobley, W. C., Gardiner, R. M., Lake, B. D., Taschner, P. E., & Nussbaum, R. L. (1999). Targeted disruption of the Cln3 gene provides a mouse model for Batten disease. The Batten Mouse Model Consortium [corrected]. *Neurobiology of Disease*, *6*(5), 321–334.

Mizukami, K., Kawamichi, T., Koie, H., Tamura, S., Matsunaga, S., Imamoto, S., Saito, M., Hasegawa, D., Matsuki, N., Tamahara, S., Sato, S., Yabuki, A., Chang, H.-S., Yamato, O., Landoni, M. F., & Thompson, E. J. (2012). Neuronal ceroid lipofuscinosis in Border collie dogs in Japan: Clinical and molecular epidemiological study (2000–2011). *The Scientific World Journal*, *383174*.

Mohammadi, S. F., Mazouri, A., Jabbarvand, M., Rahman-A, N., & Mohammadi, A. (2011). Sheep practice eye for ophthalmic surgery training in skills laboratory. *Journal of Cataract and Refractive Surgery*, *37*(6), 987–991.

Mohd Ismail, I. F. (2014). *Identification of a novel mutation in the CLN6 gene causing neuronal ceroid lipofuscinosis in South Hampshire sheep*. PhD thesis, University of Sydney, Sydney, Australia.

Mole, S. E., Michaux, G., Codlin, S., Wheeler, R. B., Sharp, J. D., & Cutler, D. F. (2004). CLN6, which is associated with a lysosomal storage disease, is an endoplasmic reticulum protein. *Experimental Cell Research*, *298*(2), 399–406.

Mole, S. E., Williams, R. E., & Goebel, H. H. (2005). Correlations between genotype, ultrastructural

morphology and clinical phenotype in the neuronal ceroid lipofuscinoses. *Neurogenetics*, *6*(3), 107–126.

Mole, S. E., Williams, R. E., & Goebel, H. H. (Eds.). (2011). *The neuronal ceroid lipofuscinoses (Batten disease)* (2nd Edition). Oxford, UK: Oxford University Press.

Montgomery, G. W. & Sise, J. A. (1990) Extraction of DNA from sheep white blood cells. *New Zealand Journal of Agricultural Research*, *33*(3), 437-441.

Moore, S. J., Buckley, D. J., MacMillan, A., Marshall, H. D., Steele, L., Ray, P. N., Nawaz, Z., Baskin, B., Frecker, M., Carr, S. M., Ives, E., & Parfrey, P. S. (2008). The clinical and genetic epidemiology of neuronal ceroid lipofuscinosis in Newfoundland. *Clinical Genetics*, *74*(3), 213–222.

Morgan, J. P., Magee, H., Wong, A., Nelson, T., Koch, B., Cooper, J. D., & Weimer, J. M. (2013). A murine model of variant late infantile ceroid lipofuscinosis recapitulates behavioral and pathological phenotypes of human disease. *PloS One*, *8*(11), e78694.

Morton, A. J., & Avanzo, L. (2011). Executive decision-making in the domestic sheep. *PLoS ONE*, *6*(1), 1–8.

Mrak, R. E., & Griffin, W. S. T. (2005). Glia and their cytokines in progression of neurodegeneration. *Neurobiology of Aging*, *26*(3), 349–54.

Nakayama, H., Uchida, K., Shouda, T., Uetsuka, K., Sasaki, N., & Goto, N. (1993). Systemic ceroid-lipofuscinosis in a Japanese domestic cat. *The Journal of Veterinary Medical Science*, *55*(5), 829–31.

Naldini, L., Blömer, U., Gage, F. H., Trono, D., & Verma, I. M. (1996a). Efficient transfer, integration, and sustained long-term expression of the transgene in adult rat brains injected with a lentiviral vector. *Proceedings of the National Academy of Sciences of the United States of America*, *93*(21), 11382–11388.

Naldini, L., Blömer, U., Gallay, P., Ory, D., Mulligan, R., Gage, F. H., Verma, I. M., & Trono, D. (1996b). In vivo gene delivery and stable transduction of nondividing cells by a lentiviral vector. *Science*, *272*(5259), 263–267.

Nault, J.-C., Datta, S., Imbeaud, S., Franconi, A., Mallet, M., Couchy, G., Letouzé, E., Pilati, C., Verret, B., Blanc, J.-F., Balabaud, C., Calderaro, J., Laurent, A., Letexier, M., Bioulac-Sage, P., Calvo, F., & Zucman-Rossi, J. (2015). Recurrent AAV2-related insertional mutagenesis in human hepatocellular carcinomas. *Nature Genetics*, *47*(10), 1187–1193.

Neufeld, E. F. (1991). Lysosomal storage diseases. *Annual Review of Biochemistry*, *60*, 257–280.

Neufeld, E. F., & Fratantoni, J. C. (1970). Inborn errors of mucopolysaccharide metabolism. *Science*, *169*(3941), 141–146.

Nguyen, J. B., Sanchez-Pernaute, R., Cunningham, J., & Bankiewicz, K. S. (2001). Convection-enhanced delivery of AAV-2 combined with heparin increases TK gene transfer in the rat brain. *Neuroreport*, *12*(9), 1961–1964.

Nibe, K., Miwa, Y., Matsunaga, S., Chambers, J. K., Uetsuka, K., Nakayama, H., & Uchida, K. (2011). Clinical and pathologic features of neuronal ceroid-lipofuscinosis in a ferret (Mustela putorius furo). *Veterinary Pathology*, *48*(6), 1185–1189.

Nitzsche, B., Frey, S., Collins, L. D., Seeger, J., Lobsien, D., Dreyer, A., Kirsten, H., Stoffel, M. H., Fonov, V. S., & Boltze, J. (2015). A stereotaxic, population-averaged T1w ovine brain atlas including cerebral morphology and tissue volumes. *Frontiers in Neuroanatomy*, *9*, 69.

Nowak, R., Keller, M., & Lévy, F. (2011). Mother-young relationships in sheep: a model for a multidisciplinary approach of the study of attachment in mammals. *Journal of Neuroendocrinology*, *23*(11), 1042–1053.

O'Brien, D. P., & Katz, M. L. (2008). Neuronal ceroid lipofuscinosis in 3 Australian shepherd littermates. *Journal of Veterinary Internal Medicine*, *22*(2), 472–475.

Ohashi, T. (2012). Enzyme replacement therapy for lysosomal storage diseases. *Pediatric Endocrinology Reviews*, *10*(Suppl 1), 26–34.

Ohmi, K., Greenberg, D. S., Rajavel, K. S., Ryazantsev, S., Li, H. H., & Neufeld, E. F. (2003). Activated microglia in cortex of mouse models of mucopolysaccharidoses I and IIIB. *Proceedings of the National Academy of Sciences of the United States of America*, *100*(4), 1902–1907.

Ojala, D. S., Amara, D. P., & Schaffer, D. V. (2015). Adeno-associated virus vectors and neurological gene therapy. *The Neuroscientist*, *21*, 84–98.

Oswald, M. J. (2004). *Neuropathogenesis of ovine neuronal ceroid lipofuscinosis*. PhD thesis, Lincoln University, Lincoln, New Zealand.

Oswald, M. J., Kay, G. W., & Palmer, D. N. (2001). Changes in GABAergic neuron distribution in situ and in neuron cultures in ovine (OCL6) Batten disease. *European Journal of Paediatric Neurology*, *5 Suppl A*, 135–142.

Oswald, M. J., Palmer, D. N., Kay, G. W., Barwell, K. J., & Cooper, J. D. (2008). Location and connectivity determine GABAergic interneuron survival in the brains of South Hampshire sheep with CLN6 neuronal ceroid lipofuscinosis. *Neurobiology of Disease*, *32*(1), 50–65.

Oswald, M. J., Palmer, D. N., Kay, G. W., Shemilt, S. J. A., Rezaie, P., & Cooper, J. D. (2005). Glial activation spreads from specific cerebral foci and precedes neurodegeneration in presymptomatic ovine neuronal ceroid lipofuscinosis (CLN6). *Neurobiology of Disease*, *20*(1), 49-63.

Palfi, S., Gurruchaga, J. M., Ralph, G. S., Lepetit, H., Lavisse, S., Buttery, P. C., Watts, C., Miskin, J., Kelleher, M., Deeley, S., Iwamuro, H., Lefaucheur, J. P., Thiriez, C., Fenelon, G., Lucas, C., Brugières, P., Gabriel, I., Abhay, K., Drouot, X., Tani, N., Kas, A., Ghaleh, B., Le Corvoisier, P., Dolphin, P., Breen, D. P., Mason, S., Guzman, N. V., Mazarakis, N. D., Radcliff, P. A., Harrop, R., Kingsman, S. M., Rascol, O., Naylor, S., Barker, R. A., Hantraye, P., Remy, P., Cesaro, P., & Mitrophanous, K. A. (2014). Long-term safety and tolerability of ProSavin, a lentiviral vector-based gene therapy for Parkinson's disease: a dose escalation, open-label, phase 1/2 trial. *Lancet*, *383*(9923), 1138–1146.

Palmer, D. N. (2015). The relevance of the storage of subunit c of ATP synthase in different forms and models of Batten disease (NCLs). *Biochimica et Biophysica Acta*, *1852*(10 Pt B), 2287–2291.

Palmer, D. N., Barry, L. A., Tyynelä, J., & Cooper, J. D. (2013). NCL disease mechanisms. *Biochimica et Biophysica Acta*, *1832*(11), 1882–1893.

Palmer, D. N., Fearnley, I. M., Medd, S. M., Walker, J. E., Martinus, R. D., Bayliss, S. L., Hall, N. A., Lake, B. D., Wolfe, L. S., & Jolly, R. D. (1989). Lysosomal storage of the DCCD reactive proteolipid subunit of mitochondrial ATP synthase in human and ovine ceroid lipofuscinoses. *Advances in Experimental Medicine and Biology*, *266*, 211–223.

Palmer, D. N., Fearnley, I. M., Walker, J. E., Hall, N. A., Lake, B. D., Wolfe, L. S., Haltia, M., Martinus, R. D., & Jolly, R. D. (1992). Mitochondrial ATP synthase subunit c storage in the ceroid-lipofuscinoses (Batten disease). *American Journal of Medical Genetics*, *42*(4), 561–567.

Palmer, D. N., Jolly, R. D., van Mil, H., Tyynelä, J., & Westlake, V. (1997). Different patterns of hydrophobic protein storage in different forms of neuronal ceroid lipofuscinosis (NCL, Batten disease). *Neuropediatrics*, *28*(1), 45–48.

Palmer, D. N., Oswald, M. J., Westlake, V. J., & Kay, G. W. (2002). The origin of fluorescence in the neuronal ceroid lipofuscinoses (Batten disease) and neuron cultures from affected sheep for studies of neurodegeneration. *Archives of Gerontology and Geriatrics*, *34*(3), 343–357.

Palmer, D. N., Neverman, N. J., Chen, J. Z., Chang, C.-T., Houweling, P. J., Barry, L. A., Tammen, I., Hughes, S. M., & Mitchell, N. L. (2015). Recent studies of ovine neuronal ceroid lipofuscinoses from BARN, the Batten Animal Research Network. *Biochimica et Biophysica Acta*, *1852*(10 Pt B), 2279–2286.

Palmer, D. N., Tammen, I., Katz, M. L., Johnson, G. S., & Drögemüller, C. (2011). Large Animal Models. In: *The Neuronal Ceroid Lipofuscinoses (Batten disease)* (2nd Edition). Mole, S. E., Williams, R. E. & Goebel H. H. (Eds.) (pp. 284–320). Oxford, UK: Oxford University Press.

Pang, J., Lauramore, A., Deng, W., Li, Q., Doyle, T. J., Chiodo, V., Li, J., & Hauswirth, W. W. (2008). Comparative analysis of in vivo and in vitro AAV vector transduction in the neonatal mouse retina: effects of serotype and site of administration. *Vision Research*, *48*(3), 377–385.

Paniagua Bravo, A., Forkert, N. D., Schulz, A., Löbel, U., Fiehler, J., Ding, X., Sedlacik, J., Rosenkranz, M., & Goebell, E. (2013). Quantitative t2 measurements in juvenile and late infantile neuronal ceroid lipofuscinosis. *Clinical Neuroradiology*, *23*(3), 189–196.

Pardridge, W. M. (2002). Drug and gene targeting to the brain with molecular Trojan horses. *Nature Reviews. Drug Discovery*, *1*(2), 131–139.

Partanen, S., Haapanen, A., Kielar, C., Pontikis, C., Alexander, N., Inkinen, T., Saftig, P., Gillingwater, T. H., Cooper, J. D., & Tyynelä, J. (2008). Synaptic changes in the thalamocortical system of cathepsin D-deficient mice: a model of human congenital neuronal ceroid-lipofuscinosis. *Journal of Neuropathology and Experimental Neurology*, *67*(1), 16–29.

Passantino, R., Cascio, C., Deidda, I., Galizzi, G., Russo, D., Spedale, G., & Guarneri, P. (2013). Identifying protein partners of CLN8, an ER-resident protein involved in neuronal ceroid lipofuscinosis. *Biochimica et Biophysica Acta*, *1833*(3), 529–540.

Passini, M. A., Dodge, J. C., Bu, J., Yang, W., Zhao, Q., Sondhi, D., Hackett, N. R., Kaminsky, S. M., Mao, Q., Shihabuddin, L. S., Cheng, S. H., Sleat, D. E., Stewart, G. R., Davidson, B. L., Lobel, P., & Crystal, R. G. (2006). Intracranial delivery of CLN2 reduces brain pathology in a mouse model of classical late infantile neuronal ceroid lipofuscinosis. *Journal of Neuroscience*, *26*(5), 1334–1342.

Passini, M. A., Watson, D. J., Vite, C. H., Landsburg, D. J., Feigenbaum, A. L., & Wolfe, J. H. (2003).

Intraventricular brain injection of adeno-associated virus type 1 (AAV1) in neonatal mice results in complementary patterns of neuronal transduction to AAV2 and total long-term correction of storage lesions in the brains of beta-glucuronidase-deficient mi. *Journal of Virology*, *77*(12), 7034–7040.

Passler, T., Walz, P. H., & Pugh, D. G. (2012). Diseases of the neurologic system. In: *Sheep and Goat Medicine* (Second Edition). Pugh, D. G. & Baird, A. N. (Eds.) (pp. 361–405). Philadelphia, USA: Elsevier - Health Sciences Division.

Peebles, D., Gregory, L. G., David, A., Themis, M., Waddington, S. N., Knapton, H. J., Miah, M., Cook, T., Lawrence, L., Nivsarkar, M., Rodeck, C., & Coutelle, C. (2004). Widespread and efficient marker gene expression in the airway epithelia of fetal sheep after minimally invasive tracheal application of recombinant adenovirus in utero. *Gene Therapy*, *11*(1), 70–78.

Peirce, J. W., Leigh, A. E., Dacosta, A. P. C., & Kendrick, K. M. (2001). Human face recognition in sheep: lack of configurational coding and right hemisphere advantage. *Behavioural Processes*, *55*, 13–26.

Peña, J. A., Cardozo, J. J., Montiel, C. M., Molina, O. M., & Boustany, R. (2001). Serial MRI findings in the Costa Rican variant of neuronal ceroid-lipofuscinosis. *Pediatric Neurology*, *25*(1), 78–80.

Perentos, N., Martins, A. Q., Watson, T. C., Bartsch, U., Mitchell, N. L., Palmer, D. N., Jones, M. W., & Morton, A. J. (2015). Translational neurophysiology in sheep: measuring sleep and neurological dysfunction in CLN5 Batten disease affected sheep. *Brain*, *138*(4), 862–874.

Pérez, V., Suárez-Vega, A., Fuertes, M., Benavides, J., Delgado, L., Ferreras, M. C., & Arranz, J. J. (2013). Hereditary lissencephaly and cerebellar hypoplasia in Churra lambs. *BMC Veterinary Research*, *9*, 156.

Pinnapureddy, A. R., Stayner, C., McEwan, J., Baddeley, O., Forman, J., & Eccles, M. R. (2015). Large animal models of rare genetic disorders: sheep as phenotypically relevant models of human genetic disease. *Orphanet Journal of Rare Diseases*, *10*, 107.

Platt, F. M., Boland, B., & van der Spoel, A. C. (2012). Lysosomal storage disorders: The cellular impact of lysosomal dysfunction. *The Journal of Cell Biology*, *199*(5), 723–734.

Pontikis, C. C., Cella, C. V, Parihar, N., Lim, M. J., Chakrabarti, S., Mitchison, H. M., Mobley, W. C., Rezaie, P., Pearce, D. A., & Cooper, J. D. (2004). Late onset neurodegeneration in the Cln3-/- mouse model of juvenile neuronal ceroid lipofuscinosis is preceded by low level glial activation. *Brain Research*, *1023*(2), 231–242.

Pontikis, C. C., Cotman, S. L., MacDonald, M. E., & Cooper, J. D. (2005). Thalamocortical neuron loss and localized astrocytosis in the Cln3Deltaex7/8 knock-in mouse model of Batten disease. *Neurobiology of Disease*, *20*(3), 823–836.

Porada, C. D., Park, P., Almeida-Porada, G., & Zanjani, E. D. (2004). The sheep model of in utero gene therapy. *Fetal Diagnosis and Therapy*, *19*(1), 23–30.

Prieur, D. J., Ahern-Rindell, A. J., & Murnane, R. D. (1991). Ovine GM-1 gangliosidosis. *The American Journal of Pathology*, *139*(6), 1511–1513.

Pritchard, D. H., Napthine, D. V, & Sinclair, A. J. (1980). Globoid cell leucodystrophy in polled Dorset

sheep. *Veterinary Pathology*, *17*(4), 399–405.

Puppo, A., Cesi, G., Marrocco, E., Piccolo, P., Jacca, S., Shayakhmetov, D. M., Parks, R. J., Davidson, B. L., Colloca, S., Brunetti-Pierri, N., Ng, P., Donofrio, G., & Auricchio, A. (2014). Retinal transduction profiles by high-capacity viral vectors. *Gene Therapy*, *21*(10), 855–865.

Rafii, M. S., Baumann, T. L., Bakay, R. A. E., Ostrove, J. M., Siffert, J., Fleisher, A. S., Herzog, C. D., Barba, D., Pay, M., Salmon, D. P., Chu, Y., Kordower, J. H., Bishop, K., Keator, D., Potkin, S., & Bartus, R. T. (2014). A phase1 study of stereotactic gene delivery of AAV2-NGF for Alzheimer's disease. *Alzheimer's & Dementia*, *10*(5), 571–581.

Rahim, A. A., Wong, A. M., Ahmadi, S., Hoefer, K., Buckley, S. M. K., Hughes, D. A., Nathwani, A. N., Baker, A. H., McVey, J. H., Cooper, J. D., & Waddington, S. N. (2012). In utero administration of Ad5 and AAV pseudotypes to the fetal brain leads to efficient, widespread and long-term gene expression. *Gene Therapy*, *19*(9), 936–946.

Raivich, G., Bohatschek, M., Kloss, C. U., Werner, A., Jones, L. L., & Kreutzberg, G. W. (1999). Neuroglial activation repertoire in the injured brain: graded response, molecular mechanisms and cues to physiological function. *Brain Research Reviews*, *30*(1), 77–105.

Rama Rao, K. V, & Kielian, T. (2015). Astrocytes and lysosomal storage diseases. *Neuroscience*, 323, 195-206.

Ramirez, A., Heimbach, A., Gründemann, J., Stiller, B., Hampshire, D., Cid, L. P., Goebel, I., Mubaidin, A. F., Wriekat, A.-L., Roeper, J., Al-Din, A., Hillmer, A. M., Karsak, M., Liss, B., Woods, C. G., Behrens, M. I., & Kubisch, C. (2006). Hereditary parkinsonism with dementia is caused by mutations in ATP13A2, encoding a lysosomal type 5 P-type ATPase. *Nature Genetics*, *38*(10), 1184–1191.

Ransohoff, R. M., & Perry, V. H. (2009). Microglial physiology: unique stimuli, specialized responses. *Annual Review of Immunology*, *27*, 119–145.

Rapti, K., Louis-Jeune, V., Kohlbrenner, E., Ishikawa, K., Ladage, D., Zolotukhin, S., Hajjar, R. J., & Weber, T. (2012). Neutralizing antibodies against AAV serotypes 1, 2, 6, and 9 in sera of commonly used animal models. *Molecular Therapy*, *20*(1), 73–83.

Rauschecker, J. P. (1998). Cortical control of the thalamus: top-down processing and plasticity. *Nature Neuroscience*, *1*(3), 179–180.

Read, W. K., & Bridges, C. H. (1969). Neuronal lipodystrophy. Occurrence in an inbred strain of cattle. *Pathologia Veterinaria*, *6*(3), 235–243.

Reinhardt, V., & Reinhardt, A. (2002). Comfortable quarters for sheep in research institutions. In: *Comfortable Quarters for Laboratory Animals* (9th Edition). Reinhardt V. & Reinhardt A. (Eds.) (pp. 83–88). Animal Welfare Institute, Washington, DC, U.S.A.

Ribera, A., Haurigot, V., Garcia, M., Marcó, S., Motas, S., Villacampa, P., Maggioni, L., León, X., Molas, M., Sánchez, V., Muñoz, S., Leborgne, C., Moll, X., Pumarola, M., Mingozzi, F., Ruberte, J., Añor, S., & Bosch, F. (2015). Biochemical, histological and functional correction of mucopolysaccharidosis Type IIIB by intra-cerebrospinal fluid gene therapy. *Human Molecular Genetics*, *24*(7), 2078–2095.

Rider, J. A., & Rider, D. L. (1988). Batten disease: past, present, and future. *American Journal of Medical Genetics*, *5*, 21–26.

Rockwell, H. E., Mccurdy, V. J., Eaton, S. C., Wilson, D. U., Johnson, A. K., Randle, A. N., Bradbury, A. M., Gray-Edwards, H. L., Baker, H. J., Hudson, J. A., Cox, N. R., Sena-Esteves, M., Seyfried, T. N., & Martin, D. R. (2015). AAV-mediated gene delivery in a feline model of Sandhoff disease corrects lysosomal storage in the central nervous system. *American Society for Neurochemistry*, *March-April*, 1–13.

Rosenbaum, B. P., Vadera, S., Kelly, M. L., Kshettry, V. R., & Weil, R. J. (2014). Ventriculostomy: Frequency, length of stay and in-hospital mortality in the United States of America, 1988-2010. *Journal of Clinical Neuroscience*, *21*(4), 623–632.

Roybal, J. L., Endo, M., Buckley, S. M. K., Herbert, B. R., Waddington, S. N., & Flake, A. W. (2012). Animal models for prenatal gene therapy: rodent models for prenatal gene therapy. *Methods in Molecular Biology* , *891*, 201–218.

Ryder, S. J., & Simmons, M. M. (2001). A lysosomal storage disease of Romney sheep that resembles human type 3 GM1 gangliosidosis. *Acta Neuropathologica*, *101*(3), 225–228.

Sack, B. K., & Herzog, R. W. (2009). Evading the immune response upon in vivo gene therapy with viral vectors. *Current Opinion in Molecular Therapeutics*, *11*(5), 493–503.

Samaranch, L., Salegio, E. A., san Sebastian, W., Kells, A. P., Bringas, J. R., Forsayeth, J., & Bankiewicz, K. S. (2013). Strong cortical and spinal cord transduction after AAV7 and AAV9 delivery into the cerebrospinal fluid of nonhuman primates. *Human Gene Therapy*, *24*(5), 526–532.

Samaranch, L., Salegio, E. A., San Sebastian, W., Kells, A. P., Foust, K. D., Bringas, J. R., Lamarre, C., Forsayeth, J., Kaspar, B. K., & Bankiewicz, K. S. (2012). Adeno-associated virus serotype 9 transduction in the central nervous system of nonhuman primates. *Human Gene Therapy*, *23*(4), 382–389.

Samaranch, L., san Sebastian, W., Kells, A. P., Salegio, E. A., Heller, G., Bringas, J. R., Pivirotto, P., DeArmond, S., Forsayeth, J., & Bankiewicz, K. S. (2014). AAV9-mediated expression of a non-self protein in nonhuman primate central nervous system triggers widepread neuroinflammation driven by antigen-presenting cell transduction. *Molecular Therapy*, *22*(2), 329–337.

Sambraus, H. H. (1985). Mouth-based anomalous syndromes. In: *Ethology of Farm Animals.* Fraser, A. F. (Ed.) (pp. 391–422). Amsterdam, The Netherlands: Elsevier.

Sánchez-Andrade, G., James, B. M., & Kendrick, K. M. (2005). Neural encoding of olfactory recognition memory. *The Journal of Reproduction and Development*, *51*(5), 547–558.

SanCristobal-Gaudy, M., Bodin, L., Elsen, J. M., & Chevalet, C. (2001). Genetic components of litter size variability in sheep. *Genetics, Selection, Evolution*, *33*(3), 249–271.

Sanders, D. N., Kanazono, S., Wininger, F. A., Whiting, R. E. H., Flournoy, C. A., Coates, J. R., Castaner, L. J., O'Brien, D. P., & Katz, M. L. (2011). A reversal learning task detects cognitive deficits in a Dachshund model of late-infantile neuronal ceroid lipofuscinosis. *Genes, Brain, and Behavior*, *10*(7), 798–804.

Sands, M. S. (2014). A Hitchhiker's guide to the blood-brain barrier: in trans delivery of a therapeutic

enzyme. *Molecular Therapy*, *22*(3), 483–484.

Sands, M. S., & Davidson, B. L. (2006). Gene therapy for lysosomal storage diseases. *Molecular Therapy*, *13*(5), 839–849.

Sands, M. S., & Haskins, M. E. (2008). CNS-directed gene therapy for lysosomal storage diseases. *Acta Paediatrica*, *97*(457), 22–27.

Santavuori, P., Rapola, J., Nuutila, A., Raininko, R., Lappi, M., Launes, J., Herva, R., & Sainio, K. (1991). The spectrum of Jansky-Bielschowsky disease. *Neuropediatrics*, *22*(2), 92–96.

Santavuori, P., Rapola, J., Sainio, K., & Raitta, C. (1982). A variant of Jansky-Bielschowsky disease. *Neuropediatrics*, *13*(3), 135–141.

Savukoski, M., Klockars, T., Holmberg, V., Santavuori, P., Lander, E. S., & Peltonen, L. (1998). CLN5, a novel gene encoding a putative transmembrane protein mutated in Finnish variant late infantile neuronal ceroid lipofuscinosis. *Nature Genetics*, *19*(3), 286–288.

Sawiak, S. J., Perumal, S. R., Rudiger, S. R., Matthews, L., Mitchell, N. L., McLaughlan, C. J., Bawden, C. S., Palmer, D. N., Kuchel, T., & Morton, A. J. (2015). Rapid and progressive regional brain atrophy in CLN6 Batten disease affected sheep measured with longitudinal magnetic resonance imaging. *PLoS ONE*, *10*(7), e0132331.

Scheerlinck, J.-P. Y., Snibson, K. J., Bowles, V. M., & Sutton, P. (2008). Biomedical applications of sheep models: from asthma to vaccines. *Trends in Biotechnology*, *26*(5), 259–266.

Scherrmann, J. M. (2002). Drug delivery to brain via the blood-brain barrier. *Vascular Pharmacology*, *38*(6), 349–354.

Schlageter, K. E., Molnar, P., Lapin, G. D., & Groothuis, D. R. (1999). Microvessel organization and structure in experimental brain tumors: microvessel populations with distinctive structural and functional properties. *Microvascular Research*, *58*(3), 312–328.

Schmiedt, M. L., Bessa, C., Heine, C., Ribeiro, M. G., Jalanko, A., & Kyttälä, A. (2010). The neuronal ceroid lipofuscinosis protein CLN5: New insights into cellular maturation, transport, and consequences of mutations. *Human Mutation*, *31*(3), 356–365.

Schmiedt, M. L., Blom, T., Blom, T., Kopra, O., Wong, A., von Schantz-Fant, C., Ikonen, E., Kuronen, M., Jauhiainen, M., Cooper, J. D., & Jalanko, A. (2012). Cln5-deficiency in mice leads to microglial activation, defective myelination and changes in lipid metabolism. *Neurobiology of Disease*, *46*(1), 19–29.

Schochet, S. S., Font, R. L., & Morris, H. H. (1980). Jansky-Bielschowsky form of neuronal ceroid-lipofuscinosis. Ocular pathology of the Batten-Vogt syndrome. *Archives of Ophthalmology (Chicago, Ill. : 1960)*, *98*(6), 1083–1088.

Schulz, A., Kohlschütter, A., Mink, J., Simonati, A., & Williams, R. (2013). NCL diseases - clinical perspectives. *Biochimica et Biophysica Acta*, *1832*(11), 1801–1806.

Schulz, A., Specchio, N., Gissen, P., de los Reyes, E., Williams, R. E., Cahan, H., Genter, F., & Jacoby, D. (2016). *Intracerebroventricular cerliponase alfa (BMN 190) in children with CLN2 disease: Interim results from a Phase 1/2, open-label, dose-escalation study*. 12th Annual WORLD Symposium, San Diego, California, USA, 29 Feb – 4 Mar 2016 (O-5; P-15).

Schwartz, M., & Shechter, R. (2010). Systemic inflammatory cells fight off neurodegenerative disease. *Nature Reviews. Neurology*, *6*(7), 405–410.

Shacka, J. J. (2012). Mouse models of neuronal ceroid lipofuscinoses: useful pre-clinical tools to delineate disease pathophysiology and validate therapeutics. *Brain Research Bulletin*, *88*(1), 43–57.

Shamir, M. H., Ofri, R., Bor, A., Brenner, O., Reicher, S., Obolensky, A., Averbukh, E., Banin, E., & Gootwine, E. (2010). A novel day blindness in sheep: Epidemiological, behavioural, electrophysiological and histopathological studies. *The Veterinary Journal*, *185*, 130–137.

Sharp, J. D., Wheeler, R. B., Lake, B. D., Fox, M., Gardiner, R. M., & Williams, R. E. (1999). Genetic and physical mapping of the CLN6 gene on chromosome 15q21-23. *Molecular Genetics and Metabolism*, *66*(4), 329–331.

Siintola, E., Partanen, S., Strömme, P., Haapanen, A., Haltia, M., Maehlen, J., Lehesjoki, A.-E., & Tyynelä, J. (2006). Cathepsin D deficiency underlies congenital human neuronal ceroid-lipofuscinosis. *Brain*, *129*(Pt 6), 1438–1445.

Siintola, E., Topcu, M., Aula, N., Lohi, H., Minassian, B. A., Paterson, A. D., Liu, X.-Q., Wilson, C., Lahtinen, U., Anttonen, A.-K., & Lehesjoki, A.-E. (2007). The novel neuronal ceroid lipofuscinosis gene MFSD8 encodes a putative lysosomal transporter. *The American Journal of Human Genetics*, *81*(1), 136–146.

Sillito, A. M., Cudeiro, J., & Jones, H. E. (2006). Always returning: feedback and sensory processing in visual cortex and thalamus. *Trends in Neurosciences*, *29*(6), 307–316.

Sleat, D. E., Donnelly, R. J., Lackland, H., Liu, C. G., Sohar, I., Pullarkat, R. K., & Lobel, P. (1997). Association of mutations in a lysosomal protein with classical late-infantile neuronal ceroid lipofuscinosis. *Science*, *277*(5333), 1802–1805.

Sleat, D. E., Lackland, H., Wang, Y., Sohar, I., Xiao, G., Li, H., & Lobel, P. (2005). The human brain mannose 6-phosphate glycoproteome: a complex mixture composed of multiple isoforms of many soluble lysosomal proteins. *Proteomics*, *5*(6), 1520–1532.

Sleat, D. E., Wang, Y., Sohar, I., Lackland, H., Li, Y., Li, H., Zheng, H., & Lobel, P. (2006). Identification and validation of mannose 6-phosphate glycoproteins in human plasma reveal a wide range of lysosomal and non-lysosomal proteins. *Molecular & Cellular Proteomics*, *5*(10), 1942–1956.

Sleat, D. E., Wiseman, J. A., El-Banna, M., Kim, K.-H., Mao, Q., Price, S., Macauley, S. L., Sidman, R. L., Shen, M. M., Zhao, Q., Passini, M. A., Davidson, B. L., Stewart, G. R., & Lobel, P. (2004). A mouse model of classical late-infantile neuronal ceroid lipofuscinosis based on targeted disruption of the CLN2 gene results in a loss of tripeptidyl-peptidase I activity and progressive neurodegeneration. *The Journal of Neuroscience*, *24*(41), 9117–9126.

Sleat, D. E., Zheng, H., & Lobel, P. (2007). The human urine mannose 6-phosphate glycoproteome. *Biochimica et Biophysica Acta*, *1774*(3), 368–372.

Smith, K. R., Dahl, H.-H. M., Canafoglia, L., Andermann, E., Damiano, J., Morbin, M., Bruni, A. C., Giaccone, G., Cossette, P., Alexander, N. A., Cooper, J. D., Chapman, H. A., Carpenter, S., Berkovic, S. F., & Bahlo, M. (2013). Cathepsin F mutations cause Type B Kufs disease, an adult-onset neuronal ceroid lipofuscinosis. *Human Molecular Genetics*, *22*(7), 1417–1423.

Smith, K. R., Damiano, J., Franceschetti, S., Carpenter, S., Canafoglia, L., Morbin, M., Rossi, G., Pareyson, D., Mole, S. E., Staropoli, J. F., Sims, K. B., Lewis, J., Lin, W.-L., Dickson, D. W., Dahl, H.-H., Bahlo, M., & Berkovic, S. F. (2012). Strikingly different clinicopathological phenotypes determined by progranulin-mutation dosage. *The American Journal of Human Genetics*, *90*(6), 1102–1107.

Sondhi, D., Hackett, N. R., Peterson, D. A., Stratton, J., Baad, M., Travis, K. M., Wilson, J. M., & Crystal, R. G. (2007). Enhanced survival of the LINCL mouse following CLN2 gene transfer using the rh.10 rhesus macaque-derived adeno-associated virus vector. *Molecular Therapy*, *15*(3), 481–491.

Sondhi, D., Johnson, L., Purpura, K., Monette, S., Souweidane, M. M., Kaplitt, M. G., Kosofsky, B., Yohay, K., Ballon, D., Dyke, J., Kaminksy, S. M., Hackett, N. R., & Crystal, R. G. (2012). Long-term expression and safety of administration of AAVrh.10hCLN2 to the brain of rats and nonhuman primates for the treatment of late infantile neuronal ceroid lipofuscinosis. *Human Gene Therapy Methods*, *23*(5), 324–335.

Sondhi, D., Peterson, D. A., Giannaris, E. L., Sanders, C. T., Mendez, B. S., De, B., Rostkowski, A. B., Blanchard, B., Bjugstad, K., Sladek, J. R. J., Redmond, D. E. J., Leopold, P. L., Kaminsky, S. M., Hackett, N. R., & Crystal, R. G. (2005). AAV2-mediated CLN2 gene transfer to rodent and non-human primate brain results in long-term TPP-I expression compatible with therapy for LINCL. *Gene Therapy*, *12*(22), 1618–1632.

Sondhi, D., Scott, E. C., Chen, A., Hackett, N. R., Wong, A. M. S., Kubiak, A., Nelvagal, H. R., Pearse, Y., Cotman, S. L., Cooper, J. D., & Crystal, R. G. (2014). Partial correction of the CNS lysosomal storage defect in a mouse model of juvenile neuronal ceroid lipofuscinosis by neonatal CNS administration of an adeno-associated virus serotype rh.10 vector expressing the human CLN3 gene. *Human Gene Therapy*, *25*, 223–239.

Souweidane, M. M., Fraser, J. F., Arkin, L. M., Sondhi, D., Hackett, N. R., Kaminsky, S. M., Heier, L., Kosofsky, B. E., Worgall, S., Crystal, R. G., & Kaplitt, M. G. (2010). Gene therapy for late infantile neuronal ceroid lipofuscinosis: neurosurgical considerations. *Journal of Neurosurgery: Pediatrics*, *6*(2), 115–122.

Staropoli, J. F., Karaa, A., Lim, E. T., Kirby, A., Elbalalesy, N., Romansky, S. G., Leydiker, K. B., Coppel, S. H., Barone, R., Xin, W., MacDonald, M. E., Abdenur, J. E., Daly, M. J., Sims, K. B., & Cotman, S. L. (2012). A homozygous mutation in KCTD7 links neuronal ceroid lipofuscinosis to the ubiquitin-proteasome system. *American Journal of Human Genetics*, *91*(1), 202–208.

Stieger, K., Cronin, T., Bennett, J., & Rolling, F. (2011). Adeno-associated virus mediated gene therapy for retinal degenerative diseases. *Methods in Molecular Biology*, *807*, 179–218.

Stoll, G., & Jander, S. (1999). The role of microglia and macrophages in the pathophysiology of the CNS. *Progress in Neurobiology*, *58*(3), 233–47.

Storkebaum, E., Lambrechts, D., Dewerchin, M., Moreno-Murciano, M.-P., Appelmans, S., Oh, H., Van Damme, P., Rutten, B., Man, W. Y., De Mol, M., Wyns, S., Manka, D., Vermeulen, K., Van Den Bosch, L., Mertens, N., Schmitz, C., Robberecht, W., Conway, E. M., Collen, D., Moons, L., & Carmeliet, P. (2005). Treatment of motoneuron degeneration by intracerebroventricular delivery of VEGF in a rat model of ALS. *Nature Neuroscience*, *8*(1), 85–92.

Streit, W. (1990). An improved staining method for rat microglial cells using the lectin from Griffonia

simplifolia (GSA I-B4). *Journal of Histochemistry and Cytochemistry*, *38*, 1683–1686.

Streit, W. J. (2000). Microglial response to brain injury: a brief synopsis. *Toxicologic Pathology*, *28*(1), 28–30.

Streit, W. J. (2002). Microglia as neuroprotective, immunocompetent cells of the CNS. *Glia*, *40*(2), 133–139.

Streit, W. J., Mrak, R. E., & Griffin, W. S. T. (2004). Microglia and neuroinflammation: a pathological perspective. *Journal of Neuroinflammation*, *1*(1), 14.

Suárez-Vega, A., Gutiérrez-Gil, B., Cuchillo-Ibáñez, I., Sáez-Valero, J., Pérez, V., García-Gámez, E., Benavides, J., & Arranz, J. J. (2013). Identification of a 31-bp deletion in the RELN gene causing lissencephaly with cerebellar hypoplasia in sheep. *PloS ONE*, *8*(11), e81072.

Sun, Y., Almomani, R., Breedveld, G. J., Santen, G. W. E., Aten, E., Lefeber, D. J., Hoff, J. I., Brusse, E., Verheijen, F. W., Verdijk, R. M., Kriek, M., Oostra, B., Breuning, M. H., Losekoot, M., den Dunnen, J. T., van de Warrenburg, B. P., & Maat-Kievit, A. J. A. (2013). Autosomal recessive spinocerebellar ataxia 7 (SCAR7) is caused by variants in TPP1, the gene involved in classic late-infantile neuronal ceroid lipofuscinosis 2 disease (CLN2 disease). *Human Mutation*, *34*(5), 706–713.

Swain, G. P., Prociuk, M., Bagel, J. H., O'Donnell, P., Berger, K., Drobatz, K., Gurda, B. L., Haskins, M. E., Sands, M. S., & Vite, C. H. (2014). Adeno-associated virus serotypes 9 and rh10 mediate strong neuronal transduction of the dog brain. *Gene Therapy*, *21*(1), 28–36.

Tammen, I., Cook, R. W., Nicholas, F. W., & Raadsma, H. W. (2001). Neuronal ceroid lipofuscinosis in Australian Merino sheep: a new animal model. *European Journal of Paediatric Neurology*, *5(Suppl.A)*, 37–41.

Tammen, I., Houweling, P. J., Frugier, T., Mitchell, N. L., Kay, G. W., Cavanagh, J. A. L., Cook, R. W., Raadsma, H. W., & Palmer, D. N. (2006). A missense mutation (c.184C>T) in ovine CLN6 causes neuronal ceroid lipofuscinosis in Merino sheep whereas affected South Hampshire sheep have reduced levels of CLN6 mRNA. *Biochimica et Biophysica Acta*, *1762*(10), 898–905.

Tardieu, M., Zé, M., Husson, B., De Bournonville, S., Deiva, K., Adamsbaum, C., Vincent, F., Hocquemiller, M., Broissand, C., Furlan, V., Ballabio, A., Fraldi, A., Crystal, R. G., Baugnon, T., Roujeau, T., Heard, J.-M., & Danos, O. (2014). Intracerebral administration of adeno-associated viral vector serotype rh.10 carrying human SGSH and SUMF1 cDNAs in children with mucopolysaccharidosis type IIIA disease: Results of a Phase I/II trial. *Human Gene Therapy*, *25*(6), 506–516.

Taylor, R. M., & Farrow, B. R. (1988). Ceroid-lipofuscinosis in border collie dogs. *Acta Neuropathologica*, *75*(6), 627–631.

Teixeira, C. A., Espinola, J., Huo, L., Kohlschütter, J., Persaud Sawin, D.-A., Minassian, B., Bessa, C. J. P., Guimarães, A., Stephan, D. A., Clara, M., Miranda, S., Macdonald, M. E., Ribeiro, M. G., & Boustany, R.-M. N. (2003a). Novel mutations in the CLN6 gene causing a variant late infantile neuronal ceroid lipofuscinosis. *Human Mutation*, *21*(5), 502–508.

Teixeira, C., Guimarães, A., Bessa, C., Ferreira, M. J., Lopes, L., Pinto, E., Pinto, R., Boustany, R.-M., Sá Miranda, M. C., & Ribeiro, M. G. (2003b). Clinicopathological and molecular characterization of

neuronal ceroid lipofuscinosis in the Portuguese population. *Journal of Neurology*, *250*, 661–667.

Tellez, J., Vliet, K. Van, Tseng, Y.-S., Finn, J. D., Tschernia, N., Almeida-Porada, G., Arruda, V. R., Agbandje-Mckenna, M., & Porada, C. D. (2013). Characterization of naturally-occurring humoral immunity to AAV in sheep. *PLoS ONE*, *8*(9), e75142.

Temin, H. M., & Baltimore, D. (1972). RNA-directed DNA synthesis and RNA tumor viruses. *Advances in Virus Research*, *17*, 129–186.

Terlecki, S., Richardson, C., Bradley, R., Buntain, D., Young, G. B., & Pampiglione, G. (1978). A congenital disease of lambs clinically similar to “inherited cerebellar cortical atrophy” (daft lamb disease). *The British Veterinary Journal*, *134*(4), 299–307.

Thelen, M., Fehr, S., Schweizer, M., Braulke, T., & Galliciotti, G. (2012). High expression of disease-related Cln6 in the cerebral cortex, purkinje cells, dentate gyrus, and hippocampal ca1 neurons. *Journal of Neuroscience Research*, *90*, 568–574.

Themis, M., Schneider, H., Kiserud, T., Cook, T., Adebakin, S., Jezzard, S., Forbes, S., Hanson, M., Pavirani, A., Rodeck, C., & Coutelle, C. (1999). Successful expression of beta-galactosidase and factor IX transgenes in fetal and neonatal sheep after ultrasound-guided percutaneous adenovirus vector administration into the umbilical vein. *Gene Therapy*, *6*(7), 1239–1248.

Thundyil, J., & Lim, K.-L. (2015). DAMPs and neurodegeneration. *Ageing Research Reviews*, *24*(Pt A), 17–28.

Torres, P. A., Zeng, B. J., Porter, B. F., Alroy, J., Horak, F., Horak, J., & Kolodny, E. H. (2010). Tay-Sachs disease in Jacob sheep. *Molecular Genetics and Metabolism*, *101*(4), 357–363.

Traboulsi, E. I., Green, W. R., Luckenbach, M. W., & de la Cruz, Z. C. (1987). Neuronal ceroid lipofuscinosis. Ocular histopathologic and electron microscopic studies in the late infantile, juvenile, and adult forms. *Graefe’s Archive for Clinical and Experimental Ophthalmology*, *225*(6), 391–402.

Tran, N. D., Porada, C. D., Almeida-Porada, G., Glimp, H. A., Anderson, W. F., & Zanjani, E. D. (2001). Induction of stable prenatal tolerance to beta-galactosidase by in utero gene transfer into preimmune sheep fetuses. *Blood*, *97*(11), 3417–3423.

Trapani, I., Banfi, S., Simonelli, F., Surace, E. M., & Auricchio, A. (2015). Gene therapy of inherited retinal degenerations: prospects and challenges. *Human Gene Therapy*, *26*(4), 193–200.

Tyynelä, J., Cooper, J. D., Khan, M. N., Shemilts, S. J. A., & Haltia, M. (2004). Hippocampal pathology in the human neuronal ceroid-lipofuscinoses: distinct patterns of storage deposition, neurodegeneration and glial activation. *Brain Pathology*, *14*(4), 349–357.

Tyynelä, J., Palmer, D. N., Baumann, M., & Haltia, M. (1993). Storage of saposins A and D in infantile neuronal ceroid-lipofuscinosis. *FEBS Letters*, *330*(1), 8–12.

Tyynelä, J., Sohar, I., Sleat, D. E., Gin, R. M., Donnelly, R. J., Baumann, M., Haltia, M., & Lobel, P. (2000). A mutation in the ovine cathepsin D gene causes a congenital lysosomal storage disease with profound neurodegeneration. *The EMBO Journal*, *19*(12), 2786–2792.

Tyynelä, J., Suopanki, J., Santavuori, P., Baumann, M., & Haltia, M. (1997). Variant late infantile

neuronal ceroid-lipofuscinosis: pathology and biochemistry. *Journal of Neuropathology and Experimental Neurology*, *56*(4), 369–375.

Url, A., Bauder, B., Thalhammer, J., Nowotny, N., Kolodziejek, J., Herout, N., Fürst, S., & Weissenböck, H. (2001). Equine neuronal ceroid lipofuscinosis. *Acta Neuropathologica*, *101*(4), 410–414.

Van Bogaert, P., Azizieh, R., Désir, J., Aeby, A., De Meirleir, L., Laes, J.-F., Christiaens, F., & Abramowicz, M. J. (2007). Mutation of a potassium channel-related gene in progressive myoclonic epilepsy. *Annals of Neurology*, *61*(6), 579–586.

van Dellen, A., Blakemore, C., Deacon, R., York, D., & Hannan, A. J. (2000). Delaying the onset of Huntington's in mice. *Nature*, *404*(6779), 721–722.

van der Bom, I. M. J., Moser, R., Gao, G., Mondo, E., Gounis, M., McGowan, S., Chaurette, J., Bishop, N., Sena-Esteves, M. S., Mueller, C., & Aronin, N. (2013). Finding the striatum in sheep: Use of a multi-modal guided approach for convection enhanced delivery. *Journal of Huntington's Disease*, *2*, 41–45.

Van der Bom, I. M. J., Moser, R. P., Gao, G., Sena-Esteves, M., Aronin, N., & Gounis, M. J. (2013). Frameless multimodal image guidance of localized convection-enhanced delivery of therapeutics in the brain. *Journal of Neurointerventional Surgery*, *5*(1), 69–72.

Vasseur, S., Paull, D., Atkinson, S., Colditz, I., & Fisher, A. (2006). Effects of dietary fibre and feeding frequency on wool biting and aggressive behaviours in housed Merino sheep. *Australian Journal of Experimental Agriculture*, *46*(6&7), 777–782.

Vesa, J., Chin, M. H., Oelgeschläger, K., Isosomppi, J., DellAngelica, E. C., Jalanko, A., & Peltonen, L. (2002). Neuronal ceroid lipofuscinoses are connected at molecular level: interaction of CLN5 protein with CLN2 and CLN3. *Molecular Biology of the Cell*, *13*(7), 2410–2420.

Vesa, J., Hellsten, E., Verkruyse, L. A., Camp, L. A., Rapola, J., Santavuori, P., Hofmann, S. L., & Peltonen, L. (1995). Mutations in the palmitoyl protein thioesterase gene causing infantile neuronal ceroid lipofuscinosis. *Nature*, *376*(6541), 584–587.

von Schantz, C., Kielar, C., Hansen, S. N., Pontikis, C. C., Alexander, N. A., Kopra, O., Jalanko, A., & Cooper, J. D. (2009). Progressive thalamocortical neuron loss in Cln5 deficient mice: Distinct effects in Finnish variant late infantile NCL. *Neurobiology of Disease*, *34*(2), 308–319.

Vuillemenot, B. R., Katz, M. L., Coates, J. R., Kennedy, D., Tiger, P., Kanazono, S., Lobel, P., Sohar, I., Xu, S., Cahayag, R., Keve, S., Koren, E., Bunting, S., Tsuruda, L. S., & O'Neill, C. A. (2011). Intrathecal tripeptidyl-peptidase 1 reduces lysosomal storage in a canine model of late infantile neuronal ceroid lipofuscinosis. *Molecular Genetics and Metabolism*, *104*(3), 325–337.

Wada, R., Tifft, C. J., & Proia, R. L. (2000). Microglial activation precedes acute neurodegeneration in Sandhoff disease and is suppressed by bone marrow transplantation. *Proceedings of the National Academy of Sciences of the United States of America*, *97*(20), 10954–10959.

Waddington, S. N., Kennea, N. L., Buckley, S. M. K., Gregory, L. G., Themis, M., & Coutelle, C. (2004). Fetal and neonatal gene therapy: benefits and pitfalls. *Gene Therapy*, *11*, S92–S97.

Waddington, S. N., Kramer, M. G., Hernandez-Alcoceba, R., Buckley, S. M. K., Themis, M., Coutelle, C., & Prieto, J. (2005). In utero gene therapy: current challenges and perspectives. *Molecular*

Therapy, *11*(5), 661–676.

Walia, J. S., Altaleb, N., Bello, A., Kruck, C., LaFave, M. C., Varshney, G. K., Burgess, S. M., Chowdhury, B., Hurlbut, D., Hemming, R., Kobinger, G. P., & Triggs-Raine, B. (2015). Long-term correction of Sandhoff disease following intravenous delivery of rAAV9 to mouse neonates. *Molecular Therapy*, *23*(3), 414–422.

Wang, J., Lozier, J., Johnson, G., Kirshner, S., Verthelyi, D., Pariser, A., Shores, E., & Rosenberg, A. (2008). Neutralizing antibodies to therapeutic enzymes: considerations for testing, prevention and treatment. *Nature Biotechnology*, *26*(8), 901–908.

Wang, H., Yang, B., Qiu, L., Yang, C., Kramer, J., Su, Q., Guo, Y., Brown, R. H., Gao, G., & Xu, Z. (2014). Widespread spinal cord transduction by intrathecal injection of rAAV delivers efficacious RNAi therapy for amyotrophic lateral sclerosis. *Human Molecular Genetics*, *23*(3), 668–681.

Warrier, V., Vieira, M., & Mole, S. E. (2013). Genetic basis and phenotypic correlations of the neuronal ceroid lipofusinoses. *Biochimica et Biophysica Acta*, *1832*, 1827–1830.

Weimer, J. M., Custer, A. W., Benedict, J. W., Alexander, N. A., Kingsley, E., Federoff, H. J., Cooper, J. D., & Pearce, D. A. (2006). Visual deficits in a mouse model of Batten disease are the result of optic nerve degeneration and loss of dorsal lateral geniculate thalamic neurons. *Neurobiology of Disease*, *22*(2), 284–293.

Weimer, J. M., Kriscenski-Perry, E., Elshatory, Y., & Pearce, D. A. (2002). The neuronal ceroid lipofuscinoses: mutations in different proteins result in similar disease . *NeuroMolecular Medicine*, *1*(2), 111–124.

Weissenböck, H., & Rössel, C. (1997). Neuronal ceroid-lipofuscinosis in a domestic cat: clinical, morphological and immunohistochemical findings. *Journal of Comparative Pathology*, *117*(1), 17–24.

Weleber, R. G. (1998). The dystrophic retina in multisystem disorders: the electroretinogram in neuronal ceroid lipofuscinoses. *Eye*, *12*(Pt 3b), 580–590.

Wessels, M. E., Holmes, J. P., Jeffrey, M., Jackson, M., Mackintosh, A., Kolodny, E. H., Zeng, B. J., Wang, C. B., & Scholes, S. F. E. (2014). GM2 gangliosidosis in British Jacob sheep. *Journal of Comparative Pathology*, *150*(2-3), 253–257.

Westlake, V. J., Jolly, R. D., Jones, B. R., Mellor, D. J., Machon, R., Zanjani, E. D., & Krivit, W. (1995). Hematopoietic cell transplantation in fetal lambs with ceroid-lipofuscinosis. *American Journal of Medical Genetics*, *57*(2), 365–368.

Wheeler, R. B., Sharp, J. D., Schultz, R. A., Joslin, J. M., Williams, R. E., & Mole, S. E. (2002). The gene mutated in variant late-infantile neuronal ceroid lipofuscinosis (CLN6) and in nclf mutant mice encodes a novel predicted transmembrane protein. *American Journal of Human Genetics*, *70*(2), 537–542.

Whitney, N. P., Eidem, T. M., Peng, H., Huang, Y., & Zheng, J. C. (2009). Inflammation mediates varying effects in neurogenesis: relevance to the pathogenesis of brain injury and neurodegenerative disorders. *Journal of Neurochemistry*, *108*(6), 1343–1359.

Wilkes, D., Li, G., Angeles, C. F., Patterson, J. T., & Huang, L.-Y. M. (2012). A large animal neuropathic

pain model in sheep: a strategy for improving the predictability of preclinical models for therapeutic development. *Journal of Pain Research*, *5*, 415–424.

Wilkinson, F. L., Holley, R. J., Langford-Smith, K. J., Badrinath, S., Liao, A., Langford-Smith, A., Cooper, J. D., Jones, S. A., Wraith, J. E., Wynn, R. F., Merry, C. L. R., & Bigger, B. W. (2012). Neuropathology in mouse models of mucopolysaccharidosis type I, IIIA and IIIB. *PloS One*, *7*(4), e35787.

Williams, R. E., & Mole, S. E. (2012). New nomenclature and classification scheme for the neuronal ceroid lipofuscinoses. *Neurology*, *79*(2), 183–91.

Williams, R. S., Lott, I. T., Ferrante, R. J., & Caviness, V. S. (1977). The cellular pathology of neuronal ceroid-lipofuscinosis. A golgi-electronmicroscopic study. *Archives of Neurology*, *34*(5), 298–305.

Winner, B., Kohl, Z., & Gage, F. H. (2011). Neurodegenerative disease and adult neurogenesis. *The European Journal of Neuroscience*, *33*(6), 1139–1151.

Wöhlke, A., Philipp, U., Bock, P., Beineke, A., Lichtner, P., Meitinger, T., & Distl, O. (2011). A one base pair deletion in the canine ATP13A2 gene causes exon skipping and late-onset neuronal ceroid lipofuscinosis in the Tibetan terrier. *PLoS Genetics*, *7*(10), e1002304.

Wolf, D. A., Banerjee, S., Hackett, P. B., Whitley, C. B., Mcivor, R. S., & Low, W. C. (2015). Gene therapy for neurologic manifestations of mucopolysaccharidoses. *Expert Opinion on Drug Delivery*, *12*(2), 283–296.

Wong, L.-F., Azzouz, M., Walmsley, L. E., Askham, Z., Wilkes, F. J., Mitrophanous, K. A., Kingsman, S. M., & Mazarakis, N. D. (2004). Transduction patterns of pseudotyped lentiviral vectors in the nervous system. *Molecular Therapy*, *9*(1), 101–111.

Woods, P. R., Storts, R. W., Shelton, M., & Menzies, C. (1994). Neuronal ceroid lipofuscinosis in Rambouillet sheep: characterization of the clinical disease. *Journal of Veterinary Internal Medicine*, *8*, 370–375.

Worgall, S., Sondhi, D., Hackett, N. R., Kosofsky, B., Kekatpure, M. V, Neyzi, N., Dyke, J. P., Ballon, D., Heier, L., Greenwald, B. M., Christos, P., Mazumdar, M., Souweidane, M. M., Kaplitt, M. G., & Crystal, R. G. (2008). Treatment of late infantile neuronal ceroid lipofuscinosis by CNS administration of a serotype 2 adeno-associated virus expressing CLN2 cDNA. *Human Gene Therapy*, *19*(5), 463–474.

Wu, J., Zhao, W., Zhong, L., Han, Z., Li, B., Ma, W., Weigel-Kelley, K. A., Warrington, K. H., & Srivastava, A. (2007). Self-complementary recombinant adeno-associated viral vectors: packaging capacity and the role of rep proteins in vector purity. *Human Gene Therapy*, *18*(2), 171–182.

Wu, T., Töpfer, K., Lin, S.-W., Li, H., Bian, A., Zhou, X. Y., High, K. A., & Ertl, H. C. J. (2012). Self-complementary AAVs induce more potent transgene product-specific immune responses compared to a single-stranded genome. *Molecular Therapy*, *20*(3), 572–579.

Xie, J., Xie, Q., Zhang, H., Ameres, S. L., Hung, J.-H., Su, Q., He, R., Mu, X., Seher Ahmed, S., Park, S., Kato, H., Li, C., Mueller, C., Mello, C. C., Weng, Z., Flotte, T. R., Zamore, P. D., & Gao, G. (2011). MicroRNA-regulated, systemically delivered rAAV9: a step closer to CNS-restricted transgene expression. *Molecular Therapy*, *19*(3), 526–535.

Xin, W., Mullen, T. E., Kiely, R., Min, J., Feng, X., Cao, Y., O'Malley, L., Shen, Y., Chu-Shore, C., Mole, S. E., Goebel, H. H., & Sims, K. (2010). CLN5 mutations are frequent in juvenile and late-onset non-Finnish patients with NCL. *Neurology*, *74*(7), 565–571.

Yamazaki, Y., Hirai, Y., Miyake, K., & Shimada, T. (2014). Targeted gene transfer into ependymal cells through intraventricular injection of AAV1 vector and long-term enzyme replacement via the CSF. *Scientific Reports*, *4*, 5506.

Yang, B., Li, S., Wang, H., Guo, Y., Gessler, D. J., Cao, C., Su, Q., Kramer, J., Zhong, L., Ahmed, S. S., Zhang, H., He, R., Desrosiers, R. C., Brown, R., Xu, Z., & Gao, G. (2014). Global CNS transduction of adult mice by intravenously delivered rAAVrh.8 and rAAVrh.10 and nonhuman primates by rAAVrh.10. *Molecular Therapy*, *22*(7), 1299–1309.

Yang, Y., & Raine, A. (2009). Prefrontal structural and functional brain imaging findings in antisocial, violent, and psychopathic individuals: a meta-analysis. *Psychiatry Research*, *174*(2), 81–88.

Yang, G. S., Schmidt, M., Yan, Z., Lindbloom, J. D., Harding, T. C., Donahue, B. A., Engelhardt, J. F., Kotin, R., & Davidson, B. L. (2002). Virus-mediated transduction of murine retina with adeno-associated virus: effects of viral capsid and genome size. *Journal of Virology*, *76*(15), 7651–7660.

Yin, L., Greenberg, K., Hunter, J. J., Dalkara, D., Kolstad, K. D., Masella, B. D., Wolfe, R., Visel, M., Stone, D., Libby, R. T., Diloreto, D., Schaffer, D., Flannery, J., Williams, D. R., & Merigan, W. H. (2011). Intravitreal injection of AAV2 transduces macaque inner retina. *Investigative Ophthalmology & Visual Science*, *52*(5), 2775–2783.

Zerah, M., Piguet, F., Colle, M.-A., Raoul, S., Deschamps, J.-Y., Deniaud, J., Gautier, B., Toulgoat, F., Bieche, I., Laurendeau, I., Sondhi, D., Souweidane, M. M., Cartier-Lacave, N., Moullier, P., Crystal, R. G., Roujeau, T., Sevin, C., & Aubourg, P. (2015). Intracerebral gene therapy using AAVrh.10-hARSA recombinant vector to treat patients with early-onset forms of metachromatic leukodystrophy: Preclinical feasibility and safety assessments in nonhuman primates. *Human Gene Therapy*, *26*(2), 113–124.

Zhang, H., Yang, B., Mu, X., Ahmed, S. S., Su, Q., He, R., Wang, H., Mueller, C., Sena-Esteves, M., Brown, R., Xu, Z., & Gao, G. (2011). Several rAAV vectors efficiently cross the blood-brain barrier and transduce neurons and astrocytes in the neonatal mouse central nervous system. *Molecular Therapy*, *19*(8), 1440–1448.

Zhao, X., Onteru, S. K., Dittmer, K. E., Parton, K., Blair, H. T., Rothschild, M. F., & Garrick, D. J. (2012). A missense mutation in AGTPBP1 was identified in sheep with a lower motor neuron disease. *Heredity*, *109*(3), 156–162.

Zincarelli, C., Soltys, S., Rengo, G., & Rabinowitz, J. E. (2008). Analysis of AAV serotypes 1-9 mediated gene expression and tropism in mice after systemic injection. *Molecular Therapy*, *16*(6), 1073–1080.

Zufferey, R., Dull, T., Mandel, R. J., Bukovsky, A., Quiroz, D., Naldini, L., & Trono, D. (1998). Self-inactivating lentivirus vector for safe and efficient in vivo gene delivery. *Journal of Virology*, *72*(12), 9873–9880.

Zufferey, R., Dull, T., Mandel, R. J., Bukovsky, A., Quiroz, D., Naldini, L., & Trono, D. (1998). Self-inactivating lentivirus vector for safe and efficient in vivo gene delivery. *Journal of Virology*, *72*(12), 9873–9880.